GeoFocus volume 30

Martin BOCHUD

Tectonics of the Eastern Greater Caucasus in Azerbaijan

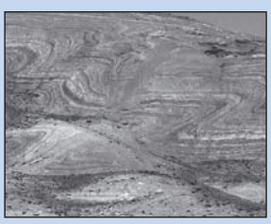

Département de Géosciences, Sciences de la Terre, Université de Fribourg (Suisse)

DEPARTMENT OF GEOSCIENCES – EARTH SCIENCES

UNIVERSITY OF FRIBOURG (SWITZERLAND)

Tectonics of the Eastern Greater Caucasus in Azerbaijan

THESIS

Presented at the Faculty of Sciences of the University of Fribourg (Switzerland) in consideration for the award of the academic grade of *Doctor rerum naturalium*

by

Martin Bochud

from

Hauterive (Fribourg), Switzerland

Thesis n° 1733

Accepted by the Faculty of Science of the University of Fribourg (Switzerland)
upon the recommendation of :

Prof. Jon MOSAR	University of Fribourg (Switzerland)	Thesis supervisor
Prof. Ulrich A. GLASMACHER	University of Heidelberg (Germany)	Examiner
Dr. Talat KANGARLI	Geological Institute of Azerbaijan (Azerbaijan)	Examiner
Dr. Marie-Françoise BRUNET	Université Pierre et Marie Curie (France)	Examiner
Prof. Christian HAUCK	University of Fribourg (Switzerland)	President of the Jury

Fribourg, the 25th of October 2011

Thesis supervisor

Prof. Jon MOSAR

Dean

Prof. Rolf INGOLD

CONTENTS

*****

ABSTRACT

The Greater Caucasus is Europe's largest and highest mountain belt and results from the inversion of the Mesozoic Greater Caucasus back-arc-type basin due to the collision of Arabia and Eurasia. The orogenic processes that led to the present mountain chain started in early Tertiary, accelerated during the Plio-Pleistocene, and are still active nowadays.

The Eastern Greater Caucasus (EGC) is located to the north of Azerbaijan. It corresponds to a doubly verging fold-and-thrust belt, with a pro- and a retro wedge actively propagating into the foreland sedimentary basins of the Kura to the south and the Terek to the north. The area is known since the antiquity for its hydrocarbon resources and its mud volcanoes. This particular context added to the high summits of its central area (Bazarduzu Mt. reaches 4466 m) and the proximity with the deep South Caspian intracontinental basin make it an unique place to investigate geodynamics of basin formation and of the orogenic structures.

The aim of this thesis is first to describe the geology and the evolution of the Eastern Greater Caucasus. Secondly we detailed structural and geomorphological features of selected areas to develop a structural model of the EGC that we export to the Greater Caucasus. Finally we tested methods like Apatite Fission Tracks (AFT), Illite Crystallinity (IC) and subsidence curves to characterize the thermal evolution and the subsidence/uplift of the area.

The structural features of the EGC result from an average NNE-SSW compressive stress. Folds have axis that slightly dip to the ESE. The EGC is cut by thrusts dipping to the NNE and SSW. They are respectively located to the S and to the N with a transition in the central part. Finally, the recent anticaucasian strike-slip fault system led to the present valley geomorphology and orientation.

Based on marine sediments at altitudes between 2000 m and 3550 m, we respectively determine uplift rates of 0.77 mm/yr since the Pliocene (~2.6 Myr) and 0.31 mm/yr since the Sarmatian (~11.6 Myr). Based on Apatite fission-track, Illite Crystallinity and subsidence studies, we determine that a fast exhumation acted on the northern area (Tahircal Zone) since the Late Miocene whereas the central area (Tufan Zone) was affected by slower uplift rates but during a longer period (since Eocene-Oligocene). This long term uplift built the highest relief of the EGC. These uplift rates of the EGC cannot be compared with the rate of 10-12 mm/yr since the Pliocene of the central Greater Caucasus in Georgia and Russia.

Several events in the EGC allow defining more than six main compressive phases since the Middle Jurassic. The first occurred before Callovian times and is expressed by Callovian deposits that unconformably lie on folded Aalenian deposits. The second is expressed by Berriasian conglomerates that transgressively cover tilted Kimmeridgian deposits. The third corresponds to an erosional event of a paleo-valley in the Sahdag-Besbarmaq Nappe and on the underlying Sahdag-Xizi Zone that is subsequently filled by Upper Cretaceous to Pliocene sediments. The fourth compressive event occurred at the end of the Upper Cretaceous and beginning of the Paleocene and is expressed by Paleocene sediments that transgressively cover deposits from the Middle Jurassic to the Cretaceous in the northern area. The fifth event corresponds to the creation of foreland basins during the Eocene and Oligocene that resulted from the building of the Greater Caucasus. The last event corresponds to the major uplift that started during Middle-Late Miocene and is based on marine sediments at high altitude.

In terms of thermal history, we observe only a weak schistosity that develops in the central part and corresponds to a very low-grade metamorphism in favorable lithologies. Apatite fission-track and illite crystallinity analyses show an increase of the metamorphism from the northern orogenic front to its central part. They

show also a decrease of the metamorphism southeastwards along the main EGC crest. AFT time-temperature models and subsidence curves show a fast burial during the Middle-Upper Jurassic and they all finish by an exhumation starting, depending on the area, from the beginning to the end of Miocene. The north is affected by an exhumation-burial period starting during the Upper Cretaceous and finishing in the Middle Miocene.

Combining our structural and geomorphological study in the EGC with literature and GIS studies on the other regions of the Greater Caucasus, we expand our findings to the whole Greater Caucasus. The Main Caucasus Thrust (MCT) is a major thrust that crosses the whole Greater Caucasus from west to east. The zone of highest topography of the Greater Caucasus is bound to the south by the MCT which shows important top to the south movement and to the north by south dipping thrusts with top to the north movement. We associate this north faults to a N-verging backthrusting system linked to a thrust ramp system to the south corresponding to the MCT. The migration of the MCT to the south during Tertiary is responsible for the formation of succesive foreland basins separated by clear changes in topography, deviation of rivers and water gaps. The geodynamic behaviour between the east and west Greater Caucasus area is not identical. This is mainly due to several factors such as the E to W decreasing plate convergence rate; the basement that outcrops only in the west; and the recent volcanism and magmatic activity that affected the central and western part of the Greater Caucasus.

Keywords: *Greater Caucasus, Azerbaijan, structural, stress, Apatite Fission Track, Illite Crystallinity, subsidence, geomorphology, GIS.*

*****

RÉSUMÉ

Le Grand Caucase est la plus haute et la plus longue chaîne de montagne en Europe. Elle est le résultat de l'inversion suite à la collision de la plaque arabique et eurasienne d'un ancien bassin d'arrière-arc mésozoïque, le « Greater Caucasus Basin ». La formation de l'actuel Grand Caucase a commencé au début du Tertiaire avec une accélération des mouvements au Pliocène-Pléistocène. Elle est encore active actuellement.

Le Grand Caucase Oriental (EGC : « Eastern Greater Caucasus ») est situé au nord de l'Azerbaijan. Il correspond à une chaîne de chevauchements et de plis à double vergences avec une propagation vers le sud dans le bassin d'avant-pays du Kura et vers le nord dans le bassin d'arrière-pays du Terek. La région est connue depuis l'Antiquité pour ses ressources en hydrocarbures et ses volcans de boue. Ce contexte particulier, ces hauts sommets de la partie centrale (le sommet du Bazarduzu atteint 4466 m d'altitude) et le proche bassin sud caspien rendent cette zone intéressante pour des études sur l'évolution et la géodynamique.

Le but de ce doctorat est dans un premier temps de décrire la géologie et l'évolution du Grand Caucase Orientale. Deuxièmement, des études structurales et géomorphologiques sur des zones sélectionnées ont été réalisées afin de définir un modèle structural de la région et de l'étendre ensuite à la totalité du Grand Caucase. Finalement, nous avons testé différentes méthodes comme les traces de fission dans l'apatite, la cristallinité de l'illite et les courbes de subsidence qui permettent entre autres de caractériser le comportement thermique et l'exhumation de la région.

Les structures géologiques du Grand Caucase Oriental sont le résultat d'une contrainte compressive de direction NNE-SSW. Les plis résultants ont un plongement axial de quelques degrés vers l'ESE. Le Grand Caucase Oriental est également découpé par de nombreux chevauchements dirigés vers le NNE et le SSW. Ils sont respectivement situés au nord et au sud du Grand Caucase Oriental avec une transition dans la région centrale.

Basé sur des sédiments marins trouvés à des altitudes de 2000 m et de 3550 m, nous avons respectivement déterminé des taux de soulèvement de surface de 0.77 mm/a depuis le Pliocène (~2.6 Ma) et de 0.31 mm/a depuis le Sarmatien (~11.6 Ma). Ces soulèvements ne sont pas comparables à ceux obtenus dans la partie centrale du Grand Caucase (Géorgie, Russie) qui atteignent des vitesses de 10 à 12 mm/a. Les traces de fission dans l'apatite, nous ont permis de déterminer que la partie centrale (Zone de Tufan) a subit des vitesses d'exhumation plus faibles mais durant une plus longue période (depuis l'Oligocène-Miocène Inf.) que la partie nord (Zone de Tahircal) où la dernière phase d'exhumation a commencé au Miocene Supérieur.

Différents événements dans le Grand Caucase Oriental ont permis de définir six phases compressives. La première s'est déroulée avant le Callovien (Jurassique Moyen). Des sédiments Callovien sont en contact transgressif sur des sédiments Aalénien plissés. La deuxième phase est déterminée par le dépôt de conglomérats Berriasien sur des dépôts marins Kimméridgien fortement inclinés. La troisième phase correspond à l'érosion d'une paléo-vallée à travers la Nappe du Sahdag-Besbarmaq et une partie de la zone de Sahdag-Xizi. Cette paléo-vallée a ensuite été comblée par des sédiments marins allant du Crétacé Supérieur au Pliocène. La quatrième phase s'est déroulée à la fin du Crétacé Supérieur et s'exprime au nord du Grand Caucase Oriental par des sédiments Paléocène transgressifs sur des dépôts marins allant du Jurassique Moyen au Crétacé. La cinquième phase est directement liée au début de la formation du Grand Caucase à l'Eocène-Oligocène où l'on voit se créer des bassins d'avant-pays qui sont remplis

par des sédiments venant de l'érosion de la nouvelle chaîne de montagne. La dernière phase correspond au soulèvement principal de la chaîne qui commence durant le Miocène et est basée sur des sédiments marins trouvés en altitude.

Au niveau de l'histoire thermique, nous avons observé une faible schistosité dans la partie centrale du Grand Caucase Oriental. Elle correspond à un métamorphisme de très faible intensité dans des lithologies favorables. Les analyses de traces de fission dans l'apatite (AFT) et de l'indice de cristallinité montrent une augmentation du métamorphisme en partant du front orogénique nord de la chaîne vers la partie centrale. Elles montrent également une diminution du métamorphisme en partant de la partie centrale vers l'ESE en suivant la crête principale de la chaîne. Les modèles temps-températures des AFT et les courbes de subsidences montrent toute un enfouissement rapide au Jurassique Moyen-Supérieur et elles se terminent par une rapide exhumation au Miocene-Pliocene. La partie nord est caractérisée par un événement intermédiaire d'exhumation-enfouissement qui commence au Crétacé Supérieur et se termine au Miocene Moyen.

En combinant les études structurales et géomorphologiques dans le Grand Caucase Oriental avec la littérature et des études SIG sur d'autres régions du Grand Caucase, nous avons pu étendre à ce dernier les structures découvertes dans la partie orientale. Le « Main Caucasus Thrust » (MCT ou chevauchement principal du Caucase) est un chevauchement qui coupe d'ouest en est la chaîne de montagne. La zone topographique élevée du Grand Caucase est limitée au sud par le MCT qui montre un déplacement important vers le sud et au nord par des failles retro-chevauchantes vers le nord. Ces failles sont liées à un système de rampe vers le sud dont le MCT est la composante principale. La migration de le MCT vers le sud pendant le Tertiaire est responsable de la formation successive de bassins d'avant pays caractérisés par des hauts topographiques, des rivières déviées et des vallées asséchées. Le comportement géodynamique entre l'est et l'ouest du Grand Caucase n'est pas identique. C'est principalement dû à différents facteurs comme la diminution de la convergence de plaque d'est en ouest, l'affleurement du socle uniquement dans la partie occidentale et le magmatisme et volcanisme récents dans la partie centrale et occidentale.

Mots-clés : *Grand Caucase, Azerbaijan, géologie structurale, contraintes, trace de fission, cristallinité de l'illite, subsidence, géomorphologie, systèmes d'information géographique.*

*****

ACKNOWLEDGMENTS

I am very grateful to my thesis director Professor Jon Mosar for giving me the opportunity to do a thesis like I imagined, for his numerous advices in the field, for his opening to new technologies and for his numerous ideas.

I would also specially thank Dr. Talat Kangarli who organized all our field trips in Azerbaijan and shared with us his unvaluable knowledge from the Eastern Greater Caucasus. He also welcomed us in his family always with great kindness and allowed us discovering the Azeri culture. I will also thank him to be examiner for this thesis.

A special thanks to Prof. Ulrich A. Glasmacher for his interesting and constructive comments in the field but also as examiner of this thesis. He introduced me to the world of the thermochronology and managed to analyse with his team the azeri samples. Thanks also to his team and colleagues including Torben Kissner and Otto Kraft (University of Heidelberg) who participated to the 2007 field trip and prepared and analysed the fission-track samples and Dr. Bertil Maechtle who gave me an introduction to quaternary method in the field

A great thanks to Dr. Marie-Françoise Brunet (CNRS, University Pierre et Marie Curie, Paris, France) who gave me the opportunity to discover the Middle East Geology, to do GIS work with her team and finally to give me, as examiner, constructive and detailed comments on this thesis.

This thesis, although it is an individual work, benefited from the collaboration of several people in the field : Annick Rast (University of Fribourg) who worked with me in the northern part of the Eastern Greater Caucasus in 2006; Prof. Nigel Mountney (University of Leeds) for his collaboration for the sedimentological part of my work and to receive me for 2 months in his research group ; Dr. Sylvia Spezzaferi who gave me the opportunity to go in Georgia; Prof. Gamkrelidze (Academy of Sciences, Georgia) and his colleagues Dr. Kakhaber Koiava and Dr. Lasha Shubitidze who organized a very interesting field trip through the Central Caucasus ; Dr. Thierry Adatte (University of Neuchâtel) and the the Centre Scientifique et technique Jean-Féger from the Total Company (Pau, France) who respectively made the illite crystallinity and organic matter analyses of our 2006 and 2007 samples.

Communicating with Azeri people would not be possible without the help of our translators: Elmir Akhmedov (2004), Ilkin Kangarli (2005), Tofig Rashidov (2006), Emin Isayev and Emil Guliyev (2007) and Elias Mammedov (2008-2009).

I would also thank the azeri families for their hospitality with special thanks to Mahir Aliyev and his family (Burovdal, 2004), to Shaxbala Hajibalayev (Tahircal, 2006), to Eyvaz and Saravat Bagirov (Xinaliq, 2006), to Heydar (Vasa, 2008) and all other persons that welcomed us with a tea, a vodka, a meal or gave us a bed.

Special thanks go to my colleagues Eva Matzenauer, Luc Braillard, Raphaelle Soulignac and Sébastien Morard for the numerous discussions and their moral support.

I owe to all my university colleagues for the numerous discussions and activities, for enduring all the “kromoks” and for the very good relationships during the 10 years of my studies at the university : Anna S.-M., André S., Bernard G., Calin T., Christian C., Elias S., Gisela T., Ildiko K.-S., Jean-Marc F., Jean-Pierre B., Jürgen von R., Marino M., Michelle C., Raymond P., Reynald D., Vincent S., Bastien M., Bertrand Y., Cécile B., Corinne S., Christina K., Claudius P., Damien A., Daniel R., Daniel W., Daniela K., David J., Elisa R., Florent H., Giordana G., Jonas T., Juanita R.-J.,

Katja von A., Kuno M., Laureline S., Maëlle L., Mario M., Martinus A., Monica C., Naomie V., Noémie S., Norbert R., Pierre V., Richard W., Roy T., Sarah G., Stephan M., Thibault L., Telm B.-A., Tobias I and all the people I forget.

A special thanks to the technical staff including Christophe N., David S., Jean-Paul B., Nicole B. and Patrick D.

I must thank also Softcom Technologies SA that gave me a very interesting work with very flexible working hours that allowed me to do my PhD and to continue to work as electronics engineer.

I will also specially thank my family for their care and support throughout the years.

Finally, the most special thanks go to my wife Ana for her love and support and for tolerating my absences from home during innumerous weeks.

I am sincerely grateful to the following organizations for their financial support:

The University of Fribourg

The Scientific co-operation between Eastern Europe and Switzerland (SCOPES) financed by the Swiss National Science Foundation

The Middle East Basins Evolution Programme

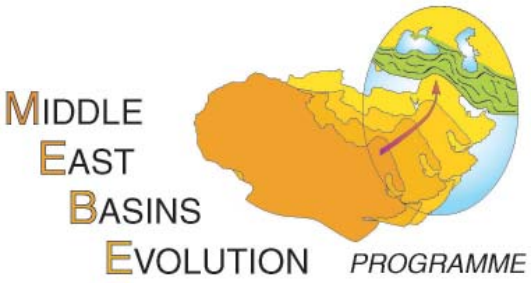

1 - INTRODUCTION

The geology of the Eastern Greater Caucasus has been studied for, at least, the last 150 years. A significant volume of published literature deals with its evolution and much with the oilfields that can be found in the surrounding sedimentary basins. Indeed, the oil history almost started here and today Azerbaijan is still one of the world strategic areas in terms of hydrocarbon resources.

Since the independence of the Azerbaijan in 1991 and the presence of international oil companies, a new impulse on geology started, and numerous studies were published most of them concerning oil exploration. The Geological Institute of Azerbaijan (GIA) is very active and numerous projects and collaborations have started. They published in 2008 the new geological map of Azerbaijan at a scale of 1:500'000 (the preceding version at the same scale was published in 1976). However the geodynamic and structural studies concerning the Eastern Greater Caucasus itself did not evolve significantly during the last decades. For the last five years several groups and international projects have started to study this very interesting area that can clearly give new data to define more precisely the geological evolution of the whole Caspian and Caucasus area.

The main aim of this work is to focus on the geodynamics of Eastern Greater Caucasus (EGC) in the north of Azerbaijan. We will discuss uplift rates of the EGC based on analytical methods. Structural styles and geodynamic behaviour of the main structural zones of the EGC will be fixed and defined based on field data collected in remote valleys.

1.1. OBJECTIVES

After a general description of the Caucasus area, the first objective is to discuss the geological context of the Eastern Greater Caucasus including the stratigraphical context, the sedimentary formations through time, the geodynamic context and the geological evolution. These descriptions are mostly based on field work.

The second objective is to define the structural zones of the Eastern Greater Caucasus. Field data and observations allow highlighting some typical tectonic features of the EGC. They help constrain the orogenic processes of the EGC and the 3 surrounding sedimentary basins: the Terek, the Kura, and the South Caspian basins.

The third objective of this thesis is to investigate the thermal evolution of the area using methods like apatite fission tracks and illite crystallinity. Combined with field observations and subsidence curves, we will try to define the uplift of the area.

The last objective is to generalize these results to the Greater Caucasus combining data like digital elevation models, earthquakes, uplift maps, and old terraces. The aim is to define the main faults crossing the Greater Caucasus and to better characterize its geodynamic behaviour.

To help to the realisation of all these objectives, a geodatabase was built. It integrates all the field data, maps, digital elevation models and other information.

1.2. PROJECT AND COLLABORATIONS

This thesis is the result of a close collaboration with the Geological Institute of Azerbaijan and it was supported by several international projects. The Eastern Greater Caucasus Project started in 2003 and included different Universities and their scientists.

Fribourg University started its geological studies in the Greater Caucasus with the Middle East Basins

Evolution Programme (MEBE). It was a 4 years effort (2003- 2006) funded by major oil companies (BP, ENI, PETRONAS, SHELL and TOTAL) and by the French research organizations (INSU-CNRS and UPMC). This multidisciplinary study of the Middle East, spanning the Arabian-Peri-Arabian and Caucasian-Caspian areas, was led by E. Barrier (CNRS – Université Pierre et Marie-Curie, Paris, France) and M. Gaetani (University of Milan, Italy). Its focus was the geodynamic evolution of the area. MEBE brought together about 300 scientists from 28 countries, representing 100 universities and research organizations. The principal MEBE products are an atlas of 14 palaeotectonic maps showing the geodynamic and tectonic evolution of the Middle East between Late Triassic and the Present and a series of four Geological Society of London Special Publications presenting the results of the regional MEBE working groups. The four volumes cover the Black Sea – Caucasus, the South Caspian – Central Iran, the Zagros-East Arabian margin and the Levant.

The Scientific Cooperation between Eastern Europe and Switzerland program (SCOPES) founded by the Swiss National Science Foundation (SNSF) and the Swiss Agency for development and Cooperation (SDC) supported the next project of the University in this area. The 3 years project named "The Eastern Greater Caucasus: geodynamics of an active mountain belt at the cross road of Europe, Middle-East and Asia", was proposed by Prof. Jon Mosar (University of Fribourg, Switzerland) and Dr. Talat Kangarli (Geological Institute of Azerbaijan). It allowed to create an effective infrastructure for scientific studies in the Eastern Greater Caucasus and to found students in the Geological Institute of Azerbaijan. Finally, this thesis itself was mainly supported by the University of Fribourg.

1.3. Fieldtrips

More than 9 fieldtrips in the Eastern Greater Caucasus since 2004 were made to first get information about the area and secondly to make detailed studies of the interesting geological outcrops.

From the 4th to the 15th May 2004, we studied several outcrops showing major geological features in the northern and southern slopes of the EGC. We also went in the foothill south of the EGC. Dr. J. Mosar and I were accompanied by Dr. Talat Kangarli (GIA, AZ), Chingiz Aliyev (GIA, AZ) and Elmir Akhmedov (translator).

The second fieldtrip corresponds to the main work for my Diploma thesis. It started from the 8th of August 2004 and finished the 24th of September. The 7 weeks were divided in two parts: 5 weeks to study the upper part of the Girdimancay River and 2 weeks for a fieldtrip to observe and study major geological outcrops in the northern slope of the EGC. For the second part I was accompanied by Prof. Jon Mosar (University of Fribourg, Switzerland), Prof. Nigel Mountney (Keele University, UK), Dr. Talat Kangarli (GIA, Azerbaijan), Elmir Akhmedov (translator) and our driver Heybat.

The aim of the third expedition from the 4th to the 13th of September 2005 was mainly to detail the northern slope around the northern Sahdag – Qizilqaya area. The people involved were Dr. J. Mosar (University of Fribourg, Switzerland), Dr. T. Kangarli (GIA, Azerbaijan), Ilkin Kangarli (translator), the driver Heybat and myself.

The 2006 expedition was the first for my PhD thesis but also for the Master thesis of Annick Rast. The main goal was to make a detailed structural study of the Sahdag – Bazarduzu area. The fieldtrip was from the 4th of August to the 13th of September 2006. During the first two weeks, I worked with Dr. T. Kangarli and we went in different places around the Eastern Greater Caucasus. After that Prof. J. Mosar, Prof. Ulrich A. Glasmacher (University of Heidelberg, Germany) and Annick Rast came and we worked one week near the Sahdag area. Finally A. Rast and I stayed and studied different places around the Sahdag area during 3 weeks.

In 2007, the main goals of the fifth fieldtrip were: an exploration of the Lesser Caucasus near Ganja, taking structural data and more fission-track samples in the central part of the EGC and finally looking the possibilities of making quaternary studies. The expedition was from the 21st of August to the 14th of September 2007. The participants were Prof. U. A. Glasmacher, Torben Kissner, Otto Kraft and Dr. Bertil Mächtle (University of Heidelberg, Germany), Dr. T. Kangarli and Emin Guliev (GIA, Azerbaijan) and myself. Finally during the second week of October I participated in a 2 days international conference for young scientists in Baku (8th and 9th of October 2007) and I also went to measure the Qaramaryam hills in the southern slope of the EGC and also looked for data and information in the GIA in Baku.

From the 8th to 19th of June 2008, the principal aim was to measure structural data from the central part of the EGC in both side of the main ridge. Prof. J. Mosar and I went in two valleys on both side of the EGC. We were accompanied by Dr. T. Kangarli and Ilyas Mammadov (translator).

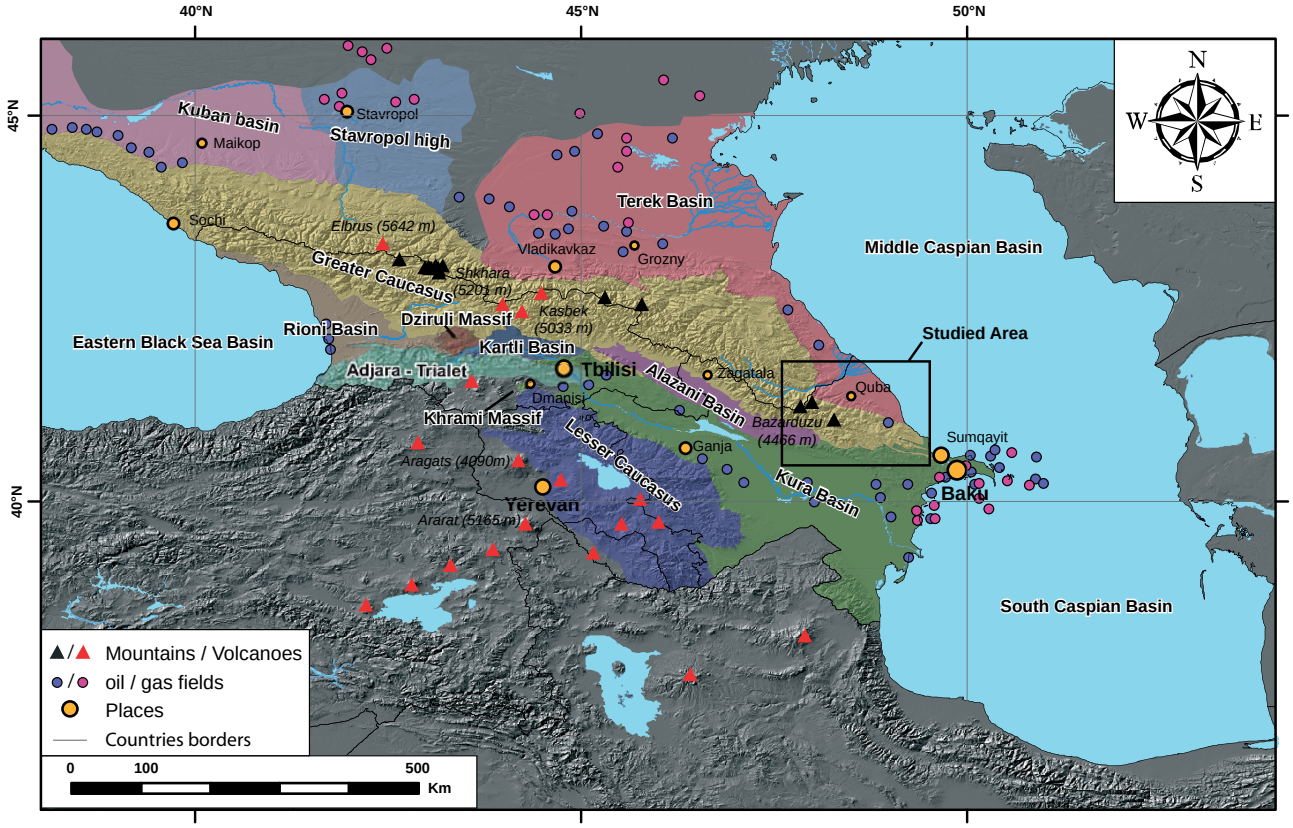

Figure 1: Tectonic units and sedimentary basins of the Greater Caucasus with main mountains, volcanoes and the main gas-oil fields.

Figure 2: The Kasbek strato volcano with its glaciers (Georgia, 2007).

Figure 3: Mud Volcanoes in Qobustan (Azerbaijan, 2004).

Figure 4: Oil fields Siyazan (Azerbaijan 2004).

Crossing the Central part of the EGC was the main goal for the 2009 expedition. The 2 weeks from the 9th to the 24th of August were perturbed by bad weather. Finally I reached to cross and to measure structural data in the valley going from Ruk Village to the summit of Babadag. Thus, I completed to the north the cross-section I did in 2004 on the southern side of this summit. I was accompanied by Dr. T. Kangarli and I. Mammadov during the fieldtrip.

1.4. Geomorphological features of the Caucasus

The main range of the Caucasus Mountains extends west to east for about 1200 km from the Taman Peninsula on the northern side of the Black Sea to the Abseron Peninsula on the Caspian Sea. The Caucasus itself is divided into two mountain systems: the Greater Caucasus and the Lesser Caucasus (fig. 1).

The Greater Caucasus itself is again divided in 2 geographical areas: the western part (Taman Peninsula – Kasbek) and the Eastern part (Kasbek – Abseron Peninsula). The division is located to the north of Tbilisi where the mountain belt is narrower (only 60 km wide) than the Eastern and Western parts (Bravard 1983).

The aim of this section is to define the geomorphological context of the mountain belt and to use the data in the next chapters to emphasize some links with the geodynamical context. As the themes of this section are not in my field of study, all the data come from literature. Whenever a paragraph is based on literature, authors are indicated at its beginning or at its end.

1.4.1. Summits and topography

The western Greater Caucasus is higher than the eastern one. It has several summits taller than 5000 m and in the eastern part no summits are higher than 4500 m. But the western northern slope goes down below 3000 m in less than 20 km and in the eastern part (Daghestan), it needs at least 40 km. In the east, summits stay at 2000 m almost until the mountain belt reaches the Terek plain (Bravard 1983).

The Elbrus Volcano (5642 m) is the highest summit of the Greater Caucasus, of Russia and of Europe (considering that the Caucasus crest located south of the Elbrus is the boundary between Eurasian and Arabian tectonic plates). Numerous summits above 5000 m are located in the area of the Elbrus: the Greater Caucasus second highest summit is the Dykh-Tau (5205 m) and just across the border, the highest summit of Georgia is the Shkhara Mountain (5201 m). North of Tbilisi, the Kasbek Volcano (5047 m) is also a major summit of Georgia. The Bazarduzu Mountain (4466 m) is the highest summit of Azerbaijan and is also the second most prominent[1] summit (2454 m) of the Greater Caucasus, just after the Elbrus (4741 m). The highest summit of the Lesser Caucasus and Armenia is the Aragats Volcano (4095 m). The Ararat volcano (5137 m) is the tallest peak of Turkey and is located just south of the Lesser Caucasus.

Table 1: Most elevated mountains of the Greater Caucasus with their elevation and prominence rank.

Elev. Rank	Prom. rank	Summit Name	Elevation	Prom.[1]
1	1	Elbrus (RU)	5642 m	4741 m
2	6	Dykh-Tau (RU)	5205 m	2002 m
3	11	Shkhara (RU/GE)	5201 m	1365 m
4	12	Koshtan-Tau (RU)	5152 m	822 m
5	16	Pushkin (RU/GE)	5100 m	110 m
6	14	Janga (Jangi-Tau) (RU/GE)	5059 m	300 m
7	3	Kasbek (GE)	5047 m	2353 m
8	15	Katyn-Tau (RU/GE)	4979 m	240 m
9	13	Tetnuld (GE)	4974 m	672 m
10	17	Shota Rustaveli (RU/GE)	4960 m	
11	4	Gora Tebulosmta (RU/GE)	4493 m	2145 m
12	2	Bazarduzu (AZ/RU)	4466 m	2454 m

1.4.2. Climate

This section is based on the works of Kotliakov & Krenke (1981) and Kurtubadze (2008).

Figure 5 shows the different climatic zones of the Caucasus. The main crest of the Greater Caucasus is a boundary between temperate and subtropical zones. (Kurtubadze 2008).

During the winter, the main crest stops the Eurasian continental polar air or the polar front depression. In the west, the mediterranean depressions reach the western Caucasus and are absorbed by the Black Sea. The Central and Eastern Caucasus climate is mostly influenced by the European and Iranian depression. At 2000 m along the main crest, the average temperature

1 In topography, the prominence of a peak is the height of the peak's summit above the lowest contour line encircling it and no higher summit. The prominence, also known as autonomous height, relative height, shoulder drop (in North America), or prime factor (in Europe), is a concept used in the categorization of hills and mountains, also known as peaks. It is a measure of the independent stature of a summit (Wikipedia).

is – 8°C. Small reliefs have a relatively high influence on the climate. (Kotliakov & Krenke 1981).

In summer, the Caucasus stays successively at the border of the Azov anticyclone that help to melt the snow and the ice or it stays in a field with a weak gradient that allow developing vertical convections with rain during the second part of the day. The temperature in summer decreases regularly with altitude: it passes from 20 to 25°C in the plain to 7-11°C at 2500 m. The 0°C isotherm stays at 3700 – 4000 m. The warmest month is July in the plain and August in the mountain. In Baku and in the Kura basin temperatures are frequently higher than 40°C. (Kotliakov & Krenke 1981).

The Central and Eastern Caucasus rainfalls reach their maxima during the summer and in the western part during the winter. In the southeast, the quantity of rain reaches 3 m/year. In the east and along the Caucasus axis, it does not rain more than 800 mm/year. Generally the southern slopes of the Greater Caucasus receive higher amounts of precipitation than the northern slopes. (Kotliakov & Krenke 1981).

1.4.3. Glaciers

This section is based on the works of Bedford & Berry (1994), Kotliakov & Touchinski (1974), Kotliakov & Krenke (1981), Milanovsky (2008), Rastvorova & Shcherbakova (1967), Shcherbakova (1973), Stokes et al. (2006) and Tzereteli (1974).

The glaciers cover an area of 1400 to 1805 km^2 in the Greater Caucasus (Bedford & Barry 1994). Kotliakov & Krenke (1981) inventory more than 2047 glaciers. In terms of morphology, hanging glaciers and glacial cirques are located mostly in the eastern and western part of the Caucasus whereas the biggest valley glaciers and glacial plateaus are mostly in the central part at altitudes between 4000 – 5000 m. Five glaciers have more than 40 km^2: Dikhsi, Bezengi, Tsanner, Lekhzur and Karaougoum glaciers. There are more glaciers on the northern slope than on the southern one, but glaciers are bigger on the southern slope. (Kotliakov & Krenke 1981; Kotliakov & Touchinski 1974; Rastvorova & Shcherbakova 1967; Shcherbakova 1973; Stokes et al. 2006; Tzereteli 1974).

During the Quaternary period, glaciations reached their maximum intensity in the highest, central part of the Greater Caucasus. The mountains in the eastern part of the Greater Caucasus are also high but the climate is dry and indications of glaciations are much more limited than in the central area. In the Lesser Caucasus and in the Armenian volcanic highlands ancient glaciations were insignificant and nowadays only small glaciers exist on the Great Ararat and on the Lesser Ararat. This is mainly due to the mountain altitudes that do not exceed 3000-4000 m (with exception of Mount Ararat) and to the arid local climate (Milanovsky 2008).

The glaciations started in the Late Pliocene in the Greater Caucasus. They can be divided in three main glacial and interglacial epochs, subdivided into phases and stages corresponding to the Early Pleistocene, the Middle Pleistocene and the Late Pleistocene-Holocene. The Quaternary glacial epoch's names are the Eltübü, Terek and Bezengi glaciations. Although the elevations of the Greater Caucasus are higher than those of the Alps, ancient and present glaciations are more important in the Alps. A peculiarity of the Greater Caucasus area is the close interaction between glacial and volcanic process. The alternation of glacial epochs and phases of volcanic activity led to the formation of a relatively hard volcanic "armor" that protected moraines from total denudation (i.e. deposits for a fourth probable Late Pliocene glaciation were preserved on the Elbrus volcanic massif). This correlation between glacial deposits and young volcanic rocks provides a unique opportunity to date glacial deposits (Milanovsky 2008).

In the studied area, the Eastern Greater Caucasus of Azerbaijan, glaciers are not present anymore. Only firns can be observed on the highest summits (Sahdag, Bazarduzu and Tufandag Mountains).

1.4.4.H ydrography

This section is based on the works of Bravard (1983), Caspers (1957), Giralt et al. (2003), Hoogendoorn et al. (2005), Mitchell & Westaway (1999) and Zenkevich (1957).

The main part of the hydrography of the Caucasus is linked with three hydrographic basins: the Caspian Sea, the Black Sea and the smaller Sea of Azov.

The Black Sea forms an almost isolated body of water. It is linked with the Mediterranean Sea through the Bosphorus strait, the Marmara Sea and the Dardanelles. The Black Sea has a surface area of 413'488 km^2 and its greatest length is 1149 km, the width 610 km. Its greatest depth is 2243m and the average depth 1197 m. The Black Sea has a positive water balance, which results in a net outflow of 300 km^3 of water per year through its link with the Aegean Sea (part of the Mediterranean Sea). Mediterranean water flows into the Black Sea as part of a 2-way hydrological exchange. The Black Sea outflow is cooler and less saline, and therefore floats over the warm, more saline Mediterranean inflow. The Black Sea also re-

Figure 5: Climate zones of the Caucasus area (KURTUBADZE 2008).

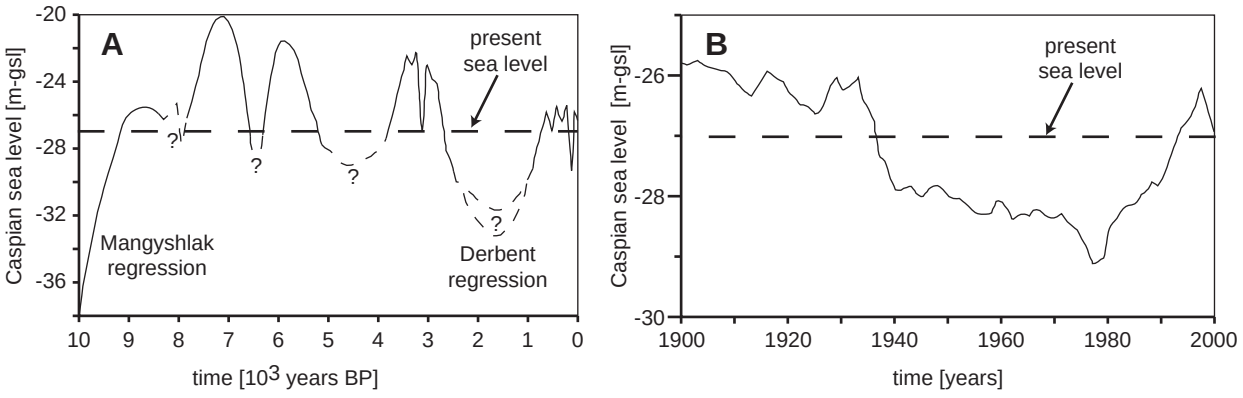

Figure 6: (A) Estimated Holocene sea-level fluctuation of the Caspian Sea (RYCHAGOV 1993a; RYCHAGOV 1993b; RYCHAGOV 1997) and (B) measured Caspian sea-level fluctuation, 1900 – 2000 AD (KLIGE & MYAGKOV 1992).

ceives river water from fluvial systems to the north of the Sea (Dnieper and Danube), from the Rioni River coming from the Caucasus and from the Sea of Azov. The Black Sea is the world's largest meromictic basin where the deep waters do not mix with the upper layers of water that receive oxygen from the atmosphere. As a result, over 90% of the deeper Black Sea volume is anoxic water (Caspers 1957).

The Sea of Azov is a shallow basin connected with the Black Sea by the Strait of Kerch. Its hydrography is controlled by the inflowing waters of the Don and the Kuban rivers. The Sea of Azov occupies a total area of 37'600 km^2. The greatest depth of the sea is 13.2 m, the average depth 7.2 m. The annual inflow of fresh water comes at 50.5 % from the Don River, 19.5% from the Kuban River and the rest from surface rainfall and groundwater. The average salinity is 1.12%. (Caspers 1957).

The Caspian Sea is the largest inland water body on the planet with its 1200 km long and 200 to 550 km wide. It is a closed reservoir of saline water (salinity of 1.2 to 1.25%). It is made up of three sub-basins (north, central and south) with an average water depth of 210 m, a maximum depth of 1024 m, an estimated surface area of about 374'000 km^2. About two-thirds of the water volume belongs to the southern part. The main water outputs of the Caspian Sea are related to evaporation (380 km^3 per year). The water inputs to the Caspian Sea are represented by river inflows (80% of the total water input), by precipitation (between 11 and 18%) and by groundwater (between 2 and 9%). The main river inflow is given by the Volga River (82%), the Ural River (3%). The other major contributor are the western rivers (Kuma, Terek, Sulak, Samur and Kura rivers) which collectively make up 11.5% of the total input, the Iranian rivers to the south that provide 3.5% of the total input and finally the Emba River in west Kazakhstan. The terraces along the coast show the variation of the sea level. The present-day water level of the Caspian Sea is situated at -27.5 m.a.s.l (fig. 6B). The lowest documented sea level is estimated at 50 m below global sea level at the end of the Pleistocene or early Holocene (Mangyshlak regression) (fig. 6A). The Derbent regression, around 1500 BP, reached a minimum of at least -32 m (fig. 6A). The Caspian Sea reaches its greater extend during the Late Akchagyl transgression 1.2 Myr ago and several other transgressions occur during the Abseron and Baku stages. During the peak of the most recent Khvalyn transgression at ~15-12 kyr, the Caspian sea reached 47 m above mean sea level (75 m above its present level) allowing it to overflow into the Black Sea via the Manych palaeo-strait. (Giralt et al. 2003; Hoogendoorn et al. 2005; Mitchell & Westaway 1999; Zenkevich 1957).

The Northern slope of the Greater Caucasus is divided by two main river systems: the Kuban River system flowing into the Azov Sea and the Terek River flowing in the Caspian Sea. The Kuban River flows 870 km from its spring near the Elbrus to the Sea of Azov. The Terek River starts flowing in the southwest of Mount Kasbek and reaches the Caspian Sea after 623 km. In the east several smaller systems drain the Caucasus: Sulak, Samur, Qusarcay, Qudiyalcay, Qaracay, Valvalacay rivers. The Kuban, Terek and Sulak rivers have their upper part perpendicular to the main axis of the Greater Caucasus and they become parallel only when they reach the steppes. The Samur River system has the particularity to flow almost parallel to the main axis since its upper part (Bravard 1983).

The southern slope of the Greater Caucasus and the Northern slope of the Lesser Caucasus are drained by the Kura River system that flows into the Caspian Sea and the Rioni River system that flows into the Black Sea. The Kura River is the largest watercourse in the southern Caucasus; its total length is 1515 km. It originates in the springs located 2720 m above sea level on the northeast slopes of Kizil-Giadik (Turkey). It then flows through the territory of Georgia and the lower reaches of the river are in Azerbaijan where it flows through the Kura Basin into the Caspian Sea. In the Kura Basin the Kura River merges with it major tributary, the Arak River. The Arak River drains the Eastern Lesser Caucasus (Hoogendoorn et al. 2005).

1.4.5. Hominid records of Dmanisi (Georgia) and Caucasus

This section is based on the works of de Lumley & Lordkipanidze (2006) and Ljubin & Bosinski (1995).

Excavations carried out since 1991 at the open-air site of Dmanisi, Georgia, have yielded four craniums, three mandibles, about 15 postcranial remains and a dozen isolated teeth. These remains correspond to at least four individuals, two adults and two adolescents. They were excavated from a precise stratigraphic, palaeontological and archaeological context above a basalt flow dated by K/Ar between 1.8 and 1.9 ± 0.01 Myr in a volcanic ash layer dated by 40Ar/39Ar to 1.80 ± 0.05 Myr. The interest of these discoveries is fourfold: (1) the dates obtained by diverse radiochronometric methods and by palaeomagnetism demonstrate, for the first time, that Man was present at the gates of Europe, in Transcaucasia at a much earlier period than that established by the classical scenario; (2) faunal and pollens analyses have revealed that the environment was close to a savannah type, but much richer in water resources than the African environment. It was a temperate climate, with a mosaic of different landscapes due to the geomorphological

diversity of the region, made up of valleys, lakes and the nearby mountains of the Greater and Lesser Caucasus; (3) the settlement of this human group could have been a direct consequence of a more humid environment, which followed a generalised aridification of the east of Georgia at the end of the Pliocene and which attracted fauna from both the east of the Eurasian continent and the north of the African continent; (4) the morphofunctional aspects of these humans are close to those of *Homo habilis* and to those of the most archaic *Homo erectus*, which were the only species known in Africa up until now. Ascribed to a new species, *Homo georgicus*, small in size measuring 1.5 m with a cranial capacity of 600 to 700 cm^3 (half of modern man's capacity), they represent the ancestors of a long European or Eurasian lineage. Two new concepts can be retained: (1) the exodus from Africa took place earlier than previously thought, dating back to at least 1.8 Myr ago. It was carried out by *Homo georgicus*, a group close to *Homo habilis*; (2) it is no longer valid to base explanations of Man's migratory capacity in terms of cranial development. *Homo georgicus*, with a small brain volume, already had the faculty to adapt to a more favourable environment for his survival (de Lumley & Lordkipanidze 2006).

Following the Dmanisi records, there is no clear evidence of hominid in this region until the Middle Pleistocene, a fact that may indicate an absence of relevant deposits, lack of fieldwork, or genuine absence. In the Middle Pleistocene, several caves were formed that were subsequently used for denning by cave bear and occasionally by hominids. Examples are Azyk in Azerbaijan, the caves of Kudaro I, II, and Tcona in Georgia and Treugol'naya in southern Russia. All except Treugol'naya have Acheulean assemblages containing some hand axes and few cleavers. Layer 7 at Treugol'naya has been dated by TL to 583 +- 25 kyr; the basal assemblage from Azyk may be slightly older, and the other caves rather young (Ljubin & Bosinski 1995).

1.5. Geology of the Greater Caucasus and its surrounding areas

The Greater Caucasus belt forms a morphological barrier along the southern margin of the Scythian Platform, running from the northern margin of the Eastern Black Sea Basin to the South Caspian Basin. It developed during several phases of deformation in Mesozoic-Cenozoic times (Brunet et al. 2009a; Brunet et al. 2003; Ershov et al. 2003; Ershov et al. 2005; Jackson et al. 2002; Kazmin & Tikhonova 2006; Khain 1975; Khain 1997; Kopp & Shcherba 1985; Saintot et al. 2006a). It is located within the active convergence zone between the Arabian and Eurasian plates. Based on the study of McClusky et al. (2000) and Vincent et al. (2007), the partitioning of Arabian – Eurasian plate convergence is divided between right-lateral strike-slip faulting on NW-SE striking faults in eastern Turkey and thrusting along the Caucasus thrust front. Total shortening across the Lesser and Greater Caucasus is 10 ± 2 mm/yr, with almost 60% of this shortening occurring across the Greater Caucasus (McClusky et al. 2000).

Several Foreland basins and tectonic units are located around the Greater Caucasus orogen (figs. 1 and 8). In the north, the western Indol – Kuban foredeep and the eastern Terek-Caspian foredeep are deep molasse basins. These foredeeps are filled with thick Oligocene to Quaternary molasse, the depth of the Pre-Mesozoic basement reaching 10 to 12 km. They are separated by the Stavropol High where the basement lies at the highest level (up to 1-2 km below the surface). In the southeast, the deep Kura intermontane trough separates the Greater Caucasus from the Lesser Caucasus. It is filled by Oligocene-Quaternary molasse reaching a thickness of 8 to 10 km and the Pre-Alpine basement has subsided in places to 10 to 12 km. Finally in the southwest, the basement plunges deep under the molasse filling of the Rioni intermontane deep. The western Rioni and the eastern Kura molasse basins are bound southward by the Lesser Caucasus Mountains, eastward by the Caspian Sea and westward by the Black Sea (Adamia et al. 2010; Brunet et al. 2003; Khain 1975). The geodynamics of all the area is influenced by super deep sedimentary basins: the Black Sea basins and the South Caspian Basin. Based on geophysical data, an oceanic crust with a depth reaching 25 km forms the basement of the South Caspian (Green et al. 2009). It is a remnant of the eastern part of the Mesozoic Great Caucasus Basin corresponding to a back-arc basin with a rifting phase starting at the Lower-Middle Jurassic (Brunet et al. 2009a; Brunet et al. 2003). In the west, the Black sea is divided into a western oceanic part and an eastern part that is floored by highly thinned continental to oceanic crust. The Andrusov-Archangelsky ridge (or mid-Black Sea ridge) divides them. Black Sea basins are interpreted as a Late Cretaceous to Eocene back-arc extensional features (Nikishin et al. 2001).

Structurally the Greater Caucasus is the deformed southern margin of the Late Paleozoic Scythian Platform (Ershov et al. 2003). The present structure of the Greater Caucasus exposes its Paleozoic basement in dominantly southward-directed thrust slices only west of longitude 44°E (fig. 7). The Jurassic and Cretaceous series are present in tight or isoclinal folds associated with thrusts across the range around the exposed Paleozoic core. The vergence of folds is predominantly

towards the south. Plio-Quaternary strata are folded into elongated, linear south vergent anticlines on the southern side of the range (between the Kura and Rioni basins). However there are north directed structures on the northern margin, especially in the northeast (Dagestan). The Moho under the range is at a depth of up to 60 km (Allen et al. 2003; Ershov et al. 1999; Ershov et al. 2003; Ershov et al. 2005). The Caucasus orogeny itself started in late Eocene times (Barrier et al. 2008a; Barrier et al. 2008b). The Pontides - Black Sea – Caucasus – South Caspian area was affected by increasingly intense compressional tectonics.

The investigated area covers the eastern part of the Greater Caucasus: the Eastern Greater Caucasus (EGC). It corresponds to the Azerbaijan part of the mountain belt. It is mostly composed of Mesozoic and Cenozoic sediments. It contains remnants of a sedimentary basin, the Greater Caucasus Trough, and, on its slopes, the erosional products of the tertiary orogeny. From a structural point of view, this area is marked by an important uplift of the central part creating remarkable thrusts to the north and to the south. It is also affected by NNE-SSW right-lateral strike-slip fault and a NNE-SSW sinistral strike-slip fault. They are highlighted by the drainage pattern of major rivers but also by mountain crests direction.

1.5.1. Earthquakes

The Greater and Lesser Caucasus are seismically active zones linked to the rapid and non-uniform plate convergence between Arabia and Eurasia (Allen et al. 2004; Allen et al. 2006; Jackson 1992; Jackson et al. 2002; Philip et al. 1989; Priestley et al. 1994; Triep et al. 1995). The Lesser Caucasus and the adjoining Anatolian Plateau show a predominance of strike-slip focal mechanisms associated with a system of vertical faults. In the Greater Caucasus, on the contrary, convergence is accommodated predominantly by reverse focal mechanisms associated to thrusting with a general N-S to NE-SW compression (Barazangi et al. 2006; Copley & Jackson 2006; Koçyigit et al. 2001; Tan & Taymaz 2006), see also discussion in Allen et al. (2004) and Jackson (1992). Slip vectors based on earthquake focal mechanisms show a general top to the south thrusting. Strike-slip mechanisms exist but are rare. Present seismicity is unevenly distributed across the GC (fig. 8). A zone with a higher seismic activity is observed on the south slope of the Greater Caucasus west of Tbilisi (Georgia) in the Racha area (Triep et al. 1995). Studies of focal mechanisms and focal depths show that this seismicity is linked to several active fault strings in the subsurface of the Gagra-Dzhava zone (Gamkrelidze & Kuloshvili 1998; Triep et al. 1995). They show south directed slip vectors.

Seismicity is extending into the Middle and South Caspian Sea (Kovachev et al. 2006). In the Abseron zone focal mechanisms show NNE-SSW oriented thrusting (Jackson et al. 2002) and seismic activity may be linked with an extension/termination of the Greater Caucasus towards the east and/or with young north-directed subduction of the South Caspian Basin to the north under the Abseron (Allen et al. 2002; Knapp et al. 2004). The seismicity further south as well as in the Qobustan desert area shows a westward component of motion relative to Eurasia, suggesting underthrusting towards the west (Jackson et al. 2002).

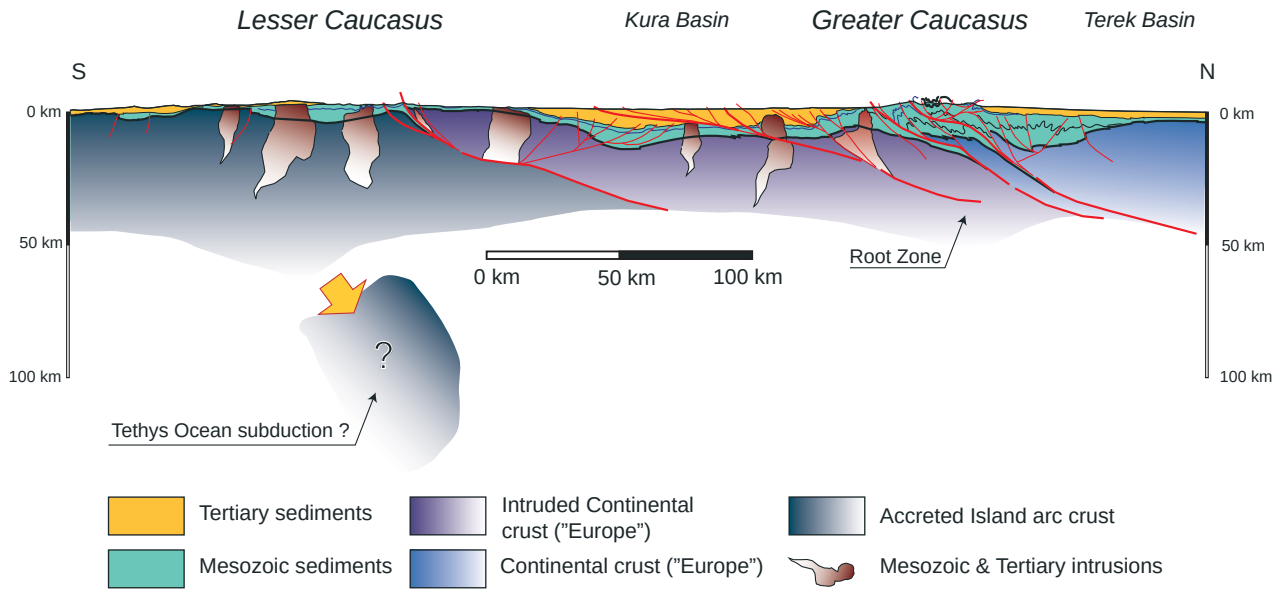

Figure 7: Simplified cross section of the eastern part of the Caucasus.

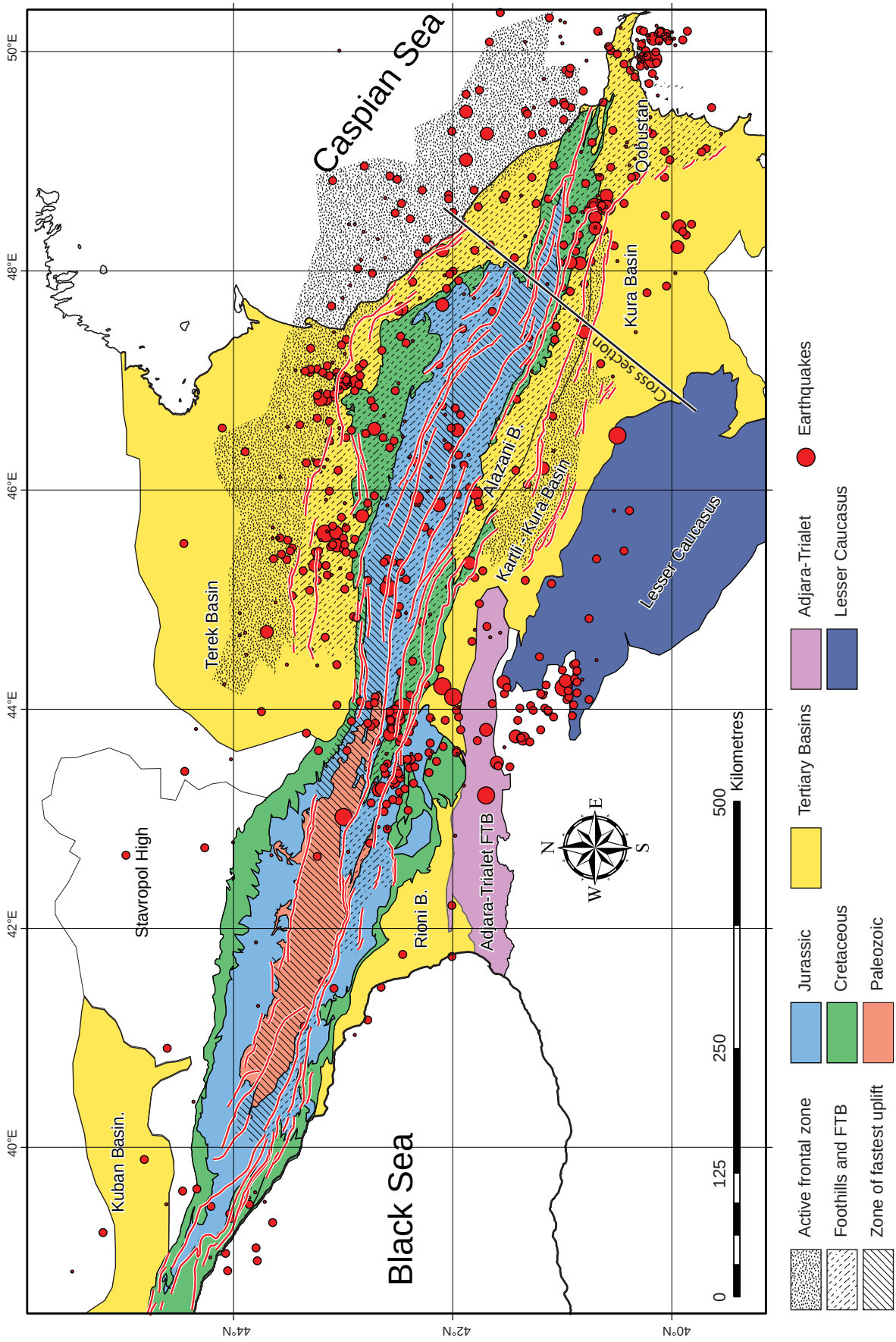

Figure 8: Simplified geological and structural map of the Greater Caucasus with the major earthquakes. Cross-section corresponds to figure 7.

Some seismic activity is also seen in the central part of the Eastern Greater Caucasus, as well as in the Kura basin. On the northern slopes, the Dagestan FTB and the recent faults in the Terek Basin show a higher concentration of earthquakes pointing to active thrust tectonics in this area.

Studies on palaeoseismology remain rare but confirm the existence of inherited faults and the possible 2000 years recurrence of high magnitude events (Rogozin & Ovsyuchenko 2005; Rogozin et al. 2002).

1.5.2. Uplift and shortening

Ershov (2005) and Philip et al. (1989) locate the main surface uplift in the central part of the mountain range and they date it of Middle Neogene age (fig 9A and 9B). Marine sediments (Budagov 1963), old marine terraces (Krasnov 1974; Mitchell & Westaway 1999; Popov et al. 2004) (fig. 9C), geomorphological (Rastvorova & Shcherbakova 1967), and thermochronological studies (Kral & Gurbanov 1996) suggest an average surface uplift rate of minimum 0.33 mm/yr to 1 mm/yr for the last 10 Myr, but Rastvorova (1967) suggested that it reaches 10 mm/yr since the last glaciations. This last assumption is mainly based on river incision and the relationship between incision and surface uplift could not be considered simple and a detailed analysis of the topography has to be done (Mitchell & Westaway 1999).

Total shortening across the Greater Caucasus is uncertain, with estimates reported in the range 5-60 km (Dotduyev 1986; Gamkrelidze & Gamkrelidze 1977). Triep et al. (1995) point out that a minimum of 33 km of shortening is needed to account for present-day relief assuming Airy isostasy. The onset of convergence in the Greater Caucasus is estimated at 2.5 Myr by Burtman (1989), although shortening may have begun as early as 5 Myr (Triep et al. 1995). Using this range of parameters (33-60 km shortening in 2.5 to 5 Myr) gives an average shortening rate in the range 7-24 mm/yr. In contrast, Westaway (1990) re-examined neotectonic information and concluded that overall shortening rates across the Greater Caucasus are likely no greater than ~5 mm/yr and that most of the convergence between Arabia and Eurasia is taken up to the south in eastern Turkey and northwestern Iran. Assuming uniform deformation rates, the GPS estimate of present-day shortening made by McClusky (2000) across the Greater Caucasus (5-6 +/- 2 mm/yr) supports Westaway (1990) analysis. According to Kadirov et al. (2008), the Eastern Greater Caucasus undergoes, in the east, a convergence rate of 10 +/- 1 mm (48° E longitude) and in the west 4 +/- 1 mm (46°E longitude).

1.5.3. Volcanoes and magmatism

The Neogene-Quaternary volcanism is limited to three areas area in the Greater Caucasus: the Kasbek area (fig. 2), the Central Georgia area and the Elbrus area (Lebedev et al. 2006). This neo-volcanism is represented by major stratovolcanoes like the Elbrus Mt. (5642 m) or the Kasbek Mt. (5047 m).

The young magmatism has involved the formation of basalt flows, stratovolcanoes and hypabyssal intrusions which have become unroofed by rapid erosion. The stratovolcanoes form a northward prolongation of a chain of similar edifices in eastern Turkey. Aragats Mt. has erupted mainly basalts, basaltic andesites and dacites, whereas Elbrus has produced mainly dacites and rhyolites. Some studies have suggested that the volcanism has been caused by subduction of an ocean basin which formerly linked the Black and Caspian Seas, by the delamination of the lower part of the thickened mantle lithosphere or by the heating of the Lower continental crust or mantle lithosphere which accompanies crustal thickening (Mitchell & Westaway 1999).

The magmatism of the Greater Caucasus that created the present volcanoes was concentrated around 2.8 Myr. Young volcanism persists for ~250 km along the western Greater Caucasus from Elbrus to Kasbek. Kasbek is considered no longer active but some eruptions of Elbrus post-date the last glaciation and fumaroles near its summit emit a vapour plume (Mitchell & Westaway 1999).

In the Lesser Caucasus, the Aragats and Ararat volcanoes are considered inactive and both are covered by an icecap. East and north of Aragats Mt., other volcanoes form the Gegham plateau and the Javakhet plateau (Mitchell & Westaway 1999).

More details about the magmatism history are in Lebedev (2006).

1.5.4. Mud Volcanoes

Azerbaijan and the South Caspian Sea are known for their hydrocarbon fields, and represent the region with the highest abundance of continental and offshore mud volcanoes (Yakubov et al. 1971). More than 400 active mud volcanoes are present in this region, both onshore and offshore (Aliyev et al. 2002; Aliyev et al. 2009; Yakubov et al. 1971). Their size is variable (heights up to 600 m and surfaces up to 10 km^2) (fig. 3).

Their presence in the South Caspian region is mainly due to three factors: (1) rapid quaternary infill of one of the world deepest sedimentary ba-

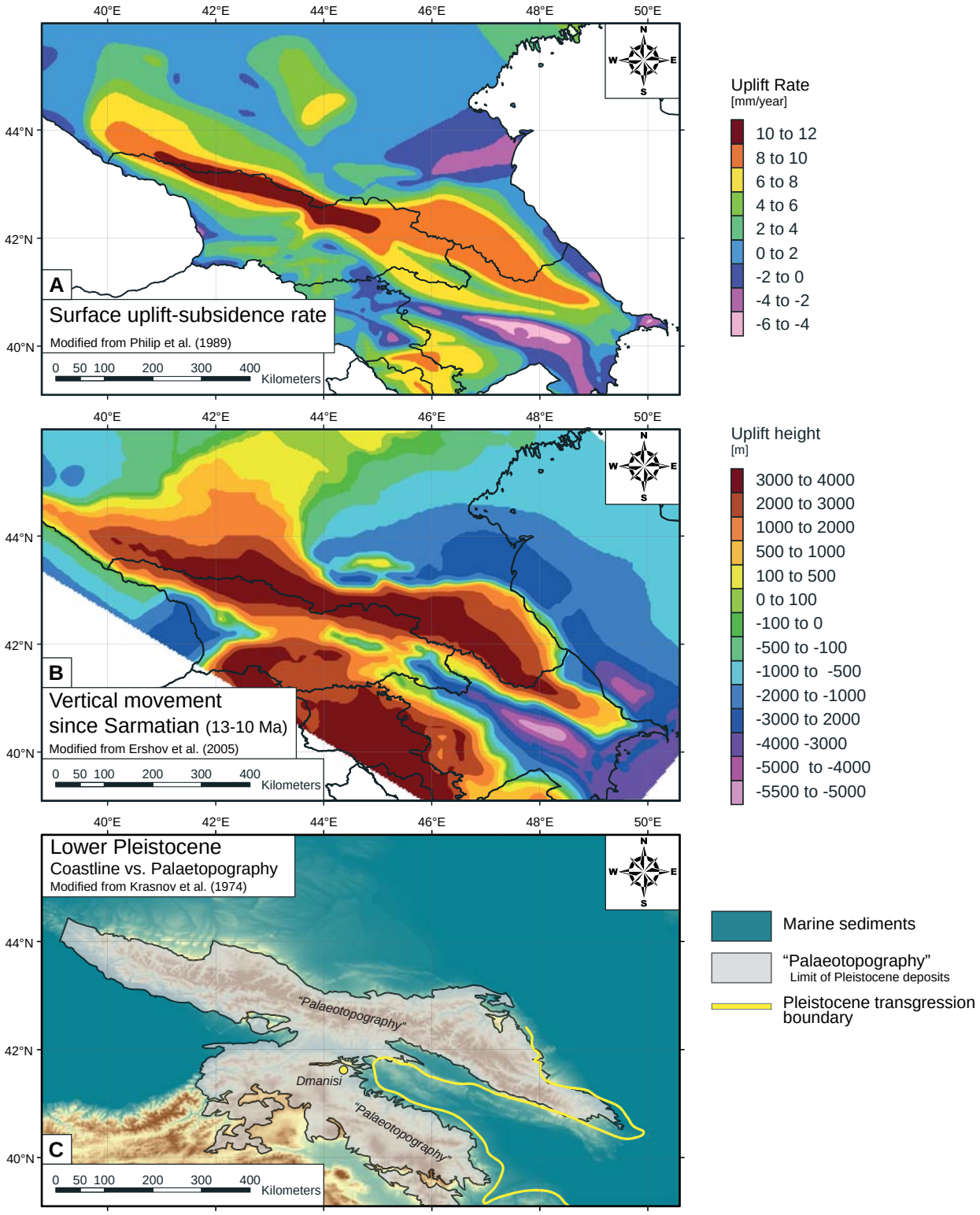

Figure 9: Maps of surface uplift rates, vertical movement, and Lower Pleistocene coastlines. (A) Uplift-subsidence rates: highest rates of 10-12 mm/year are found in the central part of the western Greater Caucasus (PHILIP et al. 1989). High subsidence is occurring in the Kura Basin; (B) Total vertical movement since Sarmatian (10-13 Myr). Strong subsidence is seen north and south of the eastern termination of the Greater Caucasus in Azerbaijan (ERSHOV et al. 2005); (C) Lower Pleistocene coastline – map of coastline (KRASNOV et al. 1974) which separates the area of the former marine domain and zone above sea-level with Pleistocene deposits, and area with unknown amount of palaeotopography. Notice the position of Dmanisi (Georgia) where hominid remnants dated back to 1.8 Myr have been discovered.

sin (up to 2.4 km/Myr); (2) diffuse methane generation in deeply buried clay units; and (3) compressional tectonics leading to anticline traps, and frequent seismicity that possibly triggers eruptions (Guliev & Panahi 2004; Inan & Yalçin 1997; Mellors et al. 2007; Nadirov et al. 1997). In this thick and under-compacted basin, hydrocarbon generation and maturation is still ongoing, particularly in the deeply buried (8.5 – 11km) Maykop Formation (Fowler et al. 2000). The main driving engine of the eruption is over pressured methane rising from source rocks and reservoirs at greater depth. A suggested scenario summarizing the birth of a mud volcanoes and the eruption mechanisms envisages that when the subsurface overpressure reaches a threshold depth where the overburden weight is exceeded, fracturing and breaching of the uppermost units occurs, sometimes facilitated by external factors (e.g. earthquakes) (Mazzini 2009). Jakubov et al. (1971) documented the intimated relationship between mud volcanoes, petroleum reservoirs, and structural traps (e.g. anticline). The feeder channels for the mud volcanoes, normally rooted below the reservoir levels (commonly at 1-3 km depth), act as a pathways for fluids during the eruptions and possibly during the dormant stage (Planke et al. 2003).

The intimate association of petroleum reservoirs and mud volcanoes in sedimentary basins make such structures interesting for hydrocarbon exploration. However mud volcanoes may also pose a geohazard for drilling and platform construction due to the potentially violent release of large amounts of hydrocarbons and mud breccias.

The seeping methane from mud volcanoes to the atmosphere can have an impact on the carbon cycle and, for Azerbaijan; it has been estimated to contribute more than 300'000 to 900'000 tons/yr to the atmosphere (Etiope et al. 2004). It is significant enough to consider it has a major source in the greenhouse-gas inventories.

1.5.5. Oil and gas field

The Abseron peninsula is famous since the Antiquity for its black pools of oil and its eternal fire. It is a major place for the Zoroastrian religion, one of the oldest religions where the fire has a major place. Many people like the Arabian explorer Al-Massoudi, Marco Polo or Alexandre Dumas praised the quantity, the medicinal effect or the quality of the oil of this region (Hoesli 2006).

The discovery of the Kerosene in 1854 by a Canadian chemist and the invention of the oil lamp increased the need for oil. Since this time, local and foreign people started to extract the petroleum : the Armenian Mirzoev, the Azeris Manatchev, Mirzabek, Moukhtarov, Naguiev and Taguiev, the Germans Liebig and Siemens (in Georgia), the Nobel family, the Rothschilds, the chemist Dimitri Mendeleev that liberated the Caucasus oil market from the heavy state taxes and concession system (Hoesli 2006).

In 1875, Robert Nobel came to Baku to find wood for weapons but eventually bought a concession and, helped by his brother Ludvig, he started to build the biggest Russian company, the Branobel. They built pipelines, tankers, tank-cars and many other tools for the oil

Country	Proved reserve of oil		Proved reserve of gas	
	[Billion Barrels]	% of World Reserve	[Billion m^3]	% of World Reserve
Armenia	-	-	-	-
Azerbaijan	7	0.52%	849.51	0.48%
Georgia	0.035	0.0026%	8.50	0.00%
Kazakhstan	30	2.24%	2406.93	1.36%
Kyrgyzstan	0.04	0.0030%	5.66	0.00%
Russia	60	4.47%	47572.30	26.86%
Chechnya [RU]	*0.0135(?)*	*0.0010% (?)*	-	-
Dagestan [RU]	*0.25 (?)*	*0.0186% (?)*	*100 (?)*	*0.056%*
Adygea [RU]	*0.56 (?)*	*0.041% (?)*	-	-
North Ossetia[RU]	*0.25 (?)*	*0.018% (?)*	-	-
Ingushetia [RU]	*0.078 (?)*	*0.006% (?)*	-	-
Kabardino-Balkaria [RU]	0.23(?)	0.017% *(?)*	-	-
Tajikistan	0.012	0.0009%	5.66	0.00%
Turkmenistan	0.6	0.0447%	2661.78	1.50%
Uzbekistan	0.594	0.0443%	1840.60	1.04%
Iran	136.15	10.1437%	28078.99	15.85%
Saudi Arabia	266.71	19.87%	7319.06	4.13%
World	1342.20732	100.00%	177103.87	100.00%

Table 2: Proven reserves of oil and gas in 2009 of the Caucasus countries and regions compared with the main world reserves (source: Energy Information Administration). (?) indicate data based on unreliable sources. Saudi Arabia and Iran own respectively the main world oil and gas reserve and Azerbaijan own the main Caucasus oil and gas reserve.

industry. To finance this empire, they first used the fund of Ludvig and of some Russian officers and finally they asked help to their brother, Alfred famous for the invention of the dynamite and a rich and famous financier in Europe. The Branobel was the world's first oil company in 1900. The company was nationalized in 1920 by the soviets and finally closed in 1959 (HOESLI 2006).

The main producer of oil and gas in the Greater Caucasus is Azerbaijan. The country has proven oil reserves of 7 x 10^9 barrels and gas reserves of 849.51 x 10^9 m^3.

The Abseron region is not the only area in the Caucasus to produce oil. In Azerbaijan, there are oil fields also in the Kura Basin and in Siyazan (fig. 4). In Russia, Grozny is also famous for its oil fountains and it is also a major refinery place. Maykop in the Kuban basin is also a main oil region in the western part of the Caucasus at the beginning of the XX^e century. Georgia has also some oil fields near Tbilisi, in the Khakheti region (east) and along the Black Sea Coast (west). Main reserves of oil and gas are listed in table 2.

At the beginning of the XXth century, Baku was the world first oil producer. In 1900, Russia produced 66.7 millions of barrels coming mostly from the Caucasus regions and representing 51.6% of the world production..

*****

2 - Geomorphology and Geology of the Eastern Greater Caucasus of Azerbaijan

2.1. Introduction

This chapter gives an overview of the geographical, paleogeographical, structural and lithostratigraphical settings of the Eastern Greater Caucasus (EGC). It is based on bibliographical work and is completed by observations made during fieldwork between 2004 and 2010.

2.2. Geographic and geomorphological setting

The EGC is located in the north of Azerbaijan. It corresponds to the eastern termination of the Greater Caucasus. It extends from the border with Georgia and runs along the border with Russia and finish near Baku, the Capital of Azerbaijan[1].

The highest summits (fig. 11) are the Bazarduzu Mt. (4466 m), the Sahdag Mt. (4243 m), and the Tufan Mt. (4191 m). They are all located in the central area of the mountain range near the border with Dagestan (Russia). Other summits like the Qizilqaya Mt., the Babadag Mt., the Qovdag Mt., Kelevu Mt. and many other are frequently cited in the geological literature because of the presence of significant outcrops.

The EGC is drained mainly by high energy rivers (fig. 11) flowing in straight and V shaped valleys. Only in the surroundings of the EGC, rivers change to an anastomosing form (i.e. Samur River in the north) or even to a meandering form (i.e. Kura River in the south).

Numerous fluvial terraces can be found in the central part, some of them resulting of temporary lakes due to landslides.

Glaciers are not present anymore in the EGC only firns can be found in places like the Bazarduzu Mt., the Sahdag Mt. and Tufan Mt. Remnants of glaciation like moraines and U shaped valley can be seen in the same area but are difficult to distinguish due to the high erodability of the rocks and also to the presence of numerous fluvial terraces.

2.2.1. Topographic setting

The studied area contains the highest summits of Azerbaijan: Bazarduzu (4466 m), Sahdag (4243 m), Tufandag (4191 m) and several other summits over 3500 m.

The northern foothills of the EGC have a delta shaped morphology incised by rivers coming from the main range. Rivers dig large valleys with a direction rotating from NE to NNE going eastward. The main valley is formed by the Samur River and some summits on its northern bank reach 1500 m (i.e. Keleg Mt. at 1535 m).

An impressive limestone cliff forming the Sahdag Mt. (4243 m) and the Qizilqaya Massif (3726 m) characterizes the northern flank of the EGC range. This natural barrier is incised by deep canyons and valleys with a NNE direction. This limestone barrier could be discerned along the northern flank until the Caspian Sea (i.e. Tangaalti canyon, Cirax castle and Besbarmaq Mt.). Some remnants of glacial morphology can be observed, such as old moraines or U-shaped valleys (near the top of Qizilqaya Mt. and on the Sahdag Mt. intermediate plain).

A flat alluvial plain, the Sahnabad plain, separates the Sahdag Mt. from the highest ridge of the central

1 To help understanding of geology, the place names, when possible, are based on the National Geospatial-Intelligence Agency (United States) place names database (http://earth-info.nga.mil/gns/html/cntry_files.html). One of the main difficulties is often to place an outcrop when, in the bibliography there are at least three spelling for one place (the Azeri, the Russian and the translated name).

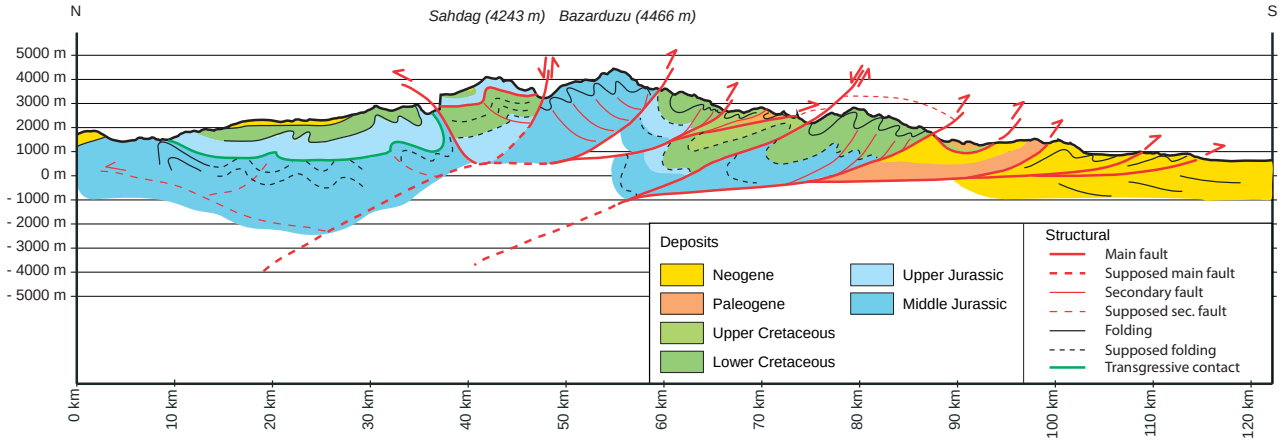

Figure 10: Synthetic tectonic cross-section of the Eastern Greater Caucasus of Azerbaijan. Adapted from KANGARLI (1982) and ERSHOV et al. (2003).

EGC (i.e. Bazarduzu Mt. and the Tufandag Mt.). Its height decreases going to the southeast. Numerous terraces can be observed along valley slopes. The central part is characterized by very steep slopes and numerous deep V-shaped valleys. Main valleys have generally a NNE direction but along the southern slope of the Sahdag Mt. and Qizilqaya Massif, they flow eastward.

The southern slope of the main range is divided in several parts. The first and highest range (i.e. Babadag Mt. at 3629 m) has some major limestone cliffs with also V-shaped valleys. From Babadag Mt. to the southeast, this ridge becomes the highest and corresponds to the watershed. To the south, after the depression formed by the upper part of the Girdimancay River valley, a second ridge reaches 2437 m (Qovdag Mt.) with gentle slopes and broader valleys. A last ridge reaching altitudes of 2322 m forms the last topographic ridge before the southern foothills.

The southern foothills are morphologically different from their northern equivalent; they are composed of several flat sedimentary basins separated by hills. Along the Girdimancay valley, three different basins can be distinguished: the east end of Alazani basin, a small basin north of the Qaramaryam hill and finally the deep Kura basin. Several small deltas are located on the northern border of these basins.

2.2.2. Climatic setting

In terms of climatic regime, the central EGC range undergoes a cold moderate mountain climate. In the EGC (contrary to the western part), southern flank is more arid than the northern one. The main mountain range is characterized by a mean annual precipitation between 500-2000 mm, a mean annual temperature smaller than 10°C and the flow regime is mostly perennial dominated by rainfall or snowmelt. Mudflows, landslides and heavy rains occur frequently and they isolate mountain villages by destroying roads sometimes during weeks. Based on field observation and inhabitants' indications, snowfalls occur throughout the year in the central part of the EGC and in winter the snow cover can reach several meters in the EGC.

During fieldtrips, temperatures of more than 50°C were observed in August in the Kura Basin and temperatures of more than 40°C in Baku.

For this study, the climatic regime of the main mountain range can be considered symmetric along the mountain range axis for precipitations and temperatures as shown in figure 12.

2.2.3. Hydrographic setting

In terms of hydrology, the main base level of the EGC area is the Caspian Sea. Several rivers drain the Eastern Greater Caucasus. The Caspian sea is characterized by major level changes. The present-day water level of the Caspian Sea is situated at 27.5 m below the water level of Baltic Sea. The lowest documented sea level is estimated at 50 m below global sea level at the end of the Pleistocene or early Holocene (Mangyshlak regression). The Derbent regression, around 1500 BP, reached a minimum of at least -32 m. The Caspian Sea reaches its greatest extent during the Late Akchagyl transgression 1.2 Myr ago and several other transgressions occur during the Abseron and Baku stages. During the peak of the most recent Khvalyn transgression at ~15-12 kyr, the Caspian sea reached 47 m above mean sea level (75m above its present level) allowing it to overflow into the Black Sea via the Manych palaeo-strait. (GIRALT et al. 2003; HOOGENDOORN et al. 2005; MITCHELL & WESTAWAY 1999; ZENKEVICH 1957). The determination of these quaternary sea level variations is mostly based on the studies of the impressive terraces along the sea shore.

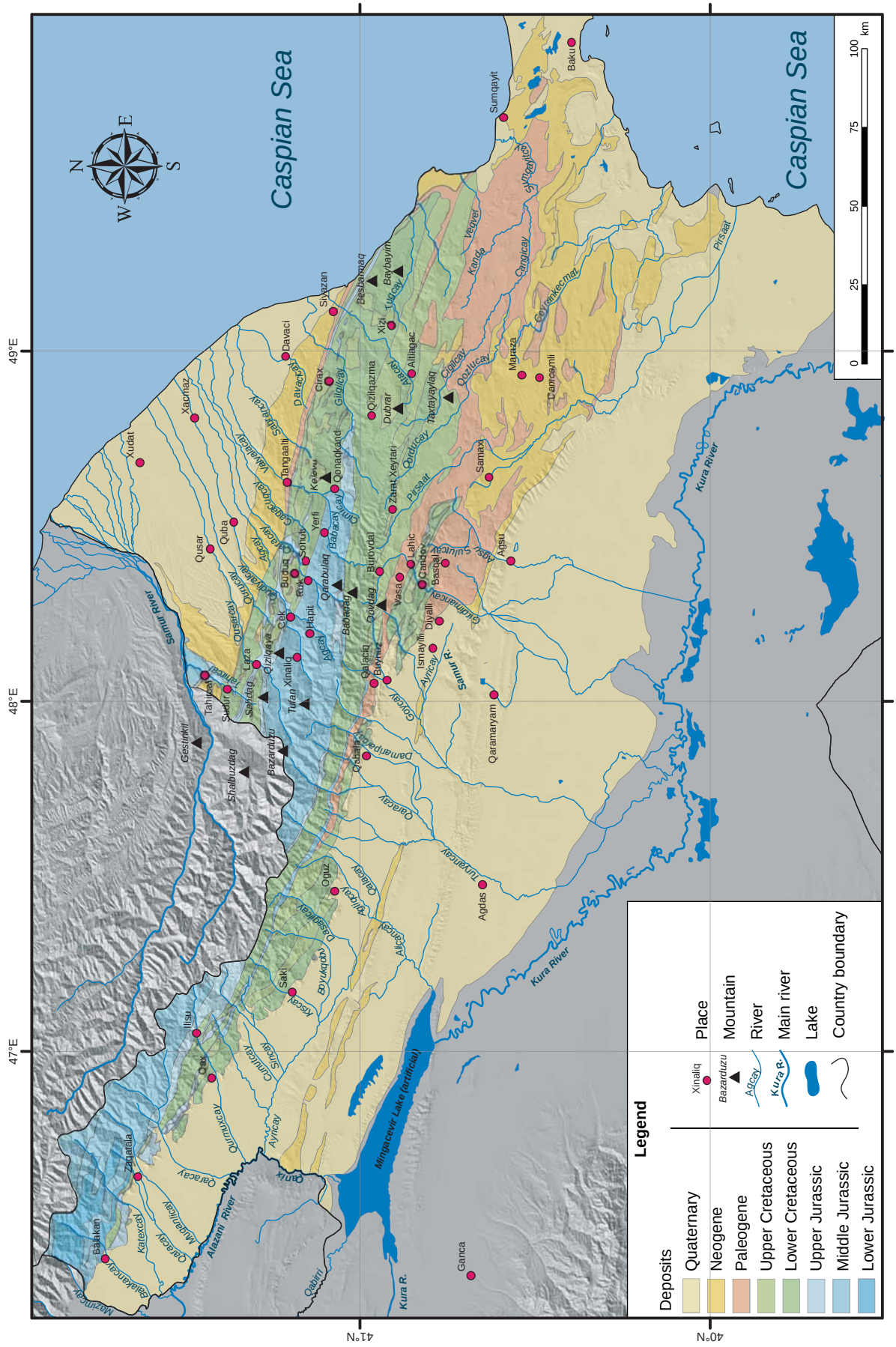

Figure 11: Simplified geological map of the Eastern Greater Caucasus of Azerbaijan with the main rivers, summits and places.

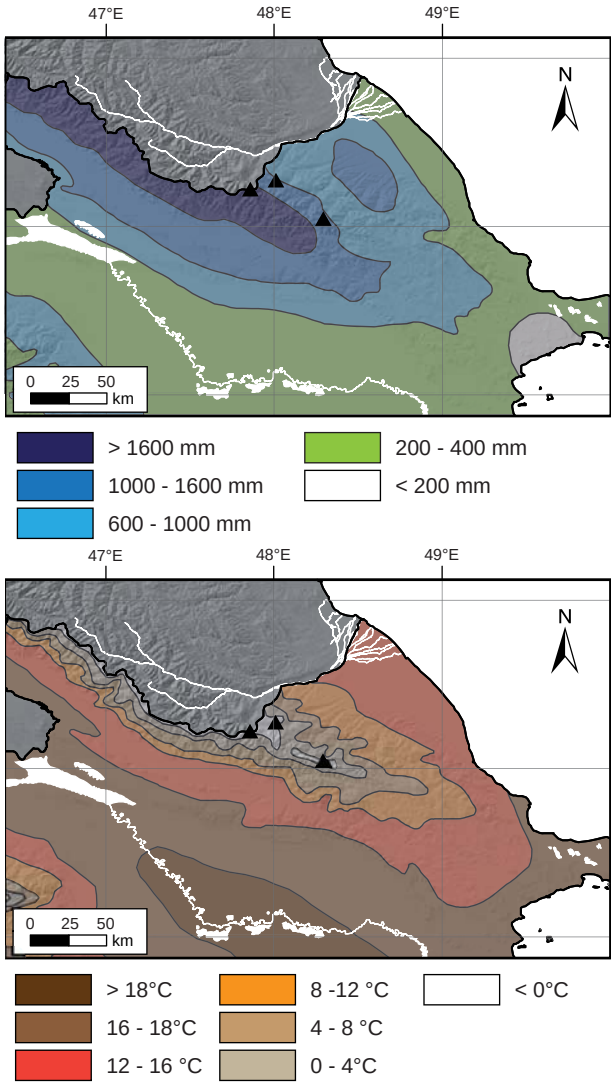

Figure 12: Mean annual precipitations and soil temperatures for Azerbaijan (EYUBOV 1993).

In the EGC of Azerbaijan, glaciers are not present anymore. Only firns can be observed on the highest summits (Sahdag, Bazarduzu and Tufandag Mountains). They cannot be considered as a main water supplier for the rivers. The watershed is not located along the main ridge (Bazarduzu, Tufandag), but south of it.

In the south, most of the rivers (i.e. Qaracay, Damiraparancay, Goycay, Girdimancay, Sulutcay, and Pirsaat) flow into the Kura River who finally reaches the Caspian Sea. From the watershed, they have mostly a north-south flow direction in the western part and a changing direction eastward of the town of Samaxi.

In the north, the Samur River is the main river which drains mostly the Dagestan Caucasus area. The majority of the rivers of the northern slope flow directly into the Caspian Sea (i.e. Qusarcay, Qudiyalcay, Valvalacay, Gilgilcay, and Atacay). Their flow direction is variable in the mountain range and when the rivers reach the plain they have a north-east flow direction.

Finally in the Eastern part of the EGC, the rivers flow directly to the east into the Caspian Sea.

2.3. Geodynamic setting

The overall geodynamic setting of the EGC corresponds to a continental collision inverting the former passive margin of the Scythian Platform and a deep Mesozoic-Tertiary basin, the Greater Caucasus Basin (GCB). The EGC corresponds to a doubly verging mountain belt with two fold and thrust belts in the northern and southern slopes and a nappe structure in the northern part of the central area. The pro-wedge (front) is located to the south and overrides the Kura Basin, whereas the retro-wedge (back) is located to the north and overrides the Terek Basin (figs. 1, 8 and 10).

A subduction initiated in Pliocene times (Allen et al. 2002; Knapp et al. 2004) when the South Caspian Basin (SCB) started subducting to the north under the eastern termination of the Greater Caucasus and the Abseron ridge. This subduction remains restricted to this eastern area.

According to Brunet et al.(2003) and Ershov et al. (2003) the depth of the Moho changes from about 40 km in the south beneath the Kura Basin to more than 50 km beneath the EGC and rises to 40 km again under the northern foreland basin.

2.4. Paleogeographic evolution

As shown and discussed by several authors (Barrier et al. 2008a; Barrier et al. 2008b; Brunet et al. 2009a; Brunet et al. 2003; Khain 1994; Nikishin et al. 2001; Sosson et al. 2010b; Zonenshain & Le Pichon 1986), the Greater Caucasus was formed as a result of shortening and closure of a former Jurassic-Eocene back-arc basin, the GCB, which was underlain by very thin continental (and possibly oceanic) crust set during the Early Jurassic. The area underwent several phases of extension and compression linked with the Tethys subduction under the Eurasian plate since the Jurassic. A major continental collision between the Arabian and Eurasian plate started in Eocene times. This long orogenic process resulted finally in one of the world's deepest sedimentary basins, the SCB (more than 25 km of sediments) and in the highest mountain belt of Europe, the Greater Caucasus Mountains (with the Elbrus Mt., 5642 m).

This chapter summarizes the evolution of this area. It is based on mainly on NIKISHIN (2001) and others authors (BRUNET et al. 2009a; BRUNET et al. 2003; KHAIN 1994; MILANOVSKI 1991; SOSSON et al. 2010b; ZONENSHAIN & LE PICHON 1986), and on the recent Middle East Basins Evolution Programme (MEBE) who published, in 2008, 14 palaeotectonic maps from the Late Norian (Upper Triassic) to the Piacenzian (Pliocene) (BARRIER et al. 2008a). Details from 6 maps on the Black Sea - Great Caucasus – Caspian Sea area are charted on figure 13. The six chosen Epochs represent periods of major changes in the studied area.

The Greater Caucasus evolution could be divided into three phases: the Proterozoic Cycle (Baikalian), the Paleozoic Cycle (Hercynian) and the Mesozoic-Tertiary Cycle (Alpine). In this study, the focus is on the Alpine cycle because it concerns mainly the building of the EGC.

The Alpine cycle is characterized by two stages: an extensional stage with the formation of deep sedimentary basins (Triassic to Eocene) and an orogenic stage (Oligocene to Quaternary). This cycle is also characterized by numerous intrusions.

The extensional stage underwent several compression and back-arc extensions phases: the Eo-Cimmerian phase in the Upper Triassic, the Mid-Cimmerian phase in Middle Jurassic times and the Late Cimmerian phase at the end of the Jurassic. These compression phases, named Cimmerian Orogeny, are related to the collision of several microplates, most of which detached from northern Gondwana in the Early Permian during the opening of the Neotethys Ocean. The Cimmerian Orogeny affected the southern Eurasia margin between Turkey and Thailand (FÜRSICH et al. 2009; ZANCHI et al. 2009). In the Caucasus, this period corresponds to a succession of subsidence phases that created the GCB and the SCB.

Based on DOUMITRACHKO & MILANOVSKII (1974), the orogenic stage could be divided in two phases: the formation of the Lesser Caucasus since the Ypresian (Eocene) and the rapid uplift of the Greater Caucasus Orogeny since Oligocene times (BARRIER et al. 2008a). The Lesser Caucasus underwent a major volcanic activity. The Greater Caucasus had an acceleration of the vertical movement since the Middle Miocene (Sarmatian). From Pliocene to Holocene times, the area underwent the major Akchagyl transgression of the Caspian Sea, the reorganisation of the river network and the Quaternary glaciations.

2.4.1. Late Triassic – Lower Jurassic compression

NIKISHIN ET AL. (2001), KAZMIN (2006) and Stampfli et al. (2001) wrote that: the remnant oceanic lithosphere of the Palaeotethys had apparently been subducted by Late Triassic to Lower Jurassic (Hettangian) times and the Cimmerian terrane collided during the Carnian with the southern margin of Eurasia. At the same time, activity along the subduction zone accelerated during Carnian to Hettangian times allowing the growth of an Eo-Cimmerian Orogeny (KAZMIN & TIKHONOVA 2006).

2.4.2. Lower and Middle Jurassic rifting and compression

As described by NIKISHIN et al. (2001), the subduction of Neotethys continued throughout the Middle Jurassic. It resulted in a Mid-Cimmerian tectonic event with an active magmatic arc, the Dzirula Massif (DzM), and a back-arc basin, the GCB. Northward, during late Aalenian-Bajocian times, a foreland basin developed on the Scythian Platform (SyP) (fig. 13 - J_1).

Also in NIKISHIN et al. (2001), the Scythian Platform (SyP) (not visible on figure 13 - J_1, located to the west) corresponded to the north-western rift shoulder of the GCB and remained an area of non-deposition during Sinemurian times. However, during the Pliensbachian and the Toarcian ages, it was transected by a system of shallow-water basins accompanied by extrusion of rhyolites, dacites, andesites and basalts. During the Upper Aalenian and the Bajocian ages, the Scythian Platform was broadly covered by shallow marine sediments deposited in a thermal subsiding basin.

NIKISHIN et al. (2001) described the large and deep GCB as a back-arc basin that was created during the Lower Jurassic. It underwent a rapid subsidence that began in Sinemurian times as indicated by the change in the Caucasus area of shallow water clastics sediments to deep water shales and turbidite sands of Pliensbachian and Lower Aalenian ages. Its extension ended between Aalenian and Bajocian ages before the onset of the Mid-Cimmerian tectonic event. Subsequently the GCB was inverted with deformations culminating in the Bajocian. Both compression cycles of Eo- and Mid-Cimmerian were accompanied by large scale subduction-related andesitic volcanic activity along the southern margin of the Greater Caucasus in the Dzirula Massif (DzM). It terminated at the end of Bathonian.

On the northern slope of the GCB, a regional unconformity at the base of Callovian sediments, could be linked to the Mid-Cimmerian inversion of this basin prior the start of a new subsidence during at the end of the Late Jurassic.

2.4.3. Upper Jurassic rift system and compression event

After the Mid-Cimmerian tectonic event, the GCB was affected by a new rifting cycle that started during the Callovian (fig. 13 – J_3). At the transition from Jurassic to Cretaceous and during the Berriasian times, the Late Cimmerian tectonic event overpowered the back-arc rift system. The main Upper Jurassic rifted basins are the SCB and the GCB, the Terek B. (TeR), the Western and Eastern Kuban basins (KbB) (Nikishin et al. 2001).

In the North Caucasus basins, including the Western and Eastern Kuban basins (KbB) and Terek Basin (TeR), thick Callovian-Upper Jurassic sequences were deposited (Koronovsky et al. 1987; Milanovski 1991; Nikishin et al. 1998a). Callovian-Lower Oxfordian deposits consist of conglomerates, silts, clay and shallow marine carbonates. During the Middle and Upper Oxfordian, a reef barrier developed around the deeper central part of these basins. The rapid Callovian-Upper Jurassic subsidence of these north Caucasus basins was probably controlled by crustal extension, related to the re-opening of the GCB. The rapid subsidence of the GCB was accompanied by rift volcanism. The lack of Upper Jurassic ophiolites in the Greater Caucasus suggests that rifting did not reach the crustal separation. Based on angular unconformities in seismic lines, the North Caucasus basins were gently deformed at the end of Tithonian and during the Berriasian and the area was uplifted (Nikishin et al. 1998a; Nikishin et al. 1998b; Nikishin et al. 2001).

In the SCB, crustal separation was probably achieved during the Callovian and was followed by Upper Jurassic sea-floor spreading (Brunet et al. 2003).

During the Kimmeridgian and Tithonian, the northern flank of the GCB was uplifted, forming a low relief high resulting in the accumulation of evaporite-dominated series (Nikishin et al. 2001).

During the Callovian and Upper Jurassic, the GCB was bordered in the south by the active Somkheto-Karabakh Volcanic Arc (SKV) (Sosson et al. 2010c).

2.4.4. Lower Cretaceous extension

As described by Nikishin et al. (2001), the Scythian Platform was tectonically stable from Berriasian to Valanginian times. However, the GCB and its surrounding basins subsided rapidly. The beginning of Aptian corresponds to a renewed phase of major back-arc extension in the northern area of the GCB (fig 13 – K_1). This phase was governed by activity along the Neotethys subduction zone.

On the Scythian Platform (SyP), sedimentation variably resumed during the Upper Berriasian to Barremian and became more widespread during Aptian-Albian. The Early Cretaceous series are interrupted by numerous regional unconformities, reflecting changing tectonics and fluctuating sea levels (Nikishin et al. 2001).

The Northern Caucasus basins, the Dagestan Basin (DgB) and the Kuban Basin (KbB), subsided rapidly during Lower Cretaceous times and particularly during Aptian and Albian times. The subsidence of the Kuban Basin was accompanied by basaltic and andesitic volcanism (Nikishin et al. 2001).

The GCB was dominated throughout Cretaceous times by thermal subsidence (Brunet et al. 2003).

In the Transcaucasus – Lesser Caucasus area, corresponding to the Somkheto-Karabakh Volcanic Arc (SKV) area, the Aptian to Turonian series consist of clastic sediments and volcanogenic rocks (Nikishin et al. 2001).

2.4.5. Upper Cretaceous and Paleogene opening of rifted basins

From Coniacian to Paleocene the intra-oceanic subduction of the Neotethys evolved to a continental subduction (Sosson et al. 2010c) (fig. 13 – K_2). Several rifting phase have been distinguished: during the Aptian-Albian (especially Middle-Upper Albian), Cenomanian-Turonian and during the Santonian.

The Scythian Platform (SyP) and the southern parts of the Russian Platform were occupied by a chalk dominated shallow water carbonate platform. However, water depths increased southwards along the northern margins of the GCB (Nikishin et al. 2001).

In the Transcaucasus - Lesser Caucasus region, a subduction-related magmatic activity is recorded until early Campanian Age. Northward, Late Turonian to Santonian alkaline basalts were extruded in Georgia under a back-arc tensional setting along the southern margin of the GCB (Nikishin et al. 2001).

The GCB and the SCB corresponded to deep water basins, characterized by terrigenous type sediments (Brunet et al. 2003; Green et al. 2009; Milanovski 1991). In the EGC, the GCB was divided in several sub-basins, i.e. the Xizi Trough and the Buduq Trough.

In Stephenson & Schellart (2010), Dercourt et al.(1986), Nikishin et al. (2001), Nikishin et al. (1998b), Zonenshain & Le Pichon (1986), the deep-water Black Sea Basin is considered to be an Early

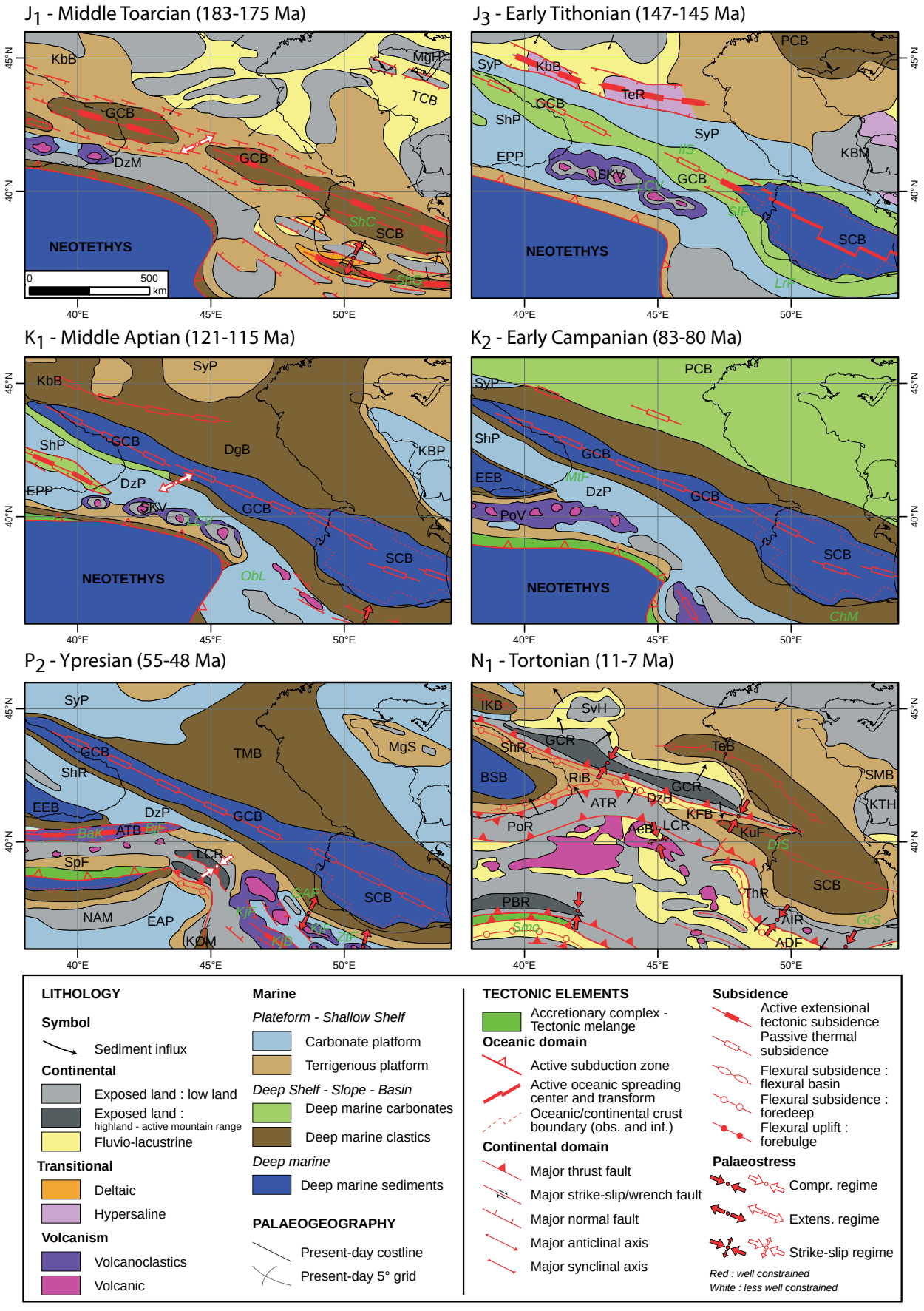

Figure 13: Paleogeographic evolution of the Greater Caucasus modified from (Barrier et al. 2008a). Abbreviations are defined in table 3.

Table 3: Abbreviations used in figure 13.

ADF	*Abu Dabbab Formation*	KbB	*Kuban Basin*	SCB	*South Caspian Basin*
AeB	*Armenian Basin*	KBM	*Kara-Bogaz Massif*	ShP	*Shatsky Platform*
AlR	*Alborz Range*	KFB	*Kartli Foreland Basin*	ShR	*Shatsky Ridge*
ATB	*Adjara-Trialeti Basin*	KjB	*Karaj Basin*	SIF	*Shal Formation*
ATR	*Achara-Trialet Range*	KjF	*Karaj Formation*	SKV	*Somkheto-Karabakh Volc.-Arc*
BaK	*Bakirköy Formation*	KOM	*Koy Ophiolite Massif*	SMB	*South Mangyshlak Basin*
BjF	*Borjomi Flysch*	KuF	*Kura Foreland Basin*	Smo	*Selmo Formation*
DgB	*Daghestan Basin*	LCR	*Lesser Caucasus Range*	SpF	*Sipikör Formation*
DIF	*Dalichai Formation*	LCV	*Lesser Caucasus Volcanics*	SvH	*Stavropol High*
DzH	*Dzirula High*	LrF	*Lar Formation*	SvM	*Stavropol Massif*
DzP	*Dzirula Platform*	MgS	*Mangyshlak Shoal*	SyP	*Scythian Platform*
EAP	*East Anatolian Platform*	MtF	*Mtavari Formation*	TeB	*Terek Basin*
EPP	*Eastern Pontides Platform*	NAM	*North Anatolian Massif*	TeR	*Terek Rift*
GAF	*Ghareh-Aghash Formation*	ObL	*Orbitolina Limestones*	ThR	*Talesh Range*
GCB	*Great Caucasus Basin*	PBR	*Puturge-Bitlis Range*	TMB	*Terek-Mangyshlak Basin*
GCR	*Great Caucasus Range*	PoR	*Pontides Range*	ZkS	*Zakatala Suite*
GrS	*Gray Series*	PoV	*Pontide Volcanic Arc*	ZtF	*Ziarat Formation*
IIS	*Illisu Suite*	RiB	*Rioni Basin*		

Cretaceous-Paleogene back-arc extensional feature that developed to the north of the Pontides-Transcaucasus magmatic arc. The Black Sea Basin is subdivided by the continental Andrusov-Archangelsky ridge (or Mid-Black Sea ridge) into a western, oceanic part and an eastern part that is floored by highly thinned continental crust. The Eastern Black Sea Basin (EEB) was separated to the northeast from the GCB by the Shatsky Platform (ShP).

The opening of the two Black Sea basins was paralleled by continuous, presumably tensional tectonics in the GCB until at least Middle Santonian times as evidenced by the volcanic activity. In the West Black Sea Basin, sea-floor spreading started during the Upper Albian and Cenomanian and continued throughout the Paleocene. In contrast, in the Eastern Black Sea Basin, crustal separation was not yet achieved.

2.4.6. Paleocene-Eocene Rift System

During the Paleocene, opening of the Western Black Sea ceased whereas the Eastern Black Sea Basin (EEB) was affected by a second rifting cycle that terminated during the Late Eocene (Banks et al. 1997; Robinson et al. 1995). Similarly the Upper Cretaceous Transcaucasus – Lesser Caucassus subduction-related magmatic belt was transected during the Paleocene-Eocene by a system of new rifts, causing its segmentation. The GCB and the SCB still underwent a passive thermal subsidence. During the Eocene volcanoclastic basins form a belt that extends from the Eastern Pontides via the Transcaucasus to the Elborz area in Iran. During the Late Eocene, rifting activity terminated in the Eastern Black Sea and in Transcaucasus area with the onset of the collisional Caucasus orogeny (Nikishin et al. 2001) (fig. 13 – P_2).

As described in Nikishin (2001), the most important rifting area in the Transcaucasus – Lesser Caucasus area was in the Adjara-Trialeti Basin **(ATB)** in Georgia. It subsided during Upper Cretaceous and Paleocene times on top of the Aptian-Turonian Transcaucasus – Lesser Caucasus magmatic arc. By Paleocene times, it had evolved into a deep-water trough in which flysch-type sediments were deposited and the basin was affected by a new subsidence phase that was accompanied by a large-scale basaltic, alkali-basaltic and andesitic volcanism and the accumulation of volcanoclastic flysch. The inversion of the area started in Lower Eocene times and it corresponds to the beginning of the building of the Lesser Caucasus Mountains.

2.4.7. Oligocene to present Caucasus orogeny

In its summary about the Mesozoic-Cenozoic evolution of the Scythian Plateform, Nikishin et al. (2001) wrote that during the Oligo-Miocene Caucasus orogeny, a northward subduction of the remnant Neotethys was followed by continent-continent collision of the Arabian Craton with the Caucasus domain. This compressive regime resulted in a thickening of the crust and lithosphere. Large-scale crustal shortening ended during the Upper Miocene and was probably followed by the detachment of the subduction slab and a delamination of the lithospheric root of the Caucasus Orogen. Related to this context, the Black Sea-Caucasus-South Caspian area was affected by increasingly intense compressional tectonics and a rapid uplift of the main orogenic areas. One of the most prominent

features of the Caucasus Orogen is the large-scale continental volcanism (Armenian, Anatolian and Azerbaijan volcanic plateaux) that occurred after the main orogenic period and located along the collision zone between Arabian Craton and the Caucasus domain (Nikishin et al. 2001) (fig. 13 – N_1).

The Lesser Caucasus Range (LCR) underwent two more magmatic pulses after the Eocene one: a late Miocene-Pliocene and a Plio-Quaternary one. The Mio-Pliocene magmatic pulse, occurring in the northern part of the Turkish–Iranian high plateau and the Lesser Caucasus, is characterized by calc-alkaline affinities reminiscent of extrusive rocks forming at active convergent margins. The Plio-Quaternary pulse is represented by alkaline rocks that occupy much of the southern part of the Turkish–Iranian plateau and the western Lesser Caucasus, and that show within-plate basalt geochemical characteristics (Dilek et al. 2010).

The Kura Foreland Basin (KuF), the Kartli Foreland Basin (KFB) and the Rioni Basin (RiB) correspond to foreland flexural basins filled with molasse sediments. In Kura Foreland Basin the thickness of Oligocene - Quaternary molasse is close to 5-8 km (Brunet et al. 2003).

In the SCB, two rapid subsidence phases took place. The first subsidence phase is linked with the onset of the Arabian-Eurasian collision in Oligocene times. The second subsidence phase during Plio-Quaternary times is linked with the Greater Caucasus, Kopet-Dagh and Alborz uplift (Brunet et al. 2003).

The GCB was intensely inverted in the collision zone between the Arabian promontory and the Eastern European Craton since Oligocene times. It underwent a fast uplift since the Middle Miocene times (Sarmatian). In its central parts (around Tbilisi), the Greater Caucasus Range (GCR) was thrusted southward over the Transcaucasus Massif. The area underwent a major Plio-Quaternary volcanic activity (Elbrus area) (Nikishin et al. 2001).

Along the northern flank of the Caucasus, a foreland basin, the Terek Basin (TeB) developed and was partly thrusted by the Dagestan thrust belt during the last phases of the Caucasus orogeny (Nikishin et al. 2001).

At the same time, the Stravopol High (SvH) was uplifted to the north of the central Greater Caucasus, whereas the westward adjacent Indolo-Kuban foreland basin (IKB) subsided rapidly; its southern margin is marked by a system of steep reverse faults (Nikishin et al. 2001).

2.5. Structural setting

The studied area is divided between three mega zones: the Eastern Greater Caucasus Mega Zone, the Qusar-Davaci Mega Zone in the north and the Kura Mega Zone in the south (fig. 14). Complete descriptions of the different zones were made by Kangarli (2005) in Russian with a summary in English.

2.5.1. Qusar-Davaci Mega Zone

The Qusar-Davaci Mega Zone includes the Xacmaz Zone (Xm) and the Quba Zones (Qb) (fig. 14).

The Quba Zone (Qb) and the Xacmaz Zone (Xm) are part from the Qusar-Davaci Mega Zone. They are separated by the Imamqulukand-Xacmaz Fault. The Paleogene and Neogene deposits cover unconformably the Mesozoic-Paleozoic deposits. The Siyazan Thrust connects the Quba Zone with the structural zones of the northern slope of the EGC (Ismailzadeh et al. 2008a; Kangarli 2005).

2.5.2. The Eastern Greater Caucasus Mega Zone

The Eastern Greater Caucasus Mega Zone is divided into 14 structural zones (fig. 14): the Tahircal Zone (Tc), the Sudur Zone (Sd), the Tengy-Besbarmaq Zone (TB), the Sahdag-Qizilqaya Nappe(SQ), the Sahdag-Xizi Zone (SX), the Qonaqkand Zone (Qk), the Tufan Zone (Tf), the Zaqatala-Qovdag Zone (ZQ), the Qovdag-Sumqayit Zone (QS), the Vandam Zone (Vm), the Basqal Nappe (Bq), the Ganih-Ayricay Zone (GA), the Samaxi-Qobustan Zone (SQ) and the Abseron zone (Ab) around Baku (Ismailzadeh et al. 2008a; Kangarli 2005).

The Tahircal Zone (Tc) is located along the northeastern border of Azerbaijan. It is characterized by folded Middle Jurassic deposits (mostly of Aalenian Age) covered by transgressive Paleogene and Neogene sediments.

The Sudur Zone (Sd) and its eastern equivalent Tengy-Besbarmaq zone (TB) crop out along the northern slope of the EGC. The Sudur zone covers transgressively the Middle Jurassic folded sediments of the Tahircal Zone. The Sudur Zone consists mostly of 5 linear anticlines in Upper Jurassic and Lower Cretaceous formations (Kangarli 2005). The southern border is in tectonic contact with the Sahdag-Xizi Zone and the Sahdag-Qizilqaya Nappe.

The Sahdag – Besbarmaq Nappe (SB) includes all impressive cliffs of the EGC northern slope. It corresponds to the southern part of the Sudur Zone but is part of the Sahdag-Xizi Zone. Because of its geologi-

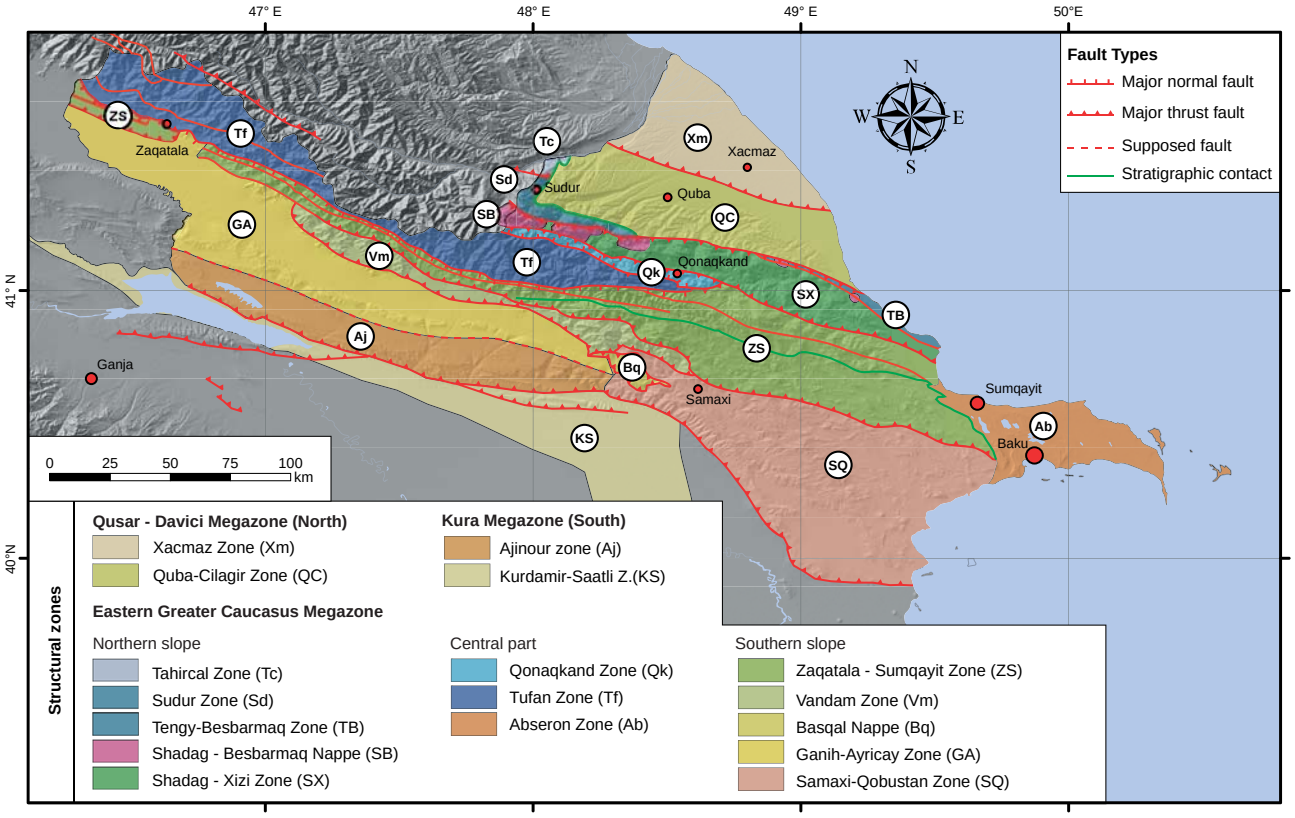

Figure 14: Structural zones of the Eastern Greater Caucasus of Azerbaijan (Modified from T. Kangarli, unpublished).

cal particularities, it is treated separately in this document. It was thrusted to the south during the Lower Cretaceous and was afterwards backthrusted to the north during the uplift of the central area of the EGC. The main part of the zone consists of the Sahdag Mt. (4243 m) and the Qizilqaya Massif (3726 m). Eastward, some remains of the nappe can be found near Sohub, Tangaalti, Cirax and the Besbarmaq Mt on the coast of the Caspian Sea. This nappe structure is only present in Azerbaijan and apparently disappears to become concordantly bedded with the underlying formations around the Shalbuzdag Mt. (4142 m) in Dagestan (Russia). The Sahdag Mt. is divided in one syncline (in the north) and one anticline (in the south) with an inverse northern flank. Eastward, the structure becomes flatter and narrower, i.e. the Qizilqaya Massif consists only of one flat syncline.

The Sahdag-Xizi Zone (SX) consists mostly of Upper Jurassic and Cretaceous deposits. In Azerbaijan, its length reaches 150 km and has a maximum width of 12-15 km. It extends from the border with Dagestan (Sahdag region) to the Caspian Sea. In its western part it is overthrusted by the Sahdag-Qizilqaya Nappe and eastward it crops out until the Caspian Sea.

The Qonaqkand Zone (Qk) is tectonically bordered by the Sahdag-Xizi Zone in the north and by the Tufan Zone in the south. It is composed of terrigenous deposits of Lower and Middle Jurassic ages in the west and of Upper Jurassic and Lower Cretaceous ages in the east. Both Sahdag-Xizi and Qonaqkand zones were overthrusted by the Sahdag-Qizilqaya Nappe during the Lower Cretaceous. The Main Caucasus Thrust separates the Qonaqkand Zone from the Tufan Zone.

The Tufan zone (Tf) corresponds to the central and highest part of the Eastern Greater Caucasus. Structurally, it consists of major folds alternating with thrust zones. It is composed of Lower and Middle Jurassic deposits and Upper Jurassic flysch. In Azerbaijan it extends from the northwestern border with Georgia until the area of Qonaqkand village in the east.

The Zaqatala – Sumqayit Zone (ZS) is the most developed zone on the southern slope of the EGC. The Zaqatala-Sumqayit Zone consists mainly of Lower Cretaceous flysches. This zone is divided in three subzones: the Zaqatala-Dubrar, the Duruji and the Qovdag-Sumqayit subzones (KANGARLI 2005).

The Vandam Zone (Vm), composed mainly of Lower Cretaceous rocks, was uplifted during the late phases of the orogen.

The Basqal Nappe (Bq) is an allochthonous Nappe thrust on Upper Miocene deposits of the Duruji subzone (Zaqatala-Sumqayit Zone). The Nappe litholo-

gies extend from Barremian to Miocene in age. Geographically, it extends from the east of the town of Ismayilli to the west of the town of Samaxi.

The Ganih-Ayricay Zone (GA), also named Alazani basin, is an asymmetric basin running parallel to the Greater Caucasus axis from the northeast of the town of Tbilisi (Georgia) to the Girdimancay River near the town of Ismayilli. Its northern border corresponds to a main thrust of the southern slope of the EGC. The sediments pile grows thicker towards the south. Quaternary deposits reach a maximum thickness of 800 m and upper Pliocene ones a maximum thickness of 1000 m (PHILIP et al. 1989).

The Samaxi-Qobustan Zone (SQ) is composed of Neogene sediments. Middle-Late Miocene sediments (with thickness up to 3600 m) are transgressively overlapped by the Pontian deposits. They are themselves overlapped by Early and Late Pliocene deposits (ISMAILZADEH et al. 2008a).

The Abseron Zone (Ab) corresponds to the eastern termination of the Greater Caucasus. It is composed of folded thick series of Miocene (1600 m), Pliocene (4240 m) and Quaternary ages (ISMAILZADEH et al. 2008a).

2.5.3. The Kura Mega Zone

The **Kura Mega Zone** is divided into five zones but our study is concerned only by the two northeastern zones: the Ajinour Zone and the Kurdamir-Saatli Zone.

The **Ajinour Zone (Aj)** is already part of the Kura Megazone but its geodynamics is clearly linked with the Greater Caucasus one. It is composed of Oligocene-Pliocene molasse deposits and is deformed by several thrusts to the south.

The **Kurdamir-Saatli Zone (KS)** is also part of the Kura Megazone. The frontal fault of the EGC can be observed in its northern area.

2.6.L ITHOSTRATIGRAPHICAL SETTING

This section is mainly based on literature and completed by field observation. A significant and detailed literature exists in Russian. The following descriptions are based on the few available translated articles and books about the Azerbaijan lithostratigraphy. ALI-ZADEH et al. (1997) and ISMAILZADEH et al. (2008a) are the main papers used to summarize the Jurassic to Quaternary deposits of the EGC. Dr. T. Kangarli also translated for this work some Russian literature about the EGC lithologies.

The text mainly focuses on the particularity of the deposits and five synthetic sections (figs. 16, 17, 18, 19 and 20) describe the different suites, their lithology and their thickness in the main structural zones of the EGC : Sudur, Sahdag-Xizi, Tufan, Zaqatala-Qovdag and Vandam zones.

2.6.1. General context

The Greater Caucasus Basin underwent several cycles of opening-closure and was successively filled by erosion products of the bordering area. Therefore lithologies from Jurassic, Cretaceous and Paleogene of the EGC are mainly represented by deep marine and slope facies. However on the northern slope, shallow marine and platform formations were deposited and represent the southern edge of the Scythian Platform. Since the beginning of the main orogen phase during Oligocene times, the eroded sediments of the uplifted area were accumulated in the surrounding foreland molasse and deep sedimentary basins. Due to major eustatic variations of the Caspian Sea during Pliocene and Quaternary times (details in section 1.4.4), marine formations were deposited alternating with continental ones at the EGC fringes. Finally, the volcanic and magmatic activity of the southern side of the Greater Caucasus Basin due to the subduction of the Paleotethys and the Neotethys resulted in major deposits and intrusions and are nowadays observable on the southern side of the EGC.

From a stratigraphic point of view, the EGC formations range from Lower Jurassic to Quaternary times. They can be subdivided into four major groups:

- Sedimentary units with important input of arc-related volcanoclastic material;
- Detrital slope to basin sediments of the southern edge of the Scythian platform;
- Carbonate platform and lagoonal environment of the southern edge of the Scythian plate;
- Detrital units (marine and continental) linked with the erosion during the building of the Greater Caucasus.

2.6.2. Jurassic Period (J)

The Jurassic sediments are widespread in the EGC with great thicknesses (>7000 - 8000 m). They were deposited since the Pliensbachian and Toarcian times in a back-arc basin configuration. During the Lower and Middle Jurassic periods, they mainly consist of slope and deep marine formations. During the Upper Jurassic they mainly consist of shallow marine depos-

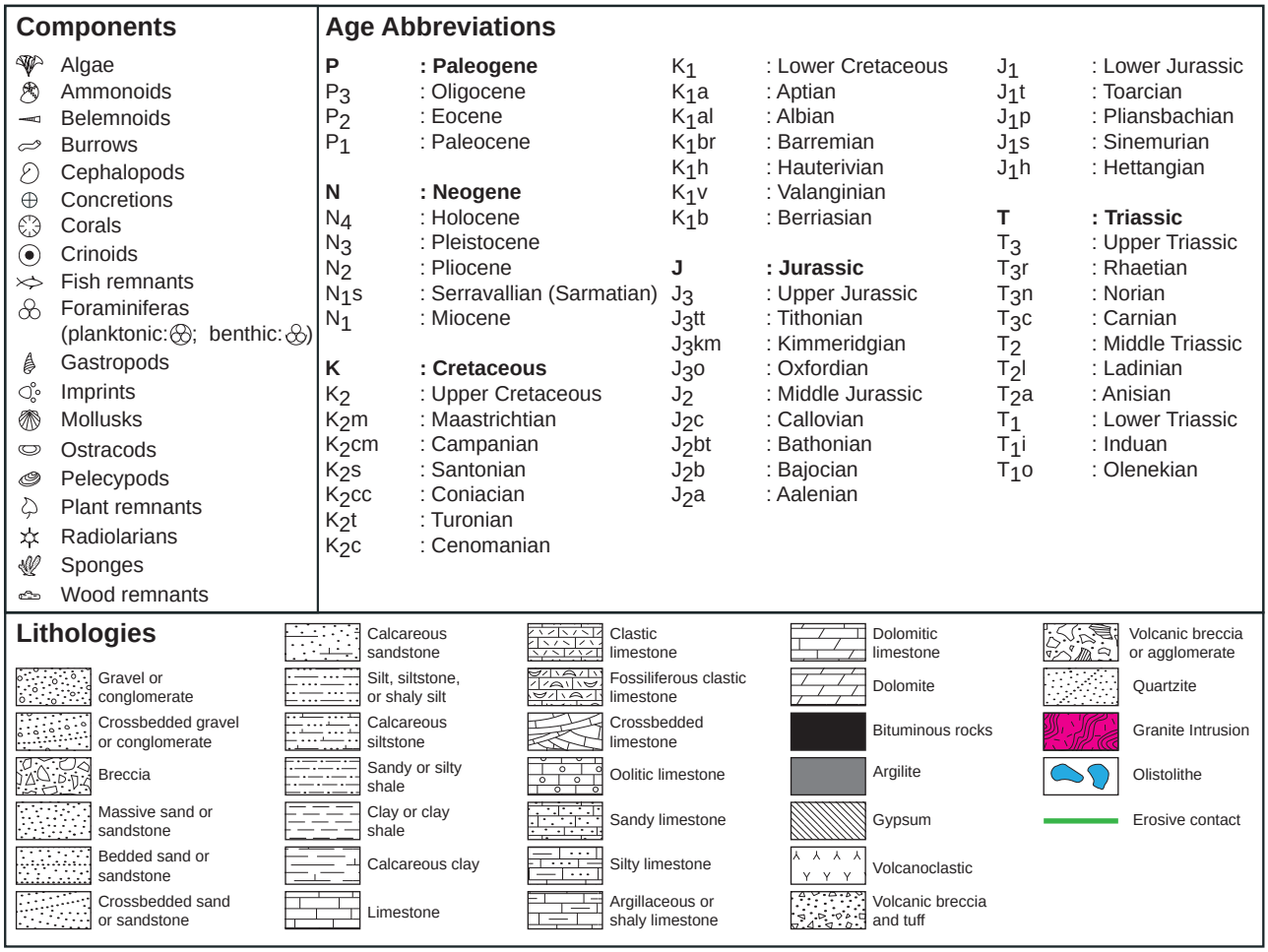

Figure 15: Legend for figures 16, 17, 18, 19 and 20.

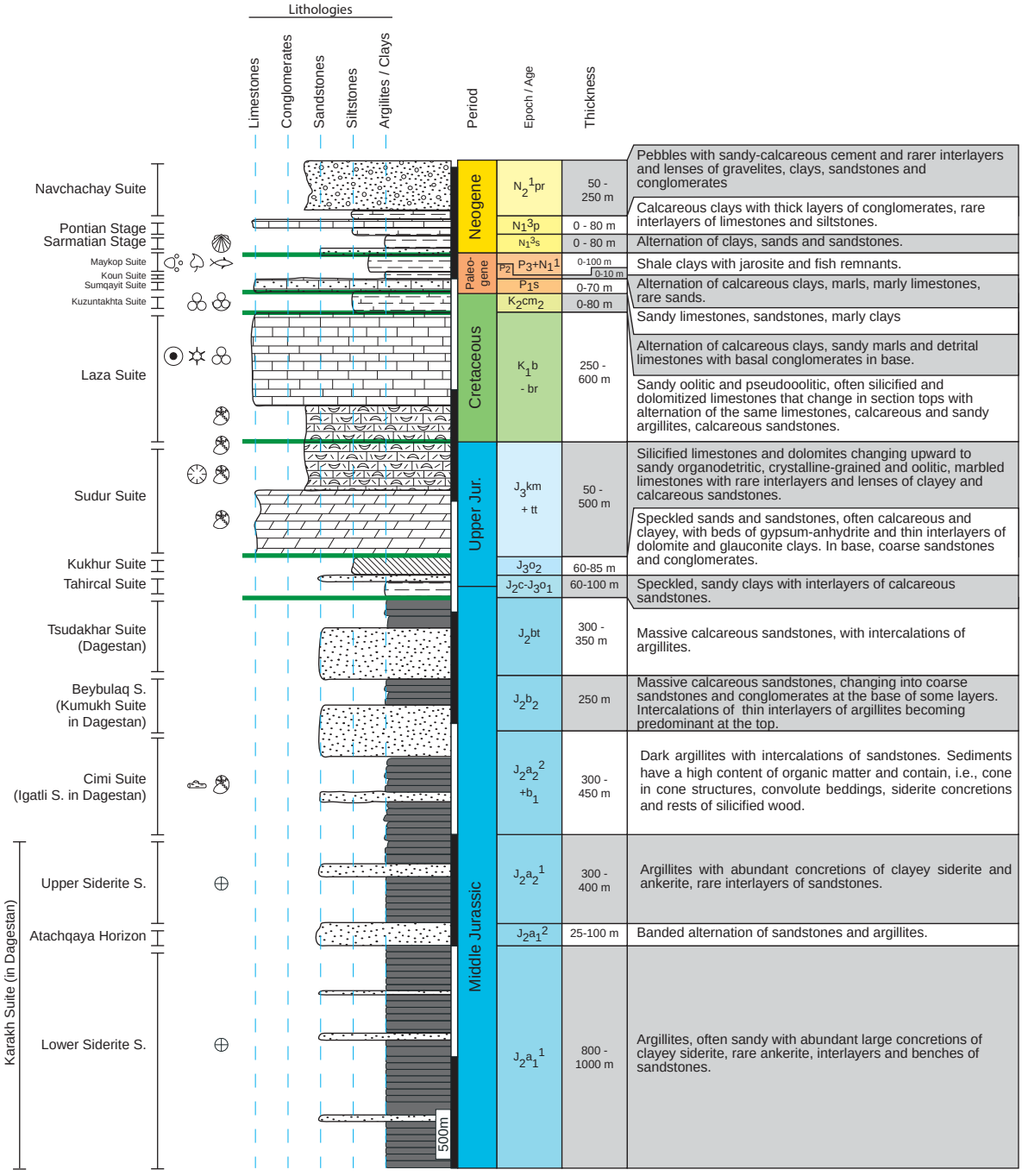

Figure 16: Lithostratigraphic log of the Tahircal-Sudur structural zone based on Ali-Zadeh et al. (1997) and Ismailzadeh et al. (2008a) and field observations. For legend refer to figure 15.

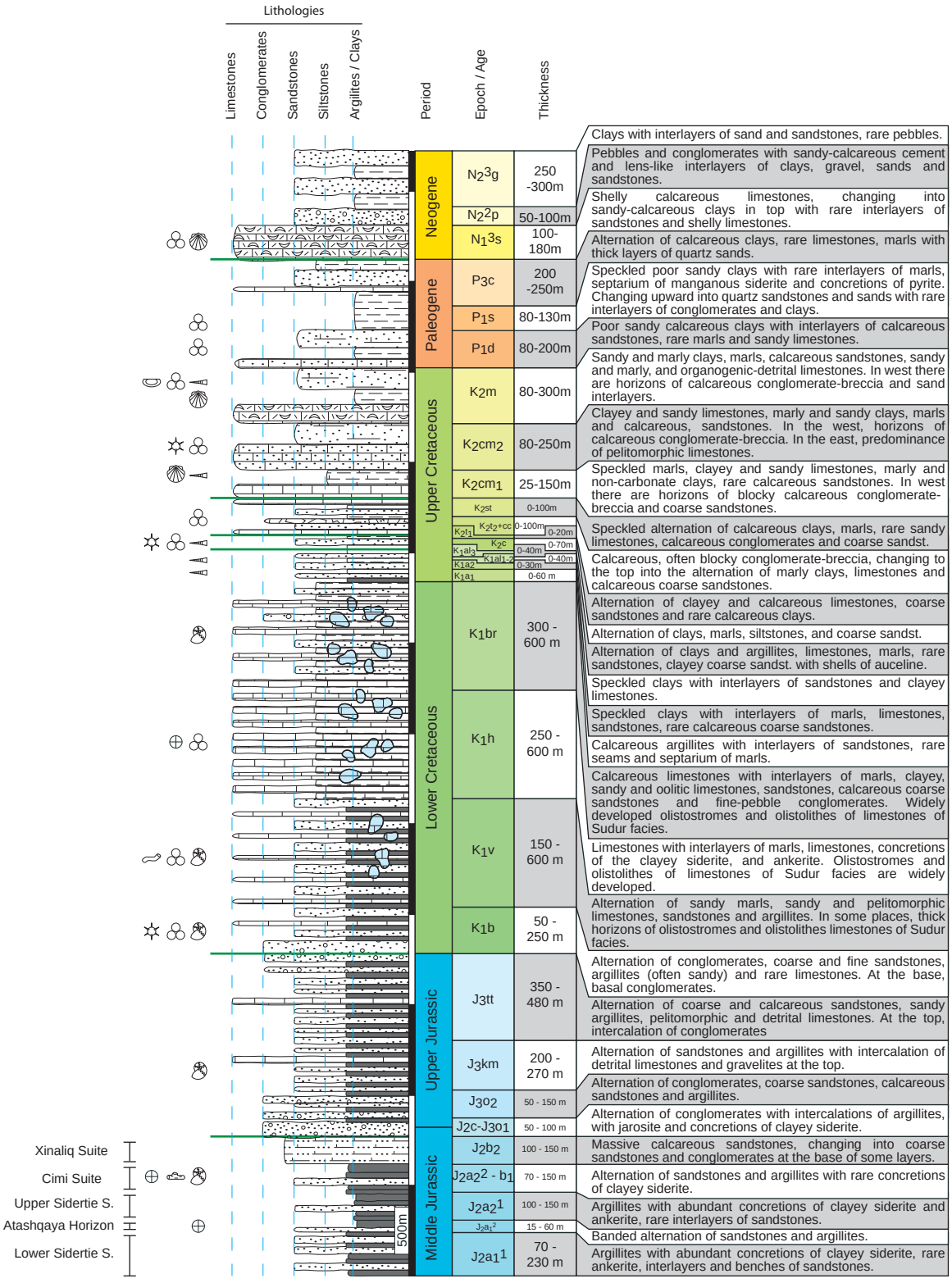

Figure 17: Lithostratigraphic log of the Sahdag-Xizi and Qonaqkand structural zone based on Ali-Zadeh et al. (1997) and Ismailzadeh et al. (2008a) and field observations. For legend refer to figure 15.

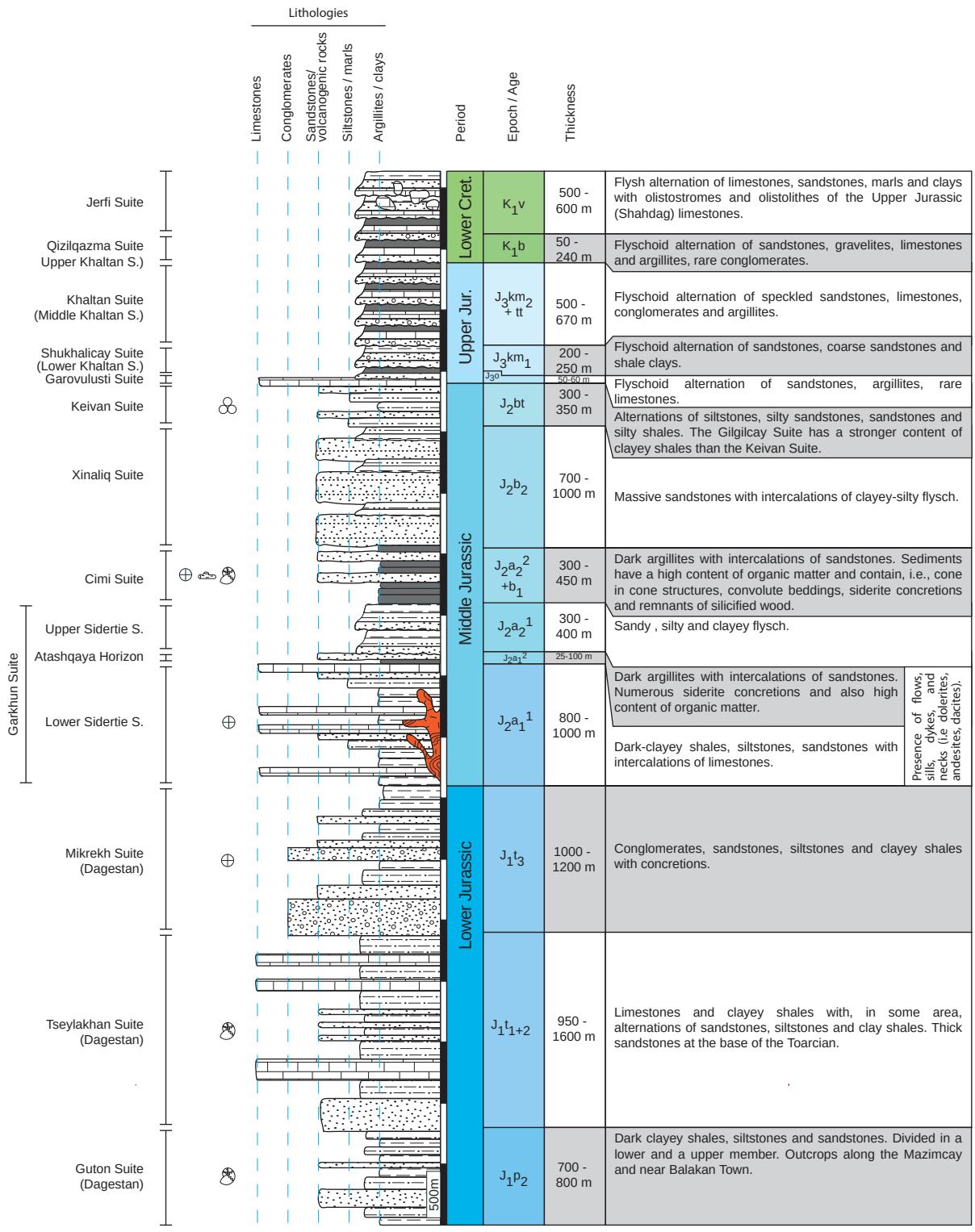

Figure 18: Lithostratigraphic log of the Tufan structural zone based on Ali-Zadeh et al. (1997) and Ismailzadeh et al. (2008a) and field observations. For legend refer to figure 15.

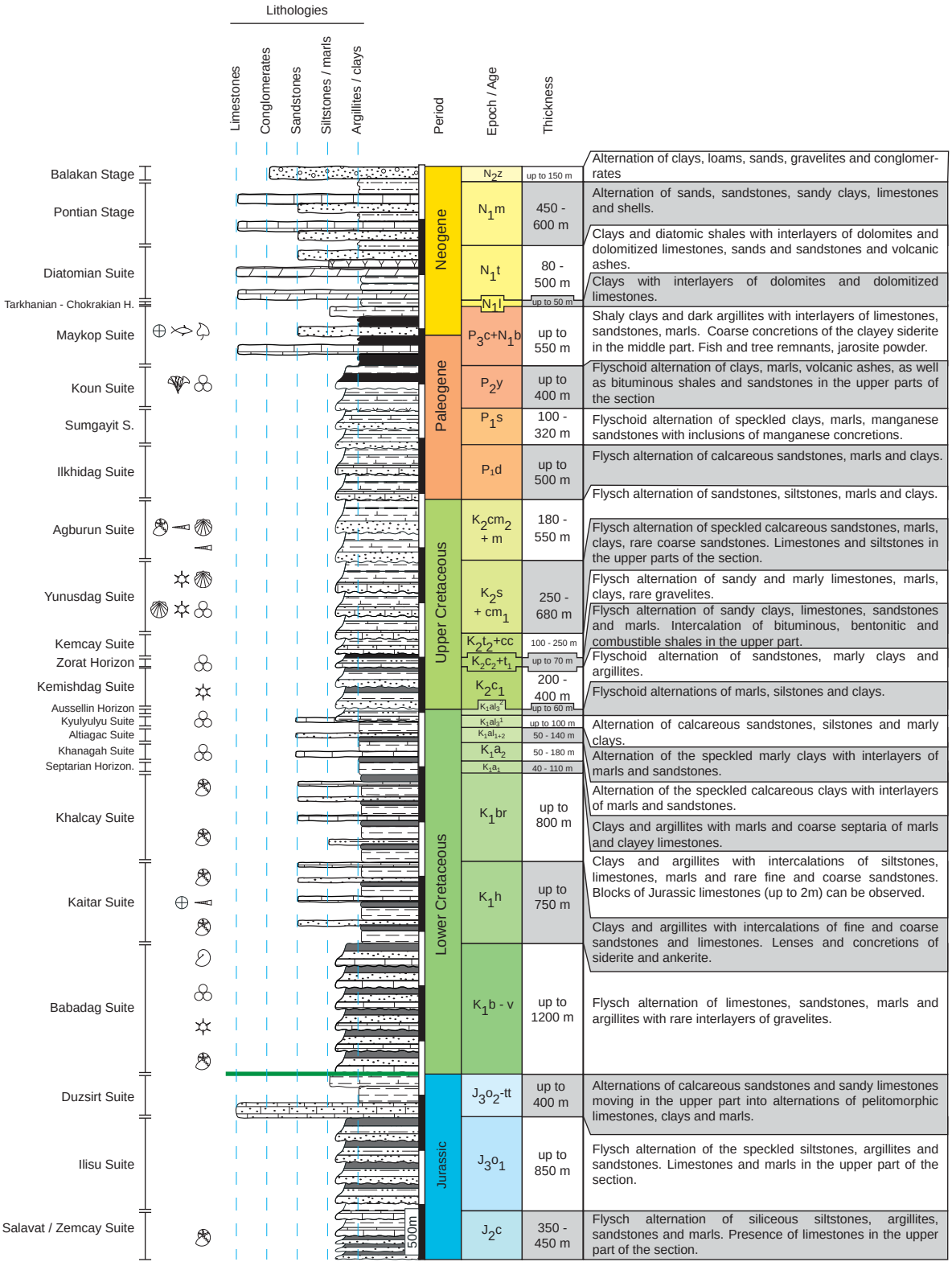

Figure 19: Lithostratigraphic log of the Zaqatala-Qovdag structural zone based on Ali-Zadeh et al. (1997) and Ismailzadeh et al. (2008a) and field observations. For legend refer to figure 15.

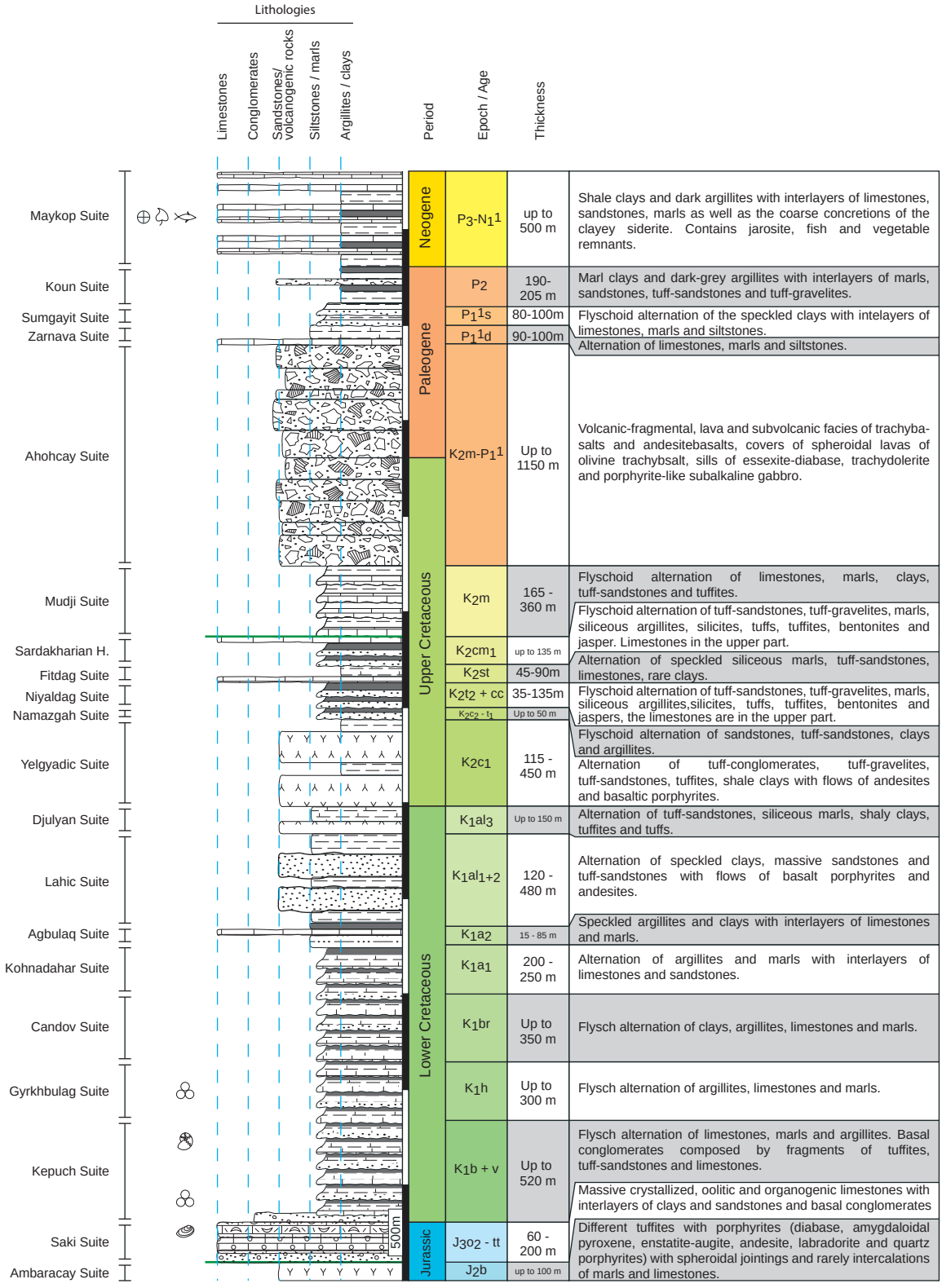

Figure 20: Lithostratigraphic log of the Vandam structural zone based on Ali-Zadeh et al. (1997) and Ismailzadeh et al. (2008a) and field observations. For legend refer to figure 15.

its and slope deposits. They are rich in natural resources like ore, oil and gas. Magmatic and effusive rocks of Jurassic age are widely spread in the Tufan zone and episodically in the Vandam zone. Within the Tufan zone, they consist of effusive and intrusive rocks of different ages and types : a sodic-basalt formation with an absolute dating of 184 Myr (Lower Jurassic), an andesite-dacite-rhyolite formation with an absolute dating of 166 Myr (Middle Jurassic) and a gabbro-diorite-tonalite formation with an absolute K-Ar dating of 150 Myr (Upper Jurassic) (ALI-ZADEH et al. 1997; ISMAILZADEH et al. 2008a).

High accumulations of sandy-silty rock and regional bituminous sediments with high contents in organic matter and the availability of surface oil and gas seepages in several region of north Azerbaijan are good indicators for oil and gas content of the Jurassic deposits. Black shale formations of Jurassic are also characterized by a high content of precious metals. Thus, a majority of ore fields and hydrocarbon seeps are associated with these deposits in the EGC (ALI-ZADEH et al. 1997; ISMAILZADEH et al. 2008a).

Lower Jurassic (J_1) Suites

During the Lower Jurassic Epoch, sediments vary from coastal-shallow facies to deeper facies after a sea transgression over the Greater Caucasus. The transgression covered a large territory of the Greater Caucasus during Pliensbachian and thick deposits were accumulated. The deepest zone of the basin was located close to the present watershed of the main Caucasian ridge. Toarcian sediments were deposited in coastal-shallow conditions and the deepening of sea occurred towards the south and east. Confined conditions were observed in Lower Jurassic basins of the Greater Caucasus and some of them contain hydrogen sulphide. Sediments were mostly carried from the northern edge of the basin.

Deposits crop mostly out in the western part of Tufan Zone (near Mazimcay and Balakancay rivers) in Azerbaijan and in Dagestan. In the EGC, 3 Lower Jurassic suites can be distinguished.

The *Guton Suite* of Upper Pliensbachian Age (J_1p) has a thickness of 800 to 1000 m. (fig. 18). It is composed of dark clayey shales, siltstones and sandstones.

The *Tseylakhan Suite* of Lower and Middle Toarcian Age (J_1t_{1-2}) has a thickness of 950 to 1600 m. (fig. 18) and is mostly composed of clayey shales and limestones.

The *Mikreh Suite* of Upper Toarcian Age (J_1t_3) has a thickness of 1000 to 1200 m. (fig. 18) and is mostly composed of clayey shales, conglomerates, sandstones and siltstones.

Middle Jurassic (J_2) Suites

During the Aalenian, the sea became shallow. Major changes in tectonic settings occurred during the Bajocian time. All over the EGC, the Middle Jurassic deposits have almost the same facies.

The Middle Jurassic Period is represented by all stages in the EGC. Deposits are represented by two main areas in the central and northern parts and by two thin lines along the northern and southern slopes of the EGC. The central area is the widest and corresponds to the Tufan zone; the northern part is considerably narrower in Azerbaijan but becomes wider in Dagestan. The line of the northern slope coincides with the axial zone of the Sudur-Tahircal and Tengy-Besbarmaq zones. The southern line goes along the limit between the Vandam and the Qovdag-Sumqayit structural zones.

In the Sudur, Tahircal and Sahdag-Xizi zones, the Middle Jurassic can be divided in, at least, 10 suites.

The *Lower Siderite Suite* corresponds to the bottom of Lower Aalenian Age ($J_2a_1^1$) and has a thickness of 800 to 1000 m. It is mainly composed of argillites with siderite concretions (figs. 16, 17 and 18).

The *Atachqaya Horizon* of the top of Lower Aalenian Age ($J_2a_1^2$) has a thickness of 25-100 m. It forms distinguishable thick sandstone layers in the middle of the argillites of the Lower and Upper Siderite suites (figs. 16, 17 and 18).

The *Upper Siderite Suite* of the lower part of the Upper Aalenian ($J_2a_2^1$) has a thickness of 300-400 m. It is mainly composed of argillite with siderite concretions (figs. 16, 17 and 18)

These three units together form the *Karakh Suite* that is mostly known in Dagestan.

The *Cimi Suite* (Igatli Suite in Dagestan) corresponds to the top of the Upper Aalenian and the Lower Bajocian ages ($J_2a_2^2$-J_2b_1). It is mainly composed of dark argillites with thin intercalations of sandstone. In the Sudur, Tahircal and Tufan zones its thickness varies from 300 to 450 m and decreases to 70-150 m in the Sahdag-Xizi Zone (figs. 16, 17 and 18). The Cimi suite is buried under the southeastern EGC and under the Qusar-Davaci Megazone (Yalama, Xudat, Xacmaz, Afurca, Kiscay, Tugcay and Baybayim dag Mt.). A typical section is located in the basin of Qaracay (near Ruk village) and Cimicay rivers. Faunistically, the Lower Bajocian deposits of the suite are divided in three parts: the lower part is characterized by ammonites *Otoites sauzei (Oppel)*, *Sphaeroceras globus*

(Buckman); the middle part by the ammonites *Stephanoceras humphriesianum (Sowerby), Stephanoceras scalare (Weisert)*; and the upper part by the ammonites *Parkinsonia parkinsoni (Sowerby)*. The suite can be seen in the Tahircal, Sudur (fig. 16), Tengy-Besbarmaq, Sahdag-Xizi (fig. 17), Tufan (fig. 18), Zaqatala-Qovdag (fig. 19), and Vandam (fig. 20) zones.

The *Beybulaq Suite* (*Kumukh Suite* in Dagestan) (fig. 16) corresponds to the Upper Bajocian Age (J_2b_2). It is composed of massive calcareous sandstones and it has a thickness of 700 to 1000 m.

In the Sahdag-Xizi Zone and in the Northern part of the Tufan Zone, the Upper Bajocian Age (J_2b_2) corresponds to the *Xinaliq Suite* (thickness of 100 to 150 m) and is also composed of thick-layered sandstones (figs. 17 and 18).

The *Tsudakhar Suite* (fig. 16) of Bathonian Age (J_2bt) outcrops in Dagestan. Its thickness reaches 300-350 m.

The *Keivan Suite* (fig. 18) from the Bathonian Age (J_2bt) consists of an alternation of argillite, siltstone and sandstone. It is dated by foraminifera in the Babacay River and Qaracay River (near Ruk villagThe thin *Ambarcay Suite* (fig. 20) (up to 100 m) of Bathonian Age (J_2bt) is located in the Vandam Zone and is mostly composed of tuffites.

The *Zemcay (or Salavat) Suite* (fig. 19) of the Lower Callovian Age (J_2c) is constituted by clayey-sandy rocks with a considerable content of carbonates. Deposits are spread in the head of Tikanlicay, Bumcay, Dasagilcay and Sincay rivers.

Upper Jurassic (J_3) Suites

Since the end of the Middle Jurassic and during the Upper Jurassic a new sea transgression occurred. Along the sea shore, restricted environments were formed allowing the deposition of evaporite (fig. 21). Suites of the Upper Jurassic consist mainly of carbonates.

Isolated outcrops of Middle-Upper Oxfordian are situated along a line starting near Tangaalti Village through Cirax Castle and finishing near the Besbarmaq Mt. The Upper Jurassic deposits are represented by all stages and crops out in most of the structural zones (Sudur, Tahircal, Tufan, Sahdag-Xizi and Zaqatala-Qovdag zones). In the northern Sudur and Tahircal zones, these sediments are transgressively bedded on the underlying Middle Jurassic deposits (fig. 21). In the Sahdag-Xizi Zone, they are also transgressively bedded on the older deposits and they can also be found as olistoliths on the Lower Cretaceous deposits. In the Tufan zone, they are concordantly bedded on the Middle Jurassic deposits. In some place (i.e. near Babadag Mt.), there is only block of several meters of Upper Jurassic breccia-limestones lying on Middle Jurassic deep sediments. The Upper Jurassic is divided at least in 9 suites.

The *Tahircal Suite* (fig. 16) of Callovian to Lower Oxfordian ages ($J_2c - J_3o_1$) has a thickness of 60-100 m and is transgressively bedded on the Bathonian. This limit corresponds to a major change in the depositional environment: from deep (Aalenian-Bathonian ages) to shallow marine deposits (Callovian-Oxfordian ages).

The *Kukhur Suite* (fig. 16) of Upper Oxfordian Age (J_3o_2) has a thickness of 60 to 85 m and has also a shallow marine facies (i.e. presence of gypsum-anhydrite) (fig. 21).

The *Sudur Suite* (fig. 16) of Tithonian and Kimmeridgian ages ($J_3km - J_3tt$) is mostly composed in its lower part of sandstones and dolomites and in its upper part of limestones. Its thickness is from 50 to 500 m. and increases southward.

The *Garovulusti Suite* (fig. 18) is very thin (50 to 60 m.) and is of Oxfordian Age (J_3o). It has a flysch facies with sandstones and sometimes limestones.

The *Shukhalicay Suite* (fig. 18) or Lower Khaltan Suite is of Lower Kimmeridgian Age (J_3km_1) and has a flysch facies with coarse sandstones.

The *Khaltan Suite* or *Middle Khaltan Suite* (fig. 18) is thicker than the previous ones (500 – 670 m.) and is of Upper Kimmeridgian Age (J_3km_2). It has a flysch facies with sandstones, limestones, conglomerates and argillites.

The *Illisu Suite* (fig. 19) of Lower Oxfordian Age (J_3o_1) is represented everywhere by alternations of shales with less thickened marls and limestones. The upper part of the suite consists of sandy and pelitomorphic shales and marls. The Ilisu Suite is developed along the southern slope of the EGC from Qabala to Balakan middle altitude mountain areas. Its thickness is up to 850 m.

The *Duzsirt Suite* (fig. 19) has a thickness that can reach 400 m. and is of Upper Oxfordian to Tithonian ages (J_3o_2- J_3tt). It is an alternation of sandstones and limestones.

The *Saki Suite* (fig. 20) of Oxfordian to Tithonian ages (J_3o - J_3tt) could be divided in three members. Near Ilisu village, the lower member consists of sand-

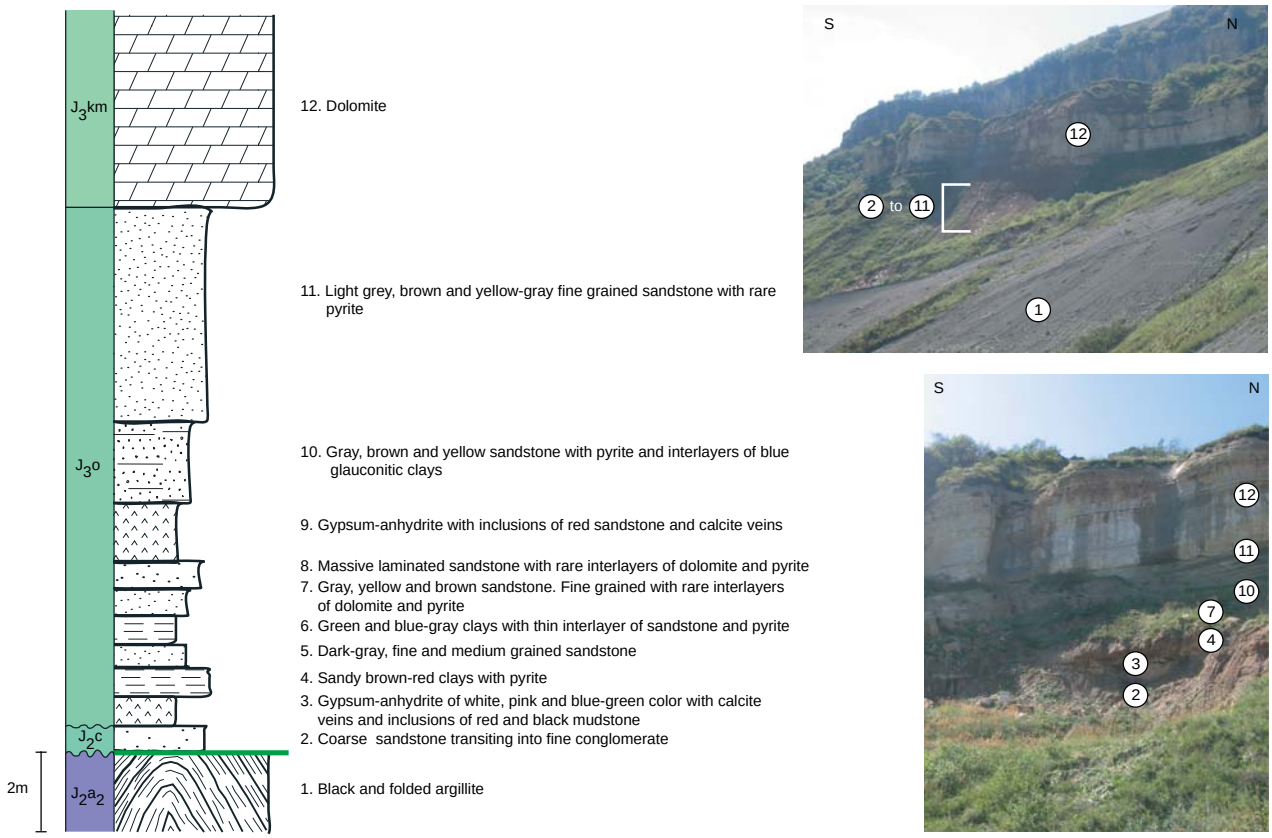

Figure 21: Stratigraphical log showing the mid-Cimmerian event. Shallow water deposits of Callovian (J2c) and Upper Jurassic (Oxfordian : J3o and Kimmeridgian : J3km) are transgressively bedded on deep water deposits of Upper Aalenian Age (J2a2). Based on fieldwork and on KANGARLI (2005).

stone and is dated from Oxfordian Age (J_3o) based on bivalves *Chlamys viminea (Sowerby)*, *Astarte ovata (Smith)* and many other. The middle member is exposed at the head of Qurmuxcay and Sincay rivers and it consists of a lower part of sandy limestones and an upper part of finely bedded limestones and sandstones with marls and clays. This middle member is of Kimmeridgian Age (J_3km), based on *Perisphinctes garnieri (Fontannes)*, *Calliphylloceras kochi (Oppel)* and others. It is mostly composed of organogenic limestones. The upper member of Tithonian Age (J_3tt) is represented by argillites, limestones and sandstones.

2.6.3. Cretaceous (K)

Sediments of Cretaceous Period consist of various lithological facies and they reach their maximum thickness (>5000 m.) on the southern slope of the EGC in the Zaqatala-Qovdag Zone. All Cretaceous ages and faunal zones are present in the EGC. Cretaceous deposits have a rapid facies change between the southern slope and the northern slope. They were deposited by an unstable regime of sedimentation. It resulted in a frequent change from turbidite facies to non-turbidite ones (ALI-ZADEH et al. 1997; ISMAILZADEH et al. 2008a).

Lower Cretaceous (K_1) Suites

Lower Cretaceous deposits have mainly a slope facies characterized by carbonate and siliciclastic turbidites. They are expressed by all stages and are concordantly built on Upper Jurassic deposits within Sudur, Sahdag-Xizi and Vandam zones. Within the Sahdag-Xizi Zone, the Valanginian-Early Aptian interval is represented by olistostromes coming from the Sahdag-Qizilqaya Nappe. They are spread in all area of the EGC and they can be divided at least in 12 suites and horizons.

Berriasian (K_1b) deposits (figs. 16, 17, 19 and 20) are present in the southern and northern slopes of the EGC. The Berriasian covers two ammonites' zones: the lower *Spiticeras obliquenodosum (Retowsky)* zone and the upper *Fauriella boissieri (Pictet)* zone. In the Xizi zone (Uqah, Dagnacay Atacay sections) the Berriasian sediments transgressively cover the different horizons of the Middle and Upper Jurassic with conglomerates at the base. In the region of Qonaqkand, Berriasian deposits are in tectonic contact with Middle Jurassic clayey shales. Berriasian-Valanginian deposits in the basins of Girdimancay, Dasagilcay, Kiscay, Sincay, Katexcay, Balakancay rivers overlie the *Saki*

Suite (Upper Jurassic). Berriasian Age is divided between several suites: the lower part of *Laza Suite* (Sudur Zone), the *Qizilqazma Suite* or *Upper Khaltan S.* (Tufan Zone), the lower part of *Babadag S.* (Zaqatala-Qovdag Zone) and the lower part of Kepuch Suite (Vandam Zone).

The Valanginian (K_1v) outcrops (figs. 16, 17, 19 and 20) are developed in the same zone as the Berriasian. The Valanginian deposits gradually evolved from the Berriasian deposits. According to ammonites *Olcostephanus Drumensis* and *Lamellaptychus didayi (Coquant)*, the Valanginian is divided respectively into a lower and an upper substage. In the eastern segment of the Zaqatala-Qovdag Trough, the deposits of Valanginian are very similar to those of the Xizi Trough. The Valanginian deposits are spread in the same suites as the Berriasian ones: the middle part of *Laza Suite* (Sudur Zone), the *Jerfi Suite* (Tufan Zone), the upper part of Babadag S. (Zaqatala-Qovdag Zone) and the upper part of *Kepuch Suite* (Vandam Zone).

Deposits of **Hauterivian age (K_1h)** (figs. 16, 17, 19 and 20) are widespread except in the northern slope (Sahdag-Qizilqaya Nappe and Sudur Zone). Due to faunal content, the Hauterivian age is divided in two substages: the lower *Lyticoceras regale (Pavlow)* zone and the upper *Speetoniceras auerbachi (Echw.)*. Foraminifera, belemnites and microfauna characterize the different suites. In all studied sections of Sahdag-Xizi Zone and also on the southern wing of Tengy-Besbarmaq anticline, lithofacies of Hauterivian deposits are significantly uniform. In eastern segment of Zaqatala-Sumqayit Zone, the Hauterivian deposits are similar to those of Xizi Zone. Hauterivian deposits correspond to the middle part of the *Laza Suite* (in Sudur Zone), to the *Kaitar Suite* (in Zaqatala-Qovdag Zone) and to the *Gyrkhbulag Suite* (in Vandam zone).

Barremian (K_1br) sediments (figs. 16, 17, 19 and 20) are widespread in all structural zones. They gradually evolve from the underlying Hauterivian deposits. These deposits are divided into two substages based on ammonites: the Lower Barremian with *Holcodiscus caillaudianus (Orbigny) and* the Upper Barremian with *Phyllopachyceras ectocostatum (Drusch)*. In the south-east the Barremian deposits have the same facies as in Sahdag and Sudur zones. Deposits of Barremian are spread in the upper part of the *Laza Suite* (in the Sudur Zone), in *the Khalcay Suite* (in Zaqatala-Qovdag Zone) and in the *Candov Suite* (in Vandam zone).

In the northern slope of the EGC, Valanginian, Hauterivian and Barremian deposits frequently include olistoliths of Upper Jurassic limestones.

Deposits of **Aptian age (K_1a)** (figs. 16, 17, 19 and 20) crop out in the Sahdag-Xizi, Zaqatala-Sumgayit, Tengy-Besbarmaq zones and they were also discovered in drillings in the northern side of EGC. In Sahdag-Qizilqaya and Sudur zones theses deposits were removed by an erosional event. The Aptian lithofacies is similar in all regions. The most complete sections of Aptian are known in south-eastern sections (Basin of Atacay River) where clays contain abundant remains of belemnites. The clayey facies of Aptian, with rich macro- and microfauna remains, can be observed in Qovdag-Sumgayit subzone (Zaqatala-Sumqayit Zone). It is divided in several suites and horizons: the *Septarian Horizon* and the *Khanaga Suite* in the Zaqatala-Qovdag Zone, the *Kohnadahar* (Lower Aptian near Candov) and the *Agbulaq Suite* (Middle-Upper Aptian) in the Vandam zone. The *Septarian Horizon* and the *Khanaga Suite* are faunistically divided into three substages: the *Dufrenoya furcate (Sowerby)* ammonite zone, the *Neohibolites inflexus (Stolley)* belemnite zone and the *Acanthohoplites multispinatus (Anthula)* ammonite zone.

Albian (K_1al) deposits (figs. 17, 19 and 20) are widespread in the same zones as the Aptian deposits and usually are concordantly bedded on them. The Albian is divided between the *Altiagac Suite*, the *Kyulyulyu Suite* and The *Ausselin Horizon* in the Zaqatala-Qovdag Zone. In central area of Sahdag-Xizi and Qovdag-Sumgayit zones, the Albian section is complete and expressed by three substages: Lower Albian and Middle Albian ages are characterized by the same facies and they contain foraminifera and belemnites *Neohibolites minimus (Lister)* and *Neohibolites pinguis (Stolley)*; Upper Albian Age contains belemnites, foraminifera and radiolarians. In section of Dubrar Mt. all three Albian substages are also known. In sections of Girdimancay River the Albian deposits are subdivided in two parts: the lower part and the upper part. Within Vandam Zone the main part of Albian section is composed of volcanoclastic rocks and is divided between the *Lahic Suite* and the *Djulyan Suite*.

Upper Cretaceous (K_2)

The Upper Cretaceous deposits have a maximal thickness in the southeastern area. Outcrops are confined to the same zones as the Lower Cretaceous ones. In the Northern slope, in observed area of Sudur Zone and Sahdag-Qizilqaya Nappe, normal marine have been accumulated. In Sahdag-Xizi, they are mainly represented by clayey and marly deposits with beds of limestones and sandstones. In Zaqatala-Qovdag Zone, they are mainly represented by flysch deposits. In the Vandam Zone, Upper Cretaceous deposits are represented by a volcanogenic-sedimentary section and flysch deposits. They are characterized by a

richness of ammonites, belemnites, inoceramus, echinoderms, corals foraminifera, ostracoda, radiolarians remains and others. In Cenomanian, Campanian and Maastrichtian deposits, spore-pollen complexes can be observed.

Deposits of **Cenomanian (K_2c)** Age (figs. 17, 19 and 20) constitute the *Kemishdag Suite* in Sahdag-Xizi and Zaqatala-Sumqayit zones and the *Yelgyadic Suite* in the Vandam zone. In Tengy-Besbarmaq Zone, deposits are discovered by drillings. In many sections Cenomanian deposits gradually evolve from Albian ones. In Sahdag-Xizi Zone, Cenomanian deposits can be observed in Buduq Trough (near Zuxur village); they are transgressive on eroded horizons of Albian and are covered unconformably by conglomerate of the Upper Turonian. In Qovdag-Sumqayit subzone (Zaqatala-Sumqayit Zone), the lithology is close to the same age deposits of Sahdag-Xizi Zone. The most complete section crops out in Dubrar Mountain and is characterized by rich complexes of benthos, planktonic foraminifers, radiolarians and pollens. In the region of Taxtayaylaq Plateau (south of Dubrar Mountain), the Cenomanian is represented by the same facies. Finally, at the base of Vandam Zone, deposits consist of tuff-conglomerate with calcareous-terrigenous flysch.

Turonian (K_2t) deposits (figs. 17, 19 and 20) crop out in Sahdag-Xizi, in the *Zorat Horizon* and *Kemcay Suite* of the Zaqatala-Sumqayit Zone and in the *Namazgah* and *Niyaldag Suite* of the Vandam Zone. Generally, they are concordantly bedded above the Cenomanian except in the Sahdag-Xizi Zone where they are transgressive on Cenomanian deposits. Lithologically the Turonian is represented by two different facies: the Lower and Upper Turonian facies. The Lower Turonian stage is generally associated with the Cenomanian stage and it consists mostly of calcareous-terrigenous facies. The Upper Turonian deposits have the same facies as the Coniacian one and both are represented by carbonate facies and have poor paleontological remains. Turonian sediments are not dispersed uniformly. In the northern slopes, Turonian deposits are exclusively represented in Sahdag-Xizi Zone and in Dubrar Mt. area. Finally, in Vandam Zone, they are represented by flysch with interbeds of tuffs and limestones.

Deposits of **Coniacian (K_2cc)** stage (figs. 17, 19 and 20) correspond to the upper part of the *Kemcay Suite* in the Zaqatala-Qovdag Zone, the upper part of the *Niyaldag Suite* in the Vandam Zone and they also outcrop in the Sahdag-Xizi Zone. In Sudur and Sahdag zones, outcrops of Coniacian deposits are unknown. Generally they concordantly cover the Turonian deposits. Faunistically the stage is characterized by a rich complex of foraminifers, radiolarians and also by rare inoceramus in the lower part. Within Sahdag-Xizi Zone, deposits have been preserved from Pre-Santonian erosion in Buduq Trough. In section of Kelevu Mt., the Coniacian stage is represented by two substages. In Qovdag-Sumqayit subzone (Zaqatala-Sumqayit Zone), the deposits are concordantly bedded on the rocks of the Upper Turonian.

Santonian (K_2s) deposits (figs. 17, 19 and 20) are concordantly bedded on Coniacian and constitute the lower part of the *Yunusdag Suite* in the Zaqatala-Qovdag Zone, the *Fitdag Suite* in the Vandam Zone and they are widespread in the Sahdag-Xizi Zone. In the latter, they are bedded on the Upper Coniacian deposits and in some places on different horizons of the Lower Cretaceous. In Qovdag-Sumqayit subzone (Zaqatala-Sumqayit Zone), the Santonian deposits are concordantly bedded on Coniacian deposits. In Sudur Zone, Sahdag-Qizilqaya Nappe and Tengy-Besbarmaq Zone these deposits are unknown. Foraminifera, rare belemnites and inoceramus characterize the Santonian deposits.

Deposits of **Campanian (K_2cm)** stage (figs. 16, 17, 19 and 20) are widespread in all basins and are represented by the same facies as the Upper Santonian ones but their thickness significantly increases. Belemnites, bivalves and foraminifers are widespread and allow distinguishing the Campanian substages. In Sudur and Tengy-Besbarmaq zones, Lower Campanian deposits of the *Kuzuntakhta Suite* are transgressive: their basal conglomerates are bedded on the Upper Barremian rocks. In Sahdag-Qizilqaya Nappe, at the base of the Upper Cretaceous section, the deposits of Lower Campanian cover unconformably the Barremian and Aptian rocks. In other zones, Campanian sediments cover the Santonian deposits and different horizons of Cretaceous and Upper Jurassic. The Campanian deposits in Qovdag and Dubrar area (Zaqatala-Sumqayit Zone) form the lower part of *Agburun Suite*; they are widespread and have similarities with those of Sahdag-Xizi Zone. On Dubrar Mt., the Lower Campanian deposits contain abundant remains of foraminifers. Southward, in section of Taxtayaylaq Plateau (south of Dubrar Mt.) area and Gilgilcay River basin the thickness of clayey beds significantly increases. In Qovdag-Sumqayit subzone (Zaqatala-Sumqayit Zone), the Campanian deposits (up to 80 m) are lithologically close to Dubrar facies and crop out along the Pirsaat River in the region of Zarat village. Good outcrops of Campanian deposits can be observed within Sahdag Zone structures, on Sahdag Mountain. The Upper Campanian is represented by the same facies as the Lower Campanian.

Maastrichtian (K_2m) deposits (figs. 17, 19 and 20) constitute the upper part of the *Agburun Suite* in

the Zaqatala-Qovdag Zone, they form the *Mudji Suite* in the Vandam Zone and also crop out in the Sahdag-Xizi Zone. Faunistically they are characterized by ammonites, belemnites, inoceramus and foraminifera. Very thin conglomerates of Lower Maastrichtian remain in Sudur Zone. In Sahdag-Xizi Zone Maastrichtian deposits have been preserved in some section of Xizi Trough as a result of recent erosive cut. On Gora Kelevu the deposits of Maastrichtian stage are represented only by the lower substage. In Zaqatala-Sumqayit Zone and Dubrar Suite, Maastrichtian deposits are widely developed and connected with Campanian by gradual transition. The complete section of Maastrichtian crops out in the area of Diyalli village. The Upper Maastrichtian is represented by the same facies as the lower stage.

2.6.4. Paleogene (P)

The Paleogene deposits are expressed by all stages and are present in all areas of the northern and southern slopes of the EGC. They are not present in the central Tufan Zone. In the northern slope, within the Sudur Zone, thin remnants unconformably lie on Lower Cretaceous carbonates. Within the Sahdag-Xizi Zone, the Paleogene deposits remain in two places: in the Buduq Trough where they are conformably bedded on Upper Cretaceous deposit and in the southeastern deposits where they are transgressive on Barremian-Early Aptian and Santonian-Campanian deposits. In the southern slope, within Qovdag-Sumqayit Subzone (Zaqatala-Sumqayit Zone), Paleogene deposits arew conformably built on Upper Cretaceous deposits. Within the Vandam Zone, they are present on both side of the uplifted part. Finally within the Samaxi-Qobustan and Abseron zones, deposits constitute the lower part of Cenozoic section. Lithologically, Paleogene formations are mainly flysch in the lower and middle parts and have a sandy-clayey lithofacies in the upper part (Ali-Zadeh et al. 1997; Ismailzadeh et al. 2008a).

Paleocene (P_1)

In the Eastern Greater Caucasus (EGC), Paleocene deposits were deposited in a marine basin. The transition from Maastrichtian to Paleocene stages was marked by a regional uplift in the NE and SW of Azerbaijan and also by an important downwarping of the central part of the basin. This downwarping was not constant and varies in space and time. The depth of the basin varied frequently from coastal to shallow water. The smallest depths areas in the Paleocene basin are the west part of the Qusar-Davaci Megazone, the Ganca and Muradxanli (Kura) regions. The deepest area was located in the Abseron Peninsula and in the central and south Qobustan (at least 5000 m of sediments). The presence of some species of nummulites and foraminifera are in favor of a mainly warm climate with certain intervals of hot climate close to tropical.

Paleocene deposits (figs. 17, 19 and 20) are spread within the Sahdag-Xizi Zone, Zaqatala-Sumqayit Zone (*Ilkhidag* and *Sumqayit suites*) and Vandam Zone (Upper part of *Ahohcay Suite*, Zarnava and Sumqayit suites). In the Sudur and Sahdag-Xizi zones they are mainly represented by clays and marls with interlayers of limestone and sandstones. In the Zaqatala-Qovdag and Vandam zones, they correspond mainly to flysch deposits.

Eocene (P_2)

Eocene deposits are widespread in the EGC and are distributed inside the *Koun Suite*. They conformably lie on the Upper Paleocene deposits and they are present in Sudur (fig. 16), Sahdag-Xizi (fig. 17), Zaqatala-Sumqayit (fig. 19), Samaxi-Qobustan, Abseron and Vandam zones (fig. 20). In some places, they contain vegetal remnants, fish fossils and jarosite. The geotectonic surroundings of the sedimentation basin were nearly the same as during the Paleocene. Only the Tufan - Sahdag area show no Eocene deposits suggestion. Stratigraphically they are divided into three parts.

The Lower Eocene is characterized by terrigenous deposits. Deposits conformably lie on the Upper Paleocene deposits. Their formation took place in a relatively deep marine basin.

The facies of the Middle Eocene deposits shows an explosive activity of the volcanic zones of the southern flank together with a wide transgression. There is sedimentation of the volcanic eruptions products. Their lacks in the north of the EGC, probably, demonstrate the role of the Sahdag uplift as a barrier on the possible way of the volcanic material to the Lower Eocene Basin. The main sources of the removal material were the Greater and Lesser Caucasus and the centers of volcanic eruption.

The Upper Eocene period is characterized by a wide transgression, by a fast downwarping of the Lower Eocene Basin, and finally by the accumulation of thick terrigenous deposits. By the end of the Upper Eocene, the velocity of downwarping was not compensated by the sedimentation and mainly deep, clayey sediments were deposited in a low oxygen environment. The centre of downwarping was located near the cities of Barda and Agcabadi where the thickness of deposit is 1200 m. The climate was probably mainly warm close to tropical (based on fauna analysis). These deposits are potential hydrocarbon source rocks.

In Vandam zone (fig. 20), magmatic formations of Eocene age are represented by intrusive bodies (Buynuz) with an absolute dating between 43 and 68 Myr.

Oligocene (P_3)

Oligocene sediments (figs. 16, 19 and 20) were accumulated in a shallow sea basin, the Maykop Basin and form the lower part of the *Maykop Suite*. This basin became shallower towards the uplifted part of the Qusar-Davaci Megazone, as well as towards the northern slopes of the Lesser Caucasus and the Talysh mountain system. It is characterized by a coastal environment towards the northern slopes of the Lesser Caucasus. The deepest portion of this basin was located in the Abseron Peninsula and northern Qobustan. In the Sahdag-Xizi Zone (fig. 17) Oligocene deposits are not widely spread and they contain concretions, fish remnants and coating of Jarosite. In Samaxi-Qobustan and Zaqatala-Sumqayit zones (fig. 19), Maykop deposits are widespread. Generally the deposits are poor in microfauna.

The Maikop Basin had good properties for accumulation, burial and transformation of organic matter into oil hydrocarbons. Accordingly, the Maykop deposits are famous for being a productive sequence of hydrocarbon EFENDIYEVA (2004).

2.6.5. Neogene (N)

In the Sahdag-Xizi Zone, the Neogene deposits had remained in Buduq Trough where they are represented by typical shallow marine sediments of Sarmatian age (Serravallian) and marine-continental deposits of Late Pliocene. Along the Caspian Coastline and in front of the EGC slopes, Middle Miocene deposits lie transgressively on the Oligocene ones.

Miocene(N_1)

The Miocene deposits (figs. 16 and 17) are widely spread in intermontane and foothill area around the EGC and also in the Caspian Sea basins. They contain oil and gas deposits and also non-ore deposits. In the EGC surroundings, all Miocene deposits are of marine origin.

Lower Miocene deposits take part of the *Maykop Suite* and are part of the *Sakaraul Regiostage* in the EGC.

Middle Miocene deposits are divided in four regiostages: the *Tarkhan*, *Chokrak*, *Karagan* and *Konk* regiostages.

The Upper Miocene deposits are divided in three regiostages: The *Sarmatian*, the *Meotic* and the *Pontian regiostages*. The *Sarmatian regiostage* deposits are spread in northern slope of the EGC, in the Abseron and Samaxi-Qobustan zones. They are especially rich faunistically. Upper Sarmatian deposits can be found at 3600 m on the Sahdag Mt. peneplain and contain *Mactra crassicolis (Sinz)*, *Mactra caspia (Eichwald)*, *Mactra sp.* and *Mactra bulgarica (Toula)* (BUDAGOV 1963). The *Miotic Regiostage* deposits are present in the same zone as the Sarmatian ones. The *Pontian Regiostage* deposits are everywhere bedded transgressively on older Miocene deposits and they are represented by three different facies: a marine, a continental and a volcanogenic facies. The marine facies is spread in the eastern Azerbaijan and is represented by coastal shallow and deep water facies. Continental and volcanogenic facies are spread in the central and western regions of Azerbaijan.

Pliocene (N_2)

Pliocene deposits have four different facies: continental, shallow coastal (up to 50 m deep), shallow (50-200 m deep) and relatively deep (up to 1000 m). They contain numerous turbidite deposits. All these facies crop out in the northern slopes of the EGC, in the Abseron and Samaxi-Qobustan zones.

The **Lower Pliocene (N_2^1)** deposits correspond to the productive series and they differ by their respective content in oil, gas and condensate but also by their facies. Their thickness can reach 5000 m. The eroded terrigenous material came from relief as the Russian platform and the Greater Caucasus. These deposits have been described precisely in numerous publications and they will not be described more precisely in this work.

The **Upper Pliocene (N_2^2)** deposits of the *Akchagyl Stage* play an important role in the geological structure of Azerbaijan oil and gas bearing area. The abundance of these deposits in Azerbaijan's rocks is accounted to the Akchagyl transgression. It began as early as the Upper Pliocene period and reached its peak in the Upper Pliocene. Therefore the boundaries of the Caspian Sea extended considerably. In the Middle Pliocene period, the major sinking zones were linked to the Terek-Caspian Trough, the South Caspian Basin and the west Turkmenian depression. In spite of a steady tectonic regime, volcanic activity took place in the peripheral parts of the depression. The evidence of this activity is the presence of interlayers of volcanic ashes in the Akchagyl deposits. Even if a regression took place at the end of the Akchagyl and Abseron stages, it was insignificant. In the Kura depression, the shores of the Akchagyl Sea overlapped not only the shores of the Early Pliocene Basin but also

those of the older basins of the Miocene Sea (including the Pontian Sea) and in some places even those of the Paleogene Sea. For this reason, the Akchagyl deposits transgressively lie on older deposits along the border of the Kura depression. In the buried structures of the Kura depression, the productive sequences are overlapped by the Akchagyl Stage without any significant signs of breaks and unconformity. In the Qusar-Davaci Megazone lowlands (in the country between the Samur River and the Valvalacay River) the *Akchagyl Stage* consists of shallow marine and fresh water facies while between the Davacicay and the Gilgilcay rivers it consists of a deep water clayey facies. In the Abseron Peninsula, Eastern and Central Qobustan, the Akchagyl section consists of the same facies having interlayers of volcanic ashes. Hydrocarbon accumulations have been discovered in the Akchagyl deposits of the Pri-Kura area. These local reservoirs are located in some anticlinal uplifts. Here the hydrocarbon is accumulated in granular reservoir rocks alternating with clayey facies.

2.6.6. Quaternary (Q)

In the EGC and its foothills, Quaternary variation of the eustatic level of the Caspian Sea reached to an alternation of marine and continental lithofacies. These variations let also one of the most prominent geologic archives directly related to uplift: the marine and river terraces. Up to 14 levels of terraces are recognized and reach into the valleys of the Greater Caucasus. The continental deposits are very thick due to the intensive erosion of the uplifting EGC. Quaternary sediments are spread all around the EGC. Volcanism adds periodic volcanoclastic deposits during Quaternary Period.

Pleistocene (Q_1)

The Pleistocene is represented by molasses-type deposits and expressed by marine, continental and transitional facies. Around the EGC, it is one of the main constituents of the old extensive alluvial fans and fills the different basins. The Greater Caucasus and the Lesser Caucasus were the main sources for clastic products. These sediments are the consequences of the erosion of the young Greater Caucasus. It thickness can reach one hundred meters in continental places, up to 1200 m in the intermontane depression (Kura and Terek basin) and up to 2000 m in the South Caspian Basin. Intercalation of periodic volcanic sediment can be observed. Oil- and gas-bearing deposits are confined mainly to the deep marine deposits in the eastern part of the Kura depression. The Pleistocene could be divided in several stages: the *Tyurjan Beds*, the *Lower* and *Upper Baku Horizon*, the *Mingechaur Beds*, the *Lower* and *Upper Khazar Horizon* and the *Lower* and *Upper Khvalyn Horizon*.

Holocene (Q_2)

Holocene Age like all the Quaternary Period is represented by marine and continental lithofacies.

The marine deposits are concentrated along the coastline and in the bottom of the Caspian Sea. Onshore they correspond mostly to small terraces of some meters and contain shells with, in some places, interlayers of mud volcanoes breccia.

The continental deposits are more widely spread than the marine deposits. They correspond to alluvial, aeolian and mud volcanic formations. In Alazani Basin (Ganih-Ayricay Zone), their thickness reaches hundreds meters but generally they are less than ten meters thick. The mud volcanoes deposits are expressed by non-laminated clays with rock fragments of different age (Cretaceous to Quaternary inclusive) and their thicknesses vary from tens to hundreds meters depending on eruptions intensity.

*****

3 - Structural geology, stress and strain across the Eastern Greater Caucasus (Azerbaijan)

M. Bochud[1,‡], J. Mosar[1], T. Kangarli[2], A. Rast[1]

[1]Earth Sciences, Department of Geosciences, University of Fribourg, Chemin du Musée 8, 1700 Fribourg, Switzerland
[2]Geological Institute of Azerbaijan (GIA), National Academy of Sciences, 29A H. Javid Av., Baku, AZ1143, Azerbaijan
[‡]Email : martin.bochud@unifr.ch

Abstract

The Eastern Greater Caucasus (EGC) corresponds to the Azeri part of the Caucasus, the Europe's largest and highest mountain belt.

The aims of this study were to explore the EGC, to find key outcrops and to measure and study them in order to improve our knowledge of the area. Several fieldtrips were made during summer periods in the remote valleys of the EGC.

The geometry of the EGC is characterized by folds with fold axes slightly deeping to the ESE with fold axes deeping to the NNE and SSW respectively in the southern and northern slopes with a change in the central part of the orogen. From north to south the EGC is cut by numerous thrusts. Both folds and thrusts can be associated to a flower structure of the orogen. However the northern slope structures geometry is influenced by the presence of the Sahdag-Besbarmaq Nappe that modified the behaviour of the area. Finally, the present valleys geomorphology and orientation is influenced by conjugate NNE-SSW and NNW-SSE strike-slip faults; secondary faults could be associated with a Riedel model.

Based on field observations and data, we deduced that the area underwent a constant NNE-SSW directed stress since the Middle Jurassic Epoch. This stress is linked successively with the closure of the Neotethys and the continent-continent collision between Arabian and Eurasian plates. The measured structures and calculated stresses are globally consistent with this main stress. However special behaviours can be locally observed. Within the structures and stresses, it is not possible to distinguish several directions of deformation but based on field observations, it is possible to see different phases in the geological evolution.

Studied outcrops show clearly an alternation of compressional and extensional events in the EGC since the Middle Jurassic Epoch. A late (probably Quaternary) strike-slip regime affected the area and influences the present geomorphology. The inversion of the Greater Caucasus Basin (GCB) and the uplift of the central area, the Tufan structural zone, probably started earlier, at the end of Eocene when the Arabian plate started to collide with Eurasian plate. Based on marine deposits in altitude, the main uplift of the EGC is post-Sarmatian (Serravallian Age – 11.6 to 13.8 Myr – 0.31 mm/yr) with an acceleration in the Pliocene (0.77 mm/yr). The present frontal active zone is located under the Qaramaryam hills in the south at the border of the Kura Basin: an anticline-syncline-anticline structure can be observed inside Plio-Quaternary sediments.

Keywords: *Eastern Greater Caucasus, structure, stress, evolution.*

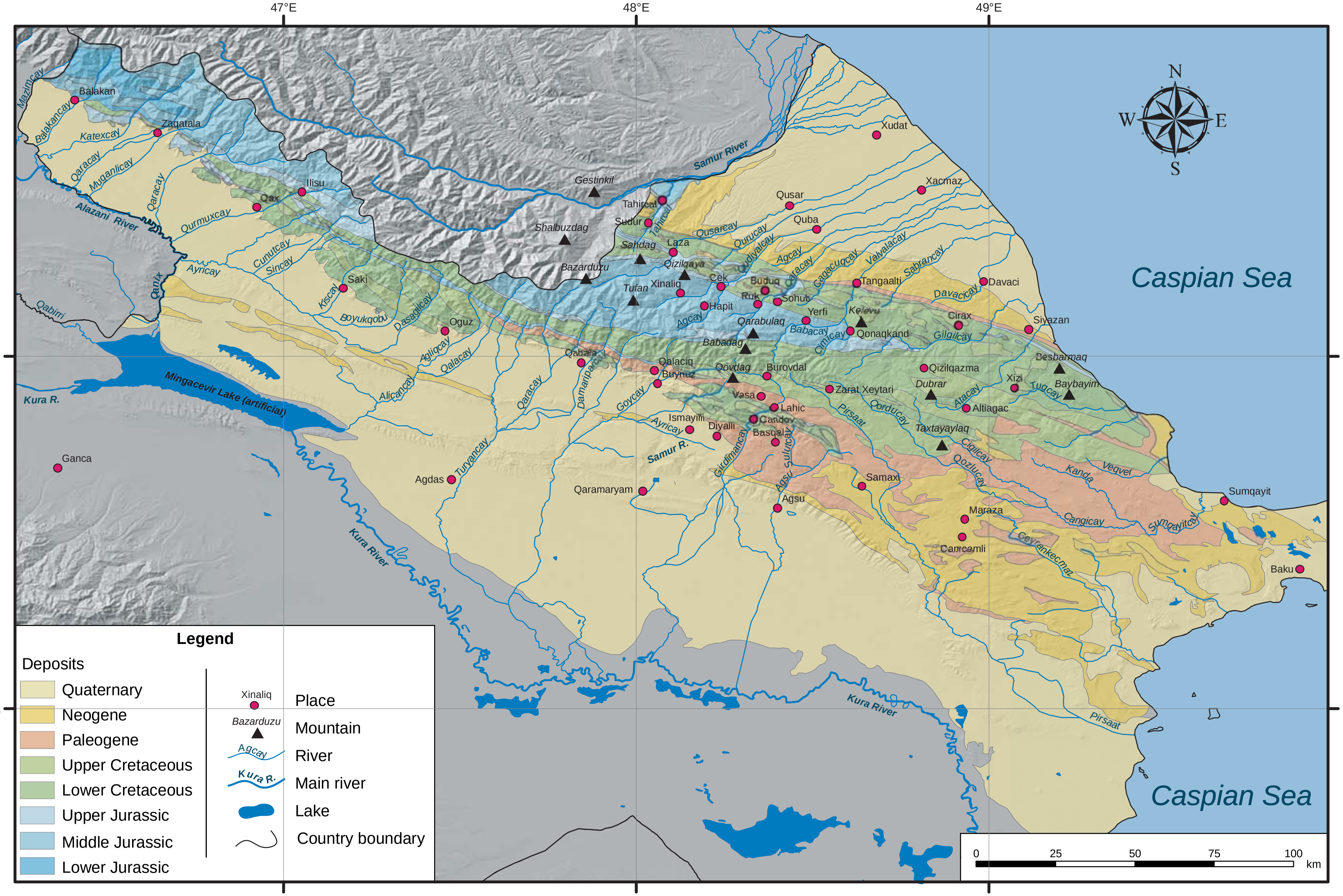

Figure 22: Simplified geological map of the EGC of Azerbaijan with the main rivers, summits and places (names based on the GEOnet Names Server (GNS) from the National Geospatial-Intelligence Agency's (NGA) of USA.

3.1. Introduction

The EGC is located in the northern part of Azerbaijan. It corresponds to the eastern termination of the Greater Caucasus and extends from the border with Georgia, goes along the border with Russia and finishes near Baku, the Azerbaijan capital (fig. 22). The country and its capital, are known for their numerous oil fields, mud volcanoes and gas seepages since Antiquity. These hydrocarbon resources are closely linked to the building history of the Caucasus and its surrounding sedimentary basins: i.e. the South Caspian Basin which is one of the world deepest intracontinental basins and underwent a rapid subsidence between Oligocene – Miocene times (Brunet et al. 2003).

The highest summits are the Bazarduzu Mt. (4466 m), the Sahdag Mt. (4243 m), and the Tufan Mt. (4191 m). All are located in the central area of the mountain range near the border with Dagestan (Russia) (fig. 22). Glaciers are not present anymore in the EGC, only firns can be found in places like Bazarduzu Mt., Sahdag Mt. or Tufan Mt. Remnants of glaciations like moraines and U shaped valley can be seen in the same area but are difficult to distinguish due to the high erodability of the rock

The EGC is drained mainly by high energy rivers flowing in straight and V shaped valleys. Only in the surroundings of the EGC, rivers change to an anastomosing form (i.e. Samur River in the north) or even to a meandering form (i.e. Kura River in the south) (fig. 22). Numerous fluvial terraces can be found in the central part, some of them associated with temporary lakes due to local landslides and others to the uplift of EGC.

A tight collaboration with the Geological Institute of Azerbaijan (GIA) made it possible to collect observation and data in key areas of the Eastern Greater Caucasus (EGC) in several expeditions since 2003. This allowed us describing and analysing the main structural features of the EGC including the paleostress field. Tectonic and paleo-tectonic structures since the early Mesozoic (early-mid Jurassic) until present were integrated into a geodynamic model of the evolution of the EGC orogen.

During fieldwork “classic” field techniques were used: notebook, compass, lens, outcrops sketches, samples and pictures. To improve the efficiency in the remote places of the EGC, we used a GPS and a field computer containing a geodatabase, detailed maps and satellite images of the area. The field data were directly entered in the geodatabase through the GPS and the field computer.

3.2. Geology of the EGC

The Greater Caucasus and its eastern part, the EGC, are the result of the inversion of a deep sedimentary Jurassic-Paleogene sedimentary basin, the Greater Caucasus Basin (GCB) and its northern passive margin. Since the Jurassic period, the Greater Caucasus Basin underwent compressional and extensional events and was successively filled by the erosion products of the bordering areas. The orogenic evolution is successively linked to the subduction of the Paleotethys (during Trias-Jurassic periods), to the subduction of the Neotethys (during Jurassic, Cretaceous and Paleocene periods) and finally to the continent-continent collision between Arabian and Eurasian plates (during Tertiary Period) (Brunet et al. 2009b; Sosson et al. 2010a).

The GCB can be considered as a back-arc basin created to the north of the Neotethys subduction, which was active from Jurassic to Paleocene (Egan et al. 2009; Ershov et al. 2005; Zonenshain & Le Pichon 1986). Remnants of the basement of this basin are present from the South Caspian Basin to the Eastern Black Sea and outcrops in the central part of the Greater Caucasus in Georgia (Brunet et al. 2009b; Sosson et al. 2010a).

The overall geodynamic setting of the EGC corresponds to a doubly verging mountain belt with a major southern pro fold-and-thrust belt and a retro fold-and-thrust belt in the north (Mosar et al. 2010). The pro-wedge is located to the south and overrides the Kura Basin (Forte et al. 2010; Philip et al. 1989), whereas the retro-wedge overrides the Terek Basin to the north. During Pliocene times, subduction initiated towards the north along the Abseron Ridge developed at the transition of the deep SCB to the shallow NCB (Egan et al. 2009; Green et al. 2009). The Abseron Ridge also forms the extension of the GC into the Caspian Sea.

The depth of the Moho changes from about 40 km in the south beneath the Kura Basin to more than 50 km beneath the EGC and rises back to 40 km under the northern foreland basin (Brunet et al. 2003; Ershov et al. 2003). The pre Jurassic basement of the Kura area shows three distinctive basins with varying depths and rises under the EGC (fig. 23) : the Western Middle Kura Basin or the Alazani Basin that forms the first foreland basin directly to the south of the EGC; the Eastern Middle Kura Basin that corresponds to the main plain between the Lesser Caucasus and the GC; the Lower Kura Basin that corresponds to the western part of the SCB.

GPS studies in the large Caucasus-Middle East region show convergence rates in the EGC area be-

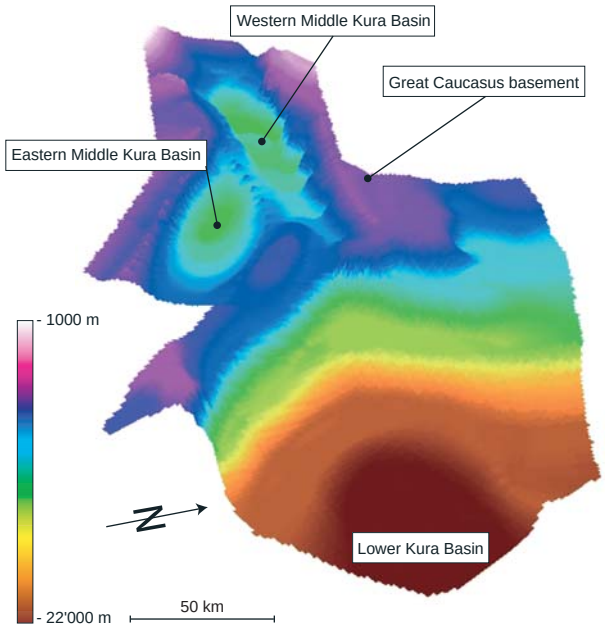

Figure 23: 3D model of the Pre Jurassic basement south of the EGC (vertical exaggeration: 5x) based on a map from Beicip Franlab. It shows that a basement high divides the Lower Kura Basin and the Eastern Middle Kura Basin. The Lower Kura Basin corresponds to the western part of the South Caspian Basin.

tween 6 to 14mm/yr (McClusky et al. 2000; Reilinger et al. 2006; Vernant et al. 2004). Detailed studies on Azerbaijan (Kadirov et al. 2008) determined convergence rates decreasing from east to west from 10±1mm/yr (48°E Long.) to 4±1 mm/yr in NW Azerbaijan (46°E. Long.). Surface uplift rates based on several types of information (see review in Mitchell & Westaway 2010 and Mosar et al. 2010) are in the range of 0.33 and 1.00 mm/yr for the last 10 Myr.

Structurally, the southern fold-and-thrust belt is characterized by major thrusts to the south with associated folds (Kangarli 2005). Some local nappes can be also observed in this area. We observe a change of structural direction from the thrusts and from axial planes that change northeastward from a NNE dip to a SSW dip in the central area. In the north, the Sahdag-Besbarmaq Nappe is the main structural element. After a first S-directed movement, the whole nappe was backthrusted to the north and folded the underlying structures of the northern area. Very low grade metamorphism can be observed in the central zone of the EGC and is generally expressed by schistosity in the argillites of the Middle Jurassic and also in the Valanginian carbonate turbidites. Finally, all the EGC structures are cross-cut by strike-slip faults: the anti-caucasian faults which exhibit general NE-SW and a N-S orientations. They clearly influence the geomorphology of the valleys. Based on GPS measurements Reilinger et al. (2006) determined a dextral strike-slip regime in Azerbaijan with velocities varying from 5.3±0.3 mm/yr in the NW, 0.7±0.4 near Ismayilli to 10.7±0.5 mm/yr near Samaxi.

Lithologies in the EGC from Jurassic, Cretaceous and Paleogene are mainly represented by deep marine and slope facies except on the northern side of the present EGC where shallow marine and platform formations were deposited and correspond to the southern shelf of the former Scythian Platform (figs. 22 and 26). Since the beginning of the main orogenic phase during Oligocene times, the eroded sediments of the uplifted area were accumulated in foreland molasse type basins: i.e. Terek and Indol-Kuban basins in the north of the Caucasus; the Rioni and Kura basins in the south, and also the deep sedimentary basin of the South Caspian Basin to the SE. A Miocene sea probably mostly covered the nascent relief of the Greater Caucasus. Remains of these marine deposits can be seen presently up to 3600 m in the EGC (Budagov 1963). Due to the major eustatic variations of the Caspian Sea during Pliocene and Quaternary times, marine formations were deposited alternating with continental ones at the EGC fringes. Finally, the volcanic and magmatic activity remnants on the southern slope of the EGC have their origin in the volcanic arc resulting from the subduction under the meridional portions of the GCS forming the present Lesser Caucasus supra-subduction volcanic arc. It resulted in major deposits of volcanogenic sediments and intrusive rocks. They are mostly of Jurassic to Middle Eocene epochs (i.e. Buynuz intrusion on the southern slope) (Sosson et al. 2010c).

3.3. EGC STRUCTURAL ZONES AND THEIR STRUCTURES

The EGC is subdivided into 3 mega zones which are divided into 17 structural zones. Some of them are themselves divided into several subzones (Ismailzadeh et al. 2008a; Kangarli 2005).

The 3 megazones are the Eastern Greater Caucasus Megazone, the Qusar-Davaci Megazone in the north and the Kura Megazone in the south (fig. 25).

The **Qusar-Davaci Megazone** corresponds to the northern foreland basins and includes to the N the Xacmaz Zone (Xm) and to the S the the Quba-Cilagir Zone (Qb). Both zones are composed of Paleogene and Neogene deposits that cover unconformably Mesozoic-Paleozoic deposits. Both zones are separated by the Imamqulukand-Xacmaz Fault with a top the south. The Siyazan Thrust separates to the S the Quba Zone from the structural zones of the northern slope of the EGC (Ismailzadeh et al. 2008a) which override the Quba Zone in a top to north movement.

The **Kura Megazone** is located between the EGC and the Lesser Caucasus and corresponds to the southern foreland basin of the EGC. In the north, it is overrides by the EGC Megazone through the southern active thrust front in a top to south movement. It is divided into five zones. Our study is concerned only by the two northeastern zones: the Ajinour Zone and the Kurdamir-Saatli Zone.

The **Eastern Greater Caucasus Mega Zone** is divided into 13 structural zones (fig. 25): the Tahircal Zone (Tc), the Sudur Zone (Sd), the Tengy-Besbarmaq Zone (TB), the Sahdag-Qizilqaya Nappe(SQ), the Sahdag-Xizi Zone (SX), the Qonaqkand Zone (Qk), the Tufan Zone (Tf), the Zaqatala-Qovdag Zone (ZQ), the Vandam Zone (Vm), the Basqal Nappe (Bq), the Ganih-Ayricay Zone (GA), the Samaxi-Qobustan Zone (SQ) and the Abseron zone (Ab) around Baku and extending towards the Abseron Ridge (Ismailzadeh et al. 2008a). The EGC structural zones and their particularities are described in the next sections. A map of the main structural zones, 5 stratigraphic sections and a synthetic cross-section of the EGC are respectively represented in figures 25, 26 and 27.

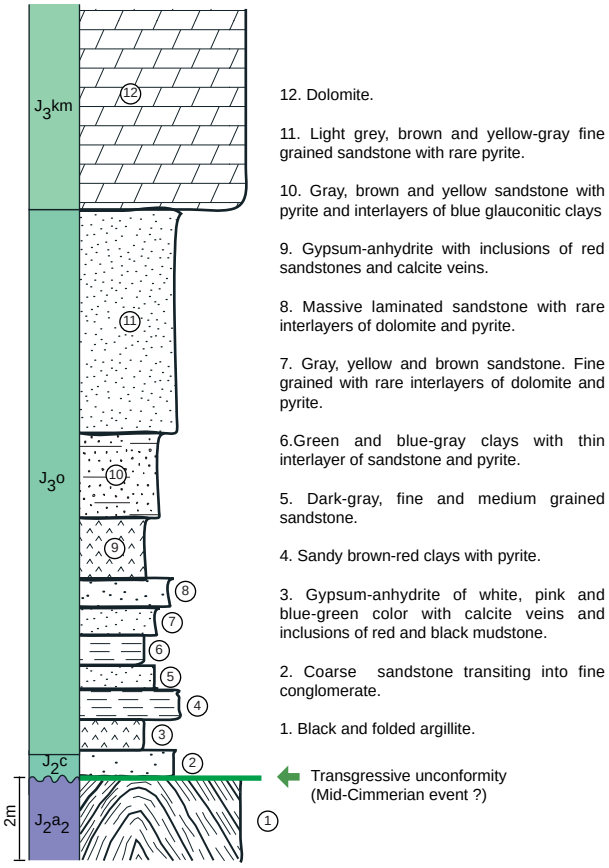

Figure 24: Transgressive contact between the deep marine and folded Upper Aalenian (J2a2) deposits and the shallow marine deposits of Callovian (J2c) and Upper Jurassic (Oxfordian: J3o and Kimmeridgian: J3km). Modified from T. Kangarli, unpublished. Located by point L1 on figure 25. Plate 3.1A, E and F.

3.3.1. Tahircal Zone

The Tahircal Zone (Tc on figs. 25, 26, 27) is located along the northern border of Azerbaijan and extends mostly into Dagestan (Russia).

Lithologically it is characterized by Middle Jurassic deep marine deposits (mostly of Aalenian Age with a thickness up to 2500 m) covered by Paleogene and Neogene marine and continental deposits (Plate 3.1 A, B, C and fig. 26). This is the second most important zone containing Middle Jurassic deposits which can be observed up to altitudes of approximatively 2000 m on the northern banks of the Samur River on the Gestinkil Mt. (Plate 3.1-A). No remnants of Cretaceous deposits can be observed in the Tahircal Valley.

Structurally, we observe three anticlines north of Tahircal Village (figs. 36 and 37-A). Bedding poles distribution show a gently ESE dipping fold axes (fig. 38-A). As illustrated on Plate 3.1-D, fold axial planes are dipping to the north. Further N, however, at the transition with the Sudur Zone fold axial surfaces are south dipping (Plate 3.1-F).

Paleogene, Neogene, Quaternary transgressive events

In the Tahircal Zone but also in the Sudur Zone, flat lying Paleogene, Neogene and Quaternary deposits transgressively overly the folded Middle Jurassic and Lower Cretaceous deposits. They illustrate several tectonic and transgressive events that uplifted older rocks and allowed their erosion. Paleocene and Lower Miocene sediments fill the inner part of the Sudur Zone synclines. Subsequently, an erosive event cuts the upper part of the Sudur Zone anticlines as well as the Paleocene-Lower Miocene deposits. Finally, a transgressive event covers the eroded area with Upper Miocene to Lower Quaternary marine to continental deposits. Total thickness of Paleogene to Quaternary sediments can reach 2000 m.

Good outcrops can be observed along the northern part of the Tahircal Valley (plate 3.1-C, D) were flat bedded Quaternary deposits lie on Middle Jurassic (Aalenian to Bathonian) deep marine sediments. In Dagestan, along the northern side of the Samur River, flat bedded Pliocene sediments are transgressive on Middle Jurassic (Bajocian, Bathonian) sediments. North of Laza Village along the Qusarcay River, thick deposits of Pliocene conglomerates can be observed.

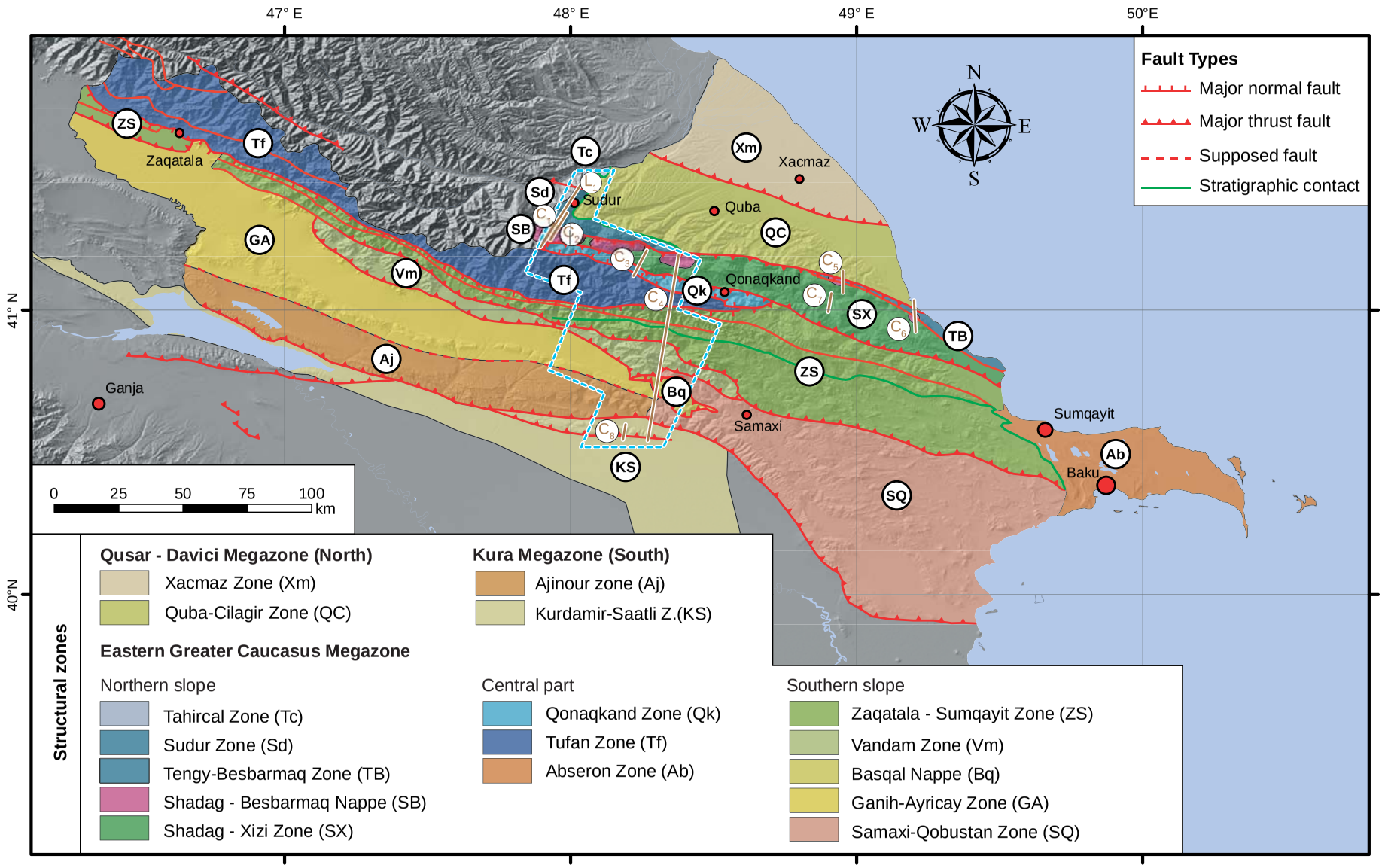

Figure 25: Simplified tectonic map of the Eastern Greater Caucasus showing the different tectonic Megazones and their zones. Cross-sections (brown line with the identifier), strati-graphical log (identifier only) and the detailed structural map (blue dots) from the chapter are also represented on the map: Cross-sections (C1), (C3), (C4) correspond to the figure 37-A, B and C; (C2) to figure 29; (C5) to figure 30; (C6) to figure 31; (C7) to figure 32, (C8) to figure 33; L1 to figure 24. Modified from Kangarli (2005).

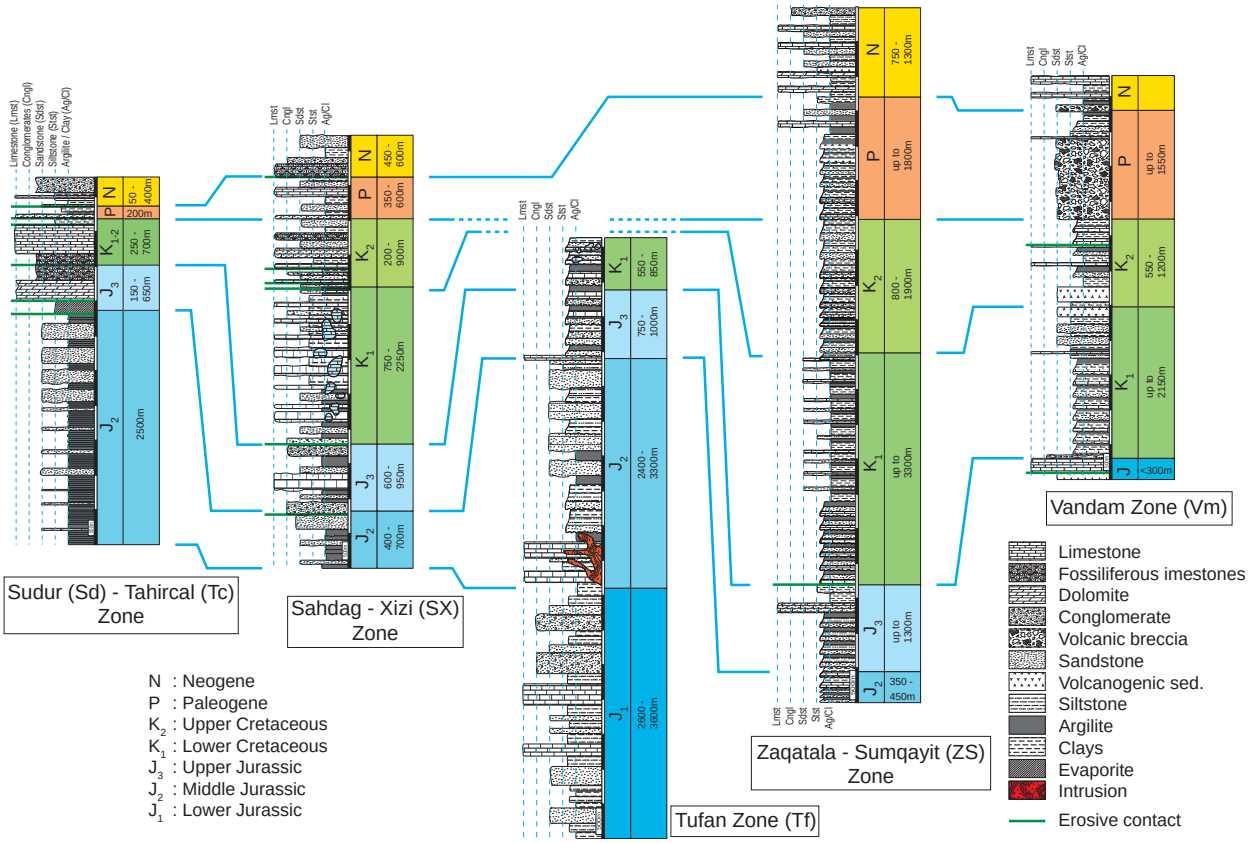

Figure 26: Stratigraphic sections of the 5 main structural zones of the EGC. J1: Lower Jurassic; J2: Middle Jurassic; J3: Upper Jurassic; K1: Lower Cretaceous; K2: Upper Cretaceous; P: Paleogene; N: Neogene.

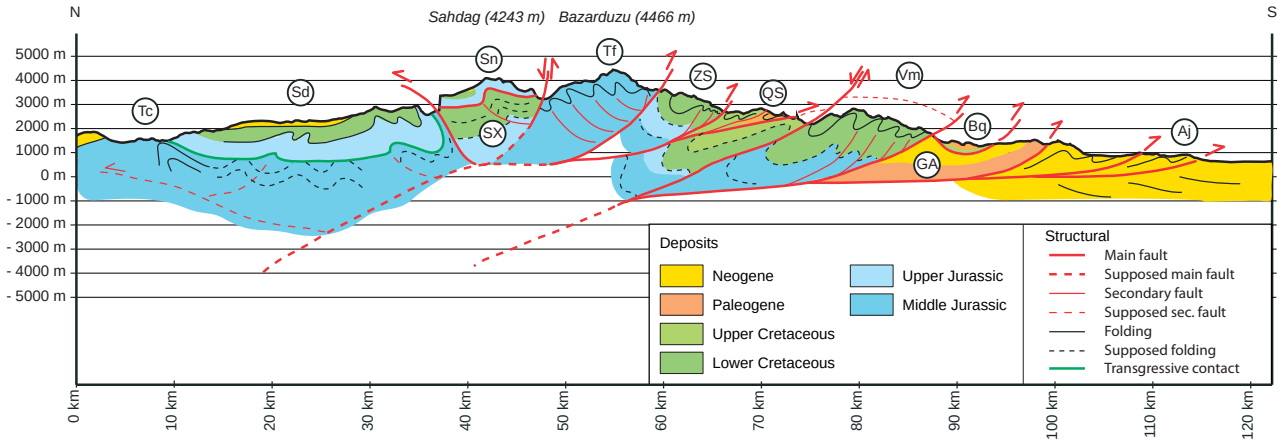

Figure 27: Simplified Cross-section with the main structures and the structural zones: Tc: Tahircal Z.; Sd: Sudur Z.; Sn: Sahdag-Besbarmaq Z.; SX: Sahdag-Xizi Z.; Tf: Tufan Z.; ZS: Zaqatala-Sumqayit Z.; QS: Qovdag-Sumqayit Z.; Vm: Vandam Z.; Bq: Basqal Nappe; GA: Ganih-Ayricay Z.; Aj: Ajinour Z.

3.3.2. Sudur and Tengy Besbarmaq zones

The Sudur Zone (Sd on figs. 25, 26, 27) and its eastern equivalent the Tengy-Besbarmaq Zone (TB on fig. 25) crop out along the northern slope of the EGC. The southern border is in tectonic contact with the Sahdag-Xizi Zone and with the Sahdag-Besbarmaq Nappe (Plate 3.2 E). The Sudur Zone contains well developed structures of several kilometers. The Tengy-Besbarmaq Zone is narrower and consists of subvertical Upper Jurassic and Lower Cretaceous deposits. Both zones are the roots of the Sahdag-Besbarmaq Nappe.

Lithologically, the Sudur Zone is mostly composed from base to top of Callovian-Oxfordian evaporites, Kimmeridgian dolomite (Plate 3.1.E, Plate 3.2-F), Lower Cretaceous shell rich limestones (Plate 3.1-G, Plate 3.2-E) and breccia limestones. The Tengy-Besbarmaq Zone is mostly composed of thick layered limestones of Upper Jurassic to Lower Cretaceous. Most of the Upper Cretaceous sediments cannot be observed.

Structurally, the Sudur Zone consists of 5 linear anticlines with their associated synclines in Jurassic and Lower Cretaceous formations (Plate 3.2-A, B and figs. 36, 37) (Kangarli 2005). 2 anticlines of 5 can be observed along the Qusarcay River. Structures along the western bank are continuous and well defined (Plate 3.2-A). Structures of the eastern bank have smaller amplitude (Plate 3.2-B) and have secondary faulting (Plate 3.2-D). Moreover the first anticline is closer to the contact with the Sahdag-Besbarmaq Nappe (Plate 3.2-B). Finally, on both sides, an inverted fold can be observed near the contact with the Sahdag-Besbarmaq Nappe (3.2-A, B, E). To the west, Middle-Upper Jurassic sediments are in contact with the Nappe while Lower Cretaceous sediments are in contact with the Nappe in the east. Based on these features, we suggest that the Qizilqaya Massif was probably more backthrusted or under different conditions than the Sahdag Mt.

Bedding planes slightly dip to NNE and SSW (fig. 38-B). Fold axis gently plunge to ESE. Based on field observation, major fold axial planes are dipping to the north except a huge fold near the contact with the Sahdag Nappe and secondary folds that have axial planes dipping to the south.

Mid-Cimmerian Event in the EGC

A pre-Callovian event marks the limit between the Tahircal and Sudur zones. Lithological and structural unconformities can be observed in the northern slope of the EGC. Aalenian deep marine and folded sediments of the Tahircal Zone are transgressively covered by shallow marine and flat lying evaporitic sediments (gypsum, anhydrite and dolomite deposits) of Callovian to Kimmeridgian ages, themselves evolving to platform and reef deposits (Plate 3.1 A, E, F, G and fig. 24).

This latter is considered to be related to an orogenic, hence compressional event since we observe rather tight folds cut by an erosive unconformity. The debate remains however open, and in the absence of any other evidence we adhere to the orogenic event explanation.

Good outcrops can be observed along the Tahircal Valley (Plate 3.1-E, F) and in Dagestan on the Gestinkil Mt. (Plate 3.1-A).

3.3.3. Sahdag – Besbarmaq Nappe

The Sahdag – Besbarmaq Nappe (SB on figs. 25, 26, 27) includes all impressive cliffs of the EGC northern slope (Plate 3.3). The main part of the zone consists of the Sahdag Mt. and the Qizilqaya Massif. Sahdag Mt. with its altitude of 4243 m, is the second highest summit of Azerbaijan (Plate 3.3-A, B, C, D). Eastward of Qizilqaya Massif, some remains of the nappe can be found near Sohub, Tangaalti, Cirax (fig. 30) and finally the Besbarmaq Mt (fig. 31) along the Caspian Sea. An offshore cliff in the Caspian Sea is also a remnant of this nappe. The nappe is only present in Azerbaijan and evolves to become a concordantly bedded series with the underlying formation around the Shalbuzdag Mt. (4142 m – Plate 3.4 A) in Dagestan (Russia). Structurally, it is part of the Sahdag-Xizi Zone, but lithologically it can be associated to the Sudur Zone. In the south, it is in contact with the Middle Jurassic deposits of the Tufan Zone (Plate 3.4-D). Due to its geological particularities, it is treated as a separate zone in this work.

Lithologically, it is composed of a thick series of Upper Jurassic and Lower Cretaceous biodetritic Mg-limestone. These deposits are frequently called “Allochtone“ deposits as opposed to the “Autochtone” deposits that correspond to the Sahdag-Xizi Zone and the “Neoautochtone” deposits that cover indifferently the two preceding formations.

Structurally, the Sahdag Mt. is divided from north to south in one syncline- one anticline (with an inverse northern flank) and one syncline (fig. 29, plates 3.3 A, B, C, D and figs. 36, 37). Eastward, the structure becomes flatter and narrower, i.e. the Qizilqaya Massif consists only of one flat syncline (Plate 3.3 F). The nappe is in tectonic contact with the underlying “Autochtone” deposits of the Sahdag-Xizi Zone. No major structural differences between Upper Jurassic and Cre-

taceous deposits are seen on Sahdag Mt. (fig. 38-C, D). Measures on Qizilqaya Massif (fig. 38-E) show a fold axis dipping to the ESE and beddings dipping to the NNE and SSW.

Upper Jurassic olistostromes

Olistostromes were observed in several parts along the northern slope of the EGC: i.e. Cek Village (Plate 3.6B), Ruk Village, Gilgilcay River. They are mostly composed of Upper Jurassic limestones. After their collapse, they were integrated in Lower Cretaceous deposits. Based on these observations, on the WNW-ESE alignment of the olistostromes along the northern slope and on their similar lithologies, we interpret Sahdag Mt. (fig. 29), Qizilqaya Massif, Chirax Mt. (fig. 30) and Besbarmaq Mt. (fig. 31) to be huge olistostromes that collapsed in a passive margin context during Valanginian - Barremian period. Small olistoliths with the same lithology were also found several kilometers south of this alignment in Middle Jurassic area (north of Babadag Mt.).

Although we consider the Sahdag Mt. and the Qizilqaya Massif as olistostromes, their sizes were certainly too big and their displacements proportionally too small to have during their setting-up a significant direction change in their structures compared to the autochtone deposits. Moreover, due to their size, they were also influenced by deformations during several tectonic events that happened from Upper Cretaceous up to now and they were probably backthrusted to the north and folded during the uplift of the central Tufan Zone.

Structural measures of an Upper Jurassic olistostrome (plate 3.3-E) lying on Aalenian deposits between the Sahdag Mt. and the Qizilqaya confirm that both are not concordantly bedded. Best fit great circle of beddings poles of the olistostrome has a SE-NW direction and its fold axis slightly dips to the NE (fig. 38-G).

The underlying Aalenian deposits of the Tufan Zone have a best fit great circle of bedding pole with a NNE-SSW direction and fold axes gently plunge to the ESE (fig. 38-F). These differences with the underlying rocks but also with the Sahdag and Qizilqaya structures suggest that this isolated block is the result of a rockfall from the surrounding Qizilqaya cliffs. Its age must still be defined: it could be recent or from the same age of the Sahdag-Besbarmaq Nappe setting-up (~Valanginian – Barremian).

3.3.4. Sahdag-Xizi Zone

The Sahdag-Xizi Zone (SX on figs. 25, 26, 27) is part of the northern slope of the EGC. In Azerbaijan, its length reaches 150 km and has a maximum width of 12-15 km. It extends from the border with Dagestan (Sahdag Mt. region) to the Caspian Sea.

Lithologically it consists mainly of calcareous-terrigenous and clayey deposits of the Upper Jurassic (up to 950 m), Lower (up to 2250 m) and Upper Cretaceous (up to 900 m) epochs (fig. 26).

Structurally, the Sahdag-Xizi Zone is cut by numerous thrusts and it is overthrust by the Sahdag-Besbarmaq Nappe (Plate 3.3 F and figs. 36, 37). It crops out until the Caspian Sea. In the studied area, the Sahdag-Xizi Zone is difficult to observe because it is covered by the Sahdag-Besbarmaq Nappe. However, it can be clearly observed in the eastern part of the EGC, near the Xizi village. Coloured and highly folded Aptian sediments of "Candy Cane" mountain (fig. 28) show fold axial planes that mostly dip to the north, fold axes that slightly dip to the ESE and most of bedding planes that dip to the SSW. Numerous thrusts to the south are also present in the area.

"Neoautochthonous" deposits

The Neoautochtonous series are formed by Turonian-Maastrichtian sediments.

Continental conglomerates of Turonian age unconformably transgress older series in the east while the unconformity is sealed by Campanian marine deposits in the west. They are in contact with the "Auto-

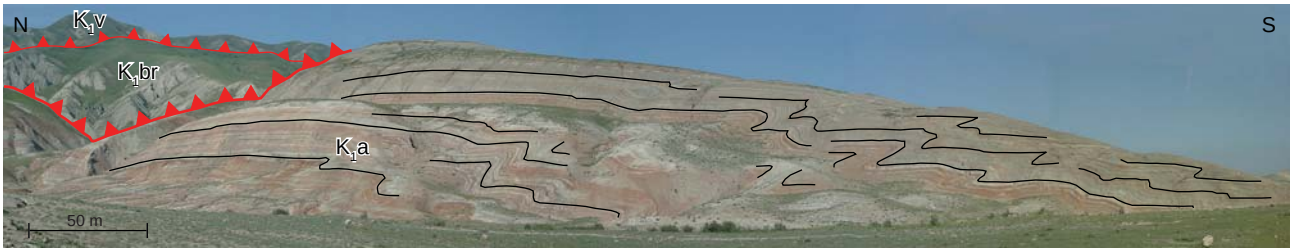

Figure 28: "Candy Cane" Mountain, east of Xizi Village. Highly folded Aptian (K1a) (red sediments) deposits overthrusted to the south by Barremian (K1br) sediments themselves overthrusted to the south by Valanginian (K1v) sediments.

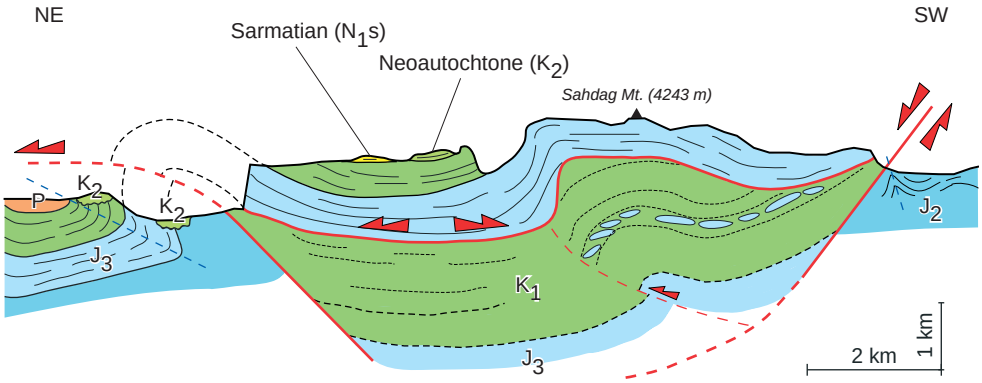

Figure 29: Sahdag Mt. (4243m) cross-section (C2 on fig. 25). It is the biggest occurrence of the Sahdag-Besbarmaq Nappe. Line A' on fig. 25. J2: Middle Juras-sic; J3: Upper Jurassic; K1: Lower Cretaceous; K2: Upper Jurassic; P: Paleo-gene; N1s: Serravalian (Sarmatian).

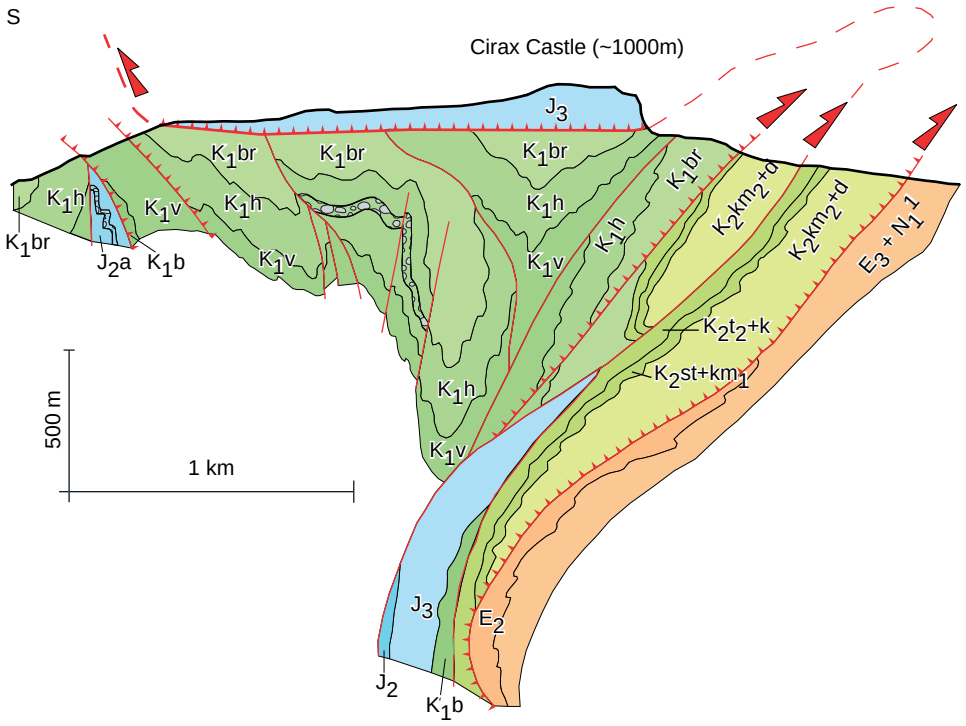

Figure 30: Cirax Castle cross-section (C5 on fig. 25) corresponding to the Sahdag-Besbarmaq Nappe overlying the Sahdag-Xizi Zone (modified from T. Kangarli). Located by line D on fig. 25. J2: Lower Jurassic; J2a: Aalenian; J3: Upper Jurassic; K1v: Ber-riasian; K1v: Valanginian; K1h: Hauterivian; K1br: Barremian; k2cm1: Lower Campanian; k2cm2: Upper Campanian; K2st: Santoni-an; E1d: Danian; E2: Eo-cene; E3: Oligocene; N1: Miocene.

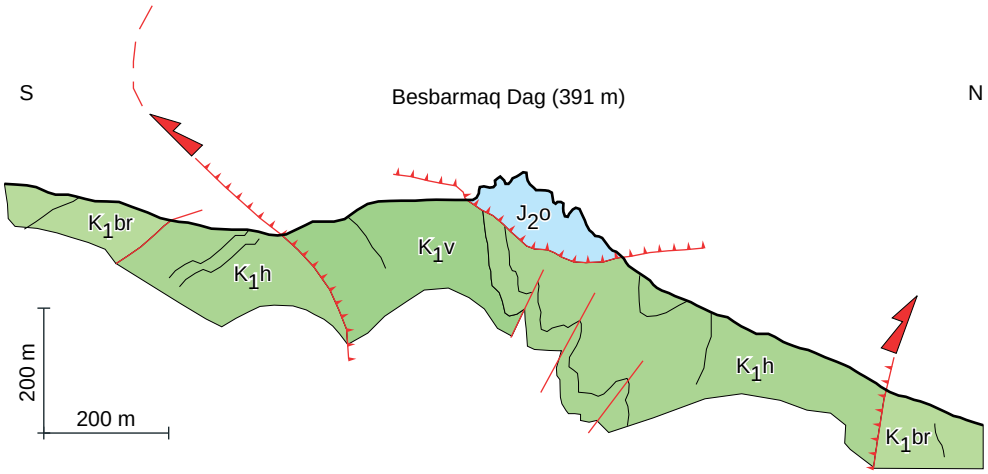

Figure 31: Besbarmaq Mt. cross section (C6 on fig. 25). It corresponds to the most eastern remnant of the Sahdag-Besbarmaq Nappe overlying the Sahdag-Xizi Zone (modified from T. Kangarli). Located by line E on fig. 25. J2o: Oxfordian; K1v: Valanginian; K1h: Hauterivian; K1br: Barremian.

chthonous" and "Allochthonous" deposits of, respectively, the Sahdag-Xizi Zone and Sahdag-Besbarmaq Nappe.

On the Sahdag Plateau at 3500 m (white deposits on Plate 3.3-C) and also north, on the Sudur Zone, sediments are of Campanian to Maastrichtian age and correspond to white patches of deep marine sediments with intercalation of brown shell rich limestones. They further outcrop on the Qizilqaya Massif north of the village of Cek where they fill a "paleovalley" that cuts across crossing the Upper Jurassic of the Sahdag-Besbarmaq Nappe and the underlying Lower Cretaceous "Autochthonous" sediments. In this area, they are thicker, also white and of deep marine origin. Eastwards, near Xizi Village, the "Neoautochtonous" deposits are made of conglomerates of Turonian Age. They form a sheet of several km^2 covering unconformably folded Albian-Aptian series (fig. 28).

3.3.5. Qonaqkand Zone

The Qonaqkand Zone (Qk on figs. 25, 26, 27) corresponds to the northeastern part of the Tufan Zone and geologically it is difficult to differentiate them.

Lithologically it is composed of terrigenous deposits of Lower and Middle Jurassic age in the west and of Upper Jurassic and Lower Cretaceous age in the east.

Structurally, it is bordered by the Sahdag-Xizi Zone in the north, by the Tufan Zone in the southwest and by the Zaqatala-Sumqayit Zone in the south. It is crosscut by numerous thrusts (figs. 36, 37). The Middle Jurassic deposits disappear eastward under younger deposits.

Berriasian transgressive event

In the eastern part of the EGC, along the Gilgilcay River, gently dipping conglomerate beds of Berriasian age overly tilted steeply dipping Upper Jurassic limestones (fig. 32). A tectonic event between these two periods of Tithonian age is thought to be at the origin of this unconformity. This area corresponds in the EGC to the easternmost outcrop of Aalenian (Middle Jurassic) deposits.

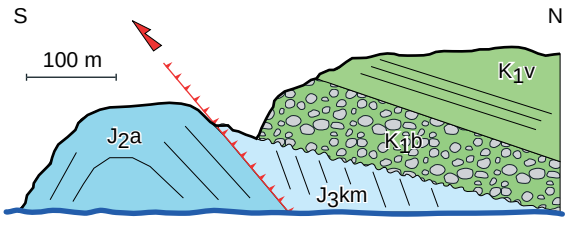

Figure 32: Cross-section along the Gilgilcay River (C7 on fig. 25) in the Qonaqkand Zone. Berriasian conglomerates are transgressive on folded Kimmeridgian deposits. Located by line F on fig. 25. J2a: Aalenian; J3km: Kimmeridgian; K1b: Berriasian; K1v: Valanginian.

3.3.6. Tufan Zone

The Tufan Zone (Tf on figs. 25, 26, 27) extends in Azerbaijan from the northwestern border with Georgia to the area of Qonaqkand village. It corresponds to the central and topographically to the highest part of the Eastern Greater Caucasus. Bazarduzu Mt. (4466 m – Plate 3.4 D and E) and Tufan Mt. (4191 m – Plate 3.4 C) are respectively the first and third highest summits of Azerbaijan and are part of this zone. The area is crossed by several remote valleys difficult to reach.

Lithologically, the zone consists mainly of thick accumulation of shaly flysch and deep marine deposits of Lower (up to 3600 m), Middle (up to 3300 m) and Upper Jurassic (up to 1000 m). There are frequently cut by sandstone intercalations (fig. 26).

Structurally, it consists of large-scale folds alternating with thrust zones (Plate 3.4-C, F, G and figs. 36, 37). A normal fault dipping to the north separates the zone from the Sahdag-Xizi Zone and Sahdag-Besbarmaq Nappe (Plate 3.3 – B) and a major thrust from the Qonaqkand Zone. In the south, it is thrust on Lower Cretaceous rocks of the Zaqatala-Qovdag Zone (Plate 3.9-D). The structural particularity of the Tufan Zone is the change of the main structure direction. Fold axial planes in the north dip to the south and they change dip to the north going south (fig. 38-F, H, I, J). A favorable lithology (mostly argillite) allowed the development of a weak schistosity in this zone. This schistosity is the witness of a very low grade metamorphism in the area.

Data from 4 major valleys were collected from west to east: the Upper Qusarcay Valley (Bazarduzu Mt. area – Plate 3.4), the Upper Qudiyalcay Valley (Plate 3.5), the Cek-Hapit Valley (Plates 3.6 and 3.7) and the Ruk-Babadag Valley (Plate 3.8 and 3.9). A NW-SE oriented cross-section based on field observation shows the changes in structural style (fig. 37A, B and C). Qudiyalcay and Cek-Hapit valleys allowed studying the northern half of the Tufan Zone and the Ruk valley allowed crossing it completely (see plates 3.6 to 3.9). Cross-sections A, B and C of figure 37 describe respectively the northern, central and southern part of the Tufan Zone. Two changes of fold axis plane and thrusts dipping direction can be seen. The first change is located near the contact between the Tufan Zone and the Sahdag-Besbarmaq Nappe (Plate 3.5 B and D). It is probably linked to the emplacement of the Sahdag-Besbarmaq Nappe. The second transition is certainly

linked to the exhumation of the central part. It is visible in the middle part of the Tufan Zone (cross-section C of figure 37 and plate 3.7 F).

3.3.7. Zaqatala – Sumqayit Zone

The Zaqatala – Sumqayit Zone (ZS on figs. 25, 26, 27) forms the main part of the southern slope of the EGC and extends almost from the border with Georgia to the town of Sumqayit (north of Abseron Peninsula) near the Caspian Sea. This zone is divided in three subzones from north to south: the Zaqatala-Dubrar (Plate 3.10), the Qovdag-Sumqayit (Plate 3.11) and the Duruji subzones (KANGARLI 2005).

Lithologically, the Zaqatala-Dubrar Subzone consists mainly of Upper Jurassic limestones and Cretaceous carbonate flysches. The Qovdag-Sumqayit Subzone is composed of marine deposits of Upper Cretaceous epoch covered by Oligocene deposits of the Maikop Formation. The Duruji Subzone is composed of deep marine Aalenian deposits (Middle Jurassic). As represented on figure 26, the Zaqatala-Sumqayit zone is mainly composed of Lower Cretaceous (up to 3300 m) and Upper Cretaceous deposits (up to 1900 m). Paleogene and Neogene sediments are thicker than on the northern slope (respectively up to 1800 m and up to 1300 m).

Structurally, the Zaqatala-Dubrar Subzone is thrust towards the S over on the Qovdag-Sumqayit and the Duruji subzones. The Duruji subzone could be interpreted as a lens of Aalenian age that was uplifted during orogeny by an underthrusting. The Zaqatala-Dubrar Subzone is composed of a main syncline near the Babadag Mt. (Plate 3.10-A, B and figs. 36, 37 and 38-K). Axial planes are generally vertical or dip to the north in this area. Outcrops observed and illustrated on Plate 3.10-C, D, E show that thrusts are generally dipping to the north and thrusting to the south. Between Babadag Mt. and Burovdal village, we studied 5 parallel valleys (fig. 38-L) that are cut by numerous thrusts dipping to the north with top to the south movement. Most of the measured bedding poles are aligned on a NNE-SSW oriented great circle. Both Qovdag Mt. stereonet (fig. 38-M) and Vasa Village stereonet (fig. 38-N) are located in the Qovdag zone-Sumqayit subzone. The Qovdag Mt. stereonet (fig. 38-M) shows that fold axes slightly dip to ESE. Measures of the Vasa Village stereonet (fig. 38-N) were mostly made in Oligocene sediments (Maykop fm.) and direction are similar to the other measures in the area.

Foreland basin formation

Inside the Qovdag-Sumqayit subzone, deep marine deposits of the Maikop formation (Eocene-Oligocene) are remnants of a foreland basin formed during the first period of building of the present Greater Caucasus orogen. A similar foreland basin with shallower marine sediments is also present on the northern slope of the EGC. These Maikop deposits are evidences for an orogenic event with foreland basin formation during the Eocene-Oligocene times.

3.3.8. Vandam Zone

The Vandam Zone (Vm on figs. 25, 26, 27) forms higher reliefs south of Zaqatala-Qovdag Zone.

Lithologically it is mainly composed of Lower Cretaceous volcanogenic sediments (Plate 3.12 A and F) remobilized in turbidite deposits. Cretaceous deposits are thinner than in the Zaqatala-Sumqayit Zone (up to 3350 m for the whole Cretaceous). The thickness of Paleogene deposit is almost identical and the Neogene deposits are thinner (fig. 26) to the ones of the Zaqatala-Sumqayit Zone.

Structurally this zone is composed of several anticlines-synclines associated with several south directed thrusts (Plate 3.12 B, C, D and cross-section C on fig. 37). The area was certainly exhumed after the Upper Miocene (see below in the Basqual Nappe section). Fold axes near the village of Lahic slightly dips to the ESE and axial planes dip to the north (fig. 38-O) (see ALLEN et al. 2003).

3.3.9. Basqal Nappe

The Basqal Nappe (Bq on fig. 25) located south of the Vandam Zone between the Girdimancay River and Samaxi Town forms an isolated outlier of a nappe deck that roots in the Zaqatala-Sumqayit Zone. This flat lying thrust sheet is isolated due to erosion and to the uplift of the Vandam Zone.

Lithologically it is composed of rocks from the Barremian to Upper Miocene deposits. Structurally the Lower Cretaceous deposits are in tectonic contact with underlying Upper Miocene deposits (Sarmatian deposits). Ages of the nappe sediments allow dating the uplift of the Vandam Zone after the Upper Miocene (south of cross-section C on fig. 37). This is an evidence for a thrusting event after the Upper Miocene (figs. 36, 37). Associated with the Upper Miocene (Sarmatian) deposits at 3600 m on the Sahdag Mt. in the northern slope, this orogenic event can be generalized to the whole EGC.

3.3.10. Ganih-Ayricay Zone

The Ganih-Ayricay Zone (GA on figs. 25 and 27), also named Alazani basin, is a piggy back basin running

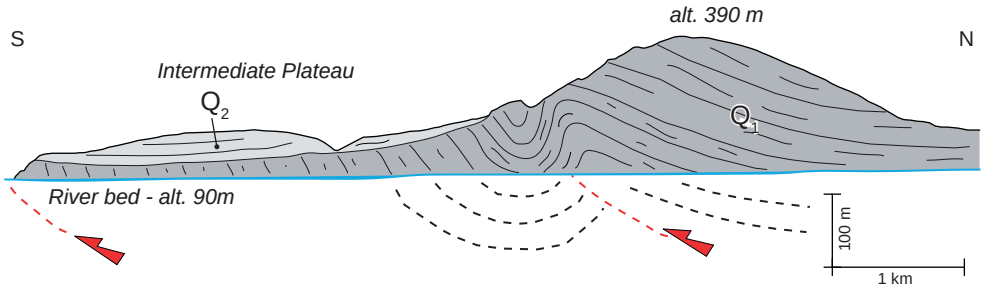

Figure 33: Cross section of the Qaramaryam hills (C8 on fig. 25). Located by line G on fig 34. Q1: Pleisto-cene; Q2 : Holocene.

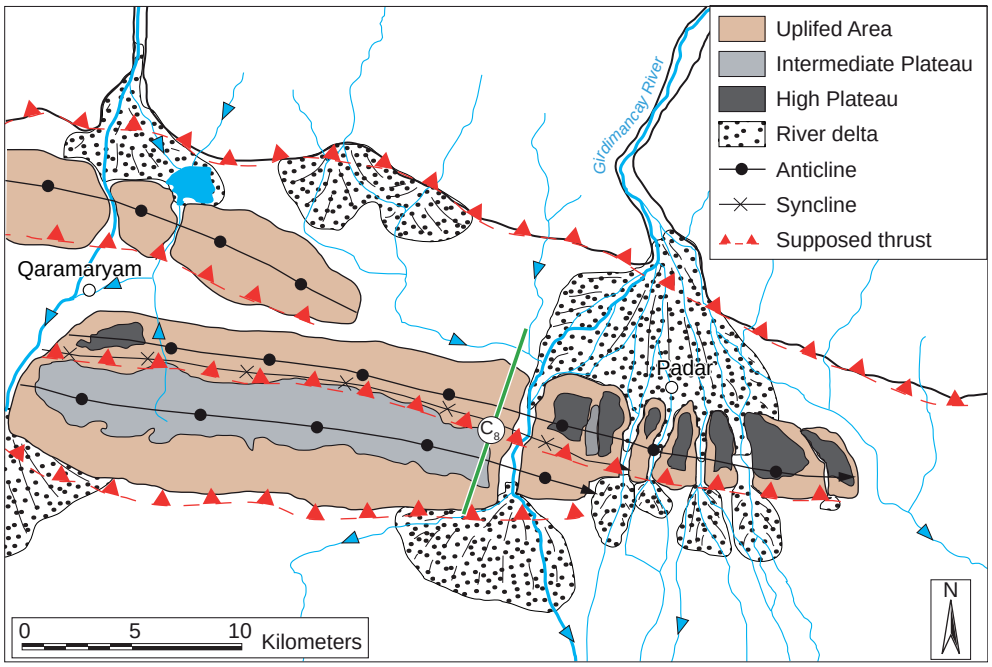

Figure 34: Structural map of Qaramaryam hills with hydrographic network and stream direction. Cross-section of figure 33 is indicated with the green line G.

parallel to the Great Caucasus axis from the northeast of Tbilisi (Georgia) to the Girdimancay River near the town of Ismayilli. Sediments thickness increases to the south. Quaternary deposits reach a maximum thickness of 800 m and Upper Pliocene ones a maximum thickness of 1000 m (Philip et al. 1989). Its northern border corresponds to a main thrust of the southern side of the EGC (figs. 36, 37).

3.3.11. Samaxi-Qobustan Zone

The Samaxi-Qobustan Zone (SQ on figs. 25) corresponds to the south eastern part of the EGC. Lithologically it is filled with Neogene sediments. Middle-Late Miocene sediments (with thickness up to 3600 m) are transgressively overlapped by the Pontian deposits. The latters are themselves overlapped by Early and Late Pliocene deposits (Ismailzadeh et al. 2008a).

3.3.12. Abseron Zone

The Abseron Zone (Ab on fig. 25) corresponds to the eastern termination of the Greater Caucasus. It forms a peninsula in the Caspian Sea. It is composed of thick series of the Miocene (1600 m), Pliocene (4240 m) and Quaternary ages (Ismailzadeh et al. 2008a).

3.3.13. Ajinour Zone (Aj) – Kura Megazone

The Ajinour Zone (Aj on figs. 25 and 27; Plate 3.13 A, B and C) is located north of the artificial Mingacevir Lake. It is already part of the Kura Megazone but it is geodynamically linked with the Greater Caucasus. This zone is continuous into the Kartli foreland folds and thrusts belt. It forms the active orogenic front in western Azerbaijan and in eastern Georgia.

It is composed of Oligocene-Pliocene molasse deposits and is deformed by several thrusts to the south.

3.3.14. Kurdamir-Saatli Zone – Kura Megazone

The Kurdamir-Saatli Zone (KS on fig. 25) is also part of the Kura Megazone. In the studied area, it is mostly composed of Pliocene and Quaternary marine and continental sediments.

Quaternary faulting in Qaramaryam Hill

The Quaternary Qaramaryam hills (figure 33 and plate 3.13 D, E, F and G) are linked to present frontal thrusts of the Southern EGC (figs. 36, 37). A syncline-anticline structure linked with these frontal active faults grew during Quaternary Period and is clearly visible in most western hill.

Data collected in Quaternary deposits of Qaramaryam hills (fig. 38-P) show a WSW – ENE trend and the fold axis slightly dips to the WSW. Since the Qaramaryam hills were formed during Quaternary times, differences with the southern slope stereonets (fig. 38 K to O) could emphasize a change in stress direction in Quaternary times or an influence of the neighbouring South Caspian Basin.

Geologically flat bedded Holocene deposits (Q_2) lie on tilted Pleistocene deposits.

Geomorphologically, two levels of plateaus can be discriminated (fig. 34). These levels were successively created by two active faults. The northern one started to act before the southern one due to the uplift of the GC located to the N. SE of Qaramaryam village, a river flows to the north although the main stream direction in the area is to the south: it could indicate that the southern fault is currently more active than the northern one. The hills' topography decreases going eastward. It indicates a progradation of the fault activity and of the related uplift to the east. Qaramaryam hills are one of the main evidences for a Quaternary tectonic activity of the EGC.

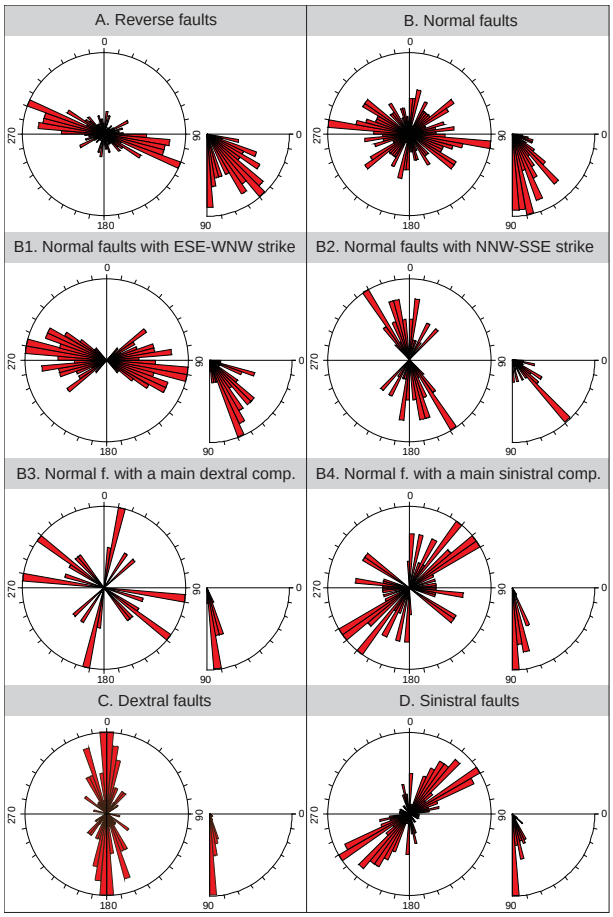

Figure 35: Rose diagrams of fault plane directions and dips for several fault movement types: A – Reverse faults (196 faults); B – Normal faults (128 faults); B1 – Sorted normal faults of B with a NNE-SSW strike; B2 - Sorted normal faults of B with a ENE-WSW strike; B3 - sorted faults of B with a main dextral component; B4 - sorted faults of B with a main sinistral component; C – Dextral faults (53 faults); D – Sinistral faults (79 faults). Direction and dip interval is 5°.

3.4. Faults analysis

Faults and striation are ubiquitous throughout the different tectonic zones of the EGC. We used these populations to address brittle deformation features and paleostress distribution.

456 measures of fault planes and their associated slickensides were made in 29 outcrops distributed in all the EGC (fig. 40). Out of 456 measured fault planes, 53 are dextral, 79 are sinistral, 196 are reverse, and 128 are normal. When sorted by their movement types, main directions can be deduced for each faults families (fig. 35).

3.4.1. Fault orientation interpretation

Reverse fault planes have an average WNW – ESE strike direction with a dip of 47.5° (fig. 35 – A) but also a second max at subvertical dip.

Normal faults have an average E - W strike direction with a subvertical dip (fig. 35 – B). But their strike distribution is wide and, as it can be observed on the detailed data stereonets of figure 40, some normal faults have a strike-slip behaviour (lineation dip < 20°). Consequently, they were sorted by fault sense trend and results are represented in four rose diagrams (fig. 35 – B1 to B4). The first component of vertical normal faulting trend has a WNW-ESE strike with a main dip of 77.5° (fig. 35 – B1). The second trend (fig. 35 – B2) corresponds also to a vertical normal faulting trend but with a NW-SE strike and a dominant dip of 47.5°. The third group (fig. 35 – B3) has a tendency of dextral faulting with a steep dip of 92.5° and three dominant strikes: a NW-SW, a WNW – ESE and a NNE-SSW. Finally, the fourth group of normal faults (fig. 35 – B4) has a tendency of sinistral faulting with a steep dip of 97.5° and two dominant strikes that are

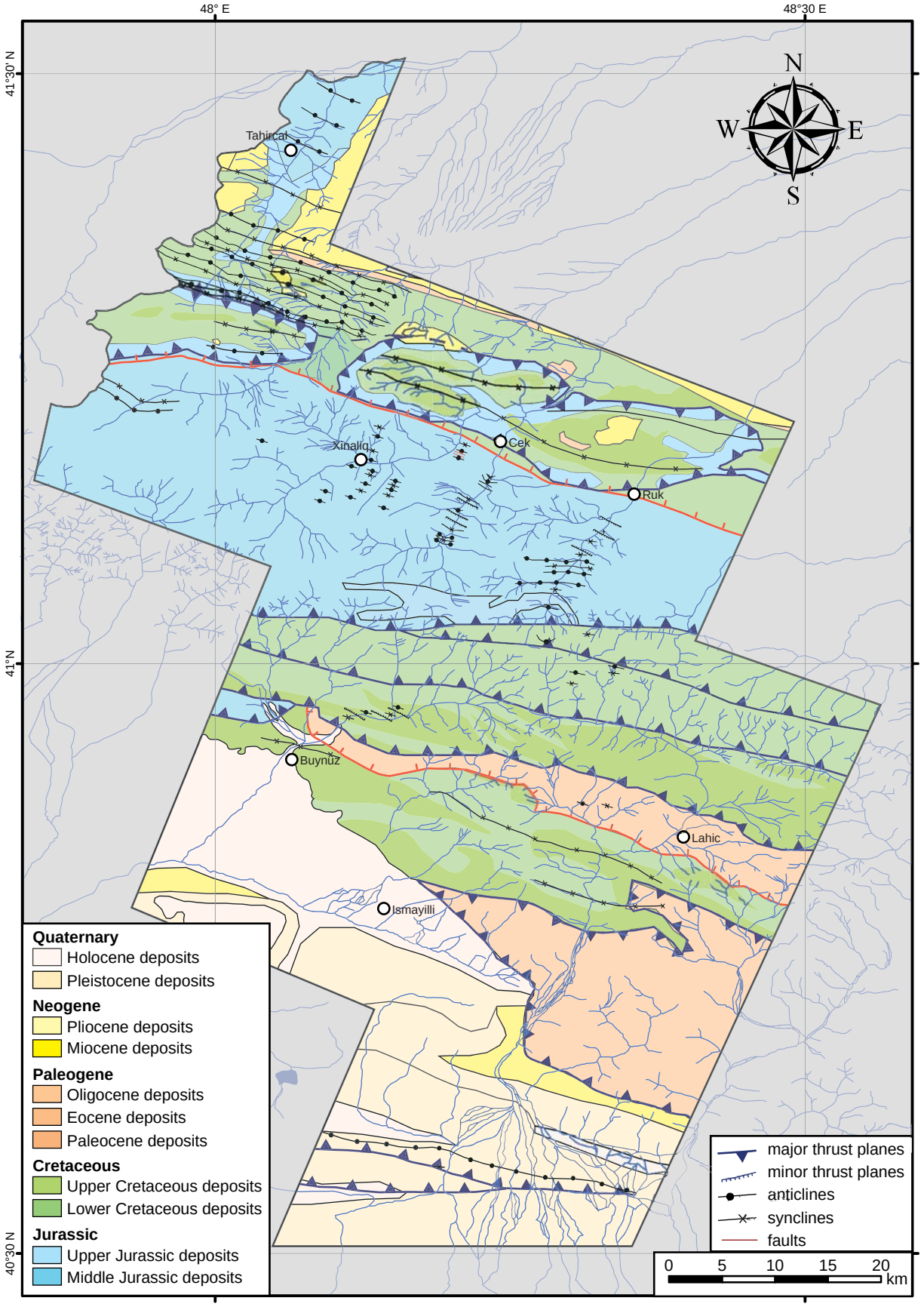

Figure 36: Detailed geological and structural map of the studied area of the EGC. Main observed structures are represented. The map is located on figure 25.

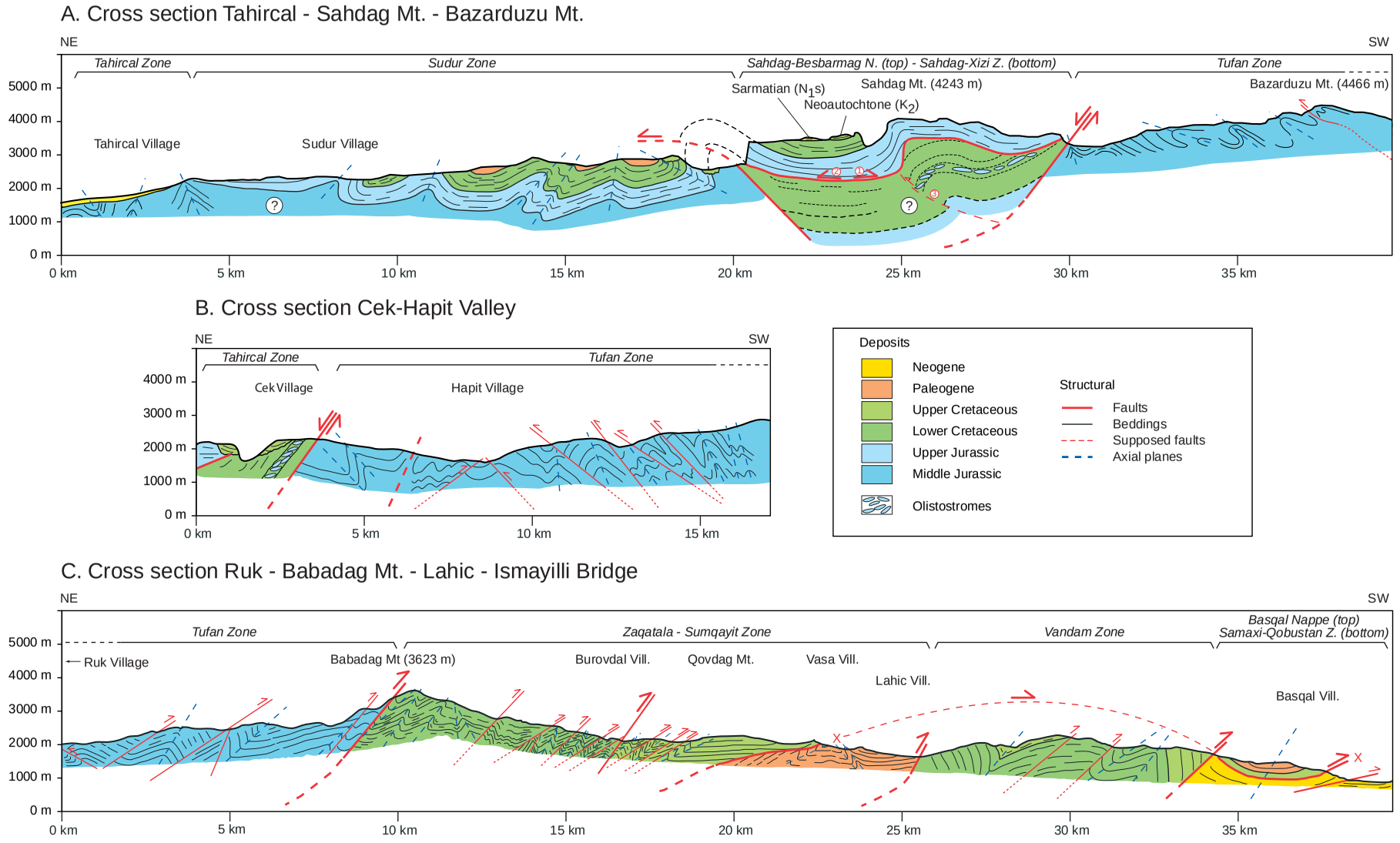

Figure 37: Cross sections crossing the EGC. and located on fig. 25: (A) Cross-section corresponds to the northern part of the EGC including the Tahircal Valley and the two highest summits of Azerbaijan, the Sahdag Mountain and the Bazarduzu Mountain. (B) Cross-section shows the contact between the Sahdag-Xizi Zone and the Tufan zone in the Cek-Hapit Valley. (C) Cross-section corresponds to the southern slope of the EGC starting from the northern slope of the Babadag Mt., going through Lahic village and finishing at the road bridge between Ismayilli and Samaxi. The cross-sections positions are shown on the simplified geological map.

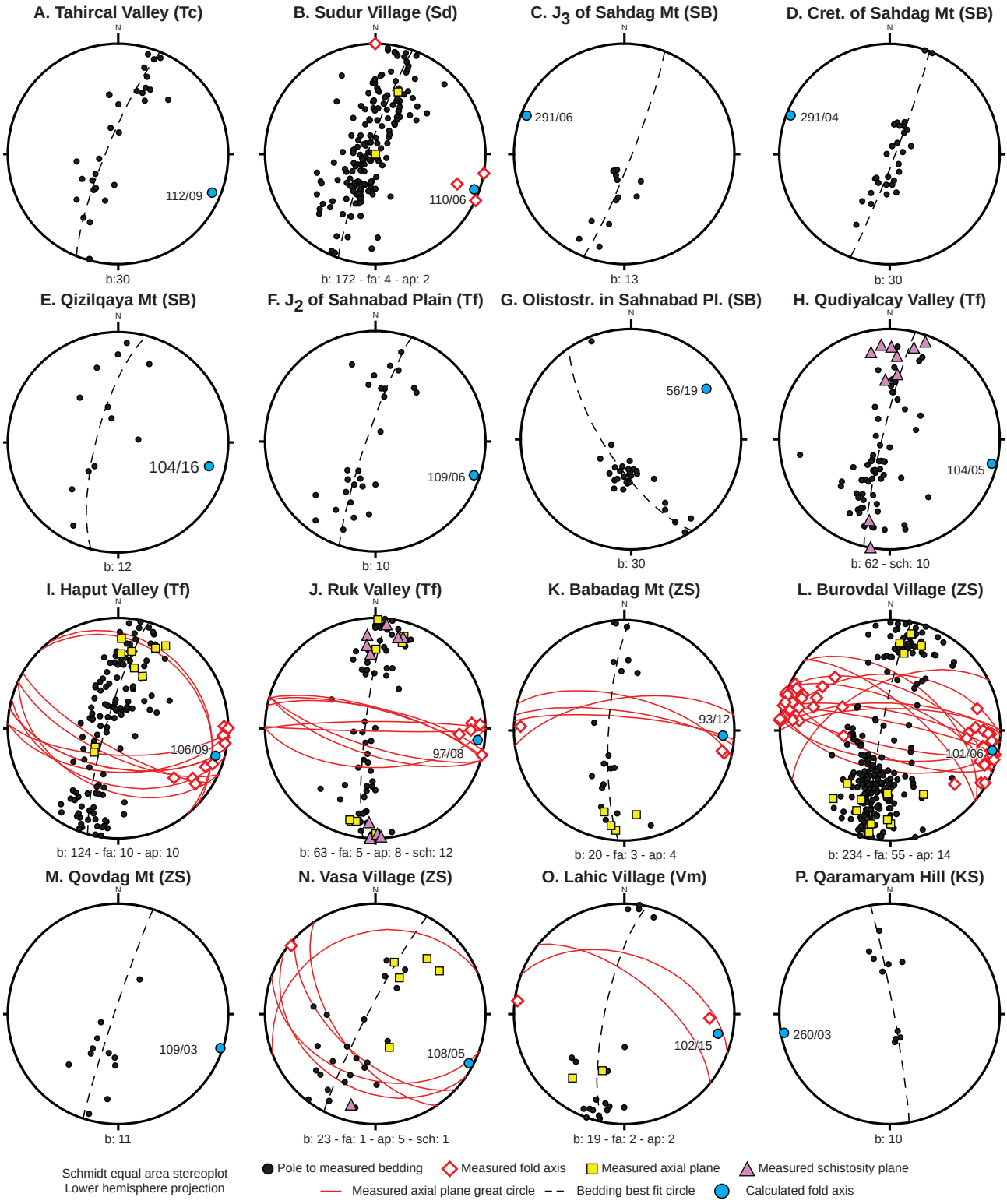

Figure 38: Stereonets of the structural data from the northern and central areas of the Eastern Greater Caucasus. The associated structural zone is indicated in parenthesis: Tc: Tahircal Zone; Sd: Sudur Z.; Tf: Tufan Z.; ZS: Zaqatala-Sumqayit Z.; Vm: Vandam Z.; KS: Kura-Saatli Z. Other Abbreviations: b: bedding; fa: fold axis; ap: axial plane; sch: schistosity plane. Stereonets are located on figure 43.

both NE-SE with a difference of ~15-20°. The dextral fault planes have a main N – S strike direction and a dominant dip of more than 95° (fig. 35 – C).

Reverse faults (fig. 35 – A) and normal faults on fig. 35 – B1 have a similar direction (NNE-SSW strike) and dip. We can suppose that they result from a NNE-SSW extensional-compressional stress perpendicular to their main direction.

Normal faults of figure 35 – B2 with a NNW-SSE direction are mainly located in the Vandam Zone (southern slope) as represented in fig. 40-28. The area underwent a fast local uplift during a late phase of Greater Caucasus that could explain a local normal faulting.

Sinistral fault planes have two dominant strikes with a NE-SE direction and are separated only by a small angle of 15-20° (fig. 35 – D).

Observed strike-slip faults show orientations compatible with a conjugate fault system combined to a Riedel Shear fault model (fig. 39A). Strike-slip faulting produces characteristic faults structure: the Riedel Shear fault system (Riedel 1929; Tchalenko 1970; Vialon et al. 1976; Wilcox et al. 1973). They will be also produced in an active strike-slip zone in an area of continuing sedimentation. A simple shear causes a related succession of faults. In a strike-slip fault system propagated in a homogenous material with a friction coefficient ϕ=30°, the first and dominant set will form at about 15° (ϕ/2) to the main fault with the same shear-sense: the dominant R shear. They are themselves associated with a second set that generally forms at about 75° (90°-ϕ/2) to the main fault: the secondary R' shears (fig. 39C). When Riedel shear segments tend to be fully linked by the development of a new shear set symmetrical to the R shear: the P shears. Finally, the last stage corresponds to the formation of a continuous fault (fig. 39B). N-S dextral faults (fig. 35 – C) and ENE-WSW sinistral faults (fig. 35 – D) correspond to a conjugate fault system (60° between the main direction) but both types have secondary faults at about 10-15° (figs. 35 – B3, B4, C and D) that could be associated to a Riedel Shear fault model Rd and Rs component.

The Rd' and Rs' component is not clearly present in our data. Based on this Riedel model the main stress is compressive with a NNE-SSW direction. This strike-slip regime is commonly named the « Anticaucasian fault system ».

In the normal fault rose-diagrams with a main dextral and sinistral component (fig. 35 – B3 and B4), the two faults families with a NW-SE and WNW-ESE directions could be related to a strike-slip system linked with the reverse-normal fault system.

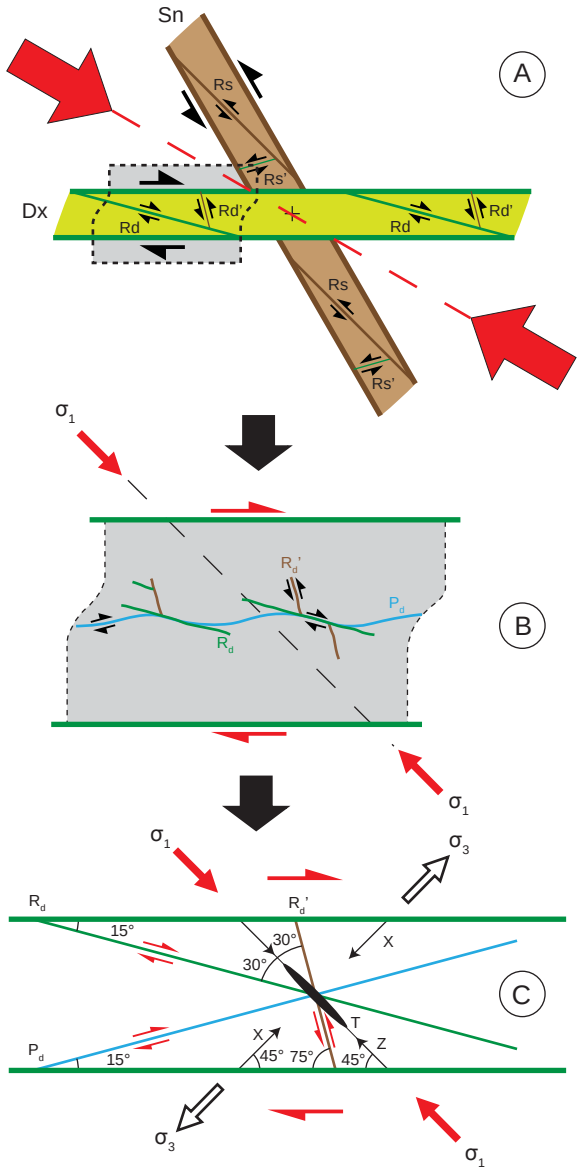

Figure 39: A – Conjugate fault system with a dextral and sinistral faults resulting from a compressive stress σ1 with respective Riedel shears; B – Detail of the dextral fault with basic Riedel shears structures (R and R') and the resulting fracture (P); C – Angular relationship between the different components of a Riedel Shear system. Angle are given for a homogenous material with a friction coefficient of ϕ = 30°. σ1: maximum stress; σ3: minimum stress; T: = tensile crack; X: max lengthening axis; Z = max shortening axis. Modified from VIALON et al. (1976).

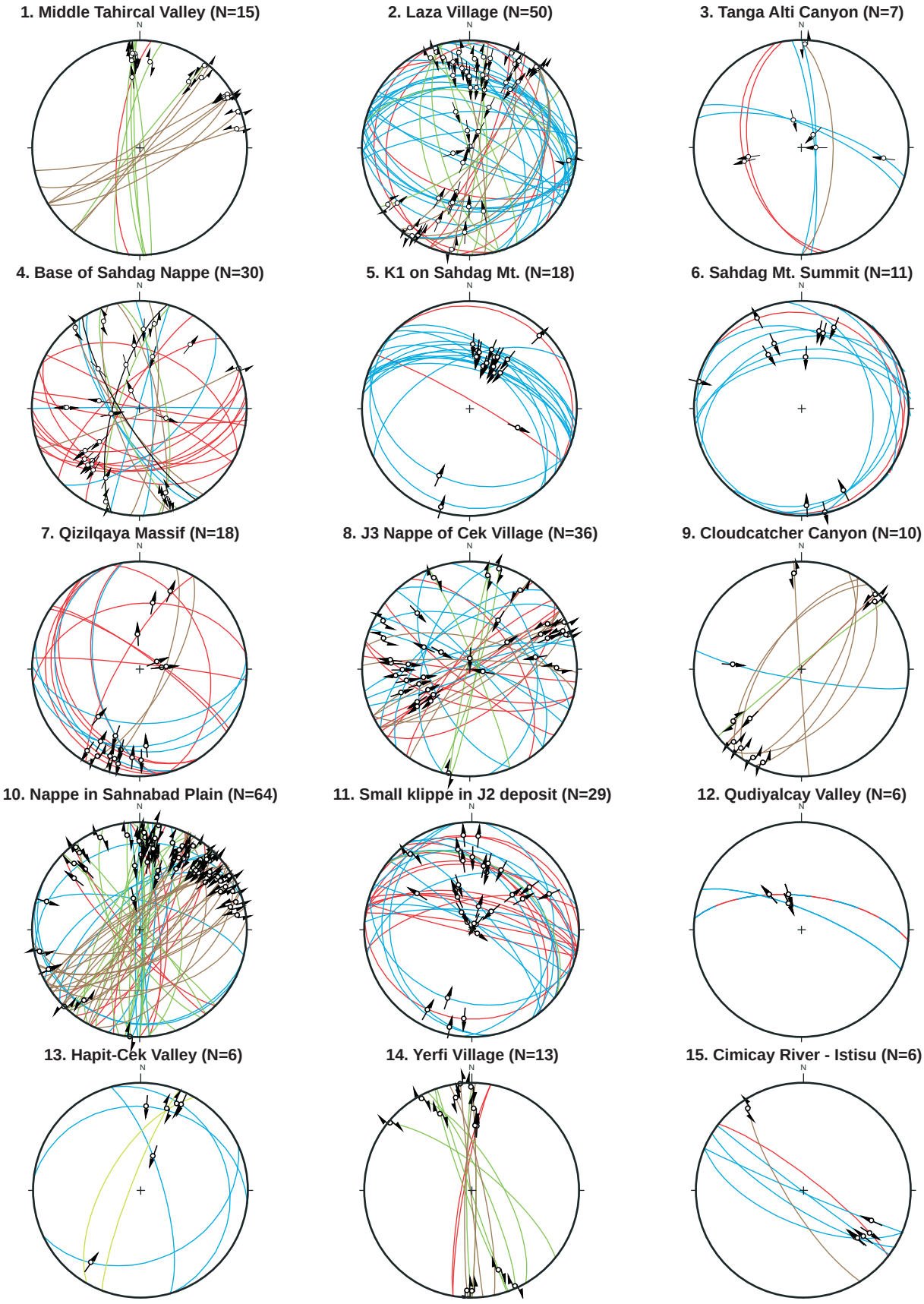

Figure 40 -1: Stereonets of the data on which the stress calculations of figure 44 are based. Stereonets are located on figure 43.

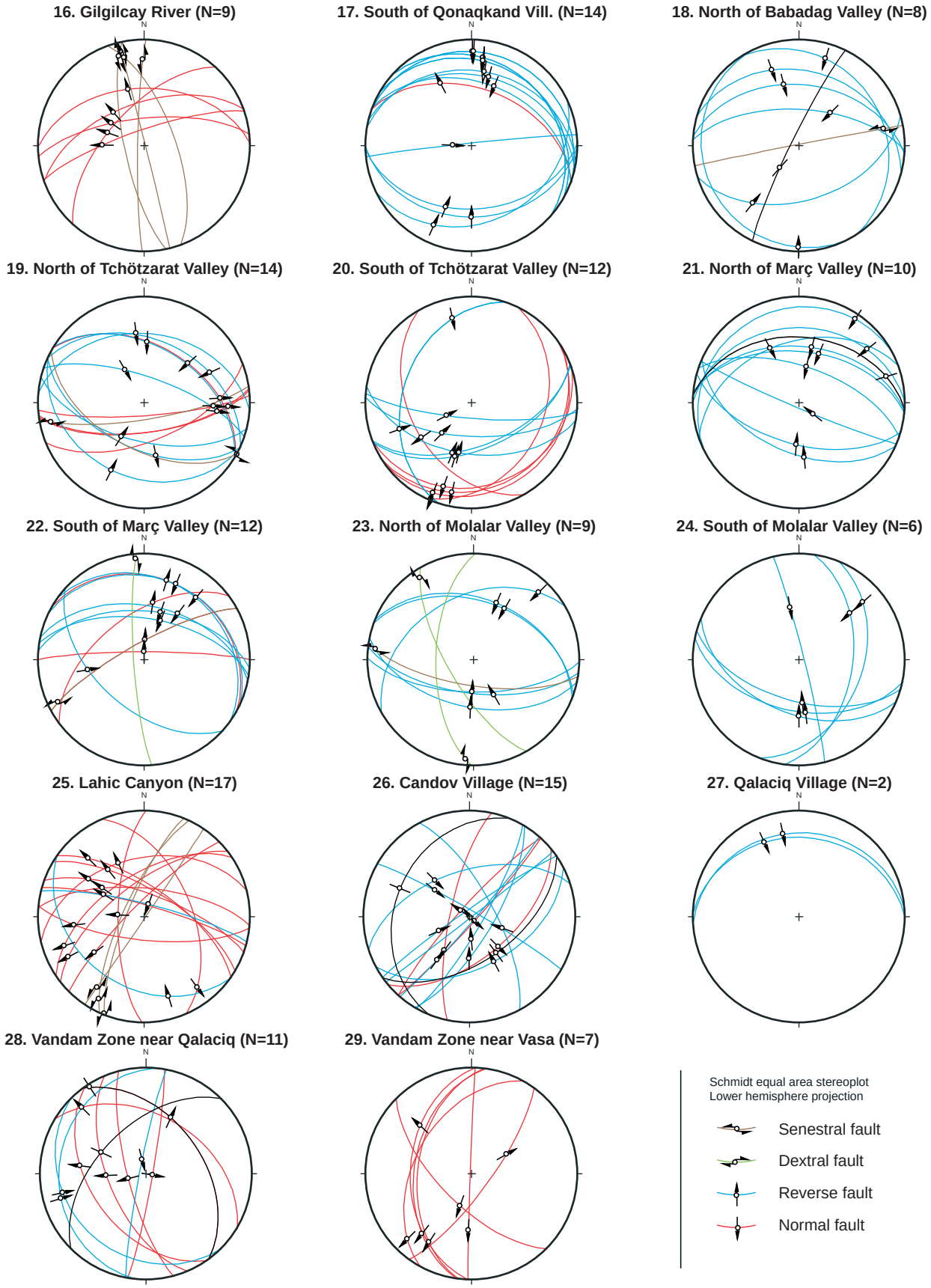

Figure 40-2: Stereonets of the data on which the stress calculations of figure 44 are based. Stereonets are located on figure 43.

3.5. Stress analysis

Stress analysis is based on the same dataset used for the fault analysis and allow us determining local paleostresses across the EGC.

3.5.1. Method for stress analysis

The stress determination is based on fault planes and their associated slickensides lineation measurements. Data have been sorted and analysed with TectonicsFP for Windows™ (Ortner et al. 2002).

For each dataset, we measured the dip direction, the dip of the fault plane and the direction, the plunge and the movement sense (dextral, sinistral, normal or reverse) of the associated lineation. Additionally the geographical position of each measure was recorded.

To calculate the 3 principal stress axes (σ_1, σ_2, σ_3), the right dihedra method defined by Angelier & Mechler (1977) was used. This graphical method provides a probability distribution stereonet of the principal stress axes for a population of faults and allows representing the 3 mains stress regimes (fig. 42).

To apply the method, a population of fault planes with their respective oriented lineation are necessary. As illustrated on figure 41 and defined by Ramsay & Lisle (2000), the perpendicular auxiliary plane and fault plane pole are determined for each fault. The movement plane is defined by the fault plane pole and the lineation. It contains the maximum extension and compression axes. Compressive and distensive dihedras are determined by the lineation sense. The dihedra method superposes the compressive and distensive dihedras of the analysed faults to build a probability distribution stereonet and determines the best fit solution for the 3 perpendicular stress axes. Practically, each counting point in a ring grid is assigned to a value of 1 if located inside a compressive dihedron and 0 in distensive dihedron. At the end the area with the highest value corresponds to the zone of highest compression (max. value on each stereonet of figure 44). The results are represented in a lower hemisphere plot with an equal area projection (Schmidt net). Eigenvectors of the best fit fault plane are given and correspond to the 3 principal stresses axes.

The right dihedra method gives the stress direction but does not give a stress amplitude ratio as proposed by inverse methods. Due to geographical distribution of the measures within one set (sometimes more than one kilometer between measures), the right dihedra method seemed to be more adapted. To apply this method, several hypotheses must be assumed (Ramsay & Lisle 2000): (1) slip movement takes place in a direction parallel to the maximum shear stress on the fault plane, consequently, the striation of the fault plane is considered as representing the direction of maximal shear stress (Peresson 1992); (2) the stress field is assumed to be homogenous within the rock mass containing sampled faults; (3) the movement of one fault exerts no influence on the slip direction of other faults.

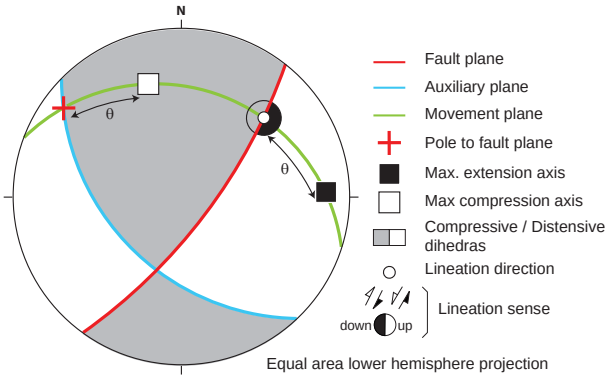

Figure 41: Stereonet of a fault plane with its lineation and the deduced movement plane, compressive and distensive dihedras and compression/extension axis. For the Right Dihedra method only the compressive and tensional dihedras are used and superposed with the other fault dihedras.

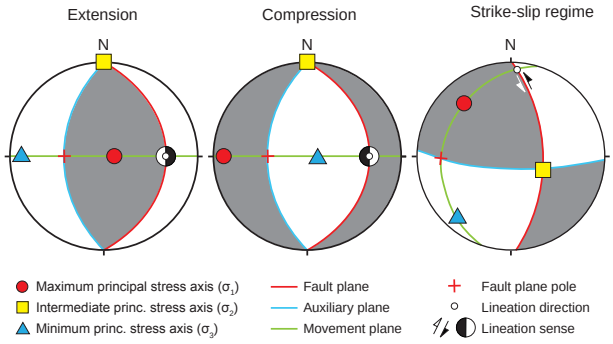

Figure 42: The 3 main stress regimes dihedras representation with principal stress axes. Extension and compression dihedras are represented respectively by a normal and reverse fault with a plane of 90/35 and a lineation 90/35 with the respective sense. Strike slip regime is illustrated by a sinistral fault with a plane of 89/62 and a lineation of 3/8.

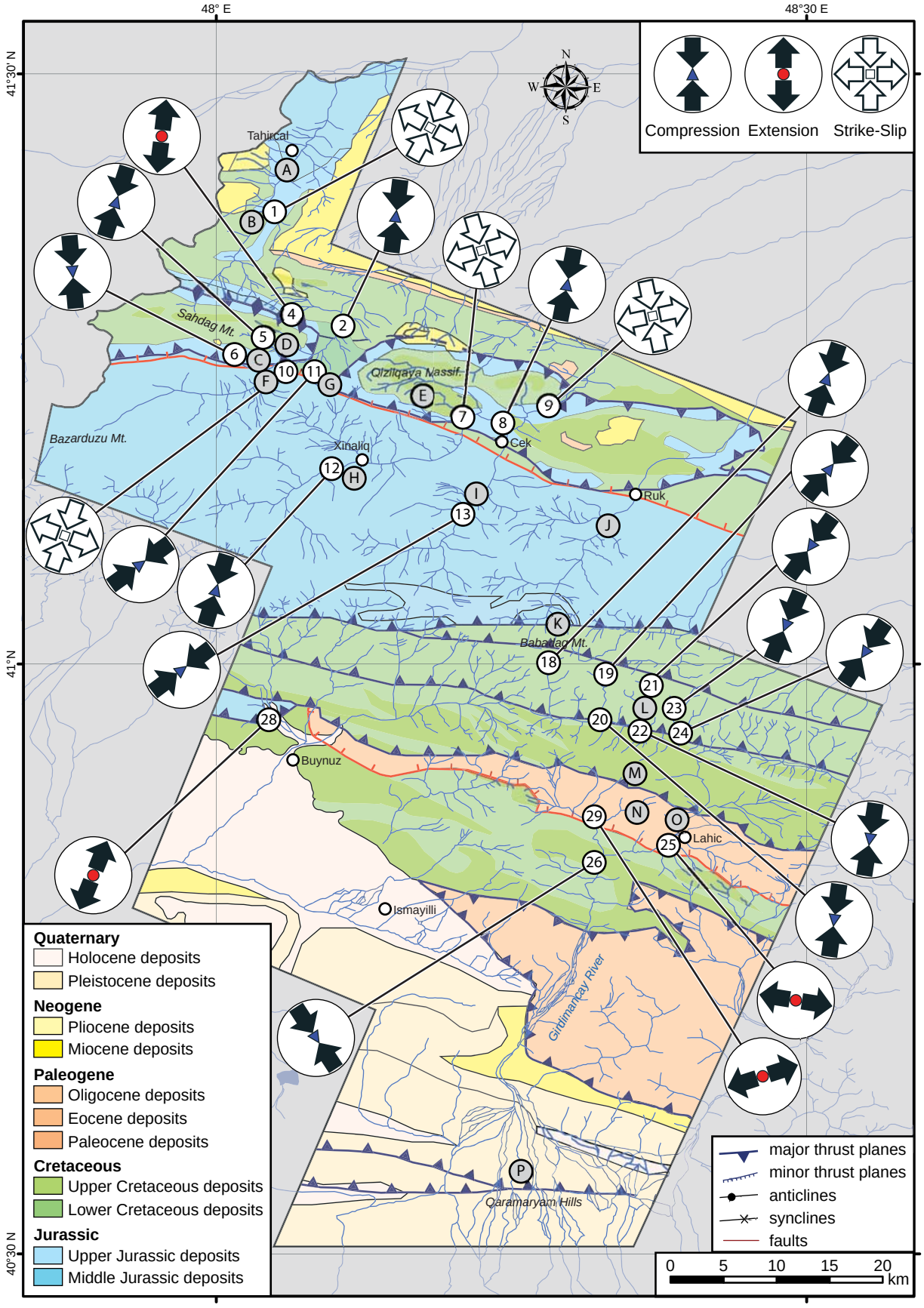

Figure 43: Detailed geological and structural map of the studied area of the EGC. Numbers in white circle correspond to those of the figures 40 and 44 (numbers 3, 14, 15 and 16 are outside the map) and letters in grey circle locate stereonets of figure 38.

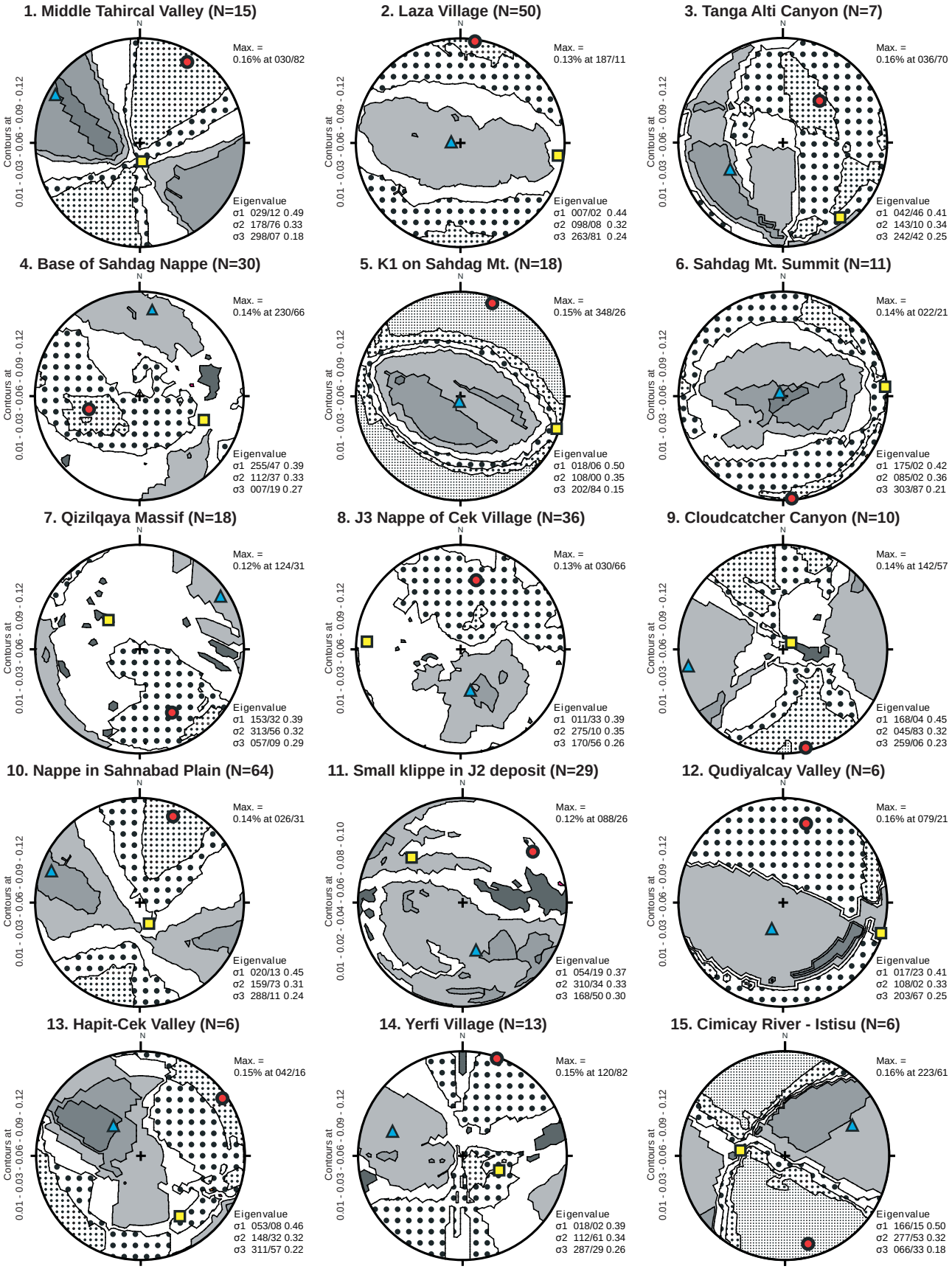

Figure 44 – 1: Stress stereonets from 29 sites across the Eastern Greater Caucasus (number refer to fig. 43). For PT analyses see appendix 1.

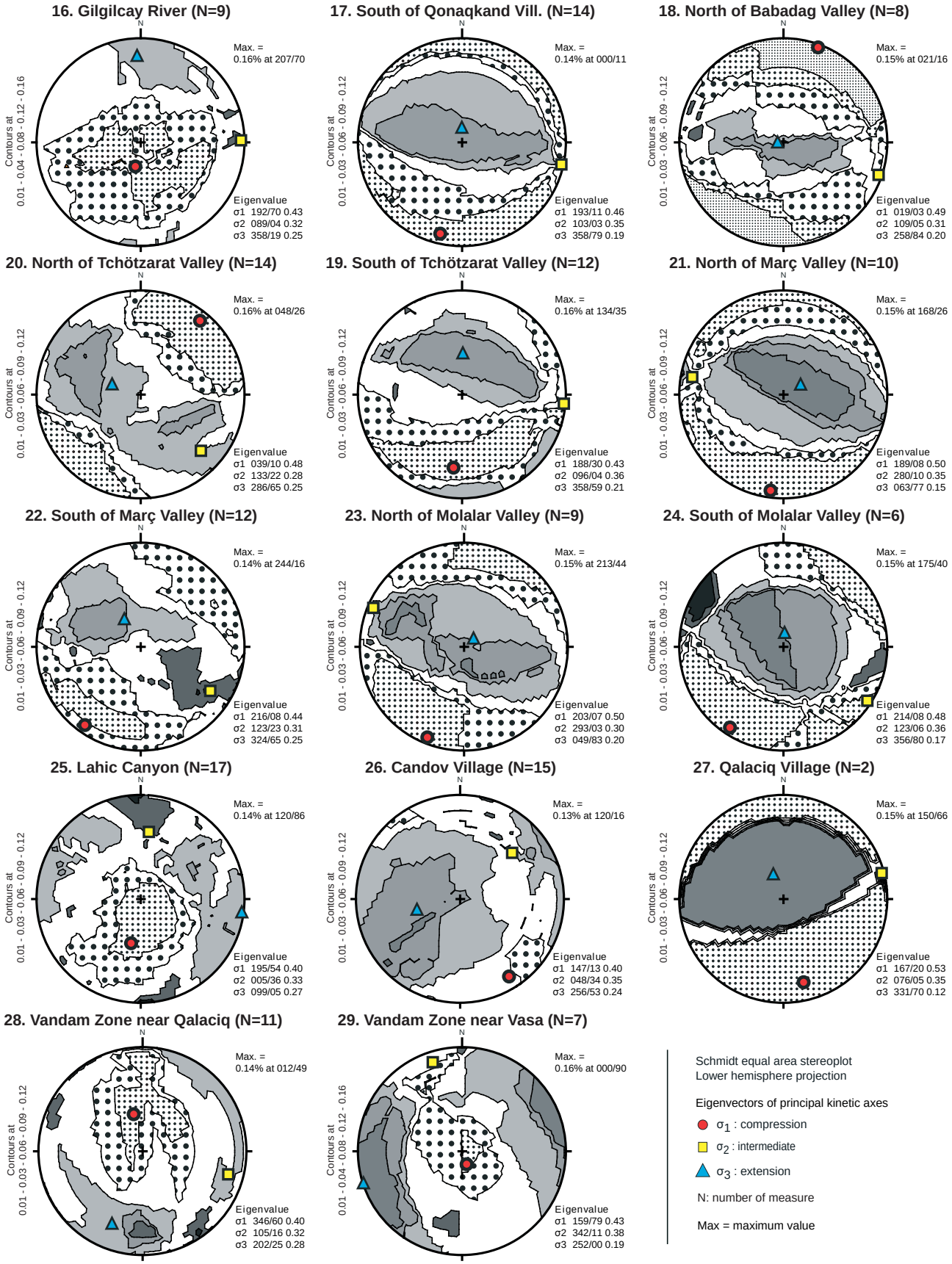

Figure 44 – 2: Stress stereonets from 29 sites across the Eastern Greater Caucasus (numbers refer to fig. 43). For PT analyses see appendix 1.

3.5.2. Results and interpretation

Of 29 investigated localities 17 show a compressional regime (figs. 43 and 44). From north to south each area is affected by this regime. Directions mainly correspond to a NNE-SSW stress. Extension regime is present along the Sahdag-Besbarmaq Nappe in the north and mainly in the southern slope. 6 out of 29 localities (figs. 43 and 44) show an extensional regime with a NNE-SSW direction. Strike-slip regime was measured in 5 localities (figs. 43 and 44) along the northern slope : 2 of them (fig. 44-1 and 14) show a strike-slip stress with a NNE σ_1 direction and the 3 others (fig. 44-7, 9 and 15) have a SSE σ_1 direction.

In the northeast structural zone, the Tahircal Zone, no faults were measured due to the lack of outcrops with good stress indicators. A strike-slip regime was observed (stereonet n°1 of figs. 43 and 44) and its behaviour is similar to the anticaucasian fault system.

The folded area of the Sudur structural zone near Laza is the result of a NNE-SSE compression (stereonet n°2 of figs. 43 and 44). Two kinds of extensional regimes can be observed: the first at the contact with the Sahdag-Besbarmaq Nappe (stereonet n°4 of figs. 43 and 44) is characterized by a NNE-SSW direction; the second in the Tangaalti Canyon further in the east is characterized by a NE-SW extension direction. σ_1 and σ_3 have a dip of almost 45° (stereonet n°3 of fig. 44) suggesting that the stress is near the limit between an extension and a compression regime.

The Sahdag-Besbarmaq Nappe is mainly characterized by thrusting (stereonets n°5, 6, and 8 of figs. 43 and 44) with a NNE-SSW direction and strike-slip regime (stereonets n°7, 9 and 10 of figs. 43 and 44) corresponding to the anticaucasian faults. Stress of a small klippe on Middle Jurassic deposits (stereonet n° 11 of figs. 43 and 44) is slightly rotated compared to the surrounding stresses. 2 of the 3 stereonet with a strike-slip regime (stereonets n°7 and 9 of figs. 43 and 44) have a ~NNW-SSE direction and therefore cannot be linked with the anticaucasian strike-slip fault system. Based on this observation, we suppose that the Nappe has a slightly different behaviour than the surrounding structural zones. This is probably due to the allochtone context but also to the sediment types that could influence the fault development: the nappe is composed at its base by a thick series of massive limestones and the underlying rocks by thick series of argillites, silts and marls (Sahdag-Xizi zone and Tufan Zone).

In the Tufan structural zone of the central part of the EGC is also characterized by thrusting resulting from a NNE-SSE compression (stereonets n°12, 13 and 17 of figs. 43 and 44). Eastwards, along the Gilgilcay River an extensional regime is acting (stereonets n°16 of figs. 43 and 44) on the area with a N-S direction. It could be explained by the uplift of the underlying Middle Jurassic rock but this hypothesis must be confirmed.

The Zaqatala-Sumqayit structural zone of the southern slope is mostly characterized by thrusting (stereonets n°18, 19, 20, 21, 22, 23 and 24 of figs. 43 and 44) with a NNE-SSW direction.

The southernmost studied area is characterized mostly by extensional stresses and one compressional stress. The westernmost extensional stress (stereonet n°28 of figs. 43 and 44) has a NNE-SSW direction. The other stresses (stereonets n°25, 26 and 29 of figs. 43 and 44) have directions that are almost perpendicular to the frequent NNE-SSW stress direction. This particularity could be explained by a local uplift of the Vandam Zone due to an underthrusting.

3.6. Synthesis and conclusion

In this section, we will propose an EGC structural model (fig. 47) based on our analyses. The geological evolution of the area will be described and compared to the regional events. Finally we will propose a geodynamic interpretation of the EGC.

To build a structural model of the EGC, we will use the observations made in the previous section and also a global structural analysis made on all the measures (fig. 45) sorted by type (bedding, fold axial plane, fold axis and fault plane).

3.6.1. EGC Structural Model

All beddings poles form a NNE-SSW oriented best fit great circle indicating a gentle ESE plunge of the regional fold axes (fig. 45-A). Rock cleavage is mainly developed in the central Tufan zone. Sandy and clayey lithology favour the formation of a sparse spaced cleavage (S_1) under low grade metamorphic condition (see chapter 4). S_1 shows an orientation ESE-WNW, with steep dips to the north and the south and is fold axial parallel. The schistosity poles (fig. 38- H and J) are also aligned on a NNE-SSW direction. Fold axes are oriented WNW-ESE with a slight dominant gentle (<10°) plunges to the ESE (number 1 on fig. 45-B). Fold axial planes poles are grouped in two zones (nb. 1 and 2 on fig. 45C) aligned parallel to bedding and schistosity planes on a NNE-SSW line. All the structure are concordant and they could result from a NNE-SSW compression stress.

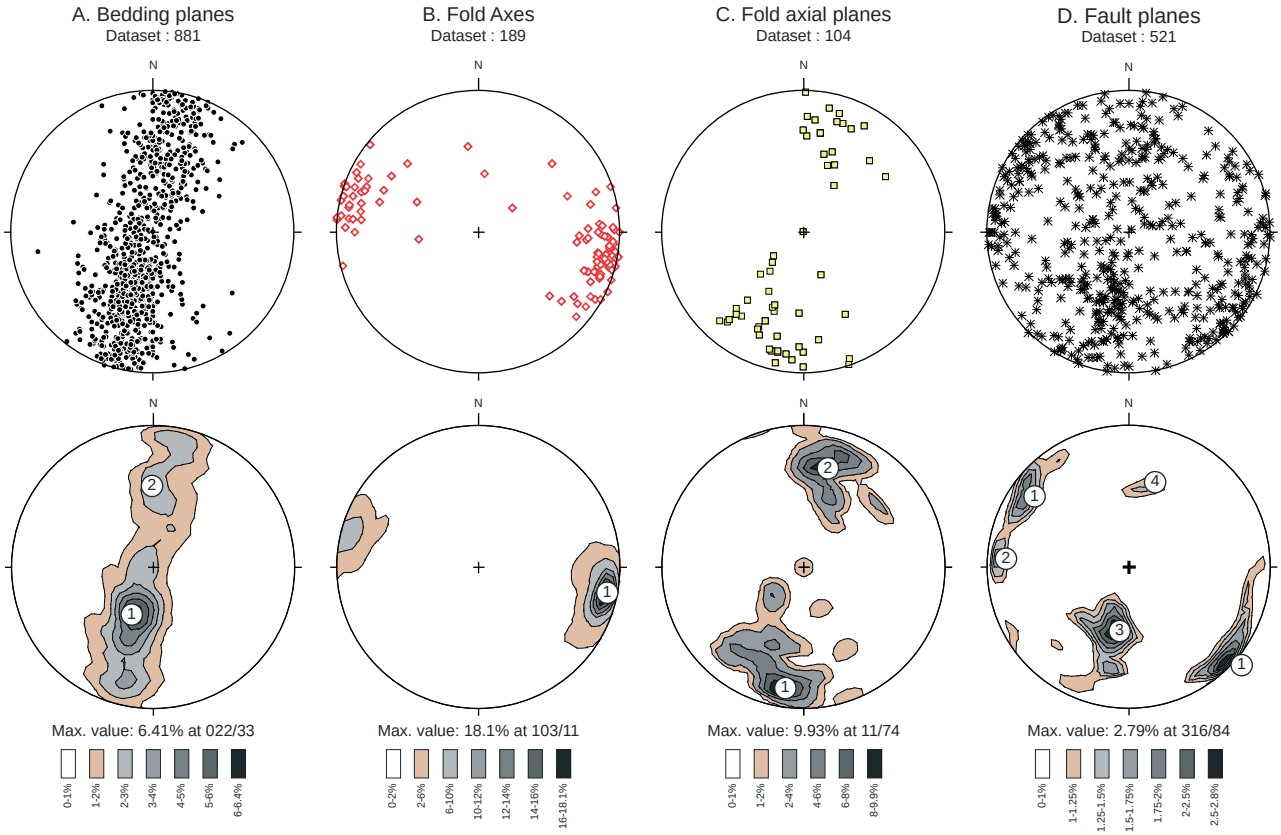

Figure 45: Structural data analysis (data stereonets in the upper row and density analyses in lower row) in equal area lower hemisphere projection of: (A) Poles of bedding planes, (B) fold axes, (C) Poles of axial planes and (D) Poles of fault planes. Peaks for each stereonet are sorted from the highest to the lowest value and numbered but their order is meaningless because the density of measures was not uniform all over the EGC.

4 main fault plane families can be distinguished: a N-S strike-slip fault system with a dextral movement (figs. 45D-1 and 35-B3, C); a NE-SW strike-slip fault system with a sinistral movement (figs. 45D-2 and 35-B4, D); WNW-ESE thrusts that dip to the NNE with top to the SSE movement (figs. 45D-3 and and 35-A); WNW-ESE thrust that dip to the SSW with top to the NNE movement (figs. 45D-4 and and 35-A). Thrusts seem to be correlated with a NNE-SSW compression. Both sinistral and dextral faults can be correlated using a conjugate fault system model resulting from a NNE-SSW directed compression. Main dextral and sinistral faults are conjugate and some secondary faults can be explained by a Riedel Model linked with a NNE-SSW main shortening direction. These strike-slip faults correspond to the Anticaucasian fault system and most of EGC valleys follow their direction. Moreover we can observe that the compression responsible for the strike slip faulting is not exactly aligned with the compression that created the thrust faults and the folds. It is slightly rotated eastward.

Finally in terms of stresses, reverse faulting results from an average NNE-SSW compression (fig 46 – column 1). Strike-slip faulting result also from an average NNE-SSW compression (fig 46 – column 3). Based on the detailed data, the resulting strike-slip fault planes have a N-S direction with a dextral movement and a NE-SW with a sinistral movement. They are commonly named anticaucasian fault system and they influence the geomorphology of the EGC. Finally, few extensional regimes are present. Extension is mostly expressed by a vertical σ_1 and σ_2 and σ_3 do not have a determined direction (fig 46 – column 2). Based on the detailed data, the extensional regime is local and therefore will not be included in the EGC structural model.

The deduced structural model of the EGC (fig. 47) is based on a general NNE-SSW compression. All bedding plane poles are distributed along a NNE to SSW oriented zone. Folds have generally steep axial planes and sub-horizontal fold axes that may gently dip to the ESE. In terms of faulting, two main systems are acting on the EGC: a thrusting system and a conjugate strike-slip fault system. The main thrusting system is composed of thrusts that dip to the SSW with top to the NNE movement and thrust that dip to the NNE with top to the SSW movement. The strike-slip faulting is a conjugate fault system with NE-SW sinistral faults and N-S dextral faults.

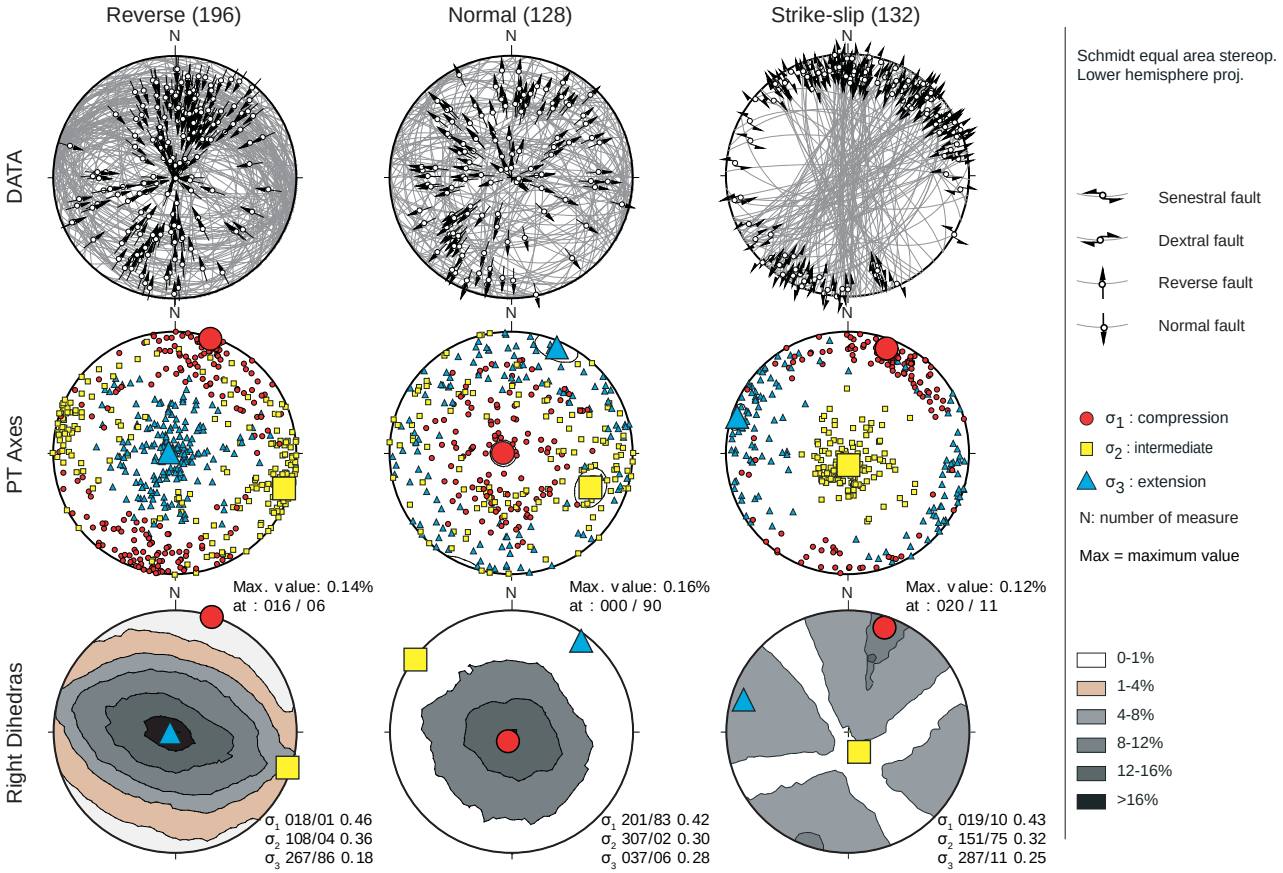

Figure 46: Analyses of all faults data sorted by main movement types (reverse, normal and strike-slip). Data stereonets in the first row, PT Axes analyses in the second row and Right Dihedra analyses in the third row.

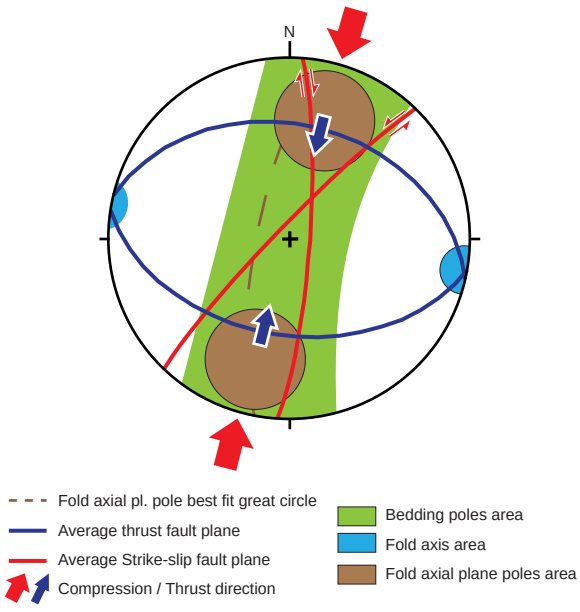

Figure 47: Stereonet of the EGC Structural Model based on our field measures and observations.

3.6.2. EGC evolution

During the Aalenian the EGC area underwent a subsidence that led to the deposition of deep marine sediments of the Tufan and Tahircal zones. This area of subsidence defined a basin which corresponds to the Greater Caucasus Basin (GCB). The evolution of the GCB basin since its opening is characterized by a succession of extensional and compressive events. The individual events can be discriminated based on field evidence and interpretation of data.

The first observed compressive event in the EGC (n°1 on fig. 48) is defined by the folded deep marine deposits of the Middle Jurassic covered by an erosional unconformity of shallow marine deposits of Callovian age in the northern Tahircal-Sudur zones. Based on sediment age, the compressive event is dated Bajocian-Bathonian (Middle Jurassic). This folding event can be possibly related to the Mid-Cimmerian event described by Fürsich et al. (2009) in northern Iran.

During the Upper Jurassic Period, thick limestones were deposited in a platform and slope context. They can be observed mainly on the northern side of the present EGC. They were submitted before the Berriasian to another compressive event (n°2 on fig. 48): Berriasian conglomerates lie on tilted Kimmeridgian slope deposit along the Gilgilcay River. This discontinuity can be related to one of the numerous compressional tectonic events that occurred during the post-rifting period of thermal subsidence in the Early Cretaceous (Brunet et al. 2009a).

During the Lower Cretaceous Period, mainly slope sediments (turbidites) were deposited. In the southern slope, they contain volcanic components. A passive margin was present at this period along the northen edge of the GCB. This period is also characterized by the collapse of kilometric size olistostromes (Sahdag-Besbarmaq Nappe) along the northern edge during the Valanginian-Barremian period.

A transgressive event (n°3 on fig. 48) occurred during the Turonian-Campanian periods that can be linked to a compressive event (underlying Albian-Aptian sediments are folded). Afterwards “Neoautochtonous” sediments were deposited and filled existing paleotopography. In the east, they are characterized by Turonian conglomerates that cover deep sediments of Albian-Aptian period; in the west, they are characterized by marly sediments of Campanian Age that were deposited on the Sudur Zone, on the Sahdag-Besbarmaq Nappe and on Sahdag-Xizi Zone. North of Cek Village and in Buduq, the “Neoautchtonous” deposits fill a paleo-valley (the Buduq Trough) eroded into the Sahdag-Besbarmaq Nappe (Upper Jurassic deposits) and the underlying Barremian and Aptian deposits of the Sahdag-Xizi Zone.

During the middle part of the Upper Cretaceous, the area underwent a renewed subsidence and thick series of marine sediments were deposited mostly in the eastern part (i.e. Dubrar Mountain).

The next event (n°4 on fig. 48) started at the end of the Upper Cretaceous and ended during the Paleocene. In the Tahircal and Sudur zones, Paleocene rocks unconformably lie on older deposits of Middle Jurassic to Cretaceous ages. This event does not correspond to the beginning of the building of the present Greater Caucasus. At this period, the area can be described as a succession of reliefs with piggy back basins.

At the end of the Eocene Epoch, the collision of the Arabian Plate with the Eurasian Plate started. The related compressional tectonic event (n°5 on fig. 48) changes the tectonic regime from a general subsidence to an uplift in the EGC area. Related to this event, foreland basins were built on both sides of the EGC and filled by marine slope deposits. To the south, a deep (100 to 3000 m) foreland basin was formed during the Oligocene Epoch: the Kura Basin. To the north of the EGC, shallower sediments were deposited in smaller basins. Filling sediments came from the erosion of the young EGC and are commonly called Maikop deposits. They are a main source rock for hydrocarbon resources in the area.

During Middle Miocene to Early Pliocene age, a shallowing up occurred in Samaxi Qobustan Zone and there are no evidences of substantial inflow of Caucasus erosion material.

During the Sarmatian (corresponding to the official Serravalian, 10-12 Myr) a general uplift of all the GCB started, however a northern foreland and shallow basin were created and sediments of Sarmatian age were deposited on the Sahdag-Besbarmaq Nappe area. These Middle Miocene marine sediments can be presently seen at more than 3600 m on the Sahdag Mt. intermediate plateau. On the southern slope Sarmatian sediments cover a large area in the Samaxi-Qobustan Zone.

The compressional tectonic event (n°6 on fig. 48) that corresponds to the main orogenic phase of the Greater Caucasus started at the end of Miocene and lasted until the beginning of the Pliocene Epoch. The Tufan Zone and the northern zones underwent uplift. In the southern slope, the emplacement of the Basqal Nappe took place (Sarmatian age) just prior to the uplift of the Vandam Zone. The formation of the Alazani Basin as a foreland piggy-back basin was linked with

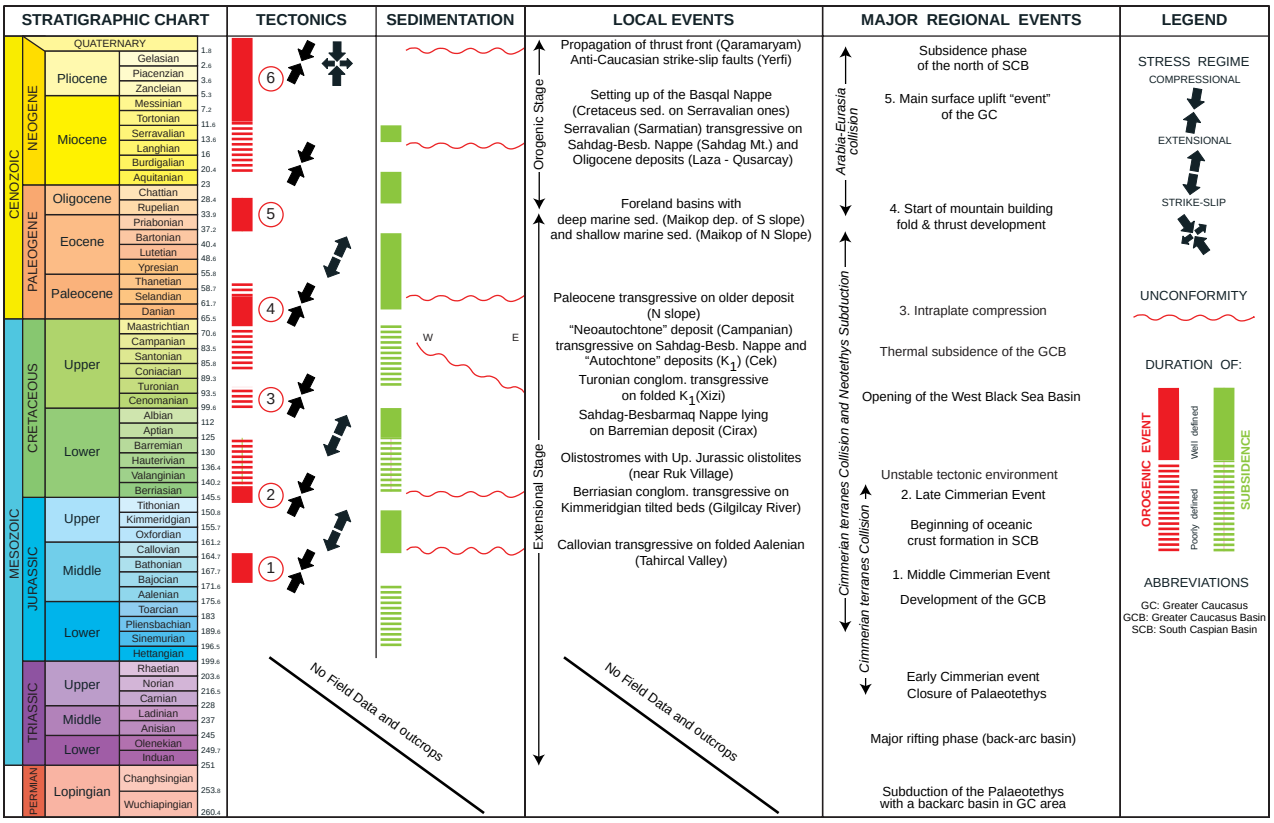

Figure 48: Summary of the tectonic and stratigraphic evolution of the eastern Greater Caucasus produced from field-based investigation. Information on major regional events has been obtained from ZONENSHAIN & LE PICHON (1986), PHILIP et al. (1989), BRUNET et al. (2003), NIKISHIN et al. (2001), SAINTOT et al. (2006a) and BARRIER et al. (2008a). Modified from EGAN et al. (2009).

the main orogenic phase of the EGC and was filled with the corresponding erosive products. The most uplifted part was to the west of the EGC and is expressed by the huge amount of exhumed Middle Jurassic deposits.

The building of the EGC is still very active. The north and the central part undergo long term uplift respectively since the Sarmatian and the Oligocene. The southern slope is characterized mainly by thrusts dipping to the north but also by local uplift (Vandam Zone, Aalenian near Qalaciq) that are closely linked with the geodynamics of the southern fold and thrust belt (underthrusting). Finally the most southern active and blind thrust is located under the Qaramaryam hills where folded Pleistocene and Holocene sediments can be observed.

3.6.3. Geodynamics of the EGC

The EGC corresponds to an asymmetrical divergent orogenic wedge with fold and thrust belts on each side. As the whole Caucasus, the EGC results from a continent-continent collision between the Arabian and Eurasian plates. Its geodynamics is particularly influenced by the presence of a deep intracontinental basin (the South Caspian Basin) with a rapid subsidence and deep forelands basins (Kura, Terek and North Caspian basins). Eastwards the prolongation of the EGC into the Caspian Sea forms a ridge, the Abseron Ridge, between the North Caspian Basin and the South Caspian Basin. Based on EGAN et al. (2009) and GREEN et al. (2009), this ridge is the result of a recent northward subduction of the South Caspian Basin under the North Caspian Basin.

The northern fold and thrust belt corresponds to the retro-wedge of the orogen and is broadening westward into Dagestan. It is dominated by folds in Jurassic and Cretaceous deposits. In this area like in the central area, Middle Jurassic deposits outcrop and are highly eroded. Based on the occurrence of marine sediments of Sarmatian age resting on Middle Jurassic series at an altitude in excess of 3600 m, we can determine uplift rate (since late Sarmatian, 11.5 Myr) of 0.31 mm/yr

The northern area is also characterized by the emplacement of kilometric olistostromes during the Lower Cretaceous. They correspond to the main block composing the Sahdag-Besbarmaq Nappe (i.e. Sahdag Mt., Qizilqaya Massif, Cirax Mt. and Besbarmaq Mt.). Based on structural measures, we deduced that they

underwent the same deformation as the adjoining areas after their emplacement. At the beginning of the Miocene, the whole nappe was backthrusted to the north.

In the central part (Tufan Zone), the transition between thrusts directed to the north and to the south can be observed. The highest part of the EGC near the Bazarduzu Mt. (4466 m) was built by thrusting and folding of Middle Jurassic sediments. This area also underwent the highest uplift of the EGC. It started at least in Eocene time at the beginning of the Greater Caucasus orogen. The uplift rate could not be directly estimated because of the lack of sediments younger than Middle Jurassic.

The southern slope is the fore-wedge of the EGC and corresponds to a well-developed fold and thrust belt. Thrusting is still active along the northern edge of the Kura Basin and thrusts dipping to the north are dominant. The area is also characterized by a “late” local uplift (Vandam Zone) probably related to underthrusting. The active frontal thrust of the EGC is located in the Kura Foreland basin (Qaramaryam hills).

Overall the EGC is cut by anticaucasian strike-slip faults with a NE-SW and N-S direction. They influence most of the valley direction and also create deep canyons in the massive limestones of the Sahdag-Besbarmaq area. Their influence on the geomorphology is recent (Pliocene to Quaternary).

The Eastern Greater Caucasus is a still active area (see chapter 5). Based on the fact that altitudes decrease going to the SE and that sediments of the central part get younger going to the SE, we deduce that the uplift acted first in the west and moves southeastwards along the main Greater Caucasus crest.

*****

PLATES

PLATE 3.1: STRUCTURES OF TAHIRCAL VALLEY

A. Gestinkil Mountain (2788 m) – Transgressive contact between deep marine folded Aalenian deposits and shallow marine Callovian deposits - (48°6’25.66”E - 41°28’49.05”N - Azm. 270°) (07.09.2005).

B. Northern bank of Samur River – Transgressive contact between folded Bajocian – Bathonian (Middle Jurassic) deep marine deposits and Pliocene continental (conglomerates and gravel) - (48°10’48.11”E - 41°29’35.89”N - Azm. 320°) (N. Mountney - 10.09.2004).

C. Western bank of Tahircal River – Recent terraces on folded Middle Jurassic deposits - (48°5’11.08”E - 41°27’2.79”N - Azm. 315°) (10.09.2004).

D. Tahircal Village – Highly folded Aalenian (Middle Jurassic) deposit under flat Quaternary terraces. The Middle Jurassic fold has a north directed axial plane - (48°4’36.86”E - 41°26’30.85”N - Azm. 286°) (08.09.2006).

E. Middle part of Tahircal Valley - Transgressive contact between folded and deep marine Aalenian deposits and shallow marine (anhydrite – gypsum – dolomite) Callovian deposits - (48°2’21.04”E - 41°26’18.25”N - Azm. 160°) (J. Mosar - 07.09.2005).

F. Same place as E –Middle Jurassic deposits fold with a south directed axial plane covered by flat Callovi-an and Upper Jurassic sediments - (48°4’5.11”E - 41°25’49.16”N - Azm. 270°) (07.09.2006).

G. Upper middle part of Tahircal Valley - Fractured Upper Jurassic rock with N-NE directed fault planes - (48°2’38.67”E - 41°23’10.73”N - Azm. 115°) (08.09.2005).

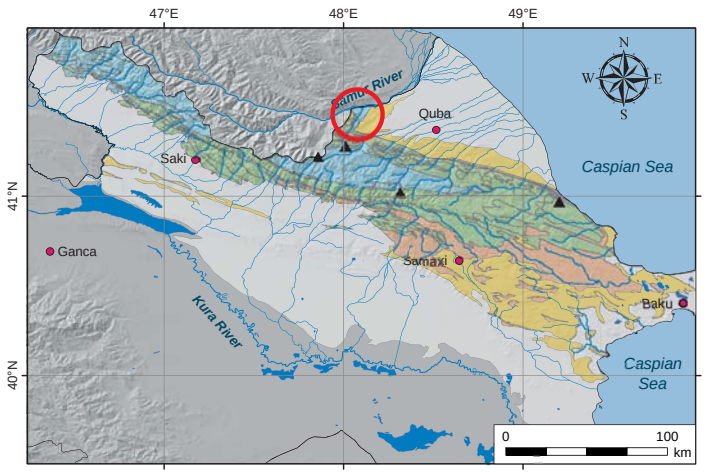

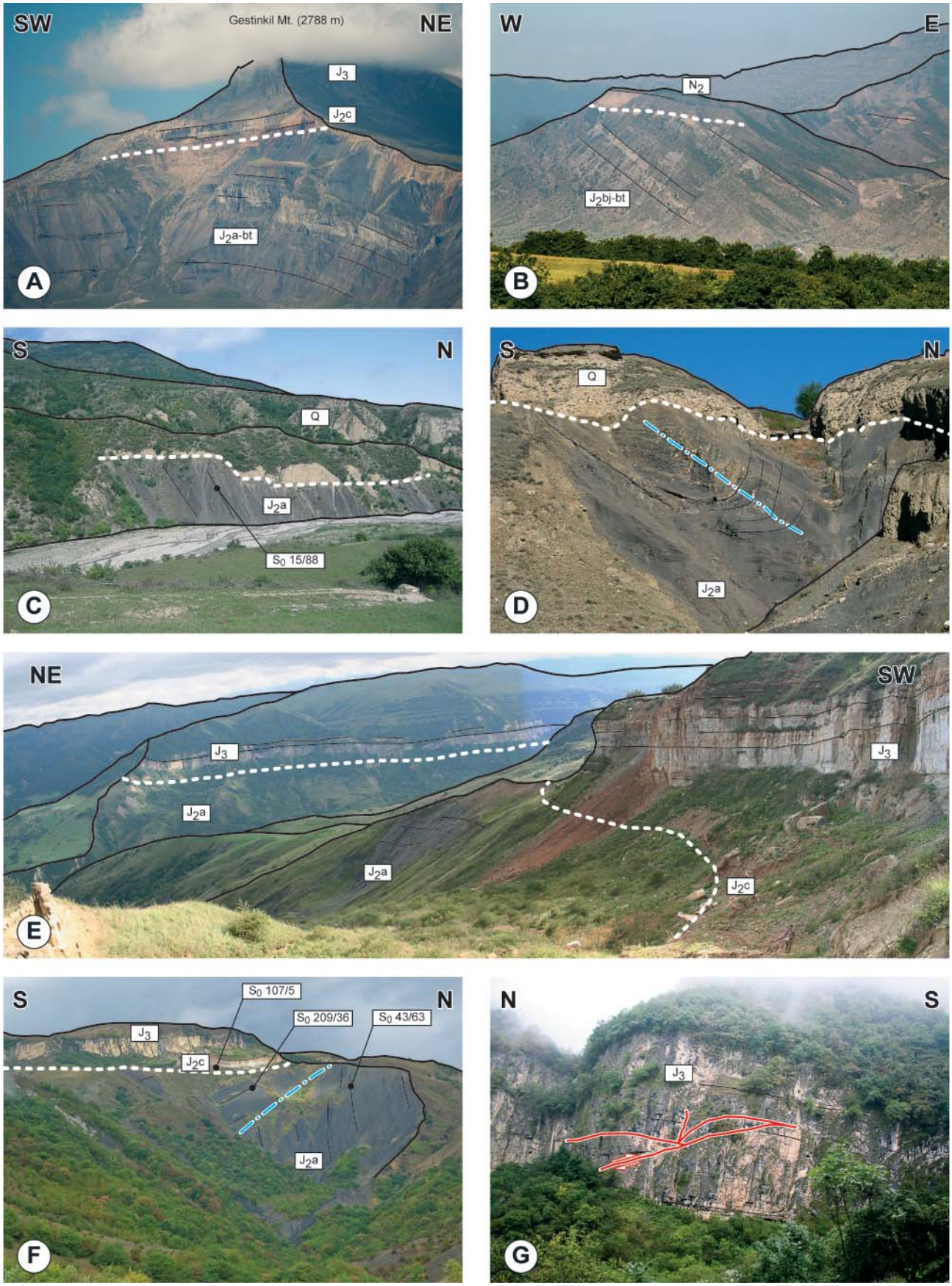
SW
Gestinkil Mt. (2788 m)
NE
J3
J2c
J2a-bt
A
W
E
N2
J2bj-bt
B
S
N
Q
J2a
S0 15/88
C
S
N
Q
J2a
D
NE
SW
J3
J2a
J2a
J3
J2c
E
S
N
S0 107/5
S0 209/36
S0 43/63
J3
J2c
J2a
F
N
S
J3
G

PLATE 3.2: STRUCTURES OF SUDUR AREA

A. Panorama along the western bank of Qusarcay River (north of Sahdag Massif) – Sahdag Massif thrust and the folded Sudur zone with north and south directed axial planes - (48°7’23.26”E - 41°16’17.13”N - Azm. 300°) (31.08.2006).

B. Panorama along the eastern bank of Qusarcay River (north of Qizilqaya Massif) – Qizilqaya Massif thrust and the folded Sudur zone with north and south directed axial planes - (48°5’34.76”E - 41°18’34.23”N - Azm. 90°) (A. Rast - 01.09.2006).

C. Eastern bank of Qusarcay River (north of Qizilqaya Massif) – Folds in Lower Cretaceous deposits with south directed axial planes - (48°7’30.02”E - 41°18’20.14”N - Azm. 110°) (02.09.2006).

D. Eastern bank of Qusarcay River – Fault bend fold with a south directed fault plane - (48°5’34.76”E - 41°18’34.23”N - Azm. 90°) (01.09.2006).

E. Eastern bank of Qusarcay River (north of Qizilqaya Massif) – Overturned fold under the Qizilqaya Mas-sif thrust with a south directed axial plane - (48°6’31.99”E - 41°16’44.37”N - Azm. 135°) (31.08.2006).

F. Western bank of Qusarcay River (north of Sahdag Massif) – Outcrop of Oxfordian deposits (Upper Jurassic), the oldest deposit and most southern outcrop of Sudur Zone in the area - (48°6’17.62”E - 41°16’52.31”N - Azm. 270°) (23.08.2006).

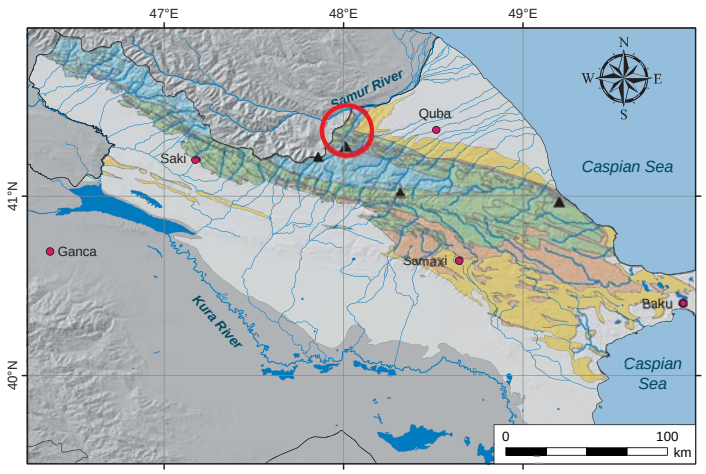

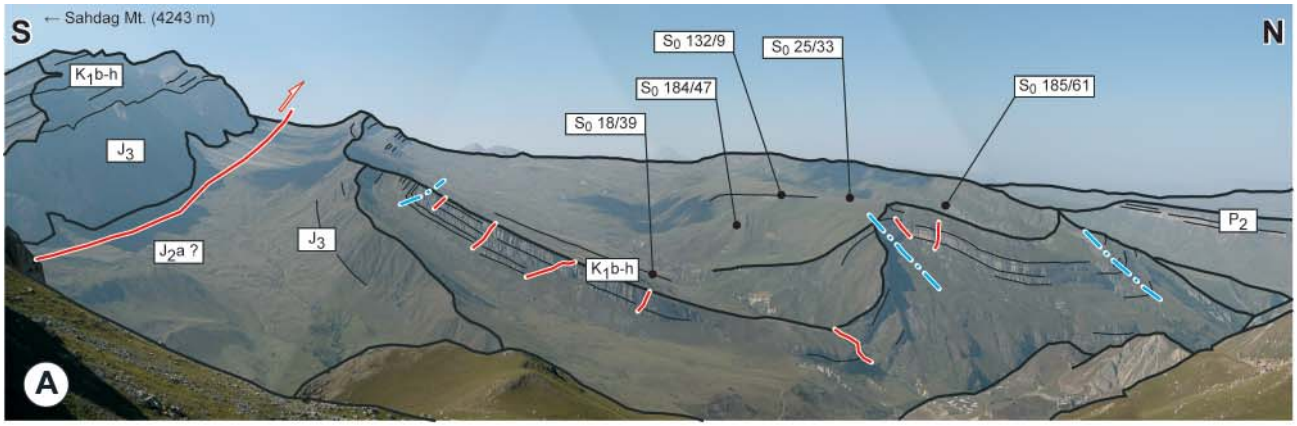
S
← Sahdag Mt. (4243 m)
N
K1b-h
J3
J2a ?
J3
K1b-h
S0 132/9
S0 25/33
S0 184/47
S0 18/39
S0 185/61
P2
A

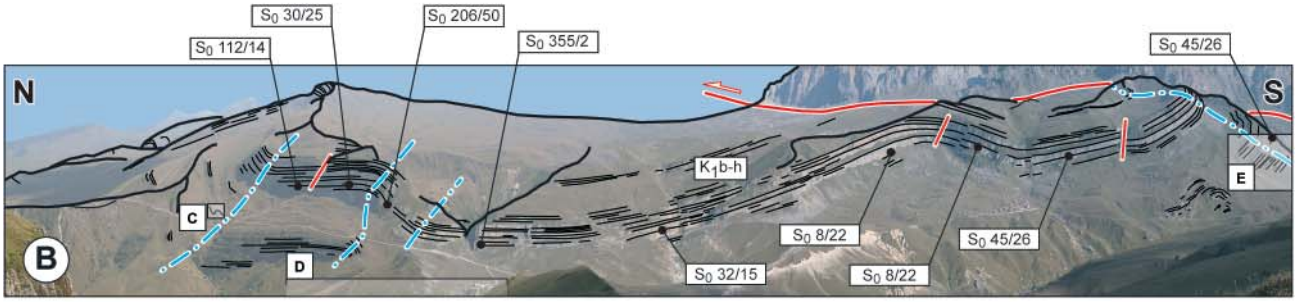
S0 30/25
S0 112/14
S0 206/50
S0 355/2
S0 45/26
N
S
K1b-h
C
D
E
S0 8/22
S0 45/26
S0 32/15
S0 8/22
B

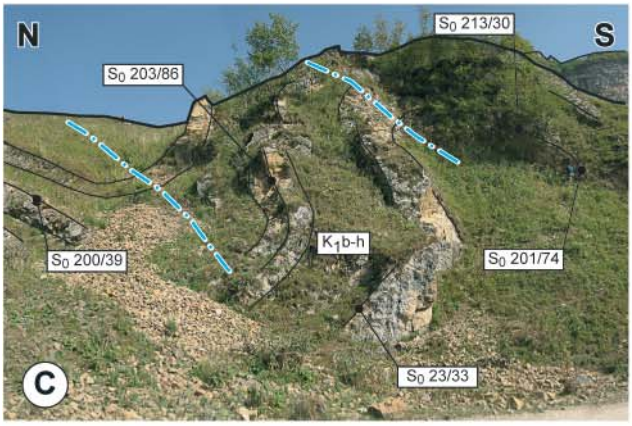
N
S
S0 213/30
S0 203/86
K1b-h
S0 200/39
S0 201/74
S0 23/33
C

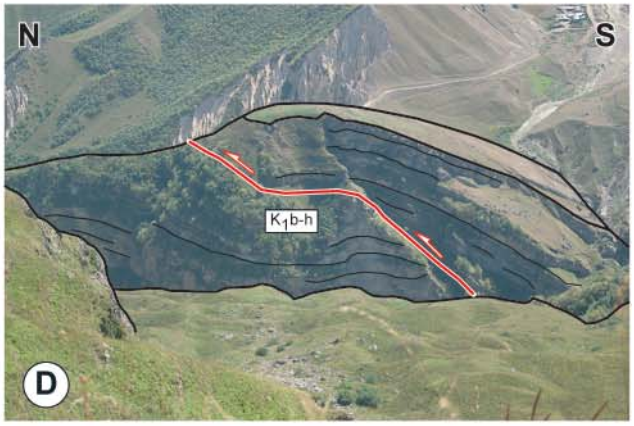
N
S
K1b-h
D

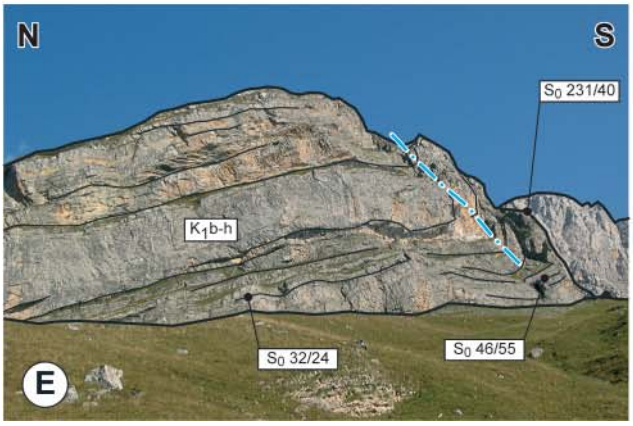
N
S
S0 231/40
K1b-h
S0 32/24
S0 46/55
E


S
N
J3o
F

PLATE 3.3: STRUCTURES OF SAHDAG MT. AND QIZILQAYA MT.

A. Panorama of the western part of the Sahdag Massif – The northern widely open syncline and the begin-ning of the anticline forming the highest part of the Sahdag Massif - (48°1’6.92”E - 41°16’51.62”N - Azm. 270°) (24.08.2006).

B. View on the Sahdag Mountain from Qizilqaya Massif – The summit area is formed by an anticline and the south-ern side by a syncline -(48°7’51.73”E - 41°13’38.88”N - Azm. 270°) (05.08.2006).

C. Sahdag main plateau – Upper Cretaceous white deposits transgressive on Lower Cretaceous deposits themselves transgressive on Upper Jurassic detritic and subvertical limestones - (48°3’0.89”E - 41°16’30.14”N - Azm. 260°) (24.08.2006).

D. Valley east of Sahdag summit – Upper Jurassic overturned bedding in contact with Lower Cretaceous normal bedding - (48°2’55.75”E - 41°16’7.23”N - Azm. 250°) (28.08.2006).

E. Between the Sahdag and Qizilqaya Massif – Klippe of Upper Jurassic in Middle Jurassic deposits – Measured beddings are not the same in the Klippe and in the Middle Jurassic deposits - (48°4’23.59”E - 41°14’4.62”N - Azm. 90°) (25.08.2006).

F. View on the Qizilqaya Massif – A large syncline build the main part of the Massif – On the right, the Upper Jurassic Klippe in Middle Jurassic deposits - (48°3’14.2”E - 41°16’18.45”N - Azm. 90°) (28.08.2006).

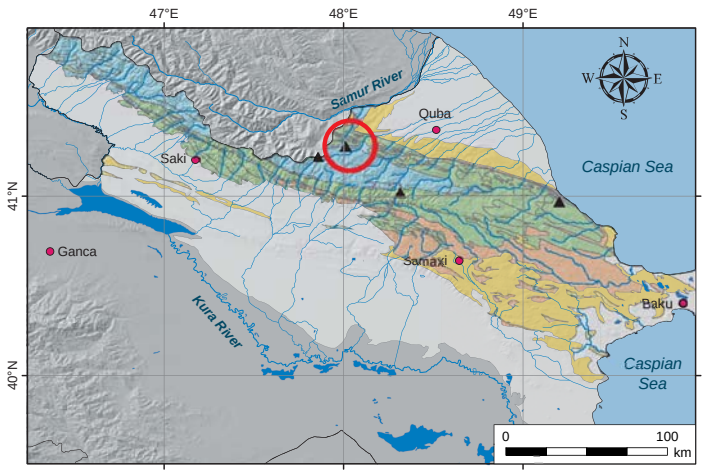

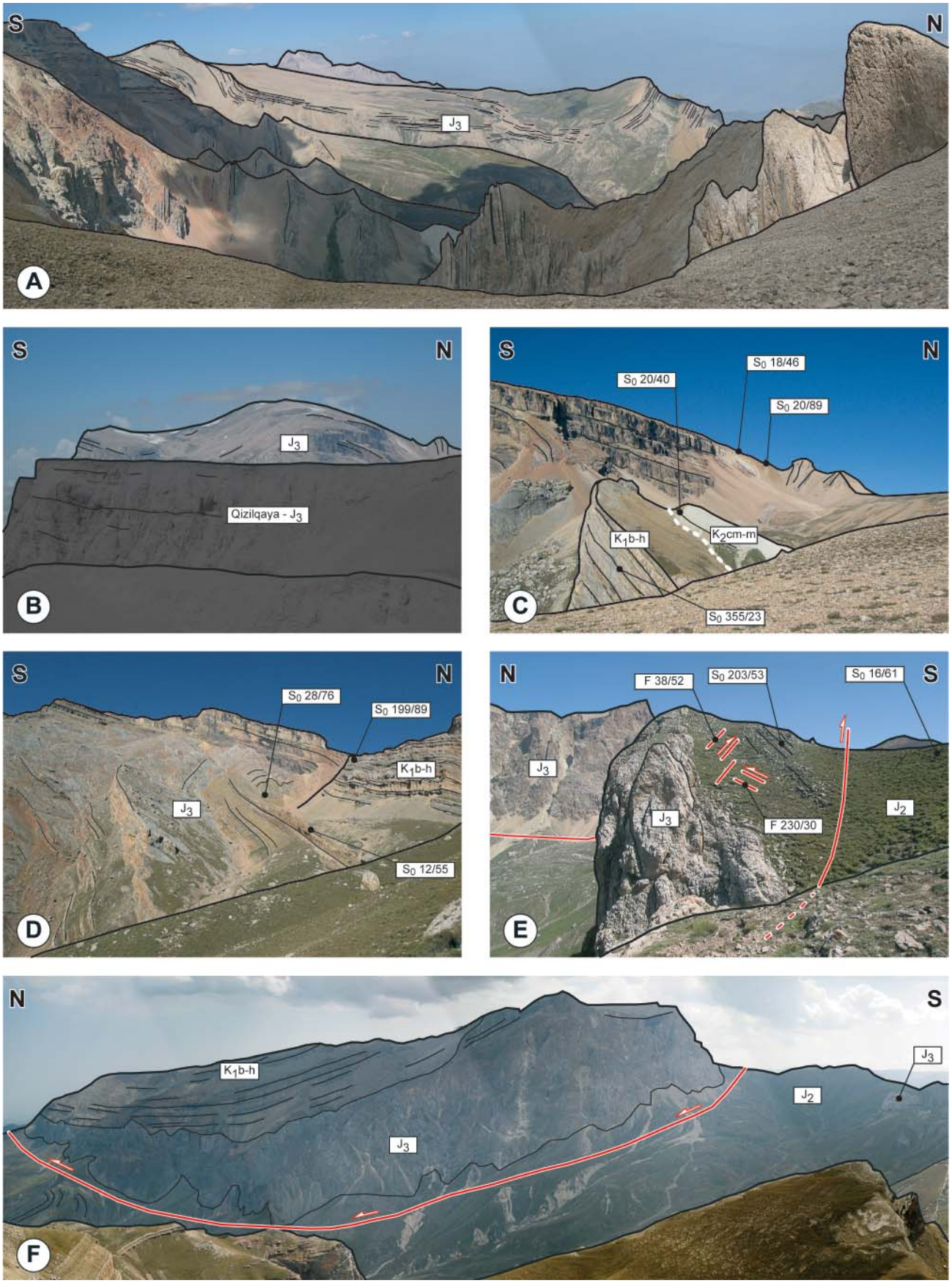
S
N
J_3
A
S
N
J_3
Qizilqaya - J_3
B
S
N
S_0 20/40
S_0 18/46
S_0 20/89
K_1b-h
K_2cm-m
S_0 355/23
C
S
N
S_0 28/76
S_0 199/89
K_1b-h
J_3
S_0 12/55
D
N
S
F 38/52
S_0 203/53
S_0 16/61
J_3
J_3
J_2
F 230/30
E
N
S
K_1b-h
J_3
J_2
J_3
F

PLATE 3.4: STRUCTURES OF TUFAN ZONE - BAZARDUZU AREA

A. View on the Sahdag equivalent in Dagestan, the Shalbuzdag (4142 m) – In the Shalbuzdag the Middle and Upper Jurassic deposit are concordantly bedded, the Nappe starts only from the Sahdag Massif to the East - (47°54’2.6”E - 41°14’0.41”N - Azm. 315°) (26.08.2006).

B. View from the eastern subsidiary summit of Bazarduzu Mountain to the Northeast on Sahdag-Qizilqaya Nappe – The nappe was first thrusted to the south and afterward backthrusted to the north - (47°54’2.6”E - 41°14’0.41”N - Azm. 90°) (26.08.2006).

C. View from the eastern subsidiary summit of Bazarduzu to the East on the Middle Jurassic deposits of the central part of the Eastern Greater Caucasus – Highly folded zone with south directed axial planes form-ing the highest area of Azerbaijan - (47°55’29.81”E - 41°13’23.38”N - Azm. 90°) (26.08.2006).

D. View on the highest summit of Azerbaijan, the Bazarduzu Mountain (4466 m) from the Qizilqaya Massif – Axial planes are south directed - (48°7’51.76”E - 41°13’38.84”N - Azm. 225°) (05.08.2006).

E. View from the eastern subsidiary summit of Bazarduzu Mountain to the West on the Middle Jurassic de-posits of the Dagestan – Folds with south directed axial planes - (47°54’2.6”E - 41°14’0.41”N - Azm. 270°) (26.08.2006).

F. View from the eastern subsidiary summit of Bazarduzu to the southeast on the Middle Jurassic deposits – Steeply inclined folds with south directed axial planes - (47°55’29.81”E - 41°13’23.38”N - Azm. 135°) (26.08.2006).

G. View on the eastern subsidiary summit of the Bazarduzu Mountain – Thrusts towards the north and their linked folds with their south directed axial planes - (47°54’47.65”E - 41°13’25.43”N - Azm. 225°) (26.08.2006).

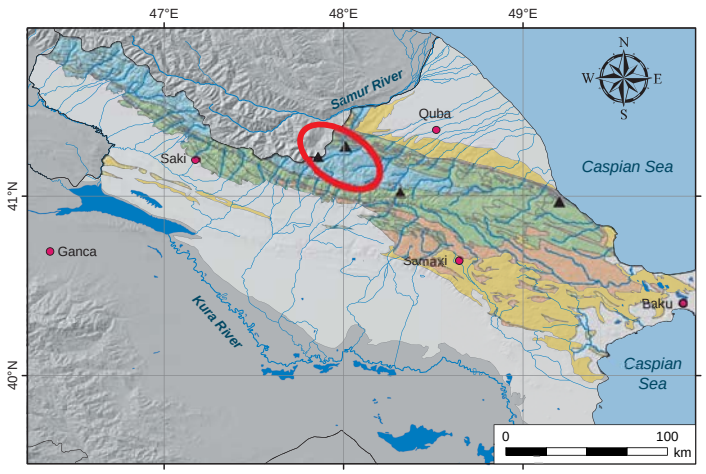

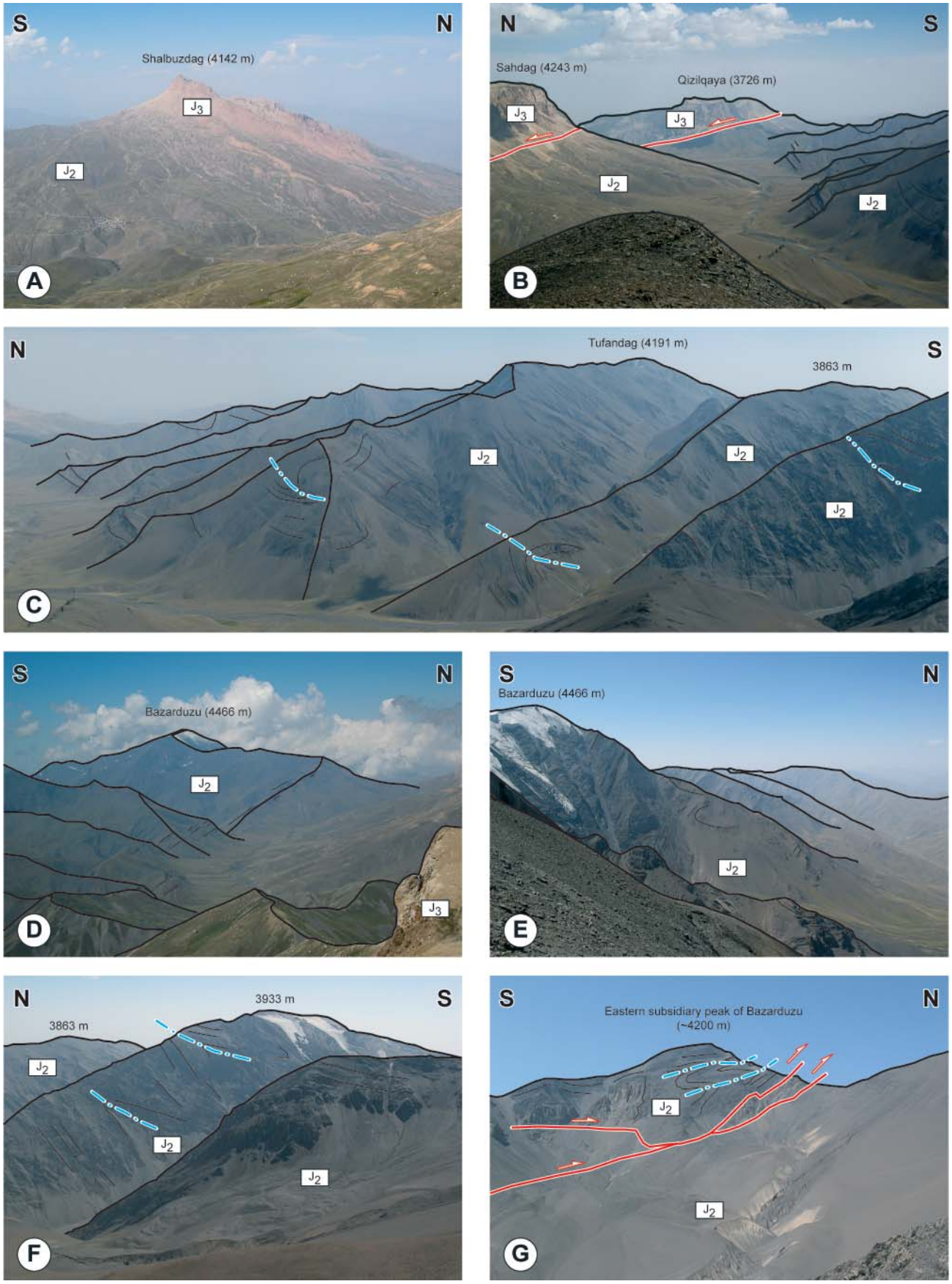
S
N
Shalbuzdag (4142 m)
J_3
J_2
A
N
S
Sahdag (4243 m)
Qizilqaya (3726 m)
J_3
J_3
J_2
J_2
B
N
Tufandag (4191 m)
S
3863 m
J_2
J_2
J_2
C
S
N
Bazarduzu (4466 m)
J_2
J_3
D
S
N
Bazarduzu (4466 m)
J_2
E
N
3933 m
S
3863 m
J_2
J_2
J_2
F
S
N
Eastern subsidiary peak of Bazarduzu
(~4200 m)
J_2
J_2
G

PLATE 3.5: STRUCTURES OF TUFAN ZONE - QUDIYALCAY VALLEY

A. Southeast of the Qizilqaya Massif along the Qudiyalcay – From north to south : backthrust of a remnant of the Sahdag-Qizilqaya Nappe, normal fault between the Hauterivian and Aalenian deposits, tight syn-cline with a south directed axial plane and an opened faulted anticline in sandstones - (48°11’24.01”E - 41°11’24.41”N - Azm. 135°) (J. Mosar - 09.09.2005).

B. Northwest of Xinaliq Village – Southern limb of an anticline with a north directed axial plane in Middle Jurassic sandstones - (48°6’47.99”E - 41°11’6.65”N - Azm. 90°) (U. A. Glasmacher - 04.09.2007).

C. West of Xinaliq Village in Middle Jurassic deposits – The south directed bedding along the road to the Sahnabad Plateau - (48°6’47.99”E - 41°11’6.65”N - Azm. 270°) (U. A. Glasmacher - 04.09.2007).

D. South of Xinaliq in Middle Jurassic deposits – Chevron folds with an overturned limb and a north di-rected axial plane - (48°7’38.83”E - 41°10’18.97”N - Azm. 82°) (U. A. Glasmacher - 05.09.2007).

E. South of Xinaliq in Middle Jurassic deposits– Anticline-syncline at the beginning of the upper valley of Qudiya-lcay River - (48°6’37.02”E - 41°10’7.12”N - Azm. 95°) (02.09.2007).

F. Upper Valley of Qudiyalcay River – north directed beddings - (48°6’37.02”E - 41°10’7.12”N - Azm. 275°) (T. Kissner - 02.09.2007).

G. View from the northern subsidiary summit of the Xinaliq Dag Mountain to the East – Folds with south and north directed axial planes - (48°6’51.7”E - 41°8’33.73”N - Azm. 72°) (03.09.2007).

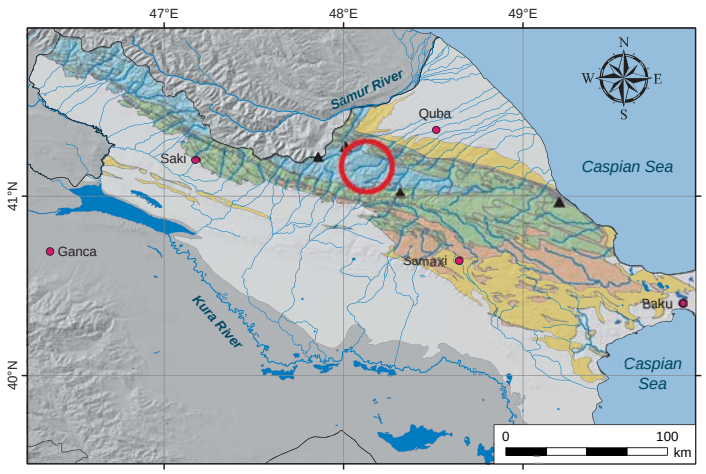

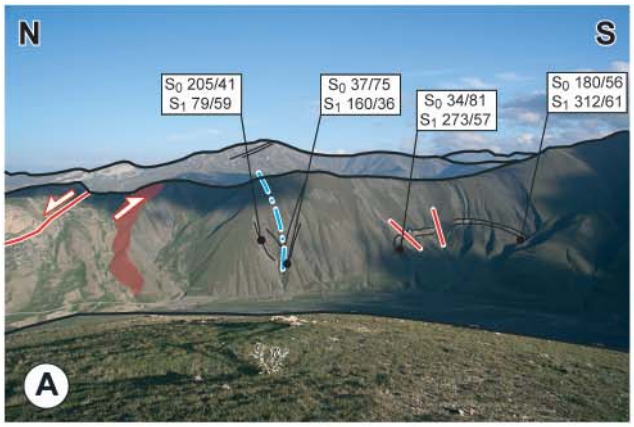
N
S
S_0 205/41
S_1 79/59
S_0 37/75
S_1 160/36
S_0 34/81
S_1 273/57
S_0 180/56
S_1 312/61
A

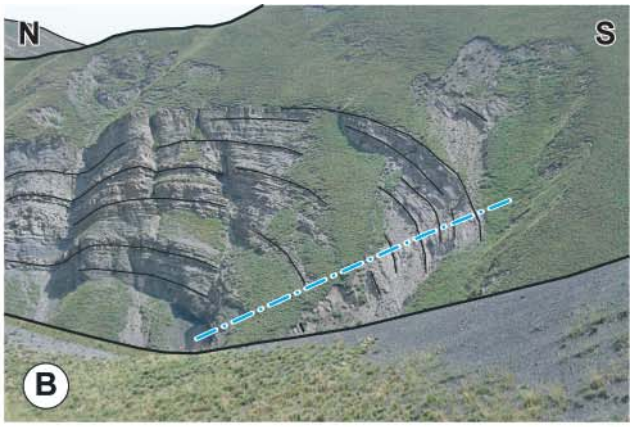
N
S
B


S
N
C

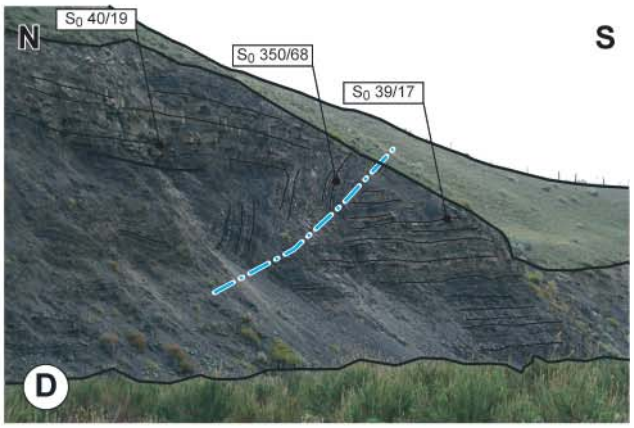
N
S
S_0 40/19
S_0 350/68
S_0 39/17
D

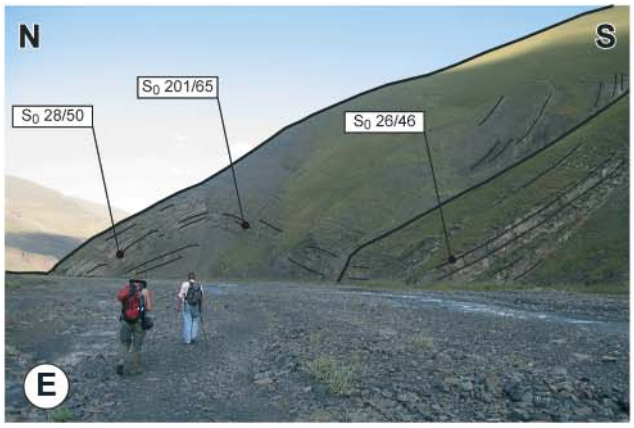
N
S
S_0 201/65
S_0 28/50
S_0 26/46
E

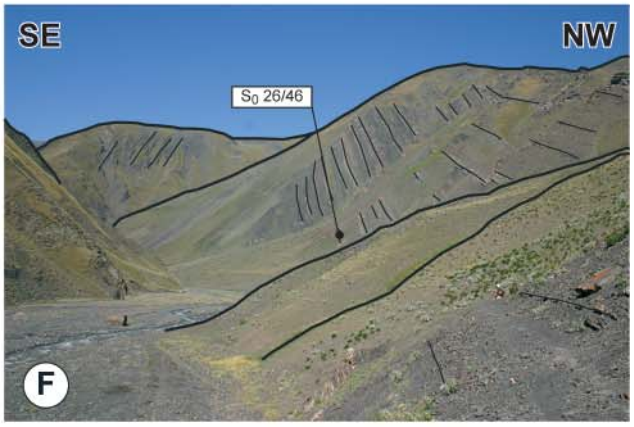
SE
NW
S_0 26/46
F

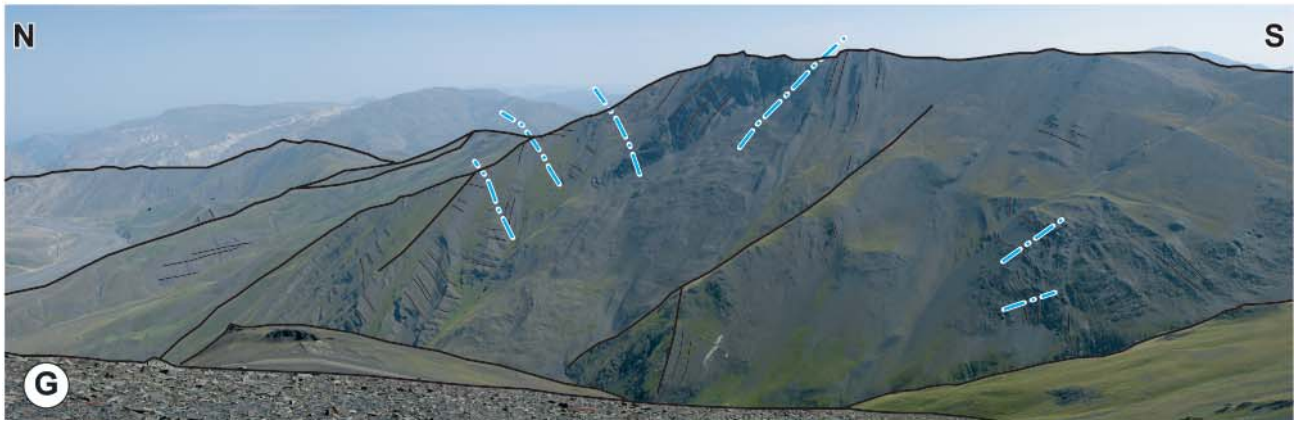
N
S
G

PLATE 3.6: STRUCTURES OF LOWER CEK VALLEY

A. North of Cek Village – Upper Cretaceous transgressively bedded on Upper Jurassic and Lower Creta-ceous deposits. The Upper Jurassic deposits are part of the Sahdag-Qizilqaya Nappe and are thrusted on the Lower Cretaceous deposits - (48°15'4.63"E - 41°11'41.07"N - Azm. 0°) (N. Mountney - 11.09.2004).

B. East of Cek Village on eastern bank of the Agcay River – Hauterivian olistostrome composed of Upper Jurassic olistoliths with a north directed bedding - (48°14'35.94"E - 41°10'55.8"N - Azm. 160°) (06.09.2005).

C. South of Alik Village on the eastern bank of the Agcay River in Middle Jurassic deposits – Syncline with a south directed axial plane - (48°14'15.99"E - 41°9'44.83"N - Azm. 315°) (14.06.2008).

D. South of Alik Village on the western bank of the Agcay River - Syncline (same as C) and anticline with south directed axial planes in Middle Jurassic deposits - (48°14'9.98"E - 41°9'46.55"N - Azm. 100°) (13.06.2008).

E. Between Alik and Hapit villages on the eastern bank of the Agcay River - Faulted zone in Middle Jurassic de-posits - (48°13'52.44"E - 41°8'54.63"N - Azm. 106°) (05.09.2007).

F. North of Hapit Village on the eastern bank of the Agcay River in Middle Jurassic deposits – Syncline with verti-cal axial plane - (48°13'24.61"E - 41°8'31.67"N - Azm. 132°) (14.06.2008).

G. Hapit Village on the western bank of the Agcay River in Middle Jurassic deposits – Syncline with a south di-rected axial plane - (48°13'15.38"E - 41°8'22.79"N - Azm. 270°) (14.06.2008).

H. South of Hapit Village on the western bank of the Agcay River in Middle Jurassic deposits – Thrust towards the north with its associate structures - (48°12'46.5"E - 41°8'3.86"N - Azm. 135°) (14.06.2008).

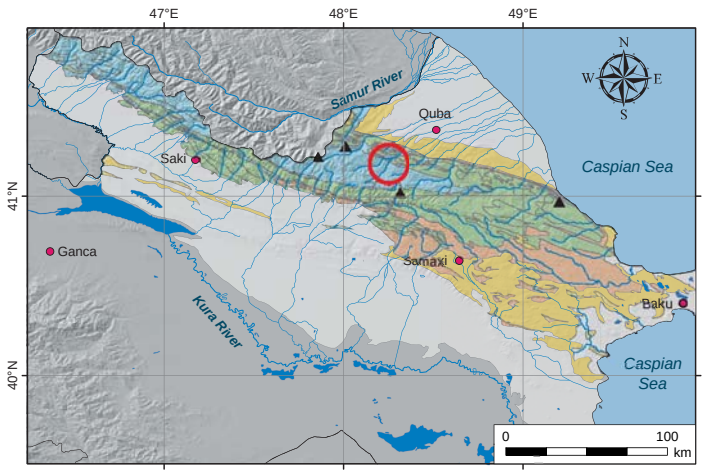

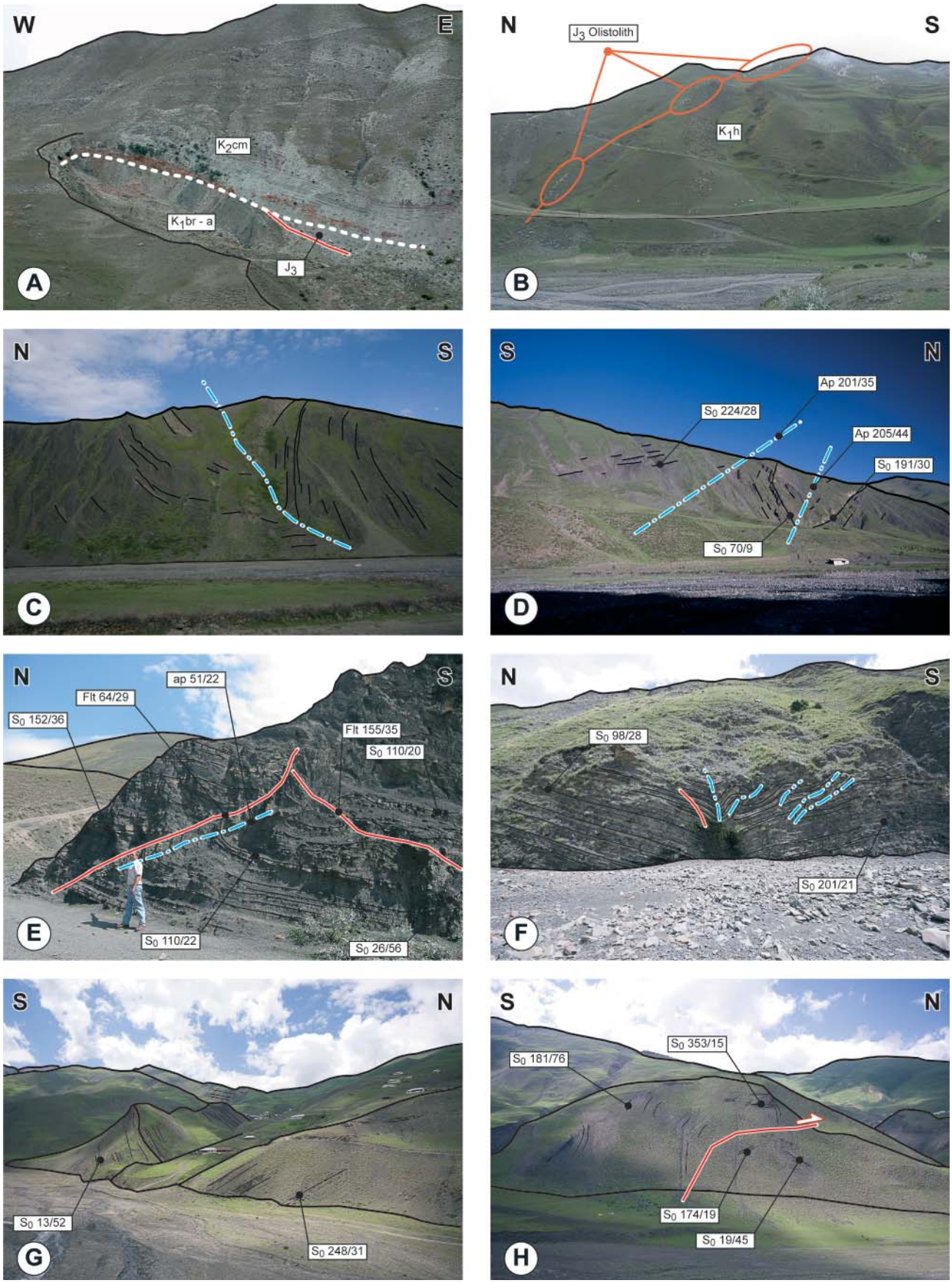
W
E
K_2cm
K_1br - a
J_3
A
N
S
J_3 Olistolith
K_1h
B
N
S
C
S
N
Ap 201/35
S_0 224/28
Ap 205/44
S_0 191/30
S_0 70/9
D
N
S
ap 51/22
Flt 64/29
S_0 152/36
Flt 155/35
S_0 110/20
S_0 110/22
S_0 26/56
E
N
S
S_0 98/28
S_0 201/21
F
S
N
S_0 13/52
S_0 248/31
G
S
N
S_0 353/15
S_0 181/76
S_0 174/19
S_0 19/45
H

PLATE 3.7: STRUCTURES OF UPPER CEK VALLEY

A. Along the eastern bank of the Agcay River - Syncline with a south directed axial plane in Middle Juras-sic deposits - (48°13’6.03”E - 41°8’27.19”N - Azm. 110°) (13.06.2008).

B. Along the eastern bank of the Agcay River – Thrust towards the north in Middle Jurassic deposits (48°12’39.36”E - 41°8’1.8”N - Azm. 135°) (14.06.2008).

C. Along the eastern bank of the Agcay River – Anticline with a south directed axial plane in Middle Jurassic deposits - (48°12’26.89”E - 41°7’40.1”N - Azm. 257°) (06.09.2007).

D. Along the eastern bank of the Agcay River – Syncline – Two thrusts towards the north with their associated anticline and syncline - (48°12’18.01”E - 41°7’25.3”N - Azm. 115°) (15.06.2008).

E. Along the western bank of the Agcay River – Highly folded and faulted zone in Middle Jurassic deposits - (48°12’10.02”E - 41°6’43.57”N - Azm. 271°) (06.09.2007).

F. Along the western bank of the Agcay River – Anticline with a subvertical axial plane in Middle Jurassic deposits - (48°11’41.77”E - 41°6’22.27”N - Azm. 292°) (06.09.2007).

G. Along the western bank of the Agcay River - Anticline with a subvertical axial plane in Middle Jurassic deposits (48°11’29.23”E - 41°6’4.08”N - Azm. 282°) (06.09.2007).

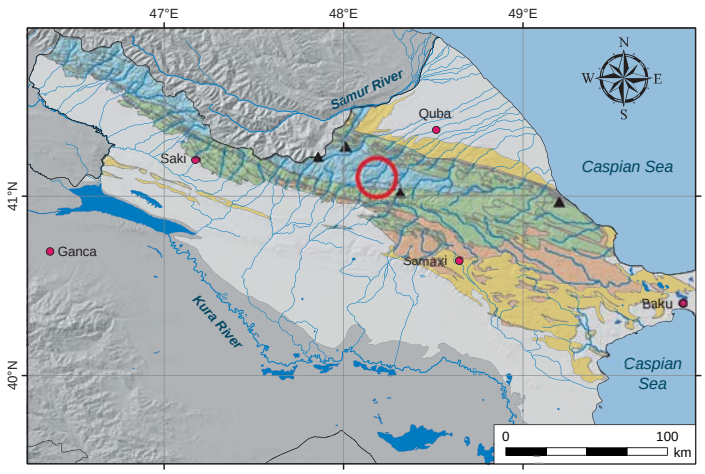


N
S
S_0 200/31
S_0 25/55
A

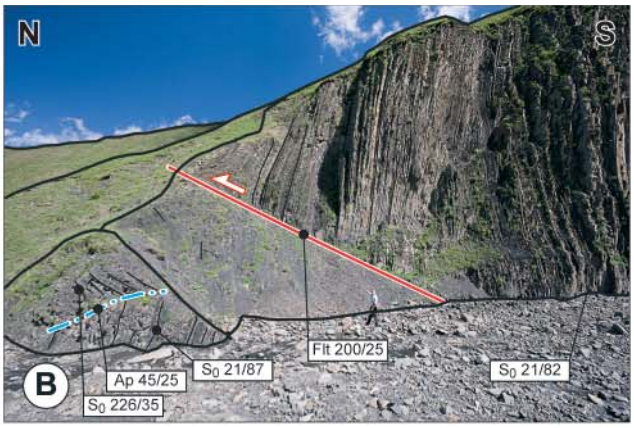
N
S
Ap 45/25
S_0 21/87
Flt 200/25
S_0 21/82
S_0 226/35
B

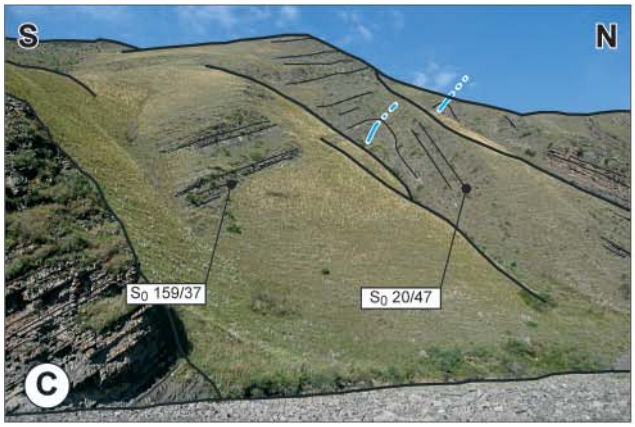
S
N
S_0 159/37
S_0 20/47
C

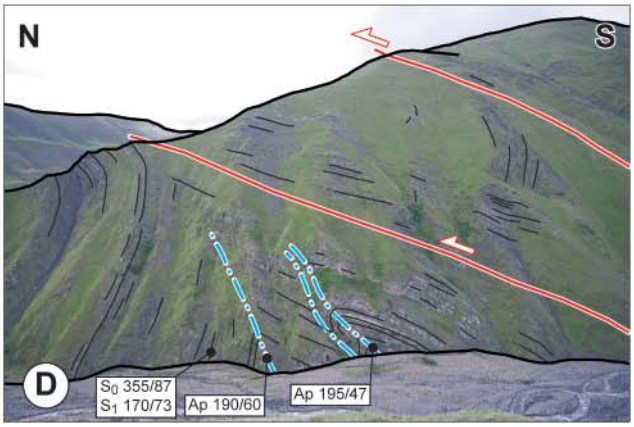
N
S
S_0 355/87
S_1 170/73
Ap 190/60
Ap 195/47
D

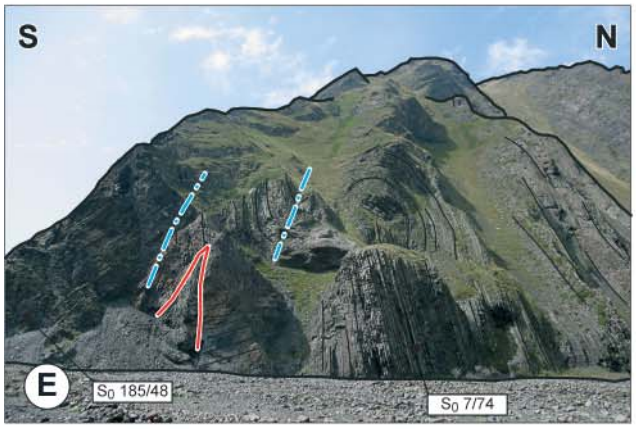
S
N
E
S_0 185/48
S_0 7/74

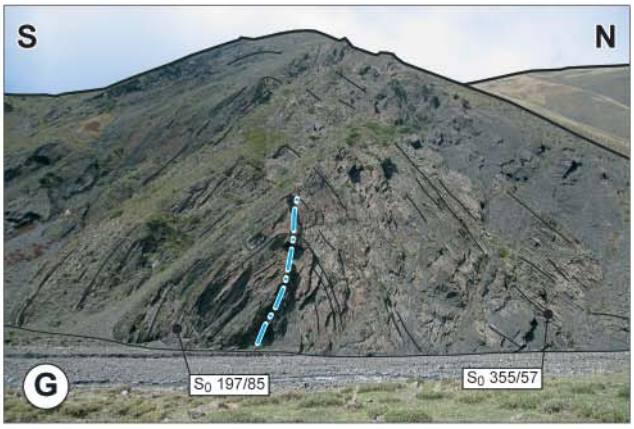
S
N
G
S_0 197/85
S_0 355/57

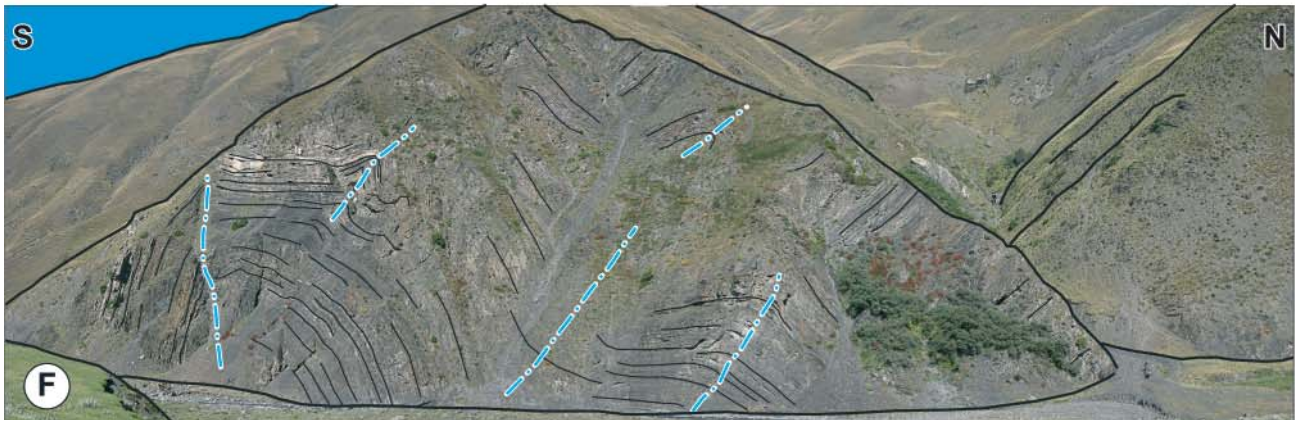
S
N
F

PLATE 3.8: STRUCTURES OF LOWER RUK VALLEY

A. South of Sohub – Valanginian deposits with Jurassic olistoliths in tectonic contact with the Aalenian deep marine sediments - (48°24’54.37”E - 41°8’10.11”N - Azm. 270°) (15.08.2009).

B. South of Ruk –Thrust towards the north with its associated folds - (48°19’34.27”E - 41°6’44.53”N - Azm. 115°) (19.08.2009).

C. Along the western bank of the Qaracay River – Secondary folds with north directed axial planes - (48°19’14.63”E - 41°6’21.92”N - Azm. 293°) (15.08.2009).

D. Lateral valley to the East- Major structure with a syncline – anticline with south directed axial planes - (48°18’40.06”E - 41°5’50.97”N - Azm. 121°) (15.08.2009).

E. Along the eastern bank of the Qaracay River – Major anticline with a subvertical - north directed axial plane (48°18’35.39”E - 41°5’27.27”N - Azm. 84°) (19.08.2009).

F. Along the western bank of the Qaracay River – Two thrusts towards the south with their associated structures - (48°18’31.58”E - 41°3’26.53”N - Azm. 322°) (18.08.2009)..

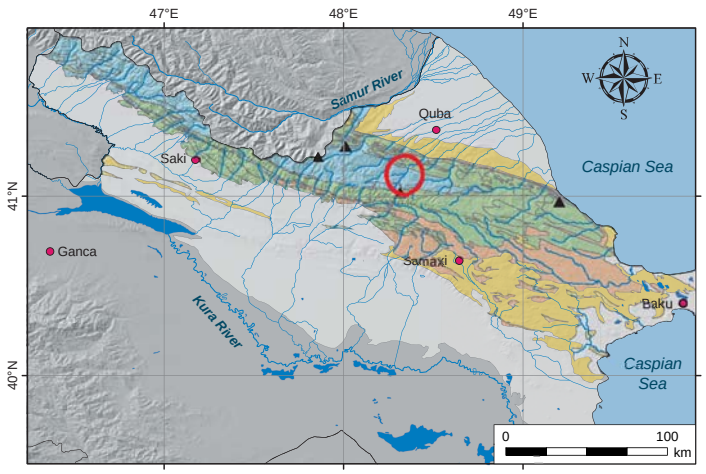

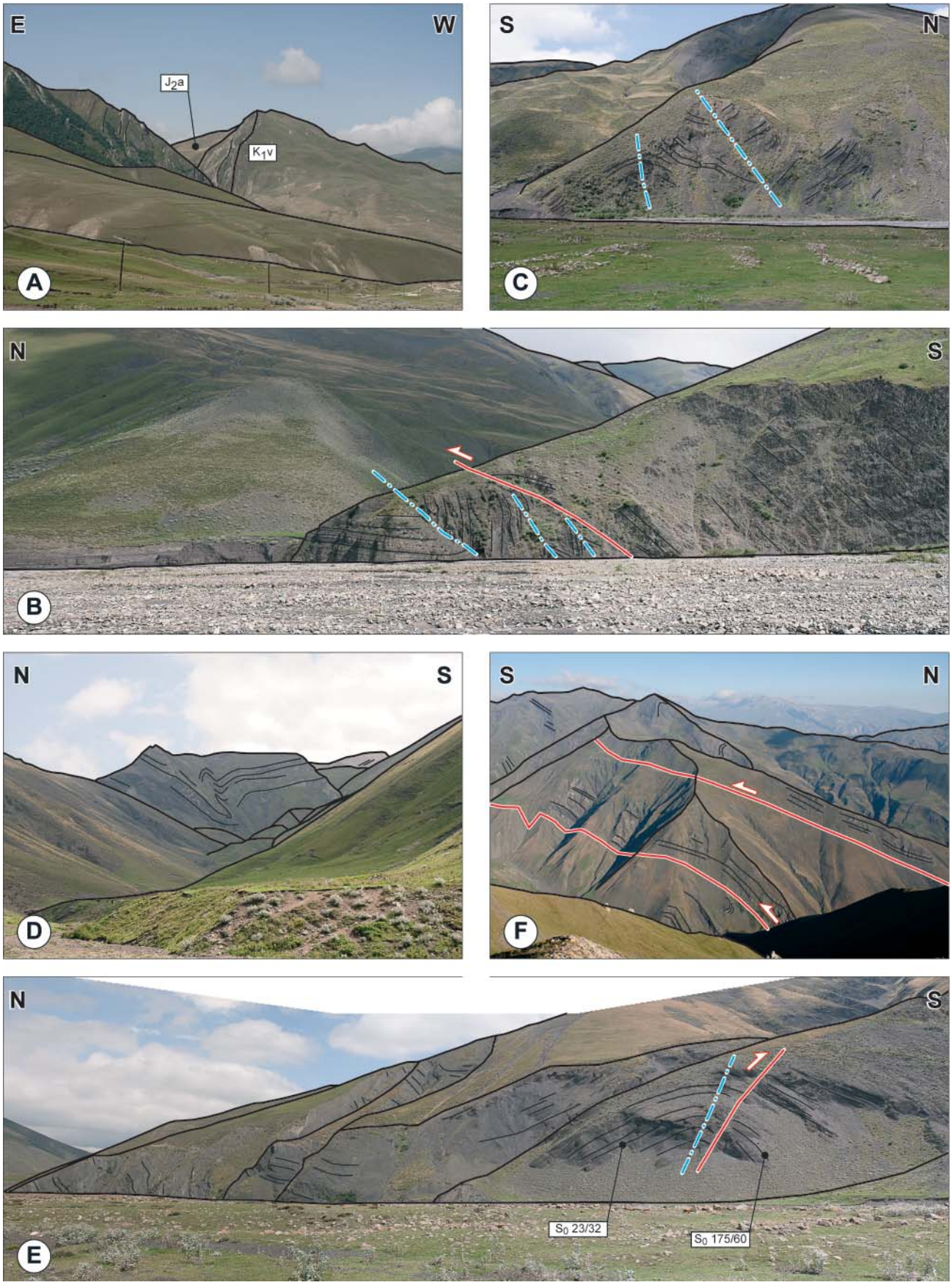
E
W
J_2a
K_1v
A
S
N
C
N
S
B
N
S
D
S
N
F
N
S
S_0 23/32
S_0 175/60
E

PLATE 3.9: STRUCTURES OF UPPER RUK VALLEY

A. Along the western bank of the Qaracay River - Thrust towards the south (same as the lower one on the Plate 3.8 F)- (48°17’43.21”E - 41°4’20.24”N - Azm. 270°) (16.08.2009).

B. Along the eastern bank of the Qaracay River - Major syncline with a north directed axial plane - (48°17’18.78”E - 41°3’47.7”N - Azm. 90°) (17.08.2009).

C. Along the western bank of the Qaracay River – Anticline with a north directed axial plane - (48°17’6.1”E - 41°2’55.26”N - Azm. 270°) (17.08.2009).

D. Valley to the west of Babadag Mt.- Contact zone between the Tufan Zone (north) and Zaqatala-Sumqayit Zone (south) - (48°18’56.09”E - 41°2’45.86”N - Azm. 240°) (18.08.2009).

E. Western flank of the Babadag Mt. - Contact zone between the Tufan Zone and Zaqatala-Sumqayit Zone (48°17’1.74”E - 41°2’34.19”N - Azm. 143°) (17.08.2009).

F. Valley to the east of Babadag Mt. – Contact zone between the Tufan Zone (north) and the Zaqatala Sumqayit Zone (south). The Zaqatala-Sumqayit deposits have south directed bedding planes - (48°18’16.64”E - 41°1’10.57”N - Azm. 90°) (30.08.2004).

G. West of Babadag Mt. – A faulted anticline from the Zaqatala-Sumqayit Zone - (48°18’2.26”E - 41°1’7.56”N - Azm. 265°) (18.08.2009).

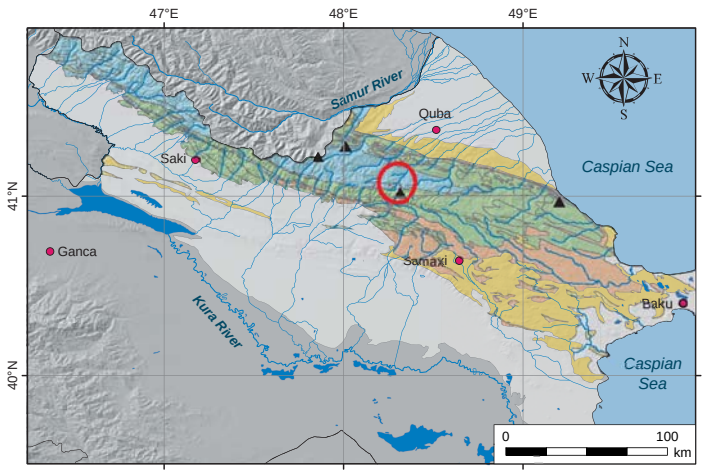

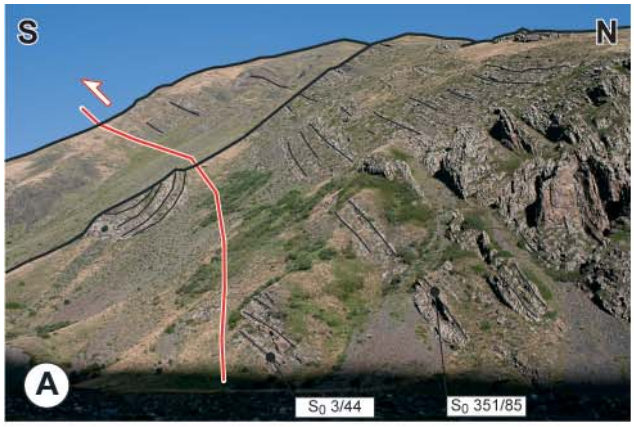
S
N
A
S0 3/44
S0 351/85


S
N
C


N
S
Ap 16/75
S0 180/80
B
S0 12/26


S
N
K1?
J2
D


N
S
E

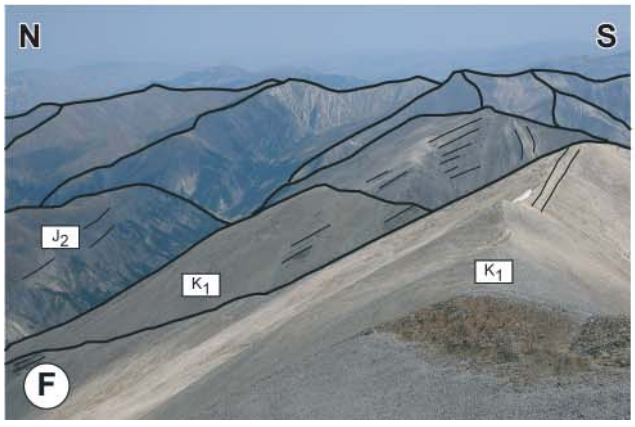
N
S
J2
K1
K1
F

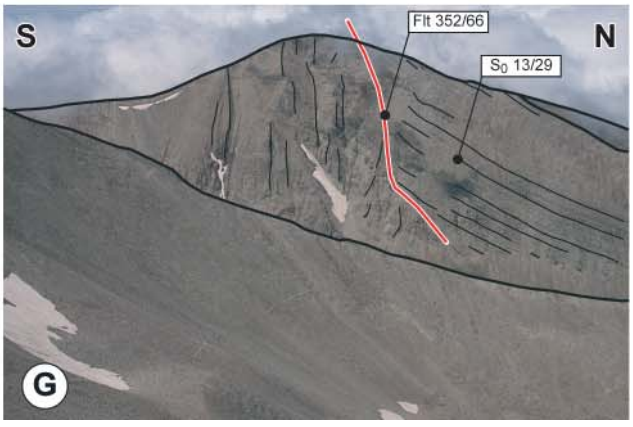
S
N
Flt 352/66
S0 13/29
G

PLATE 3.10: STRUCTURES OF BABADAG MT. AND BUROVDAL VILLAGE AREA

A. Babadag Valley (south of Badabag Mt.) in the upper part of Girdimancay River - Major syncline along the eastern flank of the valley (48°17’17.9”E - 40°59’29.29”N - Azm. 100°) (31.08.2004).

B. Tchötzarat Valley (parallel valley to east of the Babadag Valley) in the upper part of Girdimancay River - Major syncline-anticline along the eastern flank of the valley - (48°19’46.75”E - 40°59’21.27”N - Azm. 90°) (18.08.2004).

C. Babadag Valley- Thrust towards the south from the Valanginian deposits on younger deposits from Lower Cretaceous - (48°16’54.6”E - 40°59’16.04”N - Azm. 110°) (31.08.2004).

D. Març Valley (parallel valley to east of the Tchötzarat Valley) – Fault-bend fold with a north directed axial plane - (48°21’46.74”E - 40°57’42.19”N - Azm. 90°) (26.08.2004).

E. Southern part of Març Valley - Thrust towards the south with its associated folds - (48°20’10.61”E - 40°57’47.73”N - Azm. 90°) (14.08.2004).

F. Southern part of Març Valley - Anticline near the contact between the Zaqatala-Sumqayit Zone and the Qovdag Zone - (48°21’30.17”E - 40°56’53.21”N - Azm. 270°) (26.08.2004)..

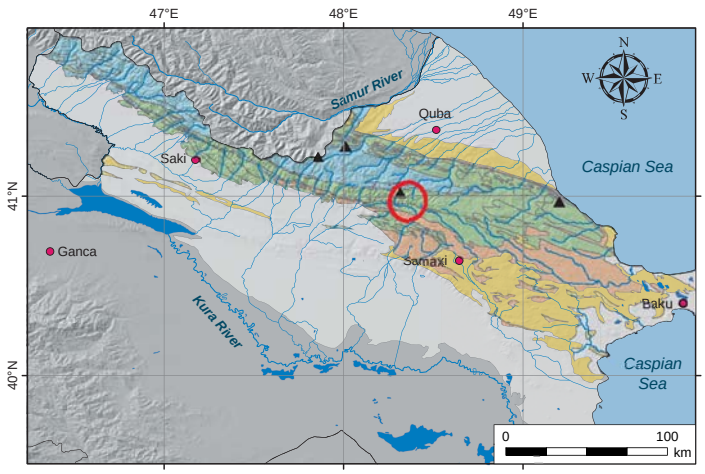


N
S
A


N
S
B

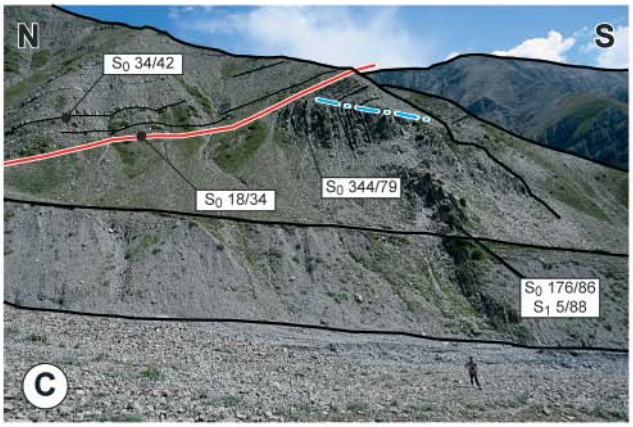
N
S
S_0 34/42
S_0 18/34
S_0 344/79
S_0 176/86
S_1 5/88
C

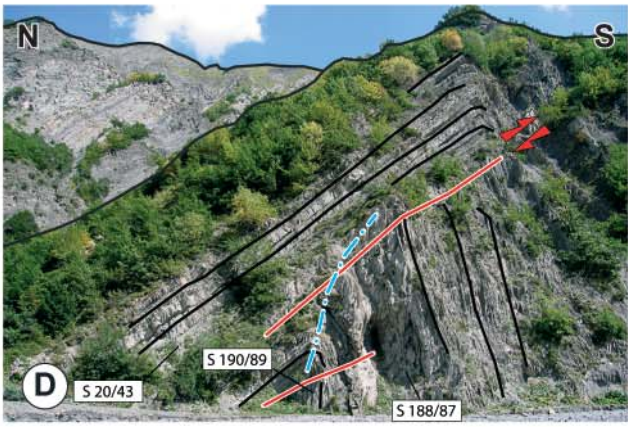
N
S
S 190/89
D
S 20/43
S 188/87


N
S
E

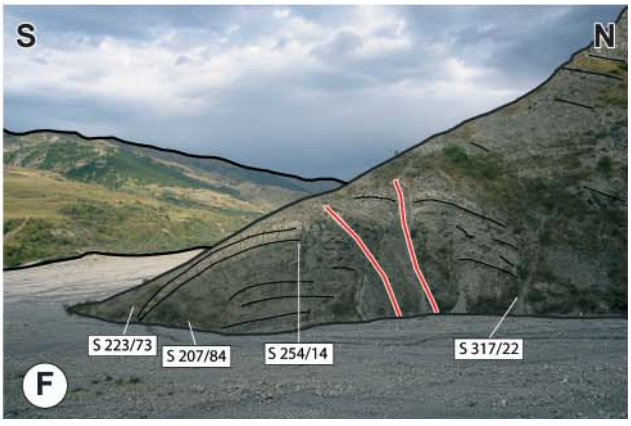
S
N
S 223/73
S 207/84
S 254/14
S 317/22
F

PLATE 3.11: STRUCTURES OF LAHIC VILLAGE AREA

A. North of Lahic – Syncline with a north directed axial plane - (48°24’39.34”E - 40°54’54.36”N - Azm. 90°) (J. Mosar - 12.05.2004).

B. North of Lahic- thrust towards the south with its associated folds - (48°25’8.63”E - 40°53’47.09”N - Azm. 150°) (J. Mosar - 12.05.2004).

C. Northeast of Lahic- Danian to Santonian deposits in a normal series and in the south a overturned syncline with a north directed axial plane (48°24’32.38”E - 40°52’16.92”N - Azm. 90°) (J. Mosar - 12.05.2004).

D. North of Vasa Village – Thrust towards the south in the Qovdag Zone at the contact between the Upper Cretaceous deposits (upper part) and Maykop (Oligocene) deposits (lower part) - (48°21’28.35”E - 40°53’29.12”N - Azm. 280°) (24.06.2008).

E. North of Vasa Village – Anticline just under the thrust described in picture D with a north directed axial plane in Maykop deposits (Oligocene) - (48°21’27.87”E - 40°53’28.11”N - Azm. 258°) (24.06.2008).

F. Northwest of Lahic along the western bank of the Girdimancay River- Small scaled folds with a south directed axial plane - (48°23’13.05”E - 40°51’8.98”N - Azm. 0°) (J. Mosar - 12.05.2004).

G. South of Vasa – Contact zone between the Qovdag-Sumqayit Zone in the north and the Vandam Zone in the south - (48°19’12.97”E - 40°51’13.63”N - Azm. 270°) (22.06.2008)..

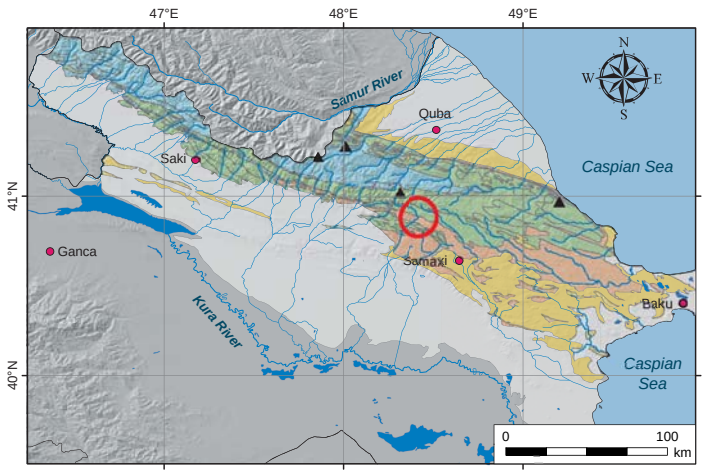

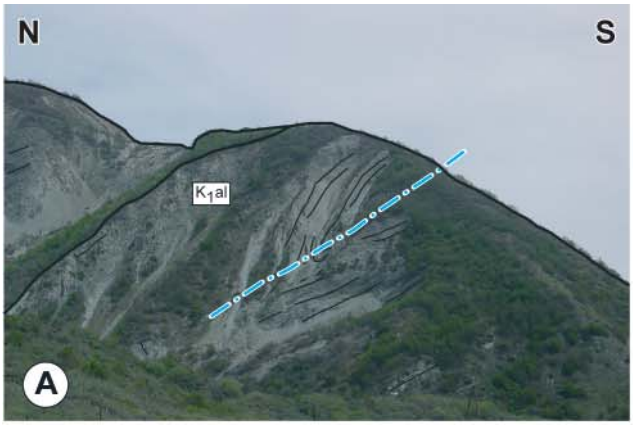
N
S
K1al
A


N
S
K2m
B


N
S
P1d
K2m
K2s
C

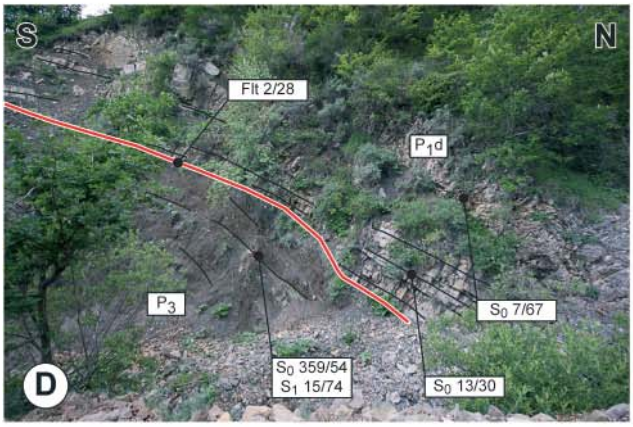
S
N
Flt 2/28
P1d
P3
S0 7/67
S0 359/54
S1 15/74
S0 13/30
D

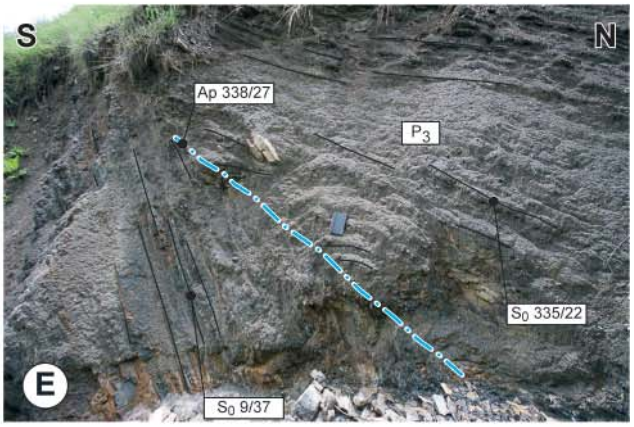
S
N
Ap 338/27
P3
S0 335/22
S0 9/37
E

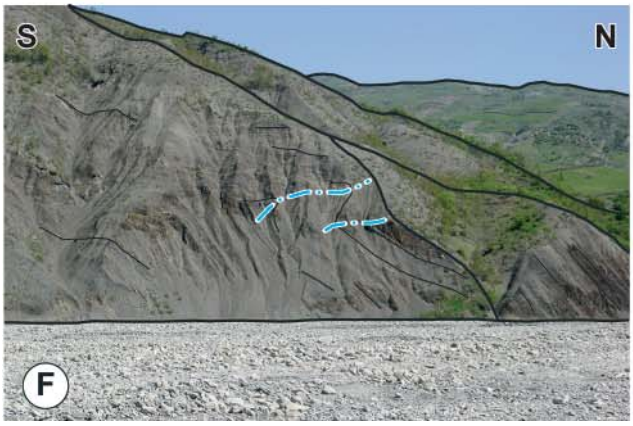
S
N
F

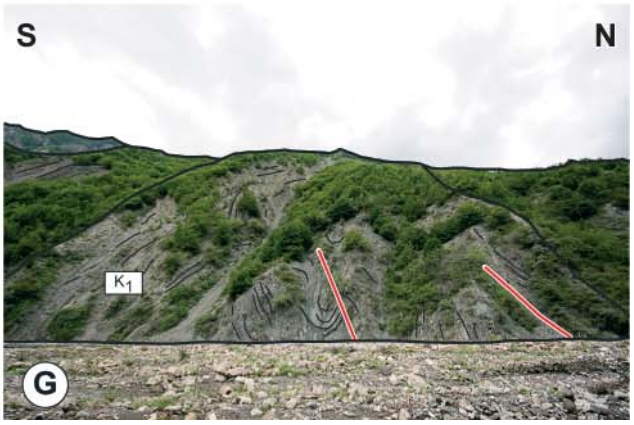
S
N
K1
G

PLATE 3.12: STRUCTURES OF GIRDIMANCAY RIVER AND SAMAXI TOWN AREA

A. Lahic Canyon – Turbidites sequence with volcanoclastic. On the left side, the contact between the Maykop (Oligocene) deposits of the Qovdag-Sumgayit Zone and the Albian deposits of the Vandam Zone - (48°20’53.18”E - 40°50’28.6”N - Azm. 90°) (10.08.2004).

B. Western bank of the Girdimancay River at the southwestern end of the Lahic Canyon – Main syncline of the Vandam Zone with a north directed axial plane - (48°20’4.5”E - 40°50’10.93”N - Azm. 270°) (U. A. Glasmacher - 29.08.2007).

C. Along the western bank of the Girdimancay River – Thrust towards the south - (48°19’40.35”E - 40°49’33.22”N - Azm. 256°) (29.08.2007).

D. Along the western bank of the Girdimancay River – Thrust towards the south - (48°19’31.87”E - 40°49’17.64”N - Azm. 270°) (29.08.2007).

E. Along the eastern bank of Girdimancay River from the Candov bridge – Extension faults in echelon - (48°19’17.17”E - 40°49’9.23”N - Azm. 136°) (29.08.2007).

F. Along the western bank of the Girdimancay River – Volcanoclastic conglomerates of Lower Cretaceous - (48°18’55.63”E - 40°47’11.27”N - Azm. 321°) (29.08.2007).

G. Along the road to Pirculu (north of Samaxi Town) – Danian deposits with a succession of an anticline and a syncline with both a north directed axial plane - (48°38’44.41”E - 40°40’45.76”N - Azm. 90°) (J. Mosar - 11.05.2004).

H. Along the road to Pirculu (north of Samaxi Town) – Maykop deposits and its overturned syncline with a north directed axial plane - (48°38’2.93”E - 40°44’7.06”N - Azm. 90°) (J. Mosar - 11.05.2004).

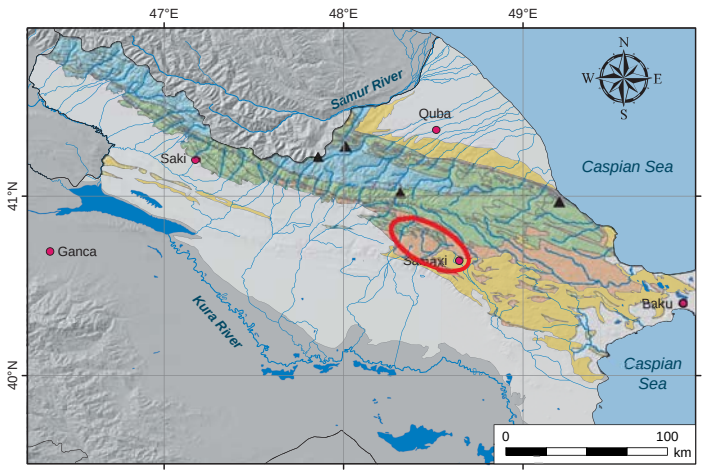

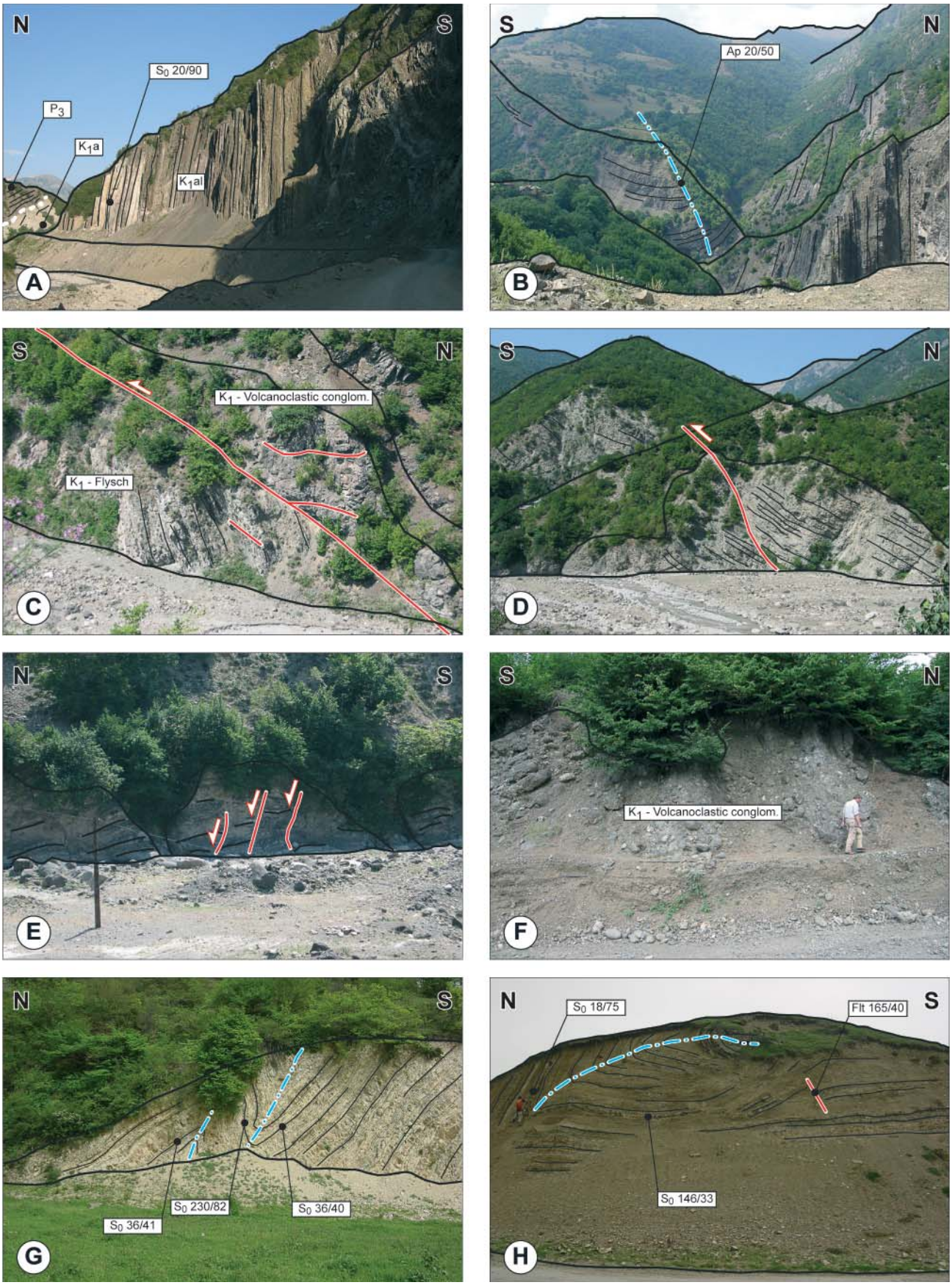
N
S
S_0 20/90
P_3
K_1a
K_1al
A
S
N
Ap 20/50
B
S
N
K_1 - Volcanoclastic conglom.
K_1 - Flysch
C
S
N
D
N
S
E
S
N
K_1 - Volcanoclastic conglom.
F
N
S
S_0 36/41
S_0 230/82
S_0 36/40
G
N
S_0 18/75
Flt 165/40
S
S_0 146/33
H

PLATE 3.13: STRUCTURES OF QARAMARYAM HILLS AND AGDAS TOWN AREA

A. Along the road from Qabala to Agdas- Contact between Quaternary conglomerates and Quaternary sandstones - (47°37’12.49”E - 40°47’23.8”N - Azm. 345°) (U. A. Glasmacher - 28.08.2007).

B. Along the road from Qabala to Agdas- Contact between Quaternary conglomerates and Quaternary sandstones - (47°37’11.27”E - 40°47’23.32”N - Azm. 135°) (U. A. Glasmacher - 28.08.2007).

C. Along the road from Qabala to Agdas- Contact between Quaternary sandstone and Pliocene deposits - (47°33’17.37”E - 40°42’45.03”N - Azm. 289°) (U. A. Glasmacher - 28.08.2007).

D. Road from Agsu to Qaramaryam – View on the Quaternary Qaramaryam hills - (48°12’3.15”E - 40°35’14.52”N - Azm. 270°) (11.10.2007).

E. Qaramaryam hills – Northern flank of the northern anticline - (48°11’58.42”E - 40°34’43.22”N - Azm. 270°) (11.10.2007).

F. Qaramaryam Hills – Central syncline of the Qaramaryam hills with a north directed axial plane - (48°11’44.83”E - 40°34’17.45”N - Azm. 90°) (11.10.2007).

G. Qaramaryam Hills – Horizontal Quaternary deposits lying on subvertical deposits (Pliocene ?) - (48°16’15.97”E - 40°36’33.03”N - Azm. 180°) (08.08.2006).

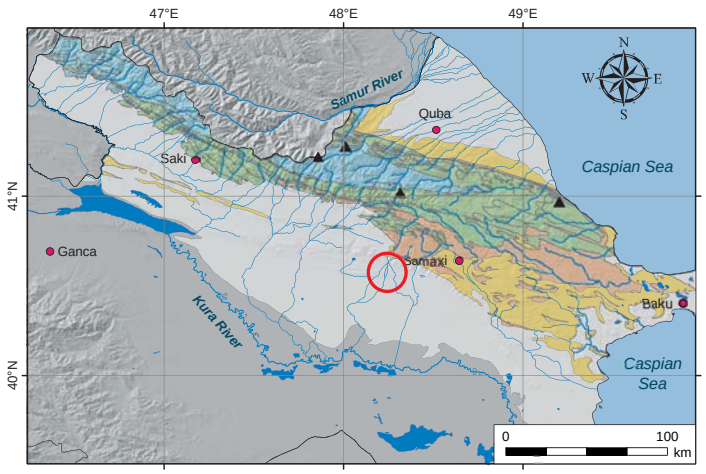

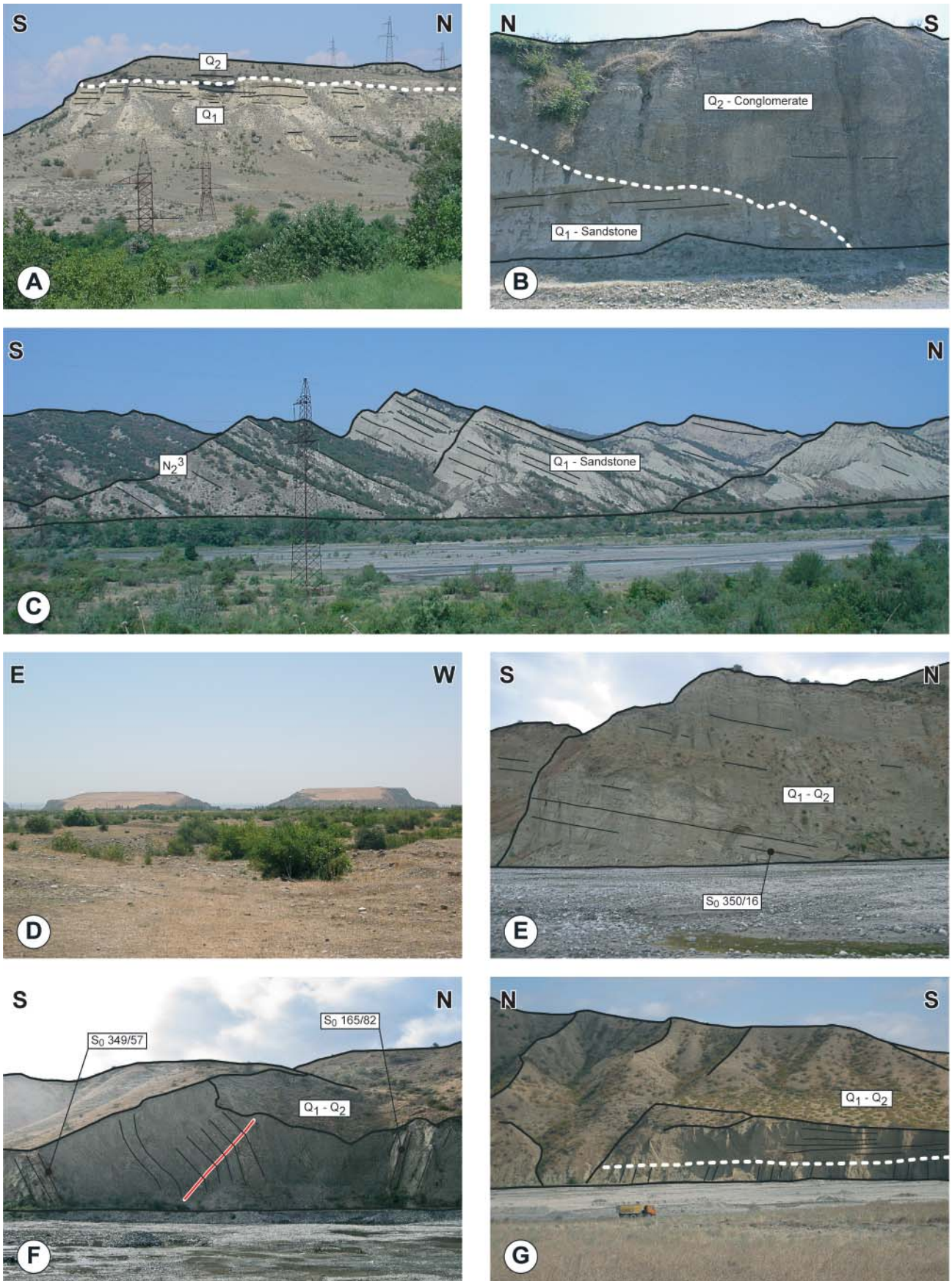
S
N
Q_2
Q_1
A
N
S
Q_2 - Conglomerate
Q_1 - Sandstone
B
S
N
N_2^3
Q_1 - Sandstone
C
E
W
D
S
N
Q_1 - Q_2
S_0 350/16
E
S
N
S_0 349/57
S_0 165/82
Q_1 - Q_2
F
N
S
Q_1 - Q_2
G

4 - Burial and exhumation : fission tracks, illite crystallinity and subsidence curve study in the EGC

M. Bochud[1,‡], J. Mosar[1], U. A. Glasmacher[2], T. Kissner[2], Otto Kraft[2], A. Rast[1], T. Kangarli[3]

[1]Earth Sciences, Department of Geosciences, University of Fribourg, Chemin du Musée 8, 1700 Fribourg, Switzerland
[2]Institute of Geosciences, University of Heidelberg, Im Neuenheimer Feld 234, 69120 Heidelberg, Germany
[3]Geological Institute of Azerbaijan (GIA), National Academy of Sciences, 29A H. Javid Av., Baku, AZ1143, Azerbaijan
[‡]Email : martin.bochud@unifr.ch

Abstract

The Greater Caucasus has undergone a fast surface uplift rate (until 12 mm/yr) since the Pliocene but only few data are available to describe it in the Eastern Greater Caucasus of Azerbaijan (EGC). Marine sediments of Sarmatian (Middle Miocene) and Pliocene age were sampled respectively at 3600 m on Sahdag Mt and at 2000m in the Buduq Trough. They allow calculating a minimum surface uplift rate of respectively 0.31 mm/yr and 0.77 mm/yr since these periods. Based on literature and on our field observations, the EGC seemed to be adapted to apply Apatite Fission-Track studies (AFT), Illite Crystallinity index (IC) and subsidence curves to better characterize its burial, exhumation and surface uplift. Samples were taken in the northern and central area of the EGC mostly in argillite sediments of Aalenian age, in Cretaceous slope deposits on Sahdag Mt. and in Pliocene conglomerates.

AFT results show that most of the samples stayed in the partial annealing zone. AFT central ages determined in the northern Pliocene conglomerates show that their components were coming from the west. Therefore, the exhumation is progressing from the central Caucasus towards the ESE. Central age differences inside the same sediments allow defining a fault between the Sahdag-Besbarmaq Nappe and the Tufan Zone. All t-T models show a fast burial during the Middle Jurassic and Lower Cretaceous and a fast exhumation that started between Miocene and Quaternary. The northern area has a more complex behaviour with an intermediate exhumation since the Upper Cretaceous followed by a burial since the beginning of Miocene.

IC analyses show an increase of metamorphism from the northern orogenic front (Samur River) towards the central part of the EGC but also a decrease of the metamorphism from the Bazarduzu Mt. area towards the ESE.

Finally 2 subsidence curves of the northern and central area show during Lower and Middle Jurassic a rapid subsidence followed by exhumation. The curves are concordant with the formation of the Greater Caucasus Basin in the central area from Upper Jurassic to Paleocene followed by the formation of a foreland basin in the north from the Paleocene to Middle Miocene (10-15 Myr). One subsidence curve emphasizes an erosive event in the middle of the Cretaceous that could not be directly related to regional event.

Based on these results, it can be deduced that the exhumation rate probably reached values of more than 1 mm/yr in the EGC and that surface uplift is propagating to the ESE. The central area underwent the most important exhumation of the area since the beginning of the orogen (Paleocene) while the northern area underwent the fastest exhumation since the Sarmatian Period (~11 Myr) or even later.

Keywords: *Eastern Greater Caucasus, Apatite Fission Track, Illite Crystallinity, Subsidence curve.*

4.1. Introduction

The Eastern Greater Caucasus (EGC) is located north of Azerbaijan and corresponds to the eastern termination of Europe's largest and highest mountain belt, the Greater Caucasus. The long building history of the Caucasus and its surrounding sedimentary basins (particularly the South Caspian Basin which is one of the world deepest intracontinental basins with a very fast subsidence) is globally well defined but few data are available for its eastern part. In this chapter, we will apply several methods to find new data to understand the geodynamic evolution of this area.

Based on the supposed fast surface uplift of the Greater Caucasus (up to 12 mm/yr in the central part, see Mitchell & Westaway (2009), on the thickness of exposed Lower and Middle Jurassic sediments in EGC (up to 6500 m) and on rock types (sandstone, argillite, siltstone) several methods like Apatite Fission Tracks (AFT), Illite Crystallinity (IC) and subsidence curves have been applied to better characterize the geodynamic evolution of the area.

Samples were collected during 2 fieldtrips in 2006 and 2007 in the northern and central part of the EGC. Preparation and analysis of the samples were made in three laboratories: the Geological Institute of the University of Neuchâtel (Switzerland), the Centre Scientifique et Technique Jean-Féger (CSTJF) of the Total Company in Pau (France) and the thermochronology Laboratory from the Institute of Geosciences of the University of Heidelberg (Germany).

4.2. Geology and evolution of the Eastern Greater Caucasus

The Greater Caucasus and its eastern part, the EGC, are the result of the inversion of a deep Jurassic-Paleogene sedimentary basin, the Greater Caucasus Basin (GCB). The latter underwent several cycles of opening-closing and was successively filled by the erosional products of the northern and southern bordering areas. Lithologies from Jurassic, Cretaceous and Paleogene of the EGC are mainly represented by deep marine and slope facies. However, along the northern slope, shallow marine and platform sediments were deposited and correspond to the southern shelf of the Scythian Platform at the northern edge of the GCB. Since the beginning of the main orogen phase during Eocene-Oligocene times, the eroded sediments of the uplifted area were accumulated in foreland molasse basins and in deep sedimentary basins such as the South Caspian Basin. A Miocene sea covered the nascent relief of the Greater Caucasus and remains can be nowadays seen up to an altitude of 3600 m in the EGC (Budagov 1963). Due to the major eustatic variations of the Caspian Sea during Pliocene and Quaternary times, marine formations were deposited alternatively with continental ones at the EGC fringes. Finally, the volcanic and magmatic activity near the Lesser Caucasus Volcanic Arc due to the subduction of the Paleotethys and the Neotethys resulted in major deposits of effusive and intrusive rocks. They are mostly of Early to Upper Jurassic and Middle Eocene epochs (i.e. Buynuz intrusion on the southern slope).

The EGC formations of the Lower Jurassic to the Holocene epochs can be subdivided into five major groups:

- Sedimentary units with important input of arc-related volcanoclastic material;
- Siliciclastic, carbonate and volcanoclastic sediments deposited along from slope to basin of the southern edge of the Scythian platform;
- Carbonate platform and lagoonal environment sediments of the southern edge of the Scythian plate;
- Continental deposits coming from the erosion of the nascent mountain belt;
- Effusive and intrusive magmatic rocks resulting of the magmatic and volcanic activity of the Lesser Caucasus.
- Structurally the northern part of Azerbaijan can be divided in 3 megazones from north to south: Qusar-Davaci Megazone, Eastern Greater Caucasus Megazone and Kura Megazone. They are themselves divided into several structural zones (figs. 49 and 50). This study concerns mostly the northern part of the EGC (fig. 53): the Tahircal Zone, the Sudur Z., the Sahdag-Xizi Z., the Sahdag-Besbarmaq Nappe and the Tufan Z

The overall geodynamic setting of the EGC is a continental collision inverting the former passive margin of the Scythian Platform and the deep Mesozoic-Tertiary basin, the GCB. The EGC corresponds to a doubly verging mountain belt with a major southern fold-and-thrust belt and a minor fold belt in the north (Mosar et al. 2010). The pro-wedge is located to the south and overrides the Kura Basin, whereas the retro-wedge is located to the north and overrides the Terek Basin. During Pliocene times the South Caspian Basin started subducting to the north under the eastern termination of the Greater Caucasus and the Abseron ridge (Allen et al. 2002; Knapp et al. 2004). The depth of the Moho changes from about 40 km in the south be-

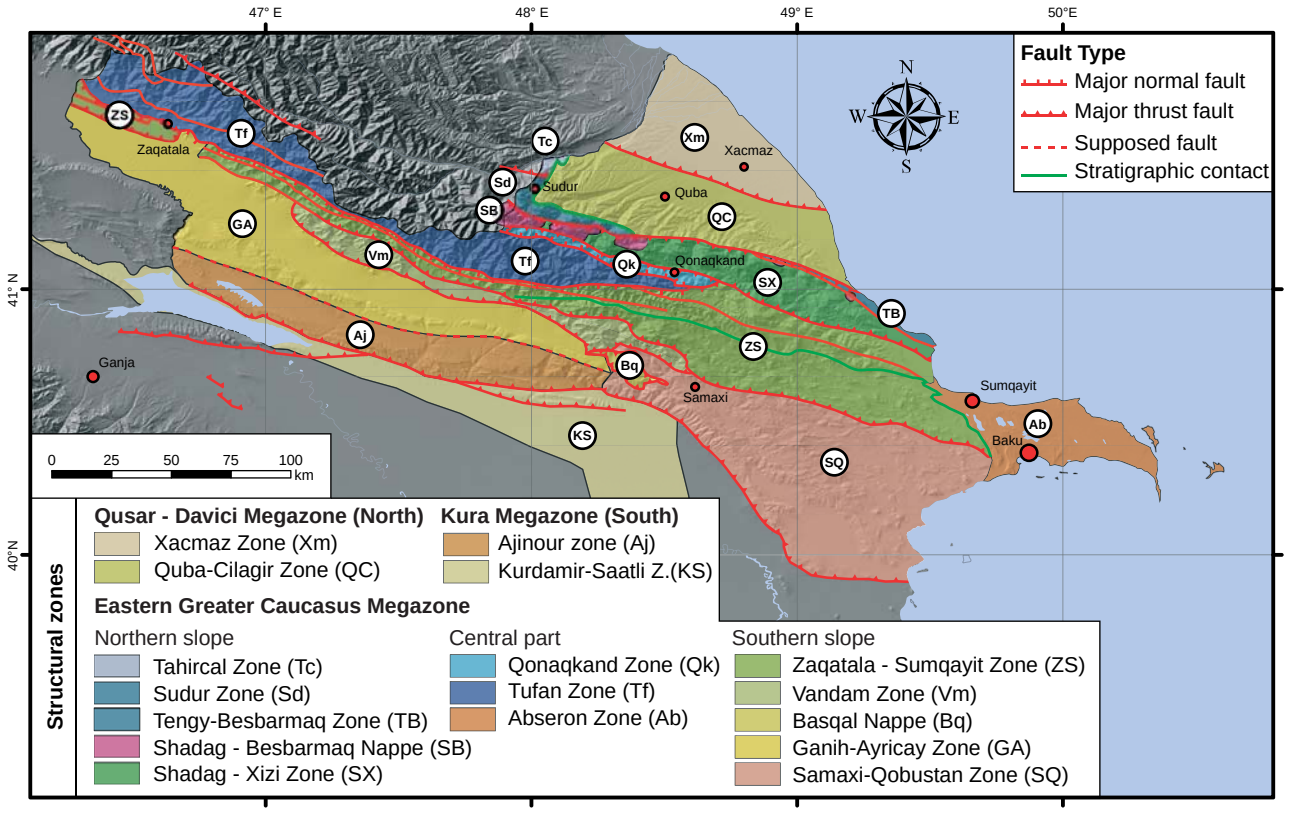

Figure 49: Simplified tectonic map of the Eastern Greater Caucasus showing the different tectonic Megazones and their zones. Modified from KANGARLI (2005).

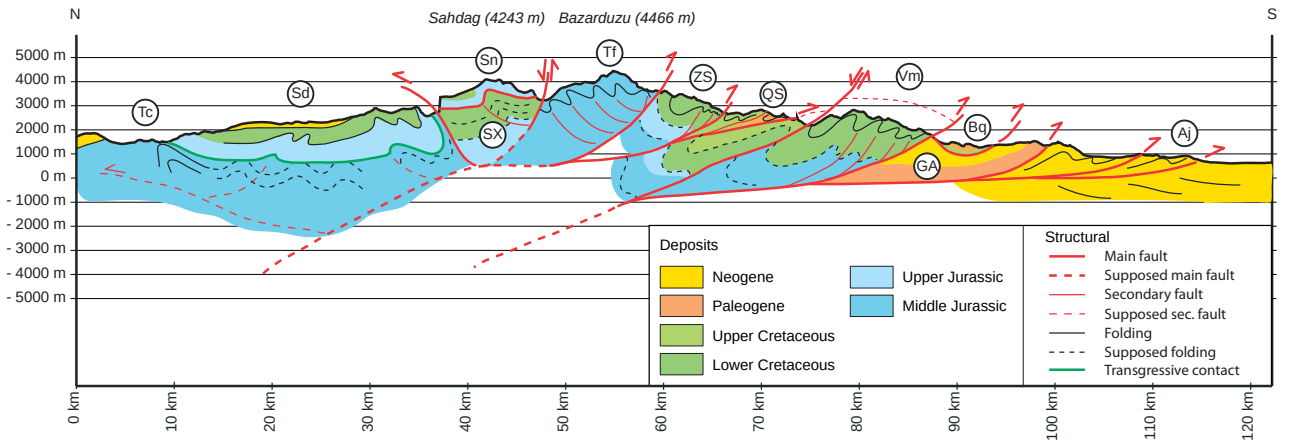

Figure 50: Simplified cross-section with main structures and structural zones: Tc: Tahircal Z.; Sd: Sudur Z.; Sn: Sahdag-Besbarmaq Nappe; SX: Sahdag-Xizi Z.; Tf: Tufan Z.; ZS: Zaqatala-Sumqayit Z.; QS: Qovdag-Sumqayit Z.; Vm: Vandam Z.; Bq: Basqal Nappe; GA: Ganih-Ayricay Z.; Aj: Ajinour Z.

neath the Kura Basin to more than 50 km beneath the Greater Caucasus and rises to 40 km again under the northern foreland basin (Brunet et al. 2003; Ershov et al. 2003).

4.2.1. Tectonic evolution of the EGC

Based on field work and literature, we distinguished five different compressional events since the Middle Jurassic and linked them with local and regional events (fig. 51).

Thick series of sediments can be observed in the Tufan Structural Zone (Tf on figs.49 and 50) located in the central part of the EGC. They confirm the subsidence phase that took place in the Greater Caucasus Basin (GCB) during Sinemurian and Pliensbachian ages and ended at the end of Aalenian (Middle Jurassic). It corresponds to the formation of a back-arc basin linked with the Neotethys subduction under European Scythian platform (Nikishin et al. 2001).

In the Tahircal Structural Zone (Tc on figs. 49 and 50), folded Aalenian deposits (deep marine sediments) can be observed under flat and shallow marine deposits (evaporite) of Callovian Age. The basin was probably uplifted and became shallow at least in its northern side. The evaporite deposits can be correlated to the Kimmeridgian-Tithonian ones described by Nikishin et al. (1998a) in the Scythian platform. This allows placing a compressional tectonic event (n°1 on fig. 51) during Bajocian and Bathonian ages. We think it can be link to the Mid-Cimmerian deformation event for which the tectonic origin is still controversed (Fürsich et al. 2009). This Mid-Cimmerian event corresponds in Alborz Mountains (Shemshak Group) to an unconformity with a sharp change in facies (Fürsich et al. 2009).

After rifting cycle (Nikishin et al. 2001), the area underwent a post rifting subsidence of the basin from Callovian to Kimmeridgian ages. In Tahircal and Sudur structural zones, shallow marine deposits of Callovian age gently evolved to reef and slope deposits during the Upper Jurassic indicating a deepening of the sedimentation realm.

The second compressional tectonic event (n°2 on fig. 51) corresponds to a weak surface uplift and compressional deformation of the older deposits. Along the Gilgilcay River in the east of the EGC, we observed an angular erosional unconformity from Berriasian (Lower Cretaceous) conglomerates on tilted Kimmeridgian deposits. We think it could be linked to one of the several compressional tectonic events that occurred during the post-rifting period of thermal subsidence, especially at the beginning of the Early Cretaceous (Brunet et al. 2009a).

At the beginning of Lower Cretaceous, a rapid subsidence of the GCB started (Nikishin et al. 2001). Corresponding thick series of Lower Cretaceous turbidites can be observed along the southern slope of the EGC in the Zaqatala-Qovdag Structural Zone (ZS on figs. 49 and 50). In the north, this period was a time of unstable tectonic environment like in the Scythian Platform (Nikishin et al. 1998a). From Late Berriasian to Barremian, it is likely a tensional regime (Nikishin et al. 2001) corresponding to a passive margin context. The formation of olistostromes during the Valanginian and Hauterivian can be observed in the Sahdag-Xizi Zone (i.e. north of Ruk Village). The setting-up of the Sahdag-Besbarmaq Nappe can be dated of this period: the youngest deposits under the Cirax Klippe are dated of Barremian Age and under the Besbarmaq Klippe of Hauterivian Age. As the general context corresponded to a continental rifting and the formation of a nappe in this context is difficult to explain, we can suppose that the Sahdag-Besbarmaq Nappe corresponds to a Mega-bloc that collapsed in a passive margin context. After the extensional regime continued throughout the Aptian and Albian: series of marine deposits can be observed along the southern slope of the EGC in the Zaqatala-Qovdag Zone but also in the eastern part of the Sahdag-Xizi Zone.

The beginning of the Upper Cretaceous (Cenomanian) corresponds to a third compressional phase (n°3 on fig. 51): we observed transgressive Turonian deposits on folded Albian-Aptian sediments. Deep valleys were dug through the Sahdag-Besbarmaq Nappe: north of Cek Village and in Buduq, a paleo-valley (the Buduq Trough) cuts the Sahdag-Besbarmaq Nappe (Upper Jurassic deposits) and the underlying Barremian and Aptian deposits. The paleo-valley is filled by Upper Cretaceous sediments.

During the middle part of the Upper Cretaceous, the area underwent an extensional phase with subsidence. Marine sediments were deposited in the north and in the south of the GCB (Nikishin et al. 2001).

The fourth compressional tectonic event (n°4, fig. 51) started at the end of the Upper Cretaceous and ended during the Paleocene. The area underwent a regional surface uplift: Paleocene deposits are unconformably overlain on older deposit mostly in the Tahircal and Sudur structural zones (Tc and Sd on figs. 49 and 50). This can be considered as beginning of the Caucasus orogen that definitively started during the Eocene. Southern and northern foreland basins are filled with the first eroded sediments of the young orogen. The Sahdag-Besbarmaq Nappe was partially back thrusted to the north during this period. Within the Zaqatala-Qovdag Zone in the south, thrusting to the south started to build succesive piggyback type basins.

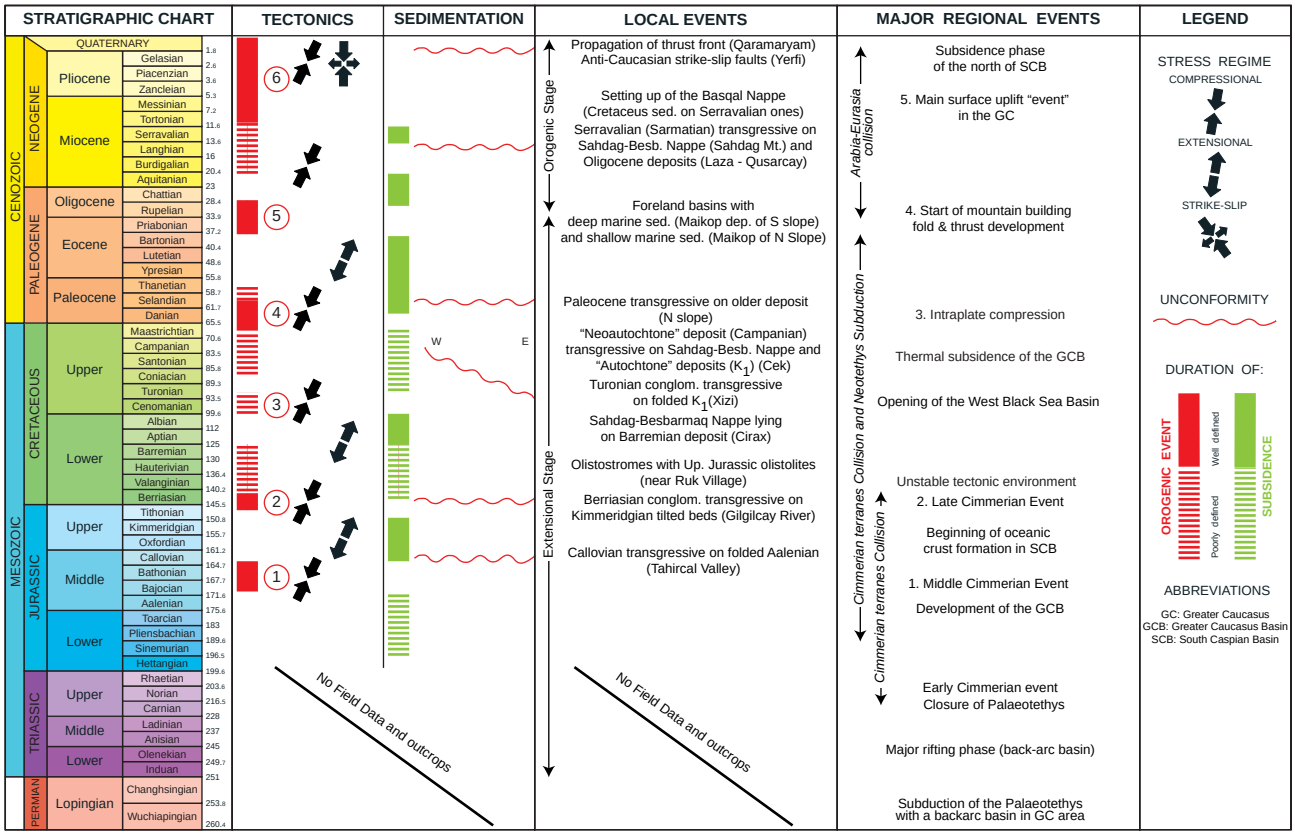

Figure 51: Summary of the tectonic and stratigraphic evolution of the eastern Greater Caucasus produced from field-based investigation. Information on major regional events has been obtained from Zonenshain & Le Pichon (1986), Philip et al. (1989), Brunet et al. (2003), Nikishin et al. (2001), Saintot et al. (2006a) and Barrier et al. (2008a).

Since the start of the building of the EGC, the area could be described as a succession of relief with intercalated piggyback basins.

At the end of the Eocene Epoch, the Arabia-Eurasia collision started. The Caucasus area underwent the fifth compressional tectonic event (n°5 on fig. 51) and the area was submitted to a main surface uplift: this is the main beginning of the present Greater Caucasus building. The erosion of this new orogen will furnish sediments for the surrounding foreland basins. Related to this event, the Kura basin, a deep (100 to 3000 m) foreland basin, was formed south of the very young EGC during the Oligocene Epoch. The productive Maikop sediments were deposited in this basin (Kopp & Shcherba 1985).

During Middle Miocene to Early Pliocene ages, a shallowing up happened in Samaxi-Qobustan Structural Zone and there are no evidences of substantial inflow of Caucasus material (Kopp & Shcherba 1985).

During the Sarmatian Age[1], a general shallowing up started. A northern foreland basin was created and sediments of Sarmatian age were deposited on the future Sahdag Mt. These Middle Miocene sediments can be presently seen at an altitude of more than 3600 m on the Sahdag Mountain. In the southern slope Sarmatian sediments cover a large area in the Samaxi-Qobustan Zone at lower altitudes (about 1000 m). Some Upper Pliocene (Akchagyl regiostage) marine clays were also found in the Buduq syncline at altitudes of 2000 m a.s.l..

The last compressional event (n°6 on fig. 51) corresponds to the main orogenic event of the Greater Caucasus during the Pliocene Epoch. The Tufan Zone and the northern zones (Tc, Sd, SX and Tf on figs.49 and 50) underwent an important surface uplift. On the southern slope, the Basqal Nappe was set up after Sarmatian Age just prior the exhumation of the Vandam Zone. The formation of the Alazani Basin as a piggyback basin to the N of the Kura Basin was linked with the main orogenic phase of the EGC and was filled with its erosive products. The western part of the EGC (near Balakan and Zaqatala towns) was the most uplifted and the oldest deposits sediments of the EGC can be found here. The EGC southeastern part corresponded to a shelf (Kopp & Shcherba 1985).

Finally, the building of the EGC is nowadays still very active and the main surface uplift zone seems to

1 Sarmatian Age corresponds to the Upper part of the Serravalian age and covers a time span of approximately 1.1 Myr between ~11.6 and 12.7 Myr before present (Harzhauser & Piller 2004).

move eastwards. Currently the southernmost blind thrust is located under the Qaramaryam hills where folded Pleistocene and Holocene sediments can be observed.

4.2.2. Surface uplift rates of the EGC

Surface uplift rates have never been precisely quantified in the EGC. However, geomorphologic studies (Mitchell & Westaway 1999) and thermochronological investigations that have been made across the Greater Caucasus show a very young surface uplift.

A study of Kral (1996) on apatite fission tracks on pre-alpine basement rocks near the Elbrus shows ages younger than 68 Myr in agreement with the general idea of an surface uplift that initiated in the Tertiary. Patterns of age distributions also indicate surface uplift of 7-4 Myr in some areas. A study by Hess (1993) on the cooling history of recent granites in the western central Greater Caucasus shows ages between 2.5 and 1.2 Myr and suggests surface uplift rates of 4 mm/yr, in the Central Greater Caucasus (Russia), but thermal modelling difficulties linked to the close vicinity of hot intrusives may significantly modify modelling results leading to overestimate surface uplift rates.

Compilation of surface uplift amount and rates (Ershov et al. 2005; Philip et al. 1989), confirm the very young surface uplift but show rates in excess of 12 mm/a, which in light of field evidence (see Mitchell & Westaway, 2009, for discussion) seem excessively fast (fig. 52). However, they consistently show that the fastest and highest surface uplift is in the centre of the range. A more recent study on apatite fission tracks on the Early Miocene Maykop series of the western Greater Caucasus (Vincent et al. 2007) shows a similar detrital provenance of the clasts on both sides (southern and northern) and suggests a minimum Early Oligocene age for subaerial surface uplift of the mountain range.

Evidence from river incision of several hundred of meters since the last glaciations suggests surface uplift rates of 10 mm/a (Rastvorova & Shcherbakova 1967) around the Central part of the Greater Caucasus. Similar deep incisions are also observed in Plio-Pleistocene sediment of the Samur River in northern Azerbaijan; however detailed studies need to confirm the fast surface uplift rates.

Detailed studies on young terraces along the Black Sea and Caspian Sea (Brod 1962; Krasnov et al. 1974), or the Kura Basin (Shirinov 1973; Shirinov 1975) exist but are all in Russian and difficult to access (Budagov 1969; Budagov 1973; Shcherbakova 1973; Shirinov 1975). For example, a terrace at 475 m a.s.l. is given as latest Pliocene in age and is found along the western shore of the Caspian Sea (in Azerbaijan) and in the Kura Basin along the foothill of the Greater and Lesser Caucasus. It reflects the location of the Pleistocene marine coastline corresponding to the Late Akchagyl transgression of the Caspian Sea (Krasnov et al. 1974; Popov et al. 2004). Its age is given between 2.5 and 1.8 Myr possibly as young as 1.2 Myr (Mitchell & Westaway 1999). Based on these data, Mitchell and Westaway (1999) determined a maximum uplift of 0.46 ±0.08 [mm/yr] in the Derbent area.

One of the best data sets to directly quantify surface uplift of the Eastern Greater Caucasus since Middle Miocene are marine sediments such as those of Sarmatian age (11.6 to 12.7 Myr after Harzhauser & Piller (2004) that we sampled at an altitude of 3550 to 3600 m a.s.l. on the Sahdag Mt. of Azerbaijan and also described by Budagov (1963). Based on these data, we determined a maximum surface uplift rate since the Middle Miocene of:

$$Uplift\ rate = \frac{3600\ [m]}{11.6\ [Myr]} = 0.31\ [mm/yr]$$

Upper Pliocene (Akchagyl regiostage) marine clays are found in the Buduq trough at altitudes of 2000 m a.s.l. between Cek and Ruk Village (Kangarli 1982) and correspond to a maximum surface uplift rate since the Upper Pliocene of:

$$Uplift\ rate = \frac{2000\ [m]}{2.6\ [Myr]} = 0.77\ [mm/yr]$$

These surface uplift rates based on field observations are more modest compared with some literature rates in excess of 10 mm/yr.

4.3. Methods and Data

Apatite Fission Track (AFT), Illite Crystallinity (IC) methods and subsidence curves were applied to find new indications to better characterize surface uplift, exhumation and metamorphism of the EGC. These methods were not applied on this area of the EGC.

4.3.1. Apatite Fission-Tracks analysis

Thermochronologic methods, such as (U-Th-Sm)/He and fission-track (FT) dating, are based on the production of an isotope or radiation damage, respectively, resulting from nuclear decay, and the subsequent, thermally controlled retention of these decay products. As described e.g. by Reiners and Brandon (2006) the radioisotopic production decreases exponentially with time but is predictable and otherwise steady, allowing the thermochronometer to keep time. Due to the thermal sensitivity of thermochronometers, thereof

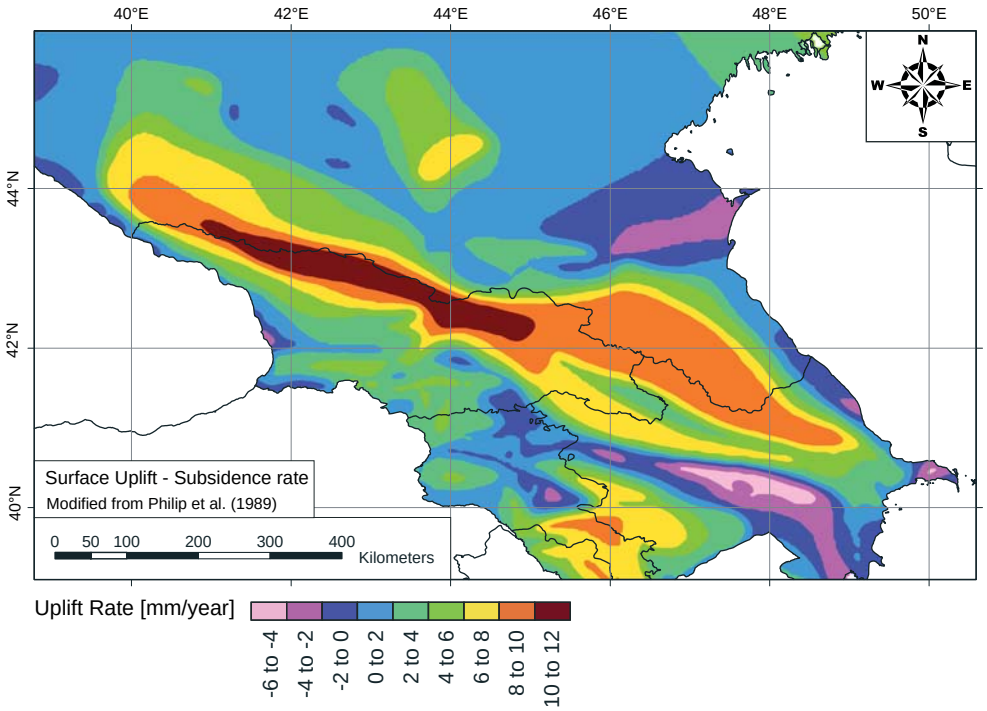

Figure 52: Surface uplift-subsidence rate map of the Greater Caucasus. Modified from PHILIP et al. (1989). Surface uplift rate in the EGC are overestimated, they certainly reach only 1 mm/yr.

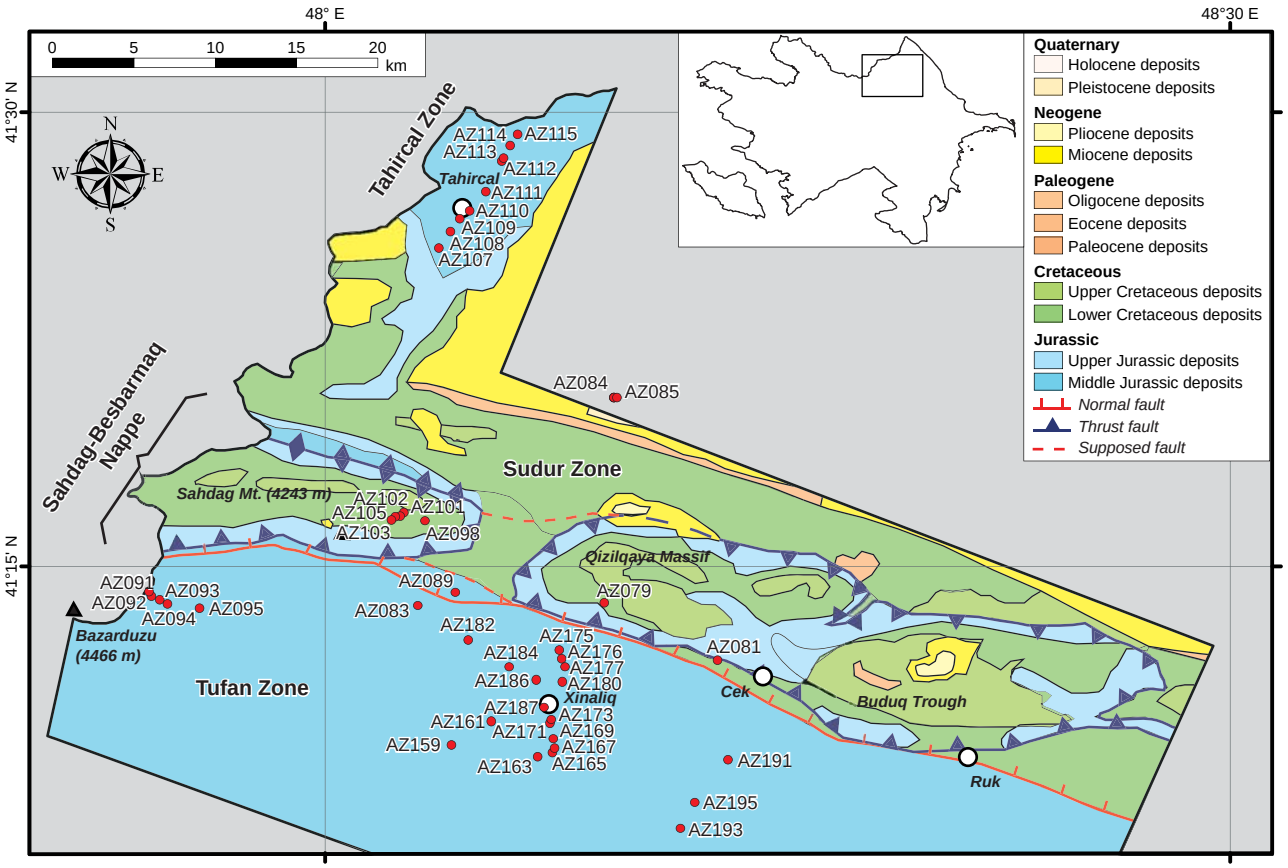

Figure 53: detailed geological map of the northern part of the EGC with analyzed samples. Four samples (AZ199, AZ201, AZ203 and AZ205) are located out of the map in along the Cimicay River that corresponds to the eastern termination of the Tufan Zone.

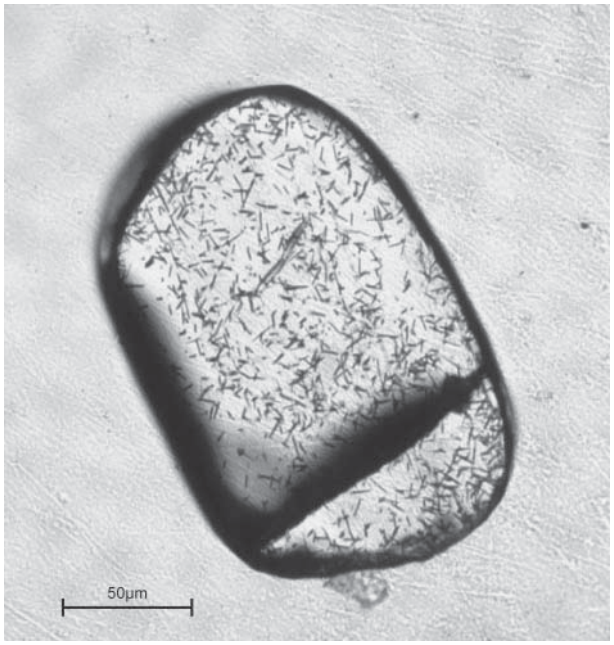

Figure 54: Apatite grain with etched pits and fission tracks (Picture from T. Kissner).

revealed ages provide information about the cooling history of the rock, rather than the crystallization ages of its minerals, which they only record at very fast cooling rates (e.g. volcanic rocks)To resolve the thermal evolution of the EGC massif, apatite fission-track (AFT) were performed. Thermal modelling was used to determine the cooling histories of individual samples and trace their exhumation though the upper crust.

Apatite fission-track thermochronology (AFT) is based in the spontaneous fission of ^{238}U, during which, the heavy fragments of this fission leave chemically etchable latent tracks in minerals (fig. 54) and natural glasses (Wagner 1972). Information on the thermal history of apatite is stored in two archives: the etch pit areal density at an artificially polished internal surface, and the length distribution of horizontal confined tracks (Lisker et al. 2009; Wagner & Van den haute 1992). Fission of ^{238}U generates spontaneous fission-tracks that are metastable in relation to temperature. The temperature sensitive annealing of fission-tracks in apatite is constraint by two important effects: 1.) the crystallographic orientation of the spontaneous tracks, and 2.) the chemical composition of the apatite. Tracks orthogonal to the c-axis anneal more rapid than tracks parallel to the c-axis (Donelick et al. 1999; Green 1981; Green 1988; Green & Durrani 1977; Laslett et al. 1984). The closure temperature (Tc) for apatites is ~110°C/10 Myr, whereas depending on the chemical composition of the apatite, the partial annealing zone (PAZ) of FT's in apatite range from ~60 to ~110°C/10 Myr (Gleadow & Duddy 1981). Decisive influence on the kinetics of annealing thereby emanates from the fluorine- and chlorine content of the apatite, with fluorapatite being more susceptible to annealing than apatite grains rich in Cl (Green et al. 1986). Despite direct measurement of the Cl content (electron probe analysis) etch pit diameter (Dpar) has been shown to be an alternate parameter for the Cl and F content of the individual apatite crystal, with Cl rich apatites showing larger etch pits than fluorapatite (Sobel & Seward 2010).

Sampling

Altogether 10 samples were processed for thermochronological analyses and yielding enough apatite grains for the analytical work (Tab. 2). Samples were collected in four different areas (fig. 53) during one field-campaign in August - September 2006: on the NE flank of Bazarduzu Mt. (AZ091, AZ092, AZ093 and AZ095) at altitude between 2834 m and 3947 m; on the Sahnabad Plain between the Sahdag Mt. and the Tufandag Mt. (AZ083 and AZ089) at an altitude of 2737 m and 3080 m; in the north of the Tahircal Valley (AZ109) at an altitude of 954 m; and finally along the Qaracay River north of Laza Village in Pliocene conglomerates (AZ084A, AZ084B and AZ085) at an altitude of 1300 m. The sampled lithologies are mainly argillite rocks of the Middle Jurassic (Aalenian) and conglomerates of Pliocene age.

Preparation

To extract apatite crystals the collected samples were processed following the general heavy mineral separation routine (Donelick et al. 2005). The samples were cleaned, crushed by a large hammer into smaller pieces, further crushed by a jar crusher, sieved, and the larger particles where milled by a barrel or roll mill. The volume of the crushed and milled samples was reduced by using a normal gold pan. Heavy minerals were further concentrated by applying the heavy liquid bromoform separation technique to the received concentrate after panning. The final concentrate was further separated with a Frantz magnetic separator and by using the heavy liquid Dijod-methan separation technique.

Following the standard techniques for heavy mineral separation, as e.g. described by Grist and Ravenhurst (1992a; 1992b), Donelick et al. (2005), apatite grains were separated and prepared for AFT analysis. The AFT grain mounts were etched in 5.5 N HNO3 for 20 (±1) s at 20 (±1) °C and afterwards covered by U-free detection muscovite. The covered grain mounts, as well as two Durango apatite age standards and three glass neutron dosimeter (CN5, top, middle, and bottom of sample batch) were irradiated at the research reactor FRM II, Munich. After irradiation the detection mica were etched in 48 % HF for 20 (±1) min at 20 (±1) °C.

AFT data acquisition was performed at the Heidelberg FT-1 system (Thermochronology and Archeometry laboratory University of Heidelberg), equipped with an Olympus® 'BX50' optical microscope and an Autoscan® 'AS3000i' 3-axis microscope stage. The entire setup is operated through the Autoscan® software Trakscan®, which also calculates the track densities. Area densities were counted by using a 50x dry objective. The fission-track ages were calculated applying the external detector method and accordant ζ-corrections (Hurford & Green 1982; Hurford & Green 1983). The ζ-value of 351.74 (±10.39) a/cm2 was obtained by counting Durango apatite age standards. All ages, 1 σ-errors, and radial plots were determined by using the computer code 'Trackkey' (Dunkl 2002). The resulting AFT ages (table 6 and fig. 56) are reported as central ages (Galbraith & Laslett 1993; Hurford 1990). Confined fission-track length were determined together with their individual angle relative to the c-axes, using the Olympus set up with a 100x dry objective and the Autoscan® computer code 'EasyLength®' (table 7). The same microscope setup was also used for Dpar measurements (etch pit size parallel to the c-axes).

t-T modelling technique

A tool for testing various geological models of time-temperature (t-T) evolution of a specific area (crustal segment) under investigation is provided by the computer code HeFTy (Ketcham 2005; Ketcham et al. 2007a; Ketcham et al. 2007b; Ketcham et al. 2009). The HeFTy algorithm considers known FT annealing kinetics and He-diffusion behaviour of apatite and zircon, and tests cooling and reheating scenarios against determined thermochronological data. Time-temperature constraints (t-T coordinates) revealed from the known geological evolution of the area have to be taken into account. Both forward and inverse modelling can be performed, constructing possible t-T paths that are in agreement with the observed thermochronological data set.

For this study, the determined AFT data set comprises single grain cooling ages, and Dpar values serving as proxy for the chlorine and fluorine content of the individual apatite crystal.

Based on our AFT data, an inverse modelling was initiated. Along the forward t-T path constraint boxes can be set, acting as starting fields for the inverse model. The software algorithm connects the fields to t-T paths and searches within the field for possible solutions. In a Monte Carlo approach a set of single t-T paths is generated, with t-T paths that best approximate the measured data provided as solution. The primary goal of the program is to define envelopes of good and acceptable results in t-T space that contain all paths passing baseline statistical criteria and that are conform to user-entered geological constraints. A good fit (purple lines on fig. 58) corresponds to a merit value of 0.50 or higher (goodness of fit, GOF ≥ 50%). This is the expected value if the t-T path and kinetic model are in fact the correct ones. An acceptable fit (grey lines on fig. 58) corresponds to a merit value of 0.05 or higher (GOF ≥ 5%), indicating that the model has not failed the null hypothesis test that forms the basis of the applied statistics (Ketcham 2009; Ketcham et al. 2009).

In this study, the HeFTy models predominantly were run with 20,000 tried t-T paths. To approach the most likely cooling history (best fit t-T path in green on fig. 58), the t-T constraint boxes were set very spacious in the first model runs and adapted successively to the acceptable and good fits of the provided solutions.

4.3.2. Illite Crystallinity index and mineral content analysis

To characterize the metamorphic degree of the samples, two kinds of analyses were applied: Illite Crystallinity and mineral content analyses based on Xray diffraction. The aim was to determine the metamorphic degree that each sample reached during its evolution.

The Illite Crystallinity index, also named the Kübler Index or Scherrer Width, is based on the full width at half-maximum heigh (FWHM) of the 10Å X-ray diffraction peak of illite-smectite interstratified (I-S) clay minerals (Adatte et al. 1996; Godet et al. 2008; Jaboyedoff et al. 2000; Kübler 1964; Kübler 1987; Kübler & Goy-Eggenberger 2001; Kübler & Jaboyedoff 2000). The method allows determining the very low grade metamorphic degree reached by sediments based on their clay composition. Three low grade metamorphism zones can be distinguished:

- The diagenesis zone with temperatures between ~100 to 200 [°C]. It corresponds to an Illite Crystallinity index > 0.33 [Δ°2θCuKα].
- The anchizone with temperature between ~200 to 300 [°C]. It corresponds to an Illite Crystallinity index between 0.22 and 0.33 [Δ°2θCuKα].
- The epizone with temperature >300°C. It corresponds to an Illite Crystallinity index <0.22 [Δ°2θCuKα].

The IC scale used here refers to a calibration for the SCINTAG XRD 2000 Diffractometer of the University of Neuchâtel and has no universal meaning.

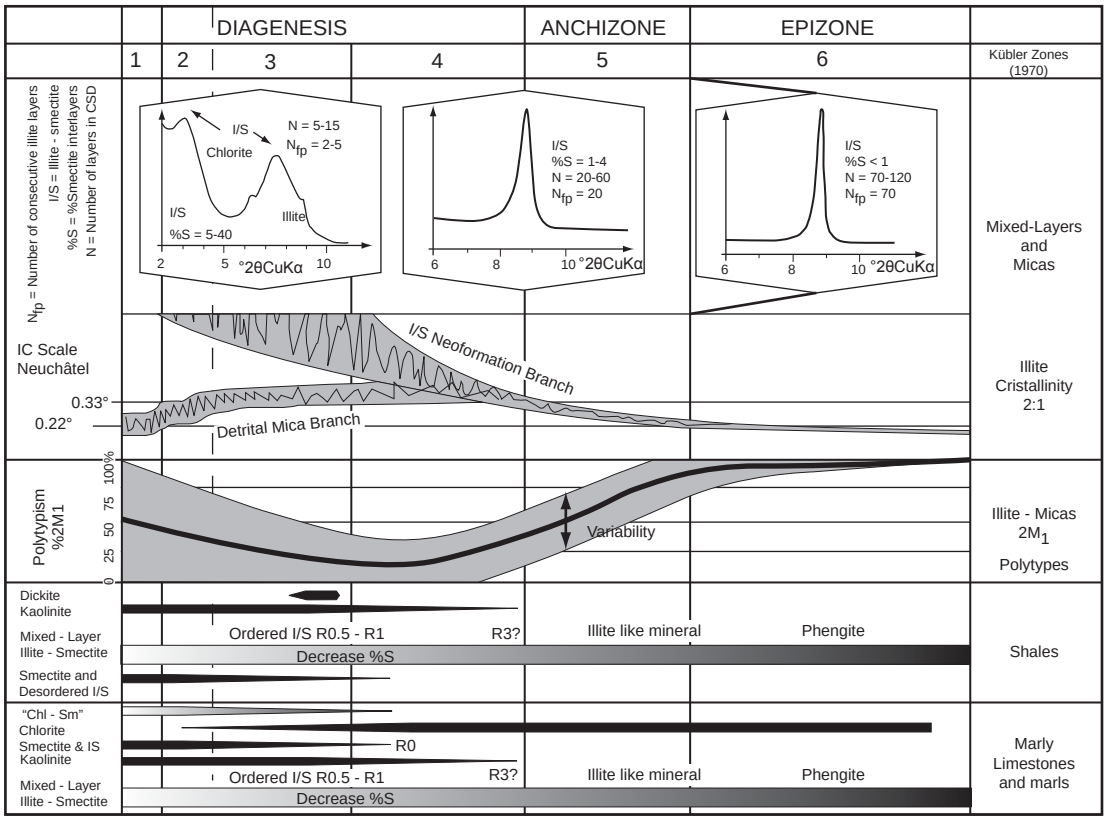

Figure 55: Equivalence between mineralogical occurrences and zones defined illite crystallinity analyses. The mineral assemblages can be deduced from this figure and are not necessarily in equilibrium. This figure summarizes the occurrences of minerals but not their fields of stability in a thermodynamic sense. The IC scale used here refers to a calibration for the Scintag diffractometer at Neuchâtel University and has no universal meaning (modified from KÜBLER & JABOYEDOFF 2000).

Mineral content is correlated with the IC index and allows also determining the temperature and the corresponding metamorphic zone (KÜBLER & JABOYEDOFF 2000) (fig. 55). Differences between mineral content, IC index value and the resulting metamorphic zone could mean a detritic origin of the sample. Variability within a same area could also mean a detritic origin of the sample.

Sampling and analyses

45 samples of 1-2 kg were taken during two fieldtrips in 2006 and 2007 (fig. 53).

23 samples were taken in 2006 in four different areas (fig. 53): on the Bazarduzu NE flank (AZ091, AZ092, AZ093, AZ094 and AZ095), on the Sahnabad Plain between the Sahdag Mt. and the Tufandag Mt. (AZ083 and AZ089), on the Sahdag-Besbarmaq Nappe (AZ079, AZ081, AZ098, AZ101, AZ102, AZ103 and AZ105) and in the north of the Tahircal Valley (AZ107, AZ108, AZ109, AZ110, AZ111, AZ112, AZ113, AZ114 and AZ115). First, they were crushed and prepared in 3 manners by A. Rast: granulometric fraction < 2µm dried at air temperature (2N), granulometric fraction < 2µm with ethylen-glycol (2G) and 2-16 µm fraction (16N). Some samples have also been analysed for AFT. Afterwards, clay mineral analyses were carried out at the Geological Institute of the University of Neuchâtel[2]. The analyses were based on methods described by Kübler (KÜBLER 1987). Small rock fragments were mixed with de-ionized water (pH 7 – 8) and agitated. The carbonate fraction was removed by addition of HCl 10% (1.25 N) at room temperature for 20 minutes or more until all carbonate was dissolved. Ultrasonic disaggregation of the rock residue was accomplished during 3 minute intervals. The insoluble residue was washed and centrifuged (5-6 times) until a neutral suspension was obtained (pH 7 – 8). Separation of different grain size fractions (2 µm and 2 – 16 µm) was obtained by centrifugation using a timed settling method based on Stokes' law. The selected fraction was then pipetted onto a glass plate and air-dried at room temperature or treated with ethylene-glycol. The oriented clay samples on air dried and glycolated slides were then XRD analysed on a SCINTAG XRD 2000 Diffractometer. Each clay mineral (e.g. chlorite,

2 The laboratory has moved now in the University of Lausanne. Contact : Dr. Thierry Adatte, Institut de géologie et paléontologie, Quartier UNIL-Dorigny, Bâtiment Anthrole 3169, 1015 Lausanne (Switzerland), email : thierry.adatte@unil.ch.

kaolinite) is characterized by specific XRD peaks expressed in intensities (counts by minutes CPM), which were measured in the size fraction 2 μm. The 2 – 16 μm fraction was used for a semi-quantitative estimate of the proportion of clay minerals.

22 samples of 1-2kg were taken in 2007 in three different areas (fig. 53): around Xinaliq (AZ159, AZ161, AZ163, AZ165, AZ167, AZ169, AZ171, AZ173, AZ175, AZ176, AZ177, AZ180, AZ182, AZ184 and AZ186), along the Cek Valley (AZ191, AZ193 and AZ195) and eastwards along the Cimicay River (AZ199, AZ201, AZ203 and AZ205). These samples were prepared and analysed in the Centre Scientifique et Technique Jean-Féger (CSTJF) of the TOTAL oil company in Pau (France). They were first crushed in 2 manners: a granulometric fraction < 5μm dried at air temperature (2N) and a granulometric fraction < 5μ.m with ethylenglycol (2G). 5 μm fraction were analysed in a Panalytical X'Pert Pro diffractometer with a X'celerator linear detector and a cobalt tube. Peaks were decomposed in the module Profile from the Diffrac-AT suite (Brüker AXS). As the laboratory does not apply anymore the Kübler Method, they did not measure the total peak width and the diffractometer is not calibrated to obtain results comparable with the first series. Consequently, we measured the FWHM of each sample directly on the delivered graph and as expected their value are not comparable with the first series. However, they can be used to evaluate a change in metamorphic grade but without classification in the Kübler Scale. Finally, no mineral content analyses were made on these samples.

4.3.3. Subsidence curves

Subsidence curves describe basin evolution through time. They include the burial curve and the tectonic subsidence curve. They are based on thicknesses, types and ages of sediment logs on which correction for effects of compaction, water depth and isostasy are applied. Combined with other information, subsidence curves can be a powerful tool to determine for example the oil and gas potential of a basin (Allen & Allen 2005). In this study we use them to determine the geohistory of the GCB from the Middle Jurassic up to now.

Data

To build 2 subsidence curves, we used the stratigraphic records of Tahircal-Sudur and Sahdag-Xizi structural zones (figs. 16 and 17 of chapter 2.6). These stratigraphic records summarize the deposits of the whole areas not from a determined section. They are mainly based on literature and completed by field observations. For the thickness parameter we decided to use the maximum thickness of each layer.

For the bathymetry of the Tahircal-Sudur and the Sahdag-Xizi curves, we use an initial value of 0-50 m and 50-100 m based on older deposit of the southern and deeper Tufan structural zone. The present bathymetries for both zones correspond to the present altitude of the deposit: respectively 850 m and 2000 m (see below).

Table 4: Sediments parameters used in the file "Easysub" to build the subsidence curves. Φ_0: initial porosity; c: lithological coefficient; ρ: sediment grain density. Parameters: # from Sawyer et al.; * from Sclater & Christie (1980); ^ from Schmoker & Halley(1982).

Lithology	Code	Φ_0 [-]	c [-]	ρ [g/cm^3]
#Limestone	1	0.45	0.54	2.71
*Sandstone	2	0.49	0.27	2.65
*Shale	3	0.63	0.51	2.72
*Chalk	4	0.70	0.71	2.71
^Dolomite	5	0.31	0.22	2.86
Evaporite	6	0.15	0.10	2.65
*Siltite	7	0.56	0.39	2.68

To build each curve, several erosive events deduced from the stratigraphical log and from field observation were introduced. For the Tahircal-Sudur zones, a first event at the end of the Middle Jurassic eroded 600 m of Bathonian and Bajocian sediments; the second event is recent (<2.6 Myr) and eroded 2800 m of sediments from Neogene to Upper Jurassic (1770 m) more 850 m of Aalenian sediments. For the Sahdag-Xizi Zone, a first event at the end of the Upper Jurassic (Berriasian transgressive on tilted Kimmeridgian), eroded about 480 m of sediments; the second event eroded about 600 m after the Albian-Aptian period. The latter is based on the hollowing out of a deep paleovalley (The Buduq-Through) in the Besbarmaq Nappe and its filling by Upper Cretaceous sediments. For both areas, numerous lacunes are described in bibliography but without the amount of eroded sediment, consequently we introduce them but with neither bathymetry nor erosion.

According to stratigraphic logs, the depth of burial curves for each zone at present time should approximatively correspond to the present sediment thickness until the Aalenian deposits base: for the Tahircal-Sudur Zone, they stay at 1100 m (near Tahircal Village) and for the Sahdag-Xizi Zone, at 4850 m (Buduq Trough).

Methods

Subsidence curves were built using the spreadsheet file "Easysub" created by J.A Uriarte, R.A. Schegg

Table 5: Lithology (Lith.), thickness (Thickn.), absolute age interval (Absolute age), today erosion (Eros.) and bathymetry interval (Bathymetry) used to build the subsidence curves. Evolution is divided in several types: Initial: initial conditions; final: final conditions; D : sediment deposition; L: sedimentological lacune; E: erosive event. Lithology is also divided in several types: Shale (Shl), Sandstone (Sdst), Limestone (Lmst), Evaporites (Evap) and Siltstone (Sltt) Data are based on literature and on field observations (see in text).

Tahircal-Sudur zones						
N°	Evol Type	Lith	Thick [m]	Eros. [m]	Abs. Ages [Myr]	Bathym. [m]
1	Initial	-			175.6-175.6	50-100
2	D	Shl	1000		172.6-175.6	100-150
3	D	Sdst	100		172.3-172.6	150-200
4	D	Shl	400		171.1-172.3	200-250
5	D	Shl	450		169.7-171.1	150-200
6	D	Sdst	250		167.7-169.7	100-150
7	D	Shl	350		165-167.7	50-100
8	E1	-		600	164.7-165	0-0
9	D	Shl	100		159.8-164.7	10-50
10	D	Evap	85		156-159.8	0-10
11	E2			0	155.6-156	0-10
12	D	Lmst	500		146-155.6	10-50
13	E3			0	145.5-146	10-50
14	D	Lmst	600		125-145.5	5-20
15	E4	-		0	77.1-125	0-0
16	D	Sdst	80		70.6-77.1	10-50
17	E5	-		0	61.1-70.6	0-0
18	D	Lmst	70		58.7-61.1	10-50
19	L1			0	55.8-58.7	10-50
20	D	Shl	10		33.9-55.8	5-50
21	D	Shl	100		20.4-33.9	200-500
22	E6			0	13.8-20.4	0-0
23	D	Sdst	80		11.6-13.8	10-50
24	L			0	7.2-11.6	10-50
25	D	Sltt	80		5.3-7.2	0-50
26	D	Sdst	250		3.6-5.3	0-50
27	Final		0	2800	0-3.6	-225
Sahdag-Xizi Zone						
1	Initial	-	0	0	175.6	50-100
2	D	Shl	230	-	171-175.6	300-500
3	D	Sdst	60	-	169.7-171	300-500
4	D	Shl	150	-	166.7-169.7	300-500
5	D	Sdst	150	-	163.7-166.7	300-500
6	D	Sdst	150	-	160.7-163.7	20-50

N°	Type	Lith	Thick [m]	Eros. [m]	Abs.Ages [Myr]	Bathym. [m]
7	E1	-	0	0	160-160.7	0
8	D	Sdst	100	-	158.6-160	50-100
9	D	Sdst	150	-	155.6-158.6	50-100
10	D	Sdst	270	-	150.8-155.6	50-100
11	D	Lmst	480	-	146-150.8	50-100
12	E2	-	0	480	145.5-146	0
13	D	Sdst	250	-	140.2-145.5	10-50
14	D	Shl	600	-	133.9-140.2	10-50
15	D	Lmst	600	-	130-133.9	10-50
16	D	Lmst	600	-	125-130	5-30
17	D	Shl	60	-	116.3-125	10-50
18	D	Shl	30	-	112-116.3	5-50
19	D	Shl	40	-	105.8-112	50-100
20	D	Shl	40	0	100-105.8	5-50
21	E3	-	0	600	99.6-100	0-0
22	D	Lmst	70	-	93.6-99.6	5-50
23	D	Lmst	20	-	92.3-93.6	10-50
24	E4	-	0	0	92-92.3	0-0
25	D	Lmst	100	-	85.8-92	10-50
26	D	Sdst	100	-	84-85.8	5-50
27	E5	-	0	0	83.5-84	0-0
28	D	Shl	150	-	78.7-83.5	5-30
29	D	Lmst	250	-	70.6-78.7	5-30
30	D	Sdst	300	-	65.5-70.6	5-50
31	D	Shl	200	-	61.1-65.5	10-50
32	D	Shl	130	-	58.7-61.1	5-50
33	L1	-	-		28.4-58.7	0
34	D	Shl	250		23-28.4	5-30
35	E6	-	-	-	13.8-23	0
36	D	Lmst	180		11.2-13.8	0-10
37	L2	-	-	0	3.6-11.2	0
38	D	Sdst	100	-	2.6-3.6	10-50
39	D	Lmst	300	-	1.8-2.6	50-100
40	Final	-	-	-	0-1.8	-2000

(University of Geneva) and modified by G. Borel. It needs to enter parameters such as lithology, sediment thicknesses, ages of the top and the bottom of the layers, today erosion and bathymetry. The spreadsheet used the computation procedure of Van Hinte (1978), Sclater & Christie (1980) and Angevine (1990). The depth-porosity laws defined by Sclater & Christie (1980) is generally used for oceanic basin modelling and when there is some emerging period (like in this study), the unpacking is too important. Table 5 contains the parameters we used to build the subsidence curves.

Thicknesses and ages were completed from synthetic stratigraphical logs based on fieldwork observations and bibliography. Known stratigraphic gaps are described on figure 51 and allow defining the "Today Erosion" parameter ("Eros." parameter in Table 5).

For lithology, this method defines 7 types of sediments with their corresponding parameters (Table 4). We change the evaporite density from an initial value of 3 [g/cm3] to a value of 2.65 [g/cm^3] corresponding to average density of the gypsum (2.31 [g/cm^3]) and the anhydrite (2.98 [g/cm^3]) with a distribution estimated at 50% for each.

Based on the lithology description of the synthetic stratigraphical logs and on field observations, approximate bathymetries were defined for each stage. Added to the decompacted sediment thicknesses, this parameter allows determining the total subsidence.

Finally the tectonic subsidence calculation is based on the laws defined by Angevine et al. (1990) using a mantle density (ρ_m) of 3.33 [g/cm^3](Parsons & Sclater 1977).

At the end, a graph depth-time allows visualizing the burial, the tectonic subsidence and the total subsidence through the geological times.

As defined by Allen & Allen (2005), the burial curve represents the maximum packed sediment thickness at a determined time for a determined level. The tectonic subsidence curve corresponds to the total subsidence with the correction of isostatic effect. This is the subsidence relative to a stationary datum (~today sea level) that would occur in an entirely water-filled basin. One benefits of working with the tectonic subsidence curves is that the subsidence history of basins can be compared without the complications of different paleobathymetric, packing and isostatic effects.

In this study, we decided to work with the burial curve and the tectonic subsidence curve with the maximum bathymetry correction. We did not use the eustatic correction.

4.4. Fission-tracks results and interpretation

Three kinds of results were deduced from fission-tracks analyses: FT central ages of each sample, pit diameters and track lengths with their corresponding t-T modelling.

4.4.1. Apatite Fission-Track age distribution

The data set exhibits a range in AFT central ages, between 12.5 (± 2.4) Ma and 89.8 (± 9.8) Myr (fig. 56, table 6 and table 7).

All central ages of Middle Jurassic samples (AZ083, AZ089, AZ091, AZ092, AZ093, AZ095, AZ109) are younger than there sedimentation age. All central age of Neogene samples are older than there sedimentation age.

Table 6: Summary of apatite fission-track data and sample location with description: Sample-location: Altitude in meter above sea-level (Alt), Latitude (Lat) and Longitude (Long) in UTM coordinates (WGS 84); Lithology (Lith): sdst: sandstone, cngl: conglomerate; Geological Age: J_2a: Aalenian, N_2: Pliocene; U (std): Uranium concentration and standard deviation in [µg/g]; n: number of counted apatite grains; ρs density of spontaneous tracks [10^5tr/cm^2]; Ns: number of spontaneous tracks; ρi: density of induced tracks [10^5 tr/cm^2]; Ni: number of induced tracks, Nd = 15391 tracks counted on CN-5; P(χ^2): probability that single grain ages are consistent and belong to the same population, test is passed if P(χ^2) >5% (Galbraith 1981). Central ages (Ctrl age) are calculated using a ζ-value of 351.27 ± 9.88 [a/cm^2]; Sample with *: Nd=15317, ages are calculated as central ages using a ζ-value of 351.27 ± 9.88 [a/cm^2].

Sample	Alt. [m.a.s.l.]	Lat [deg]	Long [deg]	Lith.	Geol. Age	U (std) [µg/g]	*N*	ρ_s [x10^5/cm^2]	N_s	ρ_i [10^5/cm^2]	N_i	P(χ^2) [%]	Ctrl age [Myr]
AZ083*	2745	41.2257	48.04839	Sdst	J_2a	32.98 (24.1)	39	5.303	693	36.467	4766	0	41.8 ± 5.4
AZ084*	1300	41.33986	48.15618	Cngl	N_2	21.53(15.7)	20	7.431	436	18.595	1091	0	83.7 ± 9.6
AZ084A	1300	41.33986	48.15618	Cngl	N_2	0.23 (0.19)	19	0.014	78	0.298	1613	0.87	14 ± 2.1
AZ085*	1300	41.33985	48.15617	Cngl	N_2	22.79 (14.8)	20	3.797	277	22.427	1636	0	37.6 ± 3.5
AZ089	3080	41.23285	48.06897	Sdst	J_2a	12.14 (12.1)	25	3.884	385	11.096	1100	0	89.8 ± 9.8
AZ091	3947	41.23344	47.90098	Sdst	J_2a	27.05 (24.9)	30	3.352	245	24.658	1802	0	35.4 ± 4.1
AZ092	3805	41.23085	47.90223	Sdst	J_2a	21.34 (13.7)	30	4.858	394	24.575	1993	0	47.6 ± 5.1
AZ093	3629	41.22879	47.90676	Sdst	J_2a	23.97 (21.6)	25	3.63	179	26.1	1287	0	39 ± 5.3
AZ095	2834	41.22428	47.32861	Sdst	J_2a	20.24 (13.2)	20	2.872	109	27.114	1029	0	36 ± 6.7
AZ109*	954	41.43801	48.07161	Sdst	J_2a	27.1 (15.7)	22	1.499	30	31.135	623	78	12.5 ± 2.4

Table 7: Detailed apatite fission-track length data: CT: confined tracks length; Lc: track length after c-axis correction; Dpar: etch pit diameter. n : number of measures; mean: mean length; std: length standard deviation; skew: skewness of distribution relative to the mean value (measure of asymmetry of the distribution).

Sample	n CT	CT mean [µm]	CT std [µm]	CT skew [µm]	Lc mean [µm]	Lc std [µm]	Lc skew [µm]	n Dpar	Dpar mean [µm]	Dpar std [µm]	Dpar skew [µm]
AZ083	51	10.92	2.16	0.43	12.15	1.91	-0.12	188	1.59	0.44	1.1
AZ084	42	9.97	1.61	0.89	n.a.	n.a.	n.a.	106	1.61	0.37	1.2
AZ084A	88	10.3	1.54	0.67	11.33	1.41	0.02	93	1.39	0.47	0.63
AZ085	15	10.72	1.71	0.30	n.a.	n.a.	n.a.	111	1.56	0.52	0.61
AZ089	44	10.21	1.22	0.27	n.a.	n.a.	n.a.	146	1.71	0.43	0.03
AZ091	62	12.83	1.82	-0.69	13.56	1.58	-0.89	156	1.27	0.32	0.30
AZ092	44	10.37	1.82	0.76	n.a.	n.a.	n.a.	154	1.33	0.37	0.80
AZ093	68	10.22	1.78	1.13	11.46	1.76	0.16	111	1.5	0.41	-0.16
AZ095	40	10.06	1.56	0.99	n.a.	n.a.	n.a.	93	1.52	0.28	-0.34
AZ109	85	10.19	1.41	0.60	11.84	1.49	-0.44	112	1.37	0.35	0.91

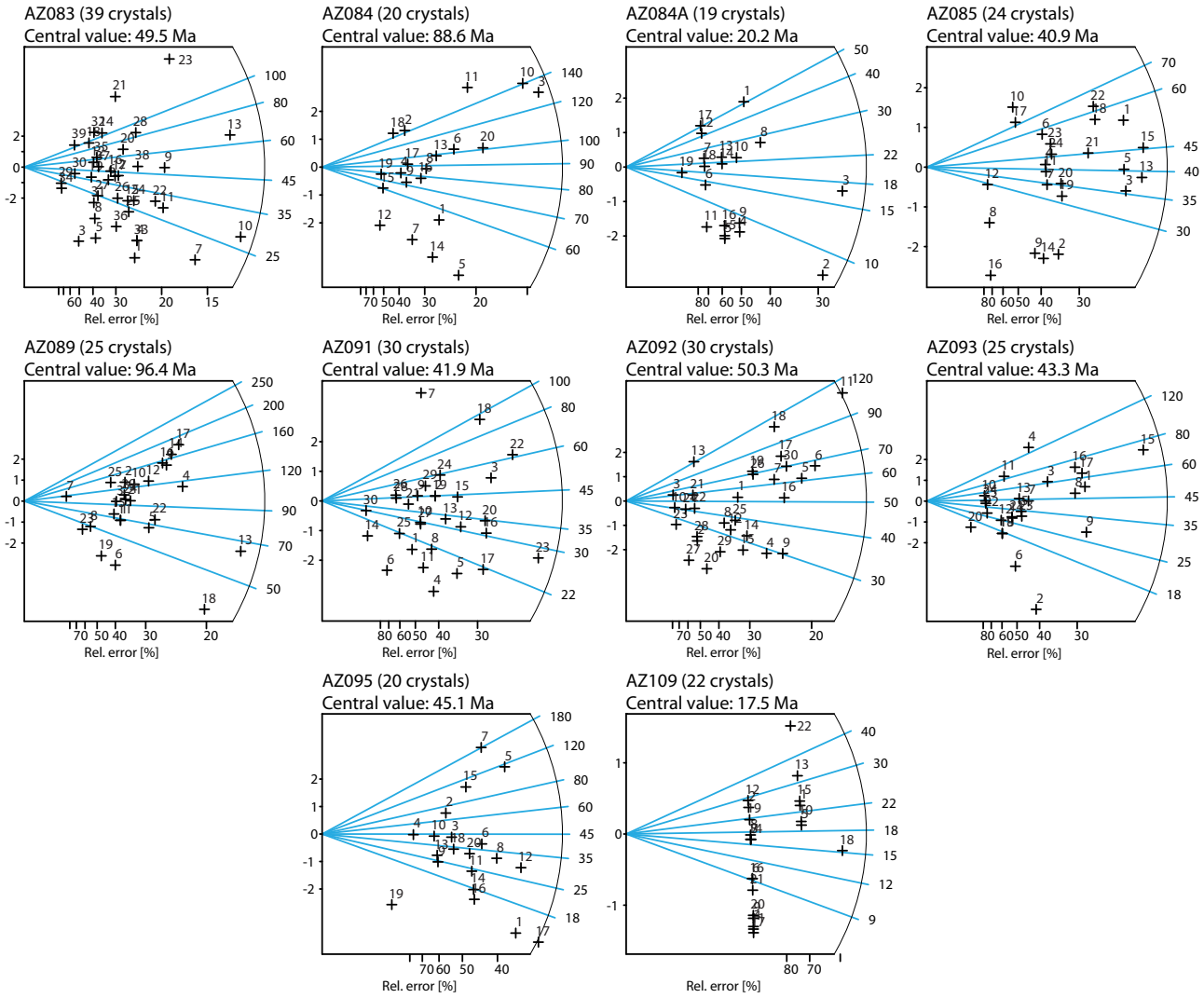

Figure 56: Radial plots after GALBRAITH (1990) of single grain age data for analyzed apatite samples. Radial plots were calculated and drawn with the TRACKKEY (ver. 4.2 g) algorithm (2002). All samples are plotted against a 2σ error.

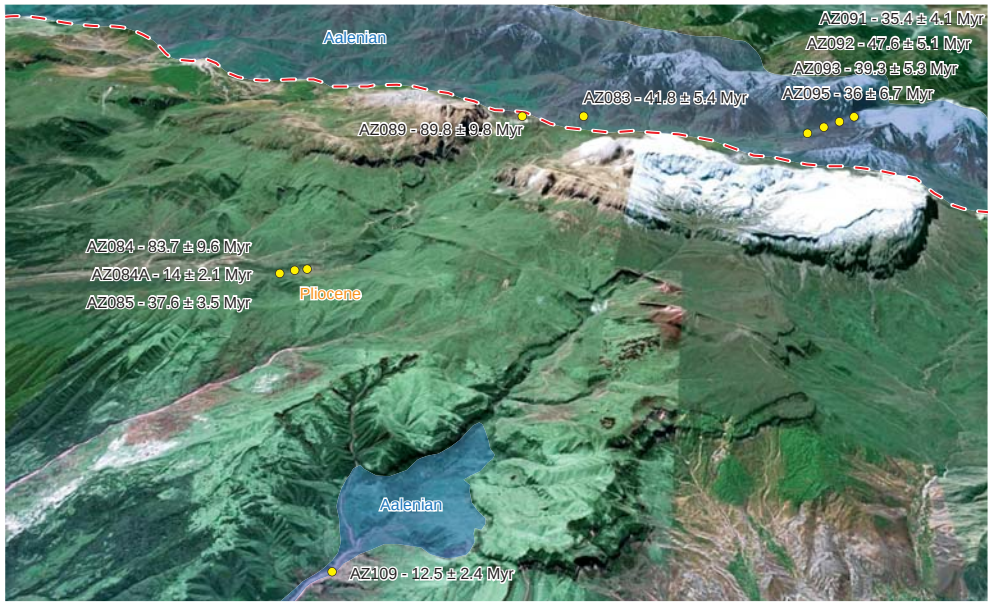

Figure 57: Samples positions with their respective AFT age. Samples AZ083, AZ089, AZ091, AZ092, AZ093, AZ095 and AZ109 are of Aalenian age. Samples AZ084 and AZ085 are of Pliocene age. Dashed red line corresponds to a supposed fault based on AFT central age difference and stratigraphical age differences.

The youngest AFT age was revealed from the lowest elevation (AZ109, 954 m.a.s.l.) that has been sampled in the northern foreland area of the EGC.

The oldest central age of 89.8 (±9.8) Myr was received from a argillite (AZ091) of Middle Jurassic (Aalenian) age located between the Sahdag and Qizilqaya mountains.

Samples of the central and highest area (AZ083, AZ091, AZ092, AZ093, AZ095) have ages between 35.4 (±4.1) Myr and 47.6 (±5.1) Myr.

4.4.2. Pit diameters (Dpar)

1270 Dpar length have been counted and their number per sample range from 93 (AZ084A and AZ095) to 188 (AZ083) (results in table 7). The mean Dpar values range from 1.27±0.32 μm (AZ091) to 1.71±0.43 μm (AZ089). The mean and standard error and the skew values of the ten samples are given in table 7.

Most of the analyzed apatites have a relatively low Dpar value despite a high variation in single grains. For the three Pliocene samples (AZ084, AZ084A and AZ085), the Dpar value is in the same range as the Dpar value of Aalenian sample.

4.4.3. Confined track length and t-T modelling

The t-T modelling is mostly based on the confined fission-track lengths. To carry out this analysis, 539 confined tracks lengths have been counted in all apatite grains used in this study (table 7). The minimum quantity of track lengths measured in a sample is 15 (AZ085) and the maximum is 88 (AZ084A). The mean track lengths show relatively low values ranging from 9.97±1.61 [μm] (AZ084) to 12.83±1.82 [μm] (AZ091).A minimum of 50 confined track lengths per sample are necessary for a good t-T modelling. AFT lengths have also to be measured in samples that reach at least one time the AFT annealing temperature. In this study, only five samples reach the 50 confined tracks. The Pliocene Age of the sample AZ084A compared to the AFT Central Age indicates that it never reached the annealing temperature and therefore cannot be used for t-T modelling. Finally, four samples were suitable for t-T modeling: AZ083, AZ091, AZ093 and AZ109. They are all of Aalenian Age.

Based on the four suitable samples, we built four t-T models (fig. 58). Models are calculated with the Hefty algorithm (Ketcham 2005; Ketcham et al. 2007a; Ketcham et al. 2007b; Ketcham et al. 2009) and were made in the Hefty v.1.6.7 software (Ketcham et al. 2009).

The constrain boxes used for A to D models are based on the sedimentological logs of the area and on the subsidence study (see below). In the case of the EGC, two general geological evolution models were tested. One that assumed a rapid heating during Middle Jurassic to Lower Cretaceous time followed by a rapide cooling during Late Neogene time and a second that add to the latters a cooling episode during Upper Cretaceous – Paleogene time.

From the resulting t-T models, burial and exhumation rates were determined for each segment of the four best fit t-T paths (table 8) and using a geothermal gradient of 20°C/km taken from Pryde (1979).

4.4.4. Interpretation

Central age results within the central area are divided in two age groups as shown in figure 57: a group composed of AZ083, AZ091, AZ092, AZ093 and AZ095 with AFT ages between 35.4 and 47.6 Myr and the sample AZ089 with an AFT age of 89.8 Myr. The first group is located in the Tufan zone and the second between the Sahdag Mt. and the Qizilqaya Massif. Lithologically, they are all of Aalenian Age. The important central AFT age difference between the two groups supports the interpretation of a north dipping normal fault between them: sample AZ089 with the old central AFT age could be considered to be part of the northern hanging wall that stay in place; the others samples with younger central AFT ages correspond to the southern footwall that underwent the surface uplift of the central part of the EGC.

The three samples taken from Pliocene conglomerates were certainly never deeply buried based on their stratigraphic ages that are younger than their central AFT ages. Pliocene samples (AZ084, AZ085) could not reach the annealing temperature. Consequently, they should be composed of inherited grains. Their central AFT ages can be related to the central AFT ages of the Aalenian samples. Indeed, the AZ084 AFT age (83.7±9.6 Myr) could be related to the Aalenian AZ089 AFT age (89.8±9.8 Myr); the AZ085 AFT age (37.6 ± 3.5) could be directly linked with the AFT ages of the central area (35.4 to 47.6 Myr). However their components must come from a source rock that had similar central AFT ages but during Pliocene age. Based on an uplift progressing towards the ESE, that mean the source rock was located to the west of the present position of the samples during Pliocene period.

Finally, t-T models and the calculated exhumation rates (table 8) confirm a fast burial during the Middle Jurassic and Lower Cretaceous periods and a fast exhumation that started between Miocene and Quaternary. The recent exhumation is not the fastest, as it could be expected, in the central and highest part (Tufan Zone) but in the northern

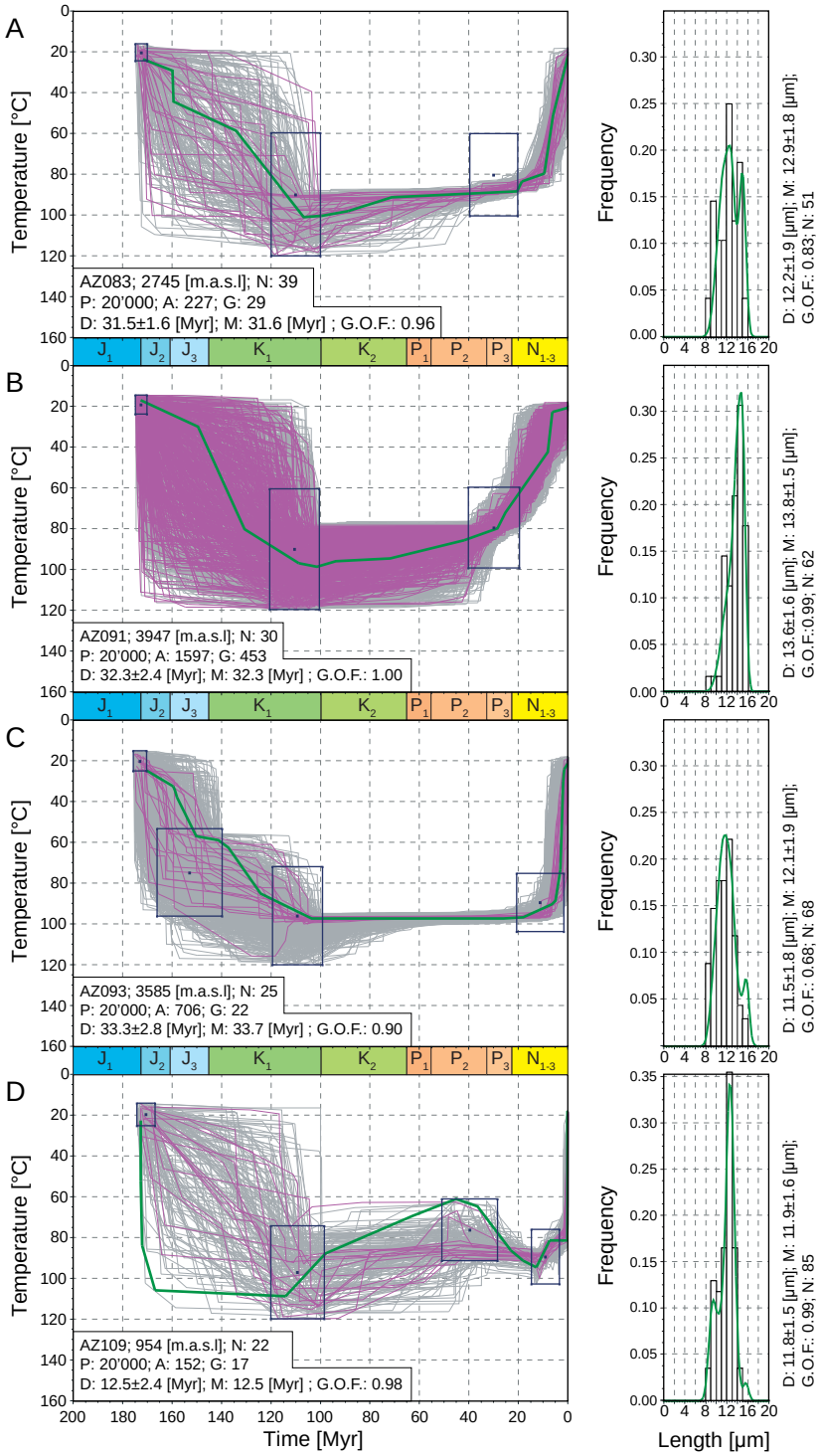

Figure 58: Track length model results using Hefty sotftware V.1.6.7 (Ketcham et al. 2009) for samples from the northern (AZ083, AZ109) and central area (AZ091, AZ093) of the Eastern Greater Caucasus. Revealed time-Temperature paths graphs illustrate the cooling history of individual samples. The left graphs to the t-T path and the right graphs to the C axes corrected confined fission-track length (CT) frequency distribution overlain by a calculated probability density function (best fit) based on the best-fit (green) path of the left graph. The modelling tests possible t–T curves that fit independent geological constraints (squares) against the AFT data set. The results in the t–T curve show three different reliability levels: grey paths correspond to "acceptable fit" t–T paths with a merit function value ≥ 0.05, purple paths correspond to "good fit" t–T paths with a merit function value ≥ 0.5. Green lines correspond to "best fit" path (Ketcham 2005; Ketcham et al. 2007a; Ketcham et al. 2007b; Ketcham et al. 2009). P: number of tested inverse models; A: acceptable fit models; G: good fit models; D: determined FT age (1-σ error) and CT; M: modelled FT age and CT; G.O.F. goodness of fit; N number of single grains and measured CT. Models A to D are based on the known geological constrains and on the data obtained with IC analyses and subsidence curves of this chapter. Models A, B and C are from the central area (Tufan Z.) and the model D from the northern area (Tahircal Z.).

Table 8: Calculation of exhumation rates for each segments of each best-fit t-T path of figure 58.

Smpl	T-T segment [°C]	t-t segment [Ma]	Cooling gradient [°C/Ma]	Exhum. Rate [mm/a]
AZ083 - 2745 [m a.s.l]	172 - 160	24 - 29	0.47	-0.024
	160 - 159	29 - 44	35.55	-1.778
	159 - 134	44 - 59	0.57	-0.028
	134 - 107	59 - 101	1.55	-0.077
	107 - 100	101 - 100	-0.08	0.004
	100 - 89	100 - 98	-0.22	0.011
	89 - 71	98 - 91	-0.38	0.019
	71 - 20	91 - 88	-0.06	0.003
	20 - 18	88 - 84	-2.45	0.122
	18 - 9	84 - 80	-0.43	0.021
	9 - 6	80 - 51	-8.06	0.403
	6 - 0	51 - 22	-4.82	0.241
AZ091 - 3945 [m a.s.l]	173 - 149	17 - 30	0.56	-0.028
	149 - 131	30 - 80	2.67	-0.134
	131 - 109	80 - 97	0.76	-0.038
	109 - 101	97 - 99	0.24	-0.012
	101 - 94	99 - 96	-0.36	0.018
	94 - 72	96 - 95	-0.06	0.003
	72 - 42	95 - 86	-0.30	0.015
	42 - 28	86 - 80	-0.43	0.022
	28 - 25	80 - 72	-2.39	0.119
	25 - 8	72 - 42	-1.73	0.087
	8 - 6	42 - 23	-10.65	0.533
	6 - 0	23 - 21	-0.33	0.017

Smpl	T-T segment [°C]	t-t segment [Ma]	Cooling gradient [°C/Ma]	Exhum. Rate [mm/a]
AZ093 - 3585 [m a.s.l]	171 - 160	25 - 33	0.72	-0.036
	160 - 159	33 - 35	2.74	-0.137
	159 - 158	35 - 38	4.12	-0.206
	158 - 150	38 - 57	2.44	-0.122
	150 - 141	57 - 59	0.22	-0.011
	141 - 137	59 - 63	0.90	-0.045
	137 - 124	63 - 85	1.73	-0.086
	124 - 103	85 - 97	0.59	-0.030
	103 - 26	97 - 97	0.00	0.000
	26 - 18	97 - 97	-0.07	0.004
	18 - 6	97 - 90	-0.55	0.028
	6 - 5	90 - 89	-1.23	0.062
	5 - 3	89 - 73	-7.63	0.382
	3 - 2	73 - 30	-38.25	1.913
	2 - 1	30 - 24	-14.13	0.706
	1 - 0	24 - 21	-2.00	0.100
AZ109 - 954 [m a.s.l]	173 - 173	23 - 52	<-100	< - 5
	173 - 172	52 - 84	55.92	-2.796
	172 - 167	84 - 106	4.19	-0.209
	167 - 114	106 - 109	0.06	-0.003
	114 - 109	109 - 103	-1.29	0.064
	109 - 98	103 - 88	-1.30	0.065
	98 - 63	88 - 69	-0.52	0.026
	63 - 45	69 - 61	-0.47	0.024
	45 - 36	61 - 65	0.43	-0.021
	36 - 23	65 - 86	1.60	-0.080
	23 - 18	86 - 91	1.02	-0.051
	18 - 13	91 - 95	0.61	-0.031
	13 - 7	95 - 81	-2.45	0.123
	7 - 0	81 - 81	0.00	0.000
	0 - 0	81 - 18	>100	> 5

part (in Tahircal and Sahdag-Xizi zones). Based on this observation, on t-T model and on the scattering of the data of sample AZ109, we think that the northern area has a more complex behaviour: the initial burial is followed by an intermediate exhumation that last during the Upper Cretaceous and Paleogene. Afterwards, a burial acted on the area since the beginning of Miocene and was finally followed by the main and recent exhumation. More precised study must be made to determine a value for the exhumation rate but it is certainly faster than 1mm/yr.

Results of the Illite Crystallinity analyses ob-tained by the two laboratories are grouped in table 9 for the 23 samples analysed at the Geological Institute of the University of Neuchâtel (Un-iNe) and in table 10 for the 22 samples analysed at the Centre Scientifique et Technique Jean-Féger (CSTJF) of the TOTAL oil company in Pau (France).

4.5. Illite Crystallinity results and interpretation

Results of the Illite Crystallinity analyses ob-tained by the two laboratories are grouped in table 9 for the 23 samples analysed at the Geological Institute of the University of Neuchâtel (UniNe) and in table 10 for the 22 samples analysed at the Centre Scientifique et Technique Jean-Féger (CSTJF) of the TOTAL oil company in Pau (France).

The 23 samples from the University of Neuchâtel are located from the northern orogenic front (Samur River – Tahircal Zone) to the central part of the EGC (Bazarduzu Mt. – Tufan Zone). Their ages vary from Aalenian to Pliocene. 8 of them (AZ089, AZ092, AZ093, AZ094, AZ105, AZ107, AZ114 and AZ115) are not suitable because the M001 peak is too small (<150 cps) to allow a good evaluation of their IC index. Four of them (AZ081, AZ101 AZ108 and AZ110) have IC index corresponding to the Epizone-Anchizone but they can be considered as detrital because they still contain smectite or kaolinite that disappear in the metamorphic zone corresponding to their IC (fig. 55). See also Rast (2007).

On figure 59, a mineralogical variation from north to south can be seen. The northern Tahircal Zone is characterized by the predominance of kaolinite, about 50% of chlorite and mica, low level (<10%) of interstratified and the absence of smectite. Based on figure

55, the Tahircal Zone could be associated to zone 3-4 of Kübler Zones corresponding to the upper part of the Diagenesis Zone. In the Sudur Zone, only a Pliocene sample was analysed and it contains all analysed mineral with the approximatively same level indicating that this sample almost did not undergo any metamorphism. Most of the samples of Sahdag-Besbarmaq Nappe contain smectite and consequently have undergone only a very low grade metamorphism. The Tufan Zone samples contain chlorite and micas but no smectite, kaolinite and interstratified. This content is typical from a sample that reached the Anchizone (zone 5 on fig. 55). These observations demonstrate that Aalenian sediments of the Tufan underwent a higher degree of metamorphism than the ones of the Tahircal Zone. Finally the sediments of Sahdag-Besbarmaq Nappe were certainly never deeply buried during their evolution.

Although the samples of the Tahircal and Sahdag Besbarmaq Nappe stays in the diagenesis metamorphic grade their minerological content is not the same: the Sahdag-Besbarmaq Nappe samples do not contain kaolinite that is normally still present at low grade metamorphism. That can mean a difference between the depositional environments of Upper Cretaceous and Aalenian periods.

In average, the Tufan and the Tahircal zones show a slightly higher metamorphism than the Sahdag-Besbarmaq Nappe and the Sudur Zone (fig. 60). In the Tahircal Zone, the metamorphism increases southward and one sample almost reach the Anchizone (AZ109). The highest degree of metamorphism is reached in the Tufan Zone (AZ095) and the Pliocene sediments of the Sudur Zone (AZ084) have the lowest degree. The IC indexes of the Sahdag-Besbarmaq Zone have a high variation (almost from the Anchizone to very low grade metamorphism) and based on the fact that they were sampled in the same area, it can be assumed that their IC indexes are inherited and do not reflect a low grade metamorphic evolution of the sediment.

The IC indexes of samples analysed by the CSTJF (fig. 61) show an increase of the metamorphism from the north towards the center of the EGC (Tufan Zone) and also a decrease from the northwest to the southeast (fig. 62). Limits between the metamorphic grades are not defined because the laboratory did not apply the Kübler Method. Consequently, they cannot be correlated with the other samples analysed in UniNe.

The Contact Zone of figure 61 corresponds to the area located between the foot of the cliff of Qizilqaya Massif and the Xinaliq Village; the Tufan Zone corresponds to the area located south of Xinaliq and Cek villages. Although the exact metamorphism zone limits are not known, an increase of metamorphism from northeast to southwest can be seen. Consequently, the Tufan Zone which is the core of the orogen has a higher degree of metamorphism than the Contact Zone located further to the north. The figure 62 represents the same samples as figure 61 but in another direction: from the northwest towards the southeast parallelly to the orogen axis. Globally, we observe a southeastward decrease of the metamorphism. On figure 62 data are grouped by location allowing detailed geographical comparison of the metamorphic grades. The samples (AZ159 and AZ161) of the area “B” (Qudiyalcay Valley south of Xinaliq) have the highest degree of metamorphism (low IC index) and they are located at the bottom of a valley reaching the center of the Tufan Zone. Samples of area “C” (Xinaliqdag Mt.) were taken along the steep slope of the mountain flank. They almost have the same degree of metamorphism although the lowest and the northeastern most sample is at an altitude of 2141 m (AZ173) and the highest and most southern sample is at an altitude of 3313m (AZ163). Based on this statement, the metamorphism increases again southwestward, perpendicularly to the orogen axis. Samples of area “A” (north of Xinaliq Village) have the lowest metamorphism degree and there is a step with the “B” and “C” areas that could probably confirm the presence of the normal fault between “B”-“C” and “A” areas that was described also in the AFT interpretation. In the area “D” (valley south of Cek Village), the central sample (AZ195) has the highest degree of metamorphism compared to samples AZ191 and AZ193. Based on this statement, it could be supposed that the center of the Tufan Zone with the highest uplift is located between these two samples. Finally, samples of the area “E” (Eastern termination of the Tufan Zone) have smaller degree of metamorphism with the highest degree located to the north and to the south.

4.5.1. Interpretation

Most of the samples analyzed by the University of Neuchâtel and represented on figure 60 are in the diagenesis zone (IC > 0.33). In the Tahircal valley, samples AZ113, AZ111 and AZ109 show a linear diminution of the IC index that could be interpreted as an increase of the metamorphism to the south until the center of the orogen. The Pliocene sample (AZ084) in the Sudur Zone has a high IC index that could mean that Pliocene deposits were not deeply buried. In the Sahdag-Besbarmaq zone, an important IC variation of the Lower and Upper Cretaceous samples (AZ079, AZ098, AZ102 and AZ103) inside the diagenesis zone and at the top of the anchizone could mean that they have a detrital origin. Finally the AZ095 sample of the Tufan zone has a low IC index (0.28) and does not contain Smectite and Kaolinite, so this sample possibly reached the Anchizone during its evolution.

Samples analyzed by TOTAL in the CSTJF of Pau (France) show clearly an increase of metamorphism to-

wards the center of the Tufan Zone. Based on this statement, the sampled area with the highest degree of metamorphism should be the Qudiyalcay Valley south of Xinaliq. The step between the illite crystallinity index on figure 62 between area "A" and areas "B"-"C" could be explained by the presence of a normal fault based on the fact that the central part that was more exhumed and corresponds to the footwall of the fault. This statement is corroborated by fission-tracks analysis.

All these assumptions are based on few samples and must be supported by new ones. However these first results can be already correlated with other methods applied in this chapter and are promising for future studies.

4.6. SUBSIDENCE CURVES ANALYSIS AND INTERPRETATION

The subsidence curve of the Tahircal - Sudur zones (fig. Figure 63) can be divided into four main phases: (1) a subsidence followed by an uplift during Lower and Middle Jurassic (events A and B); (2) a subsidence until the Aptian followed by a non-subsiding period

Table 9 : Illite Crystallinity analyses results made by the University of Neuchâtel (Switzerland) with: Lithological ages: J_2a: Aalenian, K_1: Lower Cretaceous, K_1br: Barremian, K_2: Upper Cretaceous, N_2: Pliocene : Sample-location: Altitude in meter above sea-level (Alt), Latitude (Lat) and Longitude (Long) in UTM coordinates (WGS 84); Sample fraction; M001: first mica peak; IC: Illite Crystallinity Index; IS: interstratified content; SM001: smectite content; M001; mica content; K001:Kaolinite content; C001: Chlorite content; Sample Met Zone : DIA : diagenetic zone, ANZ: Anchizone, DET: detritic, ND: not determined (M001 < 150 cps). Detailed values in appendix 2.2 Corresponding organic matter results in appendix A2.5.

Sample	Litho age	Lat WGS 84 [deg]	Long	Alt. [m]	Sample fraction	M001 [cps]	IC [°Δ2θCuKα]	IS [%]	SM001 [%]	M001 [%]	K001 [%]	C002 [%]	Type
AZ079	K_2	41.22722	48.15077	3470 m	<2µm	249.25	0.61	5.25	30.01	64.74	0.00	0.00	DIA
AZ081	K_1br	41.19564	48.21297	1980 m	<2µm	173.28	0.22	0.00	0.00	61.10	14.97	23.93	DET
AZ084*	N_2	41.33986	48.15618	1200 m	<2µm	664.78	1.11	4.84	25.37	33.84	18.29	17.66	DIA
AZ089*	J_2a	41.23285	48.06897	3080 m	<2µm	136.1	0.37	0.00	0.00	26.72	53.28	20.00	ND
AZ091*	J_2a	41.23344	47.90098	3947 m	<2µm	166.15	0.35	0.00	0.00	20.81	0.00	79.19	DIA
AZ092*	J_2a	41.23085	47.90223	3805 m	<2µm	104.53	0.22	0.00	0.00	19.93	0.00	80.07	ND
AZ093*	J_2a	41.22879	47.90676	3629 m	<2µm	103.13	0.41	3.43	0.00	19.66	0.00	76.91	ND
AZ094	J_2a	41.22662	47.91110	3477 m	<2µm	63.88	0.41	0.00	0.00	57.44	42.56	0.00	ND
AZ095	J_2a	41.22428	47.92861	2834 m	<2µm	325.48	0.28	2.02	0.00	36.49	0.00	61.50	ANZ
AZ098	K_1	41.27227	48.05244	3200 m	<2µm	181.1	0.37	0.00	0.00	100.00	0.00	0.00	DET
AZ101	K_2	41.27506	48.03913	3324 m	<2µm	172.97	0.33	0.00	47.44	36.02	0.00	16.54	DIA
AZ102	K_2	41.27478	48.03881	3332 m	<2µm	280.55	0.98	20.20	16.44	63.37	0.00	0.00	DIA
AZ103	K_2	41.27437	48.03613	3411 m	<2µm	203.63	0.63	11.61	0.00	66.59	0.00	21.80	DIA
AZ105	K_2	41.27272	48.03405	3450 m	<2µm	116.67	0.41	4.43	43.84	51.73	0.00	0.00	ND
AZ107	J_2a	41.42188	48.06016	1048 m	<2µm	117	0.17	0.00	4.36	18.22	61.24	16.18	ND
AZ108	J_2a	41.43102	48.06640	963 m	<2µm	284.28	0.18	3.98	0.00	30.54	49.79	15.69	DET
AZ109*	J_2a	41.43801	48.07161	954 m	<2µm	151.03	0.39	0.00	0.00	19.50	77.53	2.97	DIA
AZ110	J_2a	41.44228	48.07692	862 m	<2µm	163.73	0.31	2.31	0.00	14.53	57.40	25.77	DET
AZ111	J_2a	41.45288	48.08581	807 m	<2µm	160.72	0.52	8.30	0.00	47.62	17.49	26.59	DIA
AZ112	J_2a	41.46963	48.09452	735 m	<2µm	296.15	0.97	2.51	0.00	17.72	53.44	26.32	DIA
AZ113	J_2a	41.47114	48.09556	725 m	<2µm	175.6	0.59	0.00	0.00	26.70	29.10	44.20	DIA
AZ114	J_2a	41.47814	48.09918	700 m	<2µm	89.33	0.13	0.00	0.00	11.53	72.71	15.75	ND
AZ115	J_2a	41.48418	48.10333	668 m	<2µm	65.48	0.35	0.00	0.00	16.79	64.18	19.03	ND

Table 10: Illite Crystallinity analyses results made by the Centre Scientifique et Technique Jean-Féger (CSTJF) of the Total Company in Pau (France) with: Lithological ages: J_2a: Aalenian; Sample-location: Altitude in meter above sea-level (Alt), Latitude (Lat) and Longitude (Long) in UTM coordinates (WGS 84); IC: illite crystallinity index. No content analyses were made. Detailed values in appendix 2.1 Corresponding organic matter results in appendix A2.4.

Sample	Litho age	Lat WGS 84 [deg]	Long	Alt [m]	IC [°Δ2θCuKα]
AZ159	J_2a	41.14913	48.06697	2224 m	0.49
AZ161	J_2a	41.16219	48.08878	2074 m	0.56
AZ163	J_2a	41.14270	48.11435	3313 m	0.78
AZ165	J_2a	41.14504	48.12237	3063 m	0.83
AZ167	J_2a	41.14738	48.12361	2877 m	0.88
AZ169	J_2a	41.15259	48.12288	2641 m	0.83
AZ171	J_2a	41.16120	48.12101	2200 m	0.80
AZ173	J_2a	41.16308	48.12174	2141 m	0.83
AZ175	J_2a	41.20128	48.12609	2761 m	1.62
AZ176	J_2a	41.19646	48.12750	2547 m	1.60
AZ177	J_2a	41.19200	48.12932	2398 m	1.67

Sample	Litho age	Lat WGS 84 [deg]	Long	Alt [m]	IC [°Δ2θCuKα]
AZ180	J_2a	41.18380	48.12786	2212 m	1.34
AZ182	J_2a	41.20677	48.07617	2450 m	1.48
AZ184	J_2a	41.19199	48.09864	2186 m	1.51
AZ186	J_2a	41.18495	48.11352	2067 m	1.33
AZ191	J_2a	41.14105	48.21865	1826 m	1.34
AZ193	J_2a	41.10332	48.19262	2000 m	1.01
AZ195	J_2a	41.11791	48.20382	1893 m	0.66
AZ199	J_2a	41.02836	48.53844	1384 m	1.25
AZ201	J_2a	41.05013	48.55832	1314 m	1.34
AZ203	J_2a	41.04628	48.55383	1293 m	2.17
AZ205	J_2a	41.04073	48.54726	1321 m	1.66

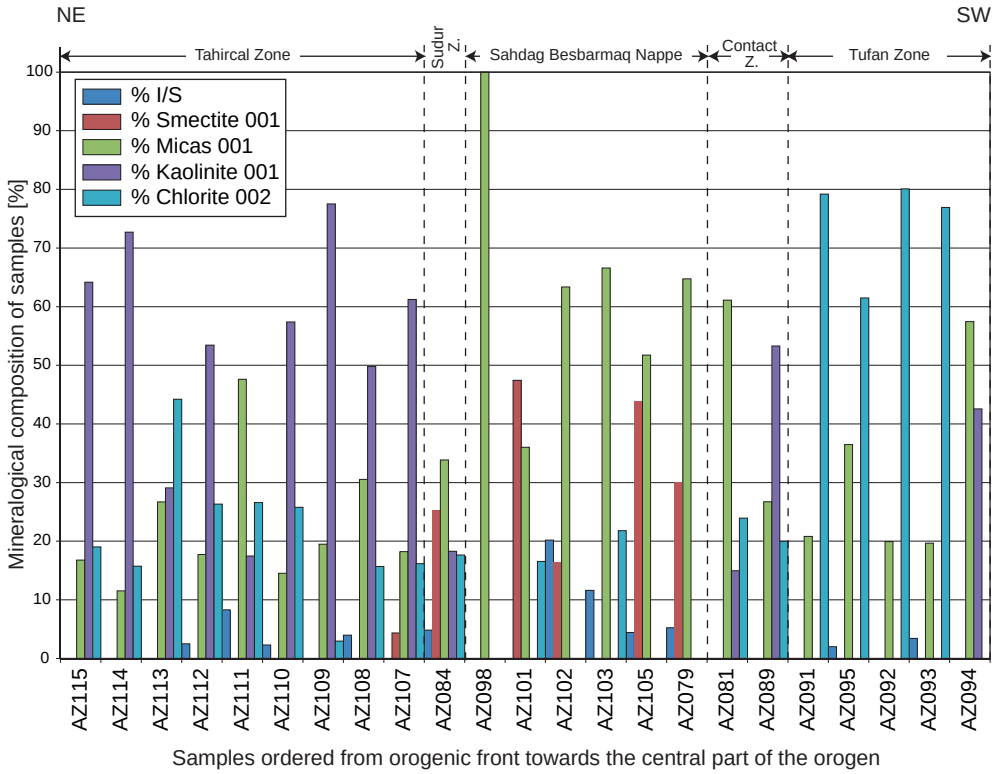

Figure 59: Mineralogical composition of the samples versus the distance away from the northern orogenic front (Samur River) to-wards the central part of the orogen. Respective structural zones are indicated on the top of the graph.

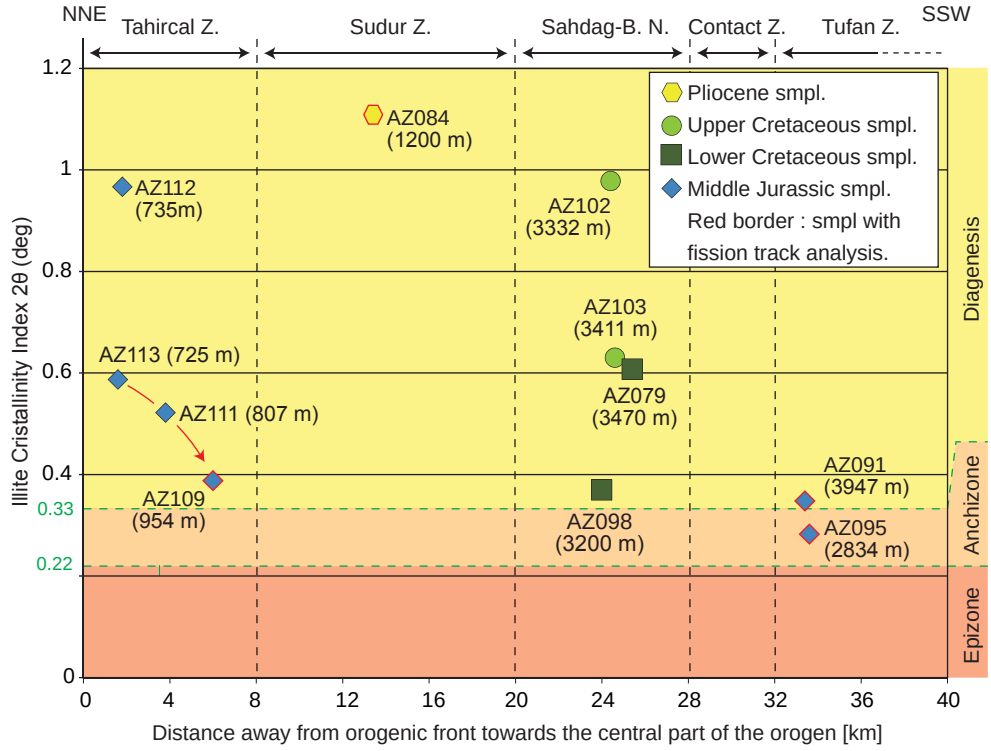

Figure 60: Illite Crystallinity In-dexes for samples analyzed in the University of Neuchâ-tel (Switzerland, 2007) ver-sus the distance away from the northern orogenic front (Samur River) towards the central part of the orogen. Samples are also divided by structural zones.

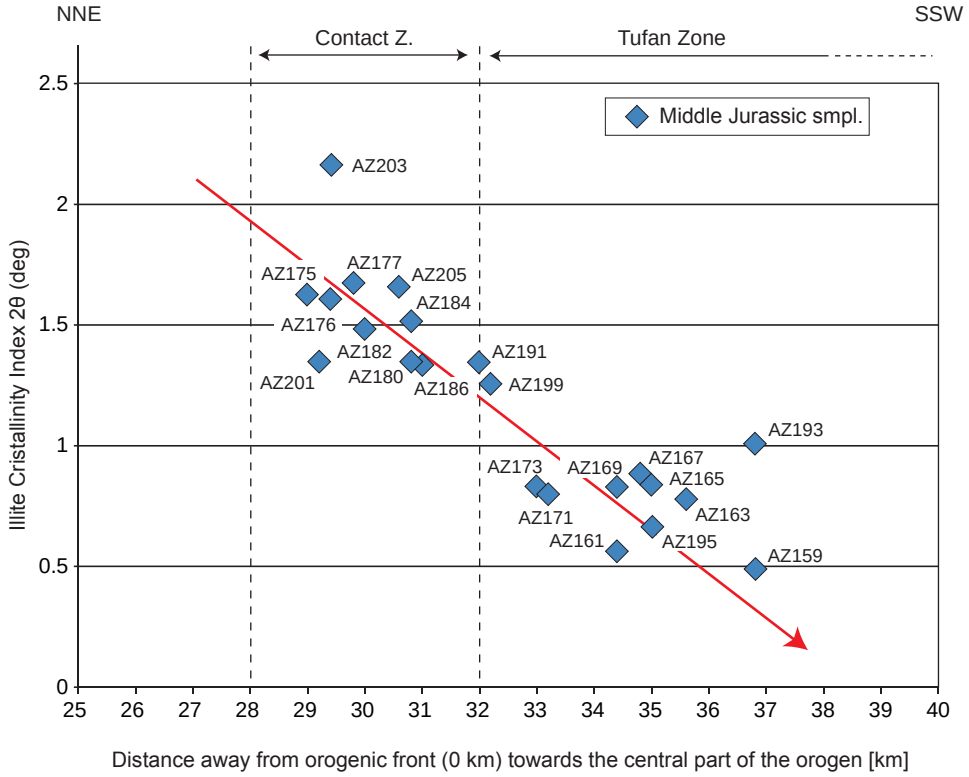

Figure 61: Illite Crystallinity Indexes for samples analysed by the CSTJF (Pau, France) versus the distance away from northern orogenic front (Samur River) towards the central part of the orogen. (Pau, France, 2008). Samples are also divided by structural zones. The red arrow indicates the increase of metamorphism. All samples are of Aalenian Age.

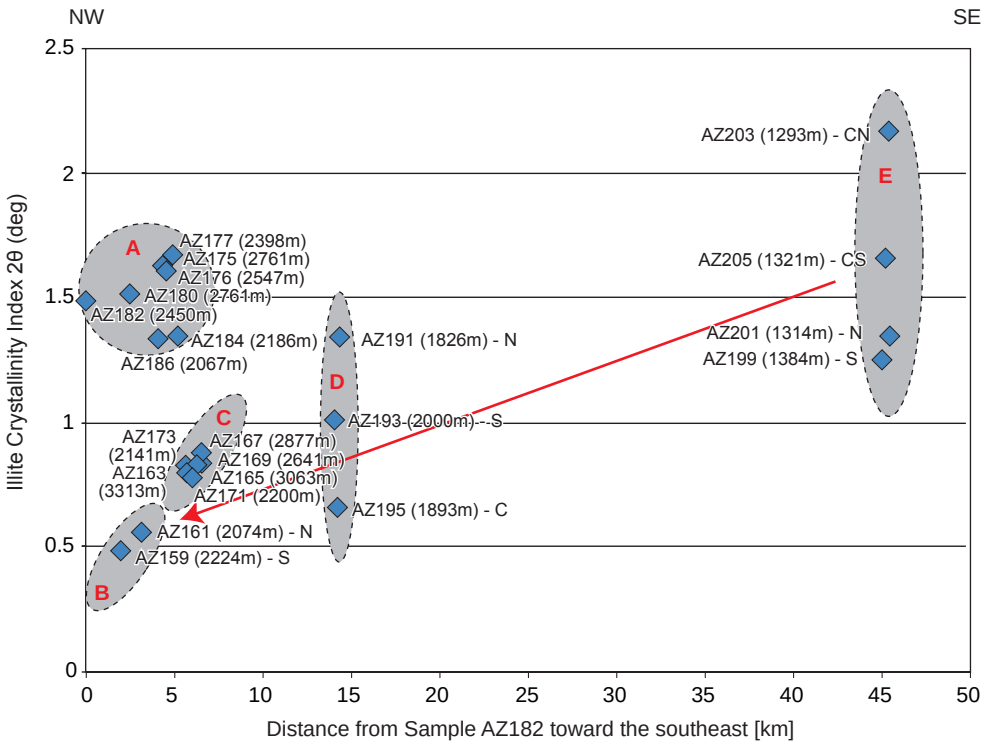

Figure 62: Illite Crystallinity Indexes for samples analysed by the CSTJF (Pau, France) versus the distance away from sample AZ182 towards the south-east Samples are also grouped by location: A: N of Xinaliq; B: Qudiyalcay Valley, S of Xinaliq; C: northern slope of Xinaliqdag Mt.; D: Cek Valley; E: Cimicay Valley. Anchizone limits are not represented because they were not given by the laboratory. The red arrow: increasing direction of metamorphism. Suffix: N = north, S = south, C=center, CN = center - north, CS = center-south.

from Upper Jurassic to the end of the Eocene (interval B to E); (3) a subsidence and a uplift of a basin from the Middle Eocene to the Middle Miocene (event E), this event is deduced from the lithology variation; (4) a fast erosion of the sediments deposited on Aalenian deposits. These Aalenian sediments outcrop in the Tahircal River and the estimated remnant thickness given by the burial curve is about 1100 m.

The subsidence curve of the Sahdag-Xizi Zone underwent 6 main events (fig. 64): (1) a subsidence phase (A) that ended during the Middle Jurassic; (2) an uplift at the end of the Middle Jurassic with some erosion (interval A to B); (3) a subsidence phase followed by an uplift from the Upper Jurassic until the beginning of the Berriasian Age (interval B-C); from Valanginian to the end of Lower Cretaceous, the area underwent a subsidence, a non-deposing period and finally an uplift (C-D); (4) afterwards, from the beginning of the Upper Cretaceous to Middle Miocene (interval D-E), (5) the area subsided slowly during ~40 Myr to finally stay quiet until the end of the Oligocene (25 Myr); (6) the next period is a little bit more active but no significant event happened. We finally reach the present with an almost complete sediments column of ~5000 m (burial curve). No recent erosion affected this area although they were uplifted at an altitude of more than 2200 m.

4.6.1. Interpretation

The first two phases A and B (subsidence followed by an erosive phase) are common to both curves and can be interpreted as the filling of the GCB followed by an uplift. This uplift phase could be possibly related to a compressive Mid-Cimmerian event. Apparently the northern Tahircal-Sudur zones were more affected than the southern Sahdag-Xizi Zones. Ershov et al. (2003) relate the uplift phase to an underthrusting of the northern slope of the GCB.

An intermediate uplift event between 150 and 140 Myr affected only the Sahdag-Xizi Zone. The period could correspond to an oceanic aperture in the SCB and the area could correspond to the breakaway from a passive margin that underwent an uplift due to a thermal rebound. (Brunet et al. 2009a)

From the end of the Valanginian, an almost non-depositing period started. In the Tahircal-Sudur zones, it lasted until the Eocene. This long term subsidence could correspond to a long term cooling of the basement. In the Sahdag-Xizi zone, this non-depositing period was interrupted by an intermediate event at the end of the Lower Cretaceous that postdates the setting up of the Sahdag-Besbarmaq Nappe and eroded valleys in it. This erosion phase is followed by a subsiding phase that allowed the continuous deposits of Upper Cretaceous deposits.

Since the Eocene-Oligocene, both area were affected by minor subsiding events. The period corresponds to the building of the Greater Caucasus. Based on sediment records, we suppose that a basin was created in the Tahircal and Sudur zones. It can correspond to a northern foreland basin linked filled with the erosive products of the young Greater Caucasus (Maykop basin). It is described in detail by Ershov et al. (1999) and Ershov et al. (2003). A non-significant subsiding phase started a little bit later in the Sahdag-Xizi Zone.

The late erosive phase of the Tahircal-Sudur Zone could be linked to a fast uplift of the area with high erosion rate corresponding to the main collisional phase of the Greater Caucasus that started in Middle Miocene (about 15 Myr). The Sahdag-Xizi Zone was also affected by this uplift, but the sediments were not eroded. An explanation could be that they were trapped and conserved in a closed paleo-valley (the Buduq Through).

4.7. General discussion and conclusion

Combined informations from literature and field observation suggest surface uplift rates between 0.1 to 10 mm/yr in the EGC. However, field evidences show an average surface uplift of 0.31 mm/yr since the Middle Miocene (Sarmatian age) with an acceleration of 0.77 mm/yr since the Pliocene (Akchagyl regiostage).

AFT t-T models validate a fast burial during the Middle Jurassic – Lower Cretaceous period followed by a quiet period in the Tufan Zone and exhumation-burial period (Upper Cretaceous – Paleogene) in the north. Finally all areas are affected by a fast exhumation since the Miocene: we determined that the exhumation was certainly slower and longer in the high Tufan Zone than in the northern and topographically lower Tahircal Zone. In the Tufan Zone, the exhumation started earlier (~40 Myr) than in the Tahircal Zone where it started after 20 Myr with an acceleration since the Pliocene.

The presence of a contact between the Tufan Zone and the Sahdag-Xizi Zone is obvious from the age difference between both zones but almost no direct evidence for a fault or a transgressive contact is visible in the field. The presence of gaz seepages and also geomorphologic indicator corroborate the existence of a fault. This is further confirmed by results from our AFT study. Thus, the AFT central age on both side of the fault zone are completely different and show clearly that the central part is younger in terms of central age than the Sahdag-Xizi Zone. The fault has a normal movement and dips to the north. The Tufan Zone with youngest AFT central ages cor-

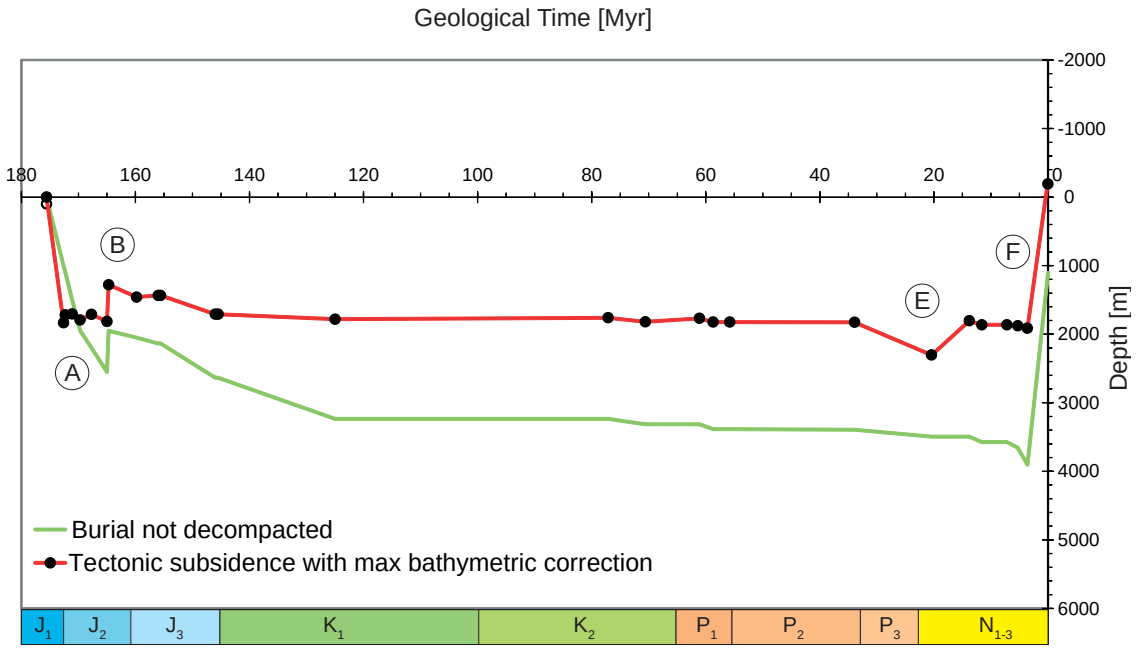

Figure 63: Subsidence curves for the Tahircal-Sudur zones. Letters A to F represent the different events described in text. Corresponding geological epochs are shown between curves: J_1: Lower Jurassic; J_2: Middle Jurassic; J_3: Upper Jurassic; K_1: Lower Cretaceous; K_2: Middle Cretaceous; P_1: Paleocene; P_2: Eocene; P_3: Oligocene; N_{1-3}: Miocene – Pliocene – Quaternary.

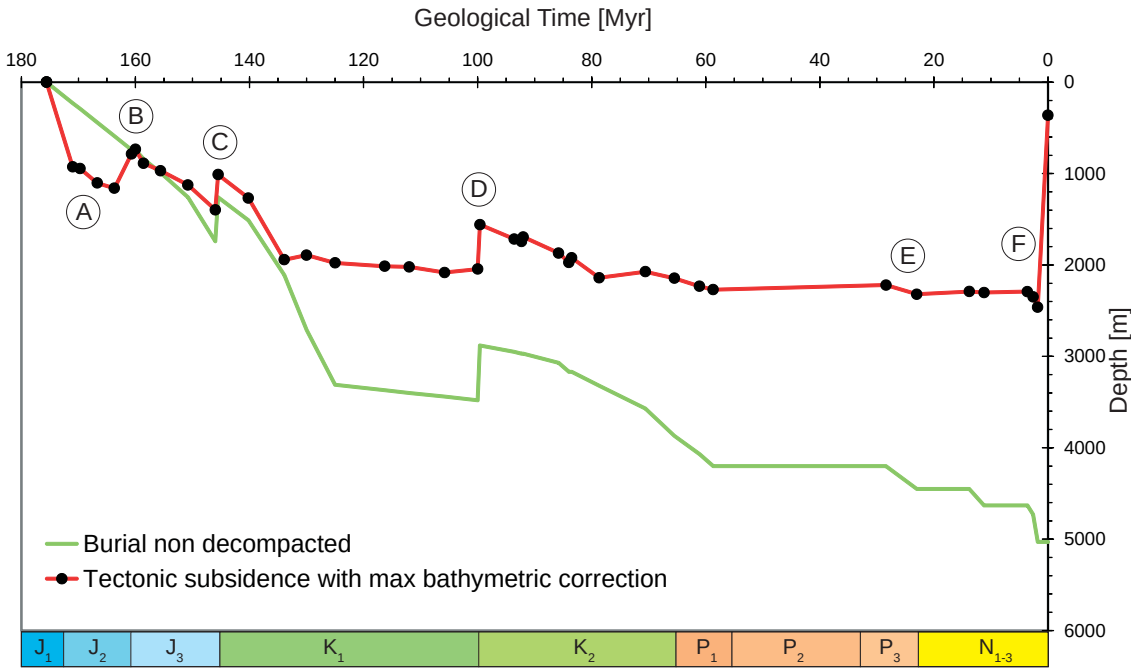

Figure 64: Subsidence curves for the Sahdag-Xizi Zone. Letters A to F represent the different events described in text. Corresponding geological epochs are shown between curves: J_1: Lower Jurassic; J_2: Middle Jurassic; J_3: Upper Jurassic; K_1: Lower Cretaceous; K_2: Middle Cretaceous; P_1: Paleocene; P_2: Eocene; P_3: Oligocene; N_{1-3}: Miocene – Pliocene – Quaternary.

responds to the footwall and was uplifted relatively to the Sahdag-Xizi Zone (hanging wall of the normal fault) that has the oldest AFT central ages. From these AFT data, no uplift rates on both sides of the fault can be deduced due to their high age dispersion and the few samples available.

Based on the determined AFT age, the Pliocene conglomerates were not reset and their AFT ages are inherited. Consequently, the source of pebbles composing Pliocene conglomerate have been determined based on AFT analysis. As the inherited central AFT ages of pebbles correspond to the age of sediments that outcrop nowadays directly south of the analysed samples, it means that, in Pliocene times, the pebbles were eroded from outcrops that were exhumed earlier and, based on the fact that the uplift is propagating southeastward, they were located to the west-northwest of the present conglomerates outcrop.

The Illite Crystallinity Index method shows an increase of metamorphism from the northern orogenic front (Samur River) towards the SSW perpendicularly to the orogen axis until the central part (Tufan Zone) but a decrease from the Bazarduzu to the ESE (Cimicay River) along the orogen axis. Topographically the higher samples have generally a lower metamorphism than the lower ones. The highest sample AZ091 with an altitude of 3947 m has almost the same crystallinity index as the AZ109 in the Tahircal Zone located at an altitude of 954 m. This observation probably indicates that the sedimentary cover was not thick on the Tufan Zone.

The 2 subsidence curves of the Sahdag-Xizi and Tahircal-Sudur zones are compatible with the sedimentary record and the evolution of the area but also with the AFT modelling. They can also be correlated with previous studies of bordering area made by Ershov et al. (1999; 2003). In the meantime, the Sahdag-Xizi Zone was submitted to an erosional event in the middle of the Cretaceous that could be linked to the setting up of the Sahdag-Besbarmaq Nappe.

In this study, we tested the AFT and Illite Crystallinity methods to see if they are applicable in the EGC. Although the studied zones were not the most favourable and the number of samples was small, all results are conclusive and indicate that the deep valleys of the Tufan Zone within Middle Jurassic deposits are certainly favorable for both Apatite Fission-Tracks and IC analyses.

*****

5- Cenozoic-Recent Tectonics and Uplift in the Greater Caucasus: a perspective from Azerbaijan

Published in : ***Sedimentary Basin Tectonics from the Black Sea and Caucasus to the Arabian Plateform*****. 2010, Geological Society, London, Special Publications, 340, p. 261-180.**

Jon Mosar[1‡], Talat Kangarli[2], Martin Bochud[1], Ulrich A. Glasmacher[3], Annick Rast[1], Marie-Françoise Brunet[4] & Marc Sosson[5]

[1]Earth Sciences, Department of Geosciences, University of Fribourg, Chemin du Musée 8, 1700 Fribourg, Switzerland
[2]Geological Institute of Azerbaijan (GIA), National Academy of Sciences, 29A H. Javid Av., Baku, AZ1143, Azerbaijan
[3]Institute of Earth Sciences, Im Neuenheimer Feld 234, 69120 Heidelberg, Germany
[4]UPMC Univ. Paris 06 – CNRS – INSU, UMR Institut des Sciences de la Terre, Paris Case 129, 4 Place Jussieu, 75005 Paris, France
[5]CNRS – GeoSciences Azur, UMR 6526, 250 Rue Albert Einstein – Sophia Antipolis, 06560 Valbonne, France
[‡]Corresponding author (email): jon.mosar@unifr.ch

Abstract

The Greater Caucasus is Europe's highest mountain belt and results from the inversion of the Greater Caucasus back-arc-type basin due to the collision of Arabia and Eurasia. The orogenic processes that led to the present mountain chain started in early Tertiary, accelerated during the Plio-Pleistocene, and are still active as shown from present GPS studies and earthquake distribution. The Greater Caucasus is a doubly verging fold-and-thrust belt, with a pro- and a retro wedge actively propagating into the foreland sedimentary basin of the Kura to the S and the Terek to the N, respectively. Based on tectonic geomorphology - active and abandoned thrust fronts - the mountain range can be subdivided into several zones with different uplift amounts and rates with very heterogeneous strain partitioning. The central part of the mountain range - defined by the Main Caucasus Thrust to the S and back-thrusts to the N - forms a triangular-shape zone showing the highest uplift and fastest rates, and is due to thrusting over a steep tectonic ramp system at depth. The meridional orogenic in front of the Greater Caucasus in Azerbaijan lies at the foothills of the Lesser Caucasus, to the south of the Kura foreland basin.

Keywords: *Greater Caucasus, tectonics, uplift, topography, seismicity*

5.1. Introduction

The Caucasus orogen lies at Europe's cross-road with Asia and Arabia, and is one of the world's outstanding mountain ranges (fig. 65). It is Europe's highest mountain range with Mt. Elbrus culminating at 5642 m a.s.l. in the western Greater Caucasus. It consists of the Greater Caucasus (GC), intermontane basins (Kura-Kartli-Rioni; ~ 200 m elevation) and the Lesser Caucasus. North of the Greater Caucasus the deep sedimentary Terek and Kuban foreland basin (> 6000 m thick; up to 1,600 m elevation) form the transition to the Scythian platform. NNW of Mount Elbrus, the Stavropol "high" forms a basement uplift, and in the east the northern slope is formed by the Dagestan foreland fold-and-thrust belt. The southern Greater Caucasus foreland, SW of Tbilisi is one of the world's earliest sites of human society with 1.8 Myr old hominoid remains of Dmanisi (Georgia) (Lordkipanidze et al. 2007). The Lesser Caucasus with lower topography (~ 3000 m), is a zone of important volcanic and seismic activity. In the east and west, the Caucasus topography is bound by two very deep sedimentary basins, the South Caspian Sea and the Black Sea, hosting some of the world's largest oil and gas provinces.

The Caucasus orogen is caused by the north directed movement of the Arabian plate squeezing a Jurassic to Early Palaeogene subduction related volcanic arc (Lesser Caucasus) as well as Jurassic to Pliocene marine sedimentary rocks and sediments (northern Lesser Caucasus, substratum of Kura-Kartli Basins and Greater Caucasus Basin) towards the Scythian plate (Gamkrelidze 1986; Hafkenscheid et al. 2006; Kazmin & Tikhonova 2006; Nikishin et al. 2001; Popov et al. 2004; Sosson et al. 2010c; Stampfli et al. 2001). Recent plate tectonic models and GPS based convergence rates (Gamkrelidze & Kuloshvili 1998; Kadirov et al. 2008; Reilinger et al. 2006; Vernant et al. 2004) suggest a moderate anticlockwise rotational component of convergence, and a complex plate boundary with vertical and horizontal strain partitioning (Jackson 1992). Recent convergence rates of up to 14 mm/a, strong earthquakes, landslides, active volcanoes, and extreme subsidence and surface uplift rates are indicative for the dynamics of the continent-continent collision. From E to W, the morphological shape and the structural features are strongly influenced by the rotational convergence of the Arabian plate and westward escape of the Anatolian Plate causing distinct tectonic regimes in the Caucasus. The Lesser Caucasus area is dominated at present by a strike-slip regime, whereas the Greater Caucasus is dominated by thrust tectonics with a main NNE-SSW direction of movement. The dominant movement is top to the south in the main range and the southern slopes. Top to the north motion is observed in the areas in the north and in Dagestan.

Hereafter we will present different aspects of Tertiary and recent tectonics, and tectonic geomorphology, especially based on detailed structural studies carried over several years in the eastern Greater Caucasus in Azerbaijan. We shall discuss their relevance for understanding the thrust kinematics and the links between tectonics, topography, seismicity and uplift in the Greater Caucasus.

5.2. Regional Tectonics and Geodynamics

The geodynamics of the Greater Caucasus orogen corresponds to an intercontinental collision zone inverting a deep Mesozoic-Tertiary basin (fig. 66) that is not located above a subduction regime, but bordered E and W by super deep sedimentary basins that have their origin in the Mesozoic and are filled with Cenozoic-Quaternary sediments. To the north and south of the Greater Caucasus are the foreland basins of the Terek-Kuban and the Kura-Khakheti-Kartli-Rioni, respectively (Daukeev et al. 2002; Ershov et al. 1999; Ershov et al. 2003; Mikhailov et al. 1999; Ulminshek 2001); to the east and west are the Caspian Sea and the Black Sea, respectively (Abrams & Narimanov 1997; Berberian 1983; Brunet et al. 2003; Ismail-Zade et al. 1987; Mangino & Priestley 1998; Narimanov 1992; Nikishin et al. 1998b; Nikishin et al. 2003; Shikalibeily & Grigoriants 1980). The Lesser Caucasus is situated above an old possibly detached subduction slab (Hafkenscheid et al. 2006). An incipient subduction is believed to occur at the northern edges of the Black Sea, whereas in the east the subduction process already initiated in Pliocene times, when the South Caspian Basin started subducting to the north under the eastern termination of the GC and the Abseron Ridge (Allen et al. 2002; Knapp et al. 2004). The detailed link of the incipient subduction to the structures such as the Main Caucasus Thrust (MCT) in the Greater Caucasus remains to be investigated. The depth of the Moho changes from about 40 km beneath the Kura basin to more than 50 km beneath the eastern Greater Caucasus and rises to 40 km again under the northern foreland basin (Brunet et al. 2003; Ershov et al. 2003).

The Greater Caucasus is a doubly verging mountain-belt (fig. 66) with two external fold-and-thrust belts (FTB) and a complex nascent axial zone (Khain 1997; Sholpo 1993). The main tectonic underthrusting appears to be towards the north - similarly as the subduction sense in the Lesser Caucasus - creating an overall asymmetry of the mountain range. The southward propagating meridional foreland FTB together with a large part of the axial zone form the pro-wedge (front) of the orogen (Adamia et al. 1981; Gamkrelidze

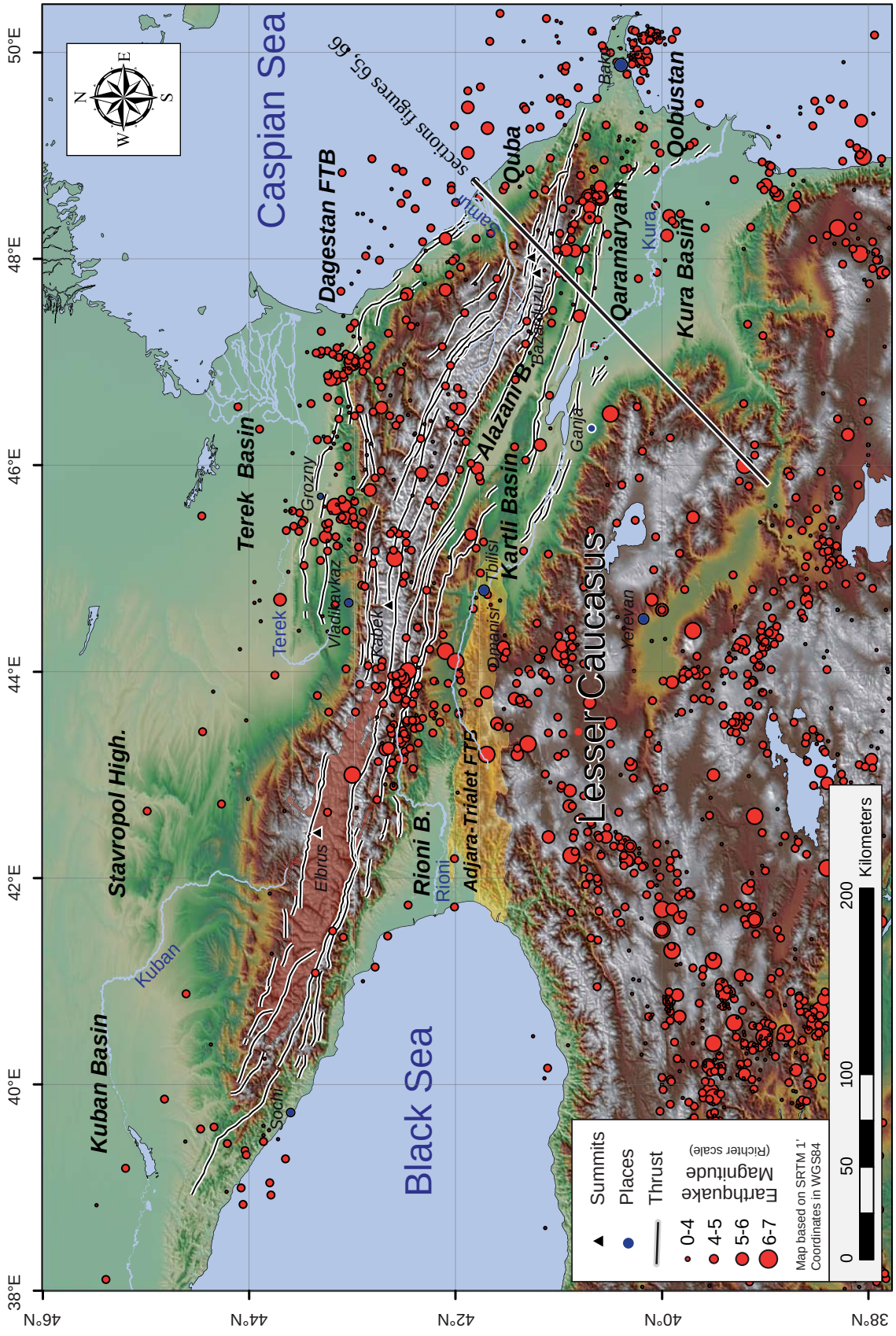

Figure 65: General map of the larger Caucasus area with topography and earthquake distribution. Not all existing thrusts are shown only a selection of the major thrusts of the Greater Caucasus relevant for the discussion. Transparent red indicates the pre-Mesozoic core. Yellow highlighted area is the Adjara-Trialet fold-and-thrust-belt.

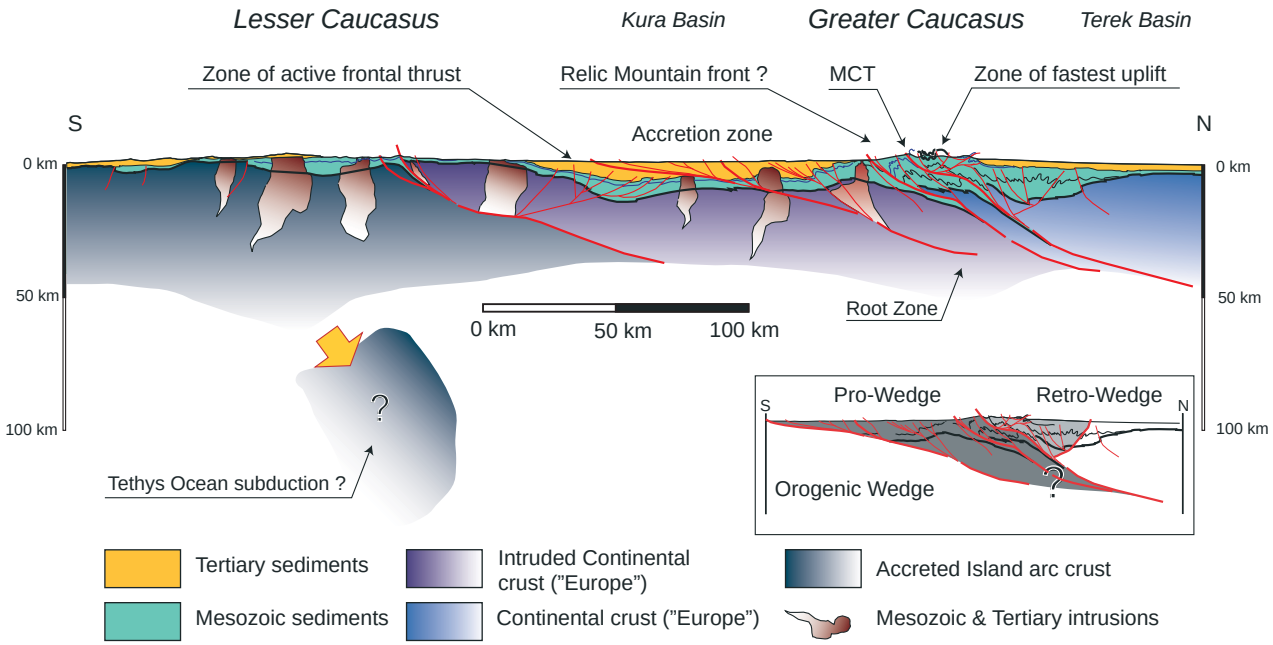

Figure 66: General crustal-scale cross-section through the eastern Greater Caucasus and the Lesser Caucasus (location see fig. 65). The Lesser Caucasus is associated with a northward subduction and possibly a detached slab (based on tomography after HAFKENSCHEID et al. (2006). No subduction is seen under the Greater Caucasus. The Greater Caucasus is a doubly verging orogenic wedge with the dominant thrusting towards the pro-wedge to the south. A retro - foreland fold and thrust belt develops to the north in Dagestan (Russia) see also figure 65. Three different types of crust have been distinguished according to their geodynamic belonging: to the south a crust intruded and associated with the Jurassic-Cretaceous supra-subduction arc volcanism in the Lesser Caucasus, in the centre the thinned and rifted and intruded southern part of the supra-subduction back-arc basin, and to the north the northern part of this extended back-arc rift system with the important Mesozoic sedimentary series of the Greater Caucasus Basin. Some major faults such as the Main Caucasus Thrust (MCT) are highlighted. The structure and the position of the thrusts at depth remains speculative, but indicate underthrusting of the terranes to the south of the Greater Caucasus and strong imbrication over a ramp system in the Greater Caucasus.

1986; GAMKRELIDZE 1997; GAMKRELIDZE & SHENGELIA 2005; KHAIN 1975). The Kura-Kartli and also the Rioni foreland basins are dissected by and incorporated into the outward propagating foreland FTB to the south of the main range. Deep seated southward migration of the orogenic front led to the inversion of the Pliocene to Late Pleistocene sediments, and the transport of the Alazani basin (figs. 65 and 72) as a piggy back basin towards the south.

Unlike in the western Greater Caucasus, a broad north-directed foreland FTB develops in the Northeast, in Dagestan and is part of the retro-wedge of the orogen (DJAVADOVA & MAMULA 1999; DOTDUYEV 1986; KOPP & SHCHERBA 1985; SOBORNOV 1994; SOBORNOV 1996; ZONENSHAIN et al. 1990). The Terek basin subsided since the early Pliocene more than 4,000 m, and recently exhibits pitted gravels of Early Pliocene age at 1,600 m elevation. This northern FTB, similarly to the southern FTB, propagates into the Tertiary-Quaternary series of the Terek Basin in the Dagestan area (fig. 66).

Whereas the axial zone of the Greater Caucasus comprises Jurassic sedimentary rocks (Azerbaijan), a pre-Mesozoic basement (Georgia, Russia), and Pliocene intrusions, both external fold-and-thrust belts consist mainly of Cretaceous and Tertiary sedimentary rocks (KHAIN 1997). The Greater Caucasus basin has developed in a back-arc setting to the southerly subduction-related volcanic arc of the Lesser Caucasus. Intrusive rocks are frequently found up into the Early Tertiary, but mainly affect the southern parts of the basin (SOSSON et al. 2010c). Volcanoclastic series derived from the Lesser Caucasus volcanic arc are now found imbricated and folded in the southern foothills of the Greater Caucasus where they form distinct tectono-sedimentary units (KANGARLI 1982; KANGARLI 2005). In situ intrusives remain however rare and are associated with igneous activity on the margins to the south of the Greater Caucasus Basin (CHALOT-PRAT et al. 2007; MENGEL et al. 1987; MUSTAFAYEV 2001).

Pliocene to Quaternary igneous activity is observed in the central part of the mountain range, in the border areas between Georgia and Russia (Chechnya). The most outstanding examples are Mount Elbrus with 5642 m a.s.l., and further east Mount Kazbek (5047m a.s.l.). These intrusions are mainly late-collisional,

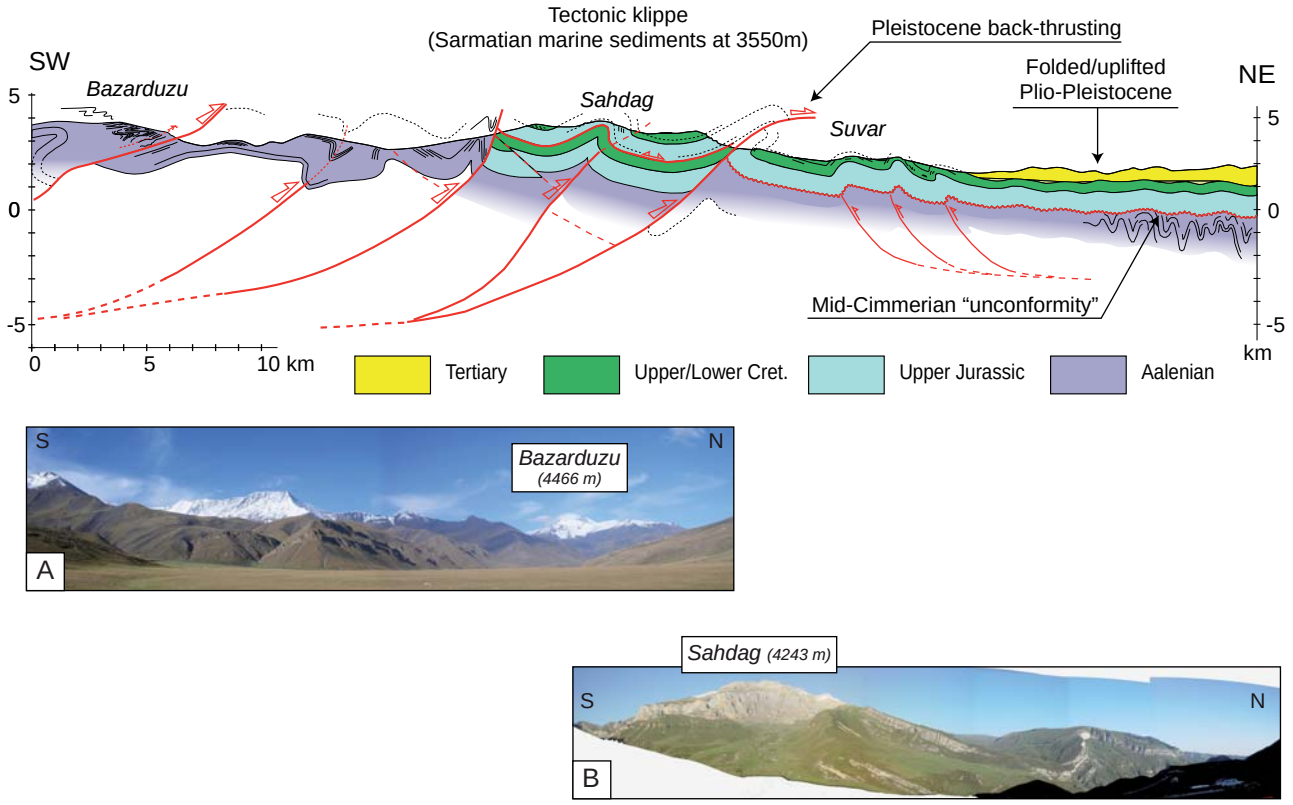

Figure 67: Cross section through the Sahdag Mountain in northeastern Azerbaijan. The section highlights the structural style at the northern edge of the mountain range. Thrusting is mainly to the north and of Plio-Pleistocene age. The Sahdag is built by a tectonic klippe that duplicates the Jurassic-Cretaceous series. The tectonic contact between the klippe and the underlying series is possibly a synsedimentary fault associated with the collapse of the carbonate platform during Cretaceous. To the north the Oxfordian overlies discordantly older folded series of the Middle to Lower Jurassic. This unconformity reflects the Mid-Cimmerian event. On the summit of the Sahdag Sarmatian rocks of marine origin document a vertical uplift of some 3550 m. Plio-Pleistocene detrital series including conglomerates are uplifted and folded (seen further east along strike the same structure). Photos: A - View to the SW from Sahnabad plain (2500 m a.s.l.) to Bazarduzu range which is the highest range in Azerbaijan culminating at more than 4000 m a.s.l. Rocks are mainly of Lower Jurassic (Aalenian) age; B - View towards the west on the Sahdag Klippe which is one of the zones of fastest uplift in the whole area. Rocks range from Cretaceous to Jurassic in age.

subalkaline granitoids that roughly range between 4.5 and 1.5 Myr (Gazis et al. 1995; Hess et al. 1993; Lebedev & Bubnov 2006; Nosova et al. 2005), and culminate with Quaternary volcanism reaching into the Holocene (Chernyshev et al. 2006; Lebedev 2005).

Several successive tectonic events are documented in the Greater Caucasus sedimentary record. Precambrian and Palaeozoic (pre-Hercynian and Hercynian) tectonic phases are recorded in the pre-Alpine basement or Palaeozoic core (for discussion and references see (Gamkrelidze & Shengelia 2005; Kazmin & Tikhonova 2006; Saintot et al. 2006a; Saintot et al. 2006b; Somin et al. 2006) and are followed by palaeotectonic events related to the Tethyan oceans (Palaeo- and Neotethys) (Barrier et al. 2008a; Nikishin et al. 1997). These palaeotectonic events included extensional structures recorded throughout the Mesozoic cover of the Greater Caucasus Basin (Dotduyev 1986), but also unconformities thought to result from compressive phases such as the "Eo-Cimmerian" (Triassic) and the "Mid-Cimmerian" (Callovian-Bajocian) which is well documented in northern Azerbaijan (fig. 67). The link of the latter unconformity to possible orogenic events remains speculative and debated.

The geometry of the Greater Caucasus sedimentary Basin is of passive margin type with numerous tilted blocks. The central part of the orogen - where the oldest series can be seen, and topography is the highest - represents a distal basin between a platform domain to the N and a distant deeper domain with a structural high (tilted block) to the S. The foreland basins associated with the orogenic evolution are filled with Tertiary and Quaternary sediments. In the south they build on top of the former distal, stretched continental margin (Greater Caucasus Basin), in the north they build on a flexural foreland underlain by a carbonate

platform (Ershov et al. 1999). During the growth of the orogen since early Tertiary the thrust front is propagating out into its own foreland basins. Especially the southern basins develop into a succession of piggy-back foreland basins, subsequently and progressively abandoned (relic thrust fronts) as the orogenic front migrates southward. A typical example of an abandoned basin is the Tertiary-Quaternary Alazani Basin (Philip et al. 1989) (figs. 65 and 72).

Distinct tectonic zones, from N to S, are separated by major thrusts (Dotduyev 1986). They correspond to the original palaeogeographic setup and build upon inherited, pre-existing (Egan et al. 2009). Lateral correlations and differences can be made between the western region in Crimea (Saintot & Angelier 2000; Saintot et al. 1998; Saintot et al. 2006a), through Georgia (Banks et al. 1997; Gamkrelidze & Gamkrelidze 1977; Gamkrelidze & Rubinstein 1974) to the Caspian Sea (Allen et al. 2003; Egan et al. 2009; Kangarli 1982; Kangarli 2005). The Adjara-Trialet FTB in Georgia located to the south of the southern limit of the Greater Caucasus in Georgia (Banks et al. 1997; Gudjabidze 2003) is of particular interest since thrusting is top to the north, opposite the direction in the GC (Gamkrelidze & Kuloshvili 1998).

One of the major structural features in the GC is the Main Caucasus Thrust (MCT) (Dotduyev 1986). This large thrust can be observed along strike of the mountain belt over a distance of more than 1000 km (figs. 70, 72 and 73). Displacement on this major thrust fault is top to the south, possibly in excess of 30 km in some places. In the west in Russia and Georgia, the MCT separates the Palaeozoic metamorphic core of the mountain range from the Jurassic cover series to the south. Further east in Georgia, Dagestan (Russia) and Azerbaijan it is found in the core of the orogen, separating rocks of different Jurassic ages. The definition of the MCT used here is according to Dotduyev (1986). Some recent papers (Kadirov et al. 2008) mistakenly label the thrust separating the Alazani Basin from the terrains in higher topographic elevations to the north as MCT. This latter thrust is believed to be a relic thrust front of early Tertiary age. In eastern Azerbaijan, east of mount Bazarduzu (the highest summit in Azerbaijan, fig. 65), we lose the trace of the MCT and fieldwork has shown that is relayed by a string of fault-related folds.

5.3. Active tectonics, Convergence and Uplift

5.3.1. Earthquakes and active faults

The Greater and Lesser Caucasus are seismically active zones linked to the rapid and non-uniform plate convergence between Arabia and Eurasia (Allen et al. 2004; Allen et al. 2006; Jackson 1992; Jackson et al. 2002; Philip et al. 1989; Priestley et al. 1994; Triep et al. 1995) (fig. 65). The Lesser Caucasus and the adjoining Anatolian Plateau show a predominance of strike-slip focal mechanisms associated with a system of vertical faults. In the Greater Caucasus, on the contrary, convergence is accommodated predominantly by reverse focal mechanisms associated to thrusting with a general N-S to NE-SW compression (Barazangi et al. 2006; Copley & Jackson 2006; Koçyigit et al. 2001; Tan & Taymaz 2006), see also discussion in Allen et al. (2004) and Jackson (1992). Slip vectors based on earthquake focal mechanisms show a general top to the south thrusting. Strike-slip mechanisms exist but are rare. Present seismicity is unevenly distributed across the GC (figs. 65, 72 and 73). A zone with a higher seismic activity is observed on the south slope of the Greater Caucasus west of Tbilisi (Georgia) in the Racha area (Triep et al. 1995). Studies of focal mechanisms and focal depths show that this seismicity is linked to several active fault strings in the subsurface of the Gagra-Dzhava zone (Gamkrelidze & Kuloshvili 1998; Triep et al. 1995). They show south directed slip vectors. These faults are located to the south and are structurally in the footwall of the MCT. To the west this fault system links to the MCT precisely where this latter shows an important bend, and is stepping back (to the north) into the mountain range (figs. 65, 72 and 73). We suggest that the MCT is developing a new splay, and that the higher seismicity in this region is due this propagation of the MCT to the SW and to a lower structural level (fig. 72). To the east this fault system may be correlated with the thrust fault at the front of the Alazani Basin. It is relevant to notice that elsewhere in the Greater Caucasus the largest earthquakes known (earthquakes > magnitude 6, both historical and measured) are all located in the vicinity of the MCT. We interpret this to show the importance of the MCT to the present day in the deformation processes, since large earthquakes occur along large faults accommodating important displacement. The MCT appears to be a major thrust in the development of the Greater Caucasus.

Seismicity is extending into the Middle and South Caspian Sea (Kovachev et al. 2006). In the Abseron zone focal mechanisms show NNE-SSW oriented thrusting (Jackson et al. 2002) and seismic activity may be linked with an extension/termination of the Greater Caucasus towards the east and/or with young north-directed subduction of the South Caspian Basin to the north under the Abseron (Allen et al. 2002; Knapp et al. 2004). The seismicity further south as well as in the Qobustan desert area shows a westward component of motion relative to Eurasia, suggesting underthrusting towards the west (Jackson et al. 2002).

Some seismic activity is also seen in the central part of the eastern Greater Caucasus, as well as in the Kura basin. On the northern slopes, the Dagestan FTB and the recent faults in the Terek Basin show a higher concentration of earthquakes pointing to active thrust tectonics in this area.

Studies on palaeoseismology remain rare but confirm the existence of inherited faults and the possible 2000 year recurrence of high magnitude events (Rogozin & Ovsyuchenko 2005; Rogozin et al. 2002).

5.3.2. Convergence and Uplift

Studies based on GPS technologies in the larger Caucasus area, including Turkey, Arabia and Iran have confirmed the global picture of convergence across the Caucasus (McClusky et al. 2000; Nilforoushan et al. 2003; Reilinger et al. 2006). The average convergence of Arabia and Eurasia of 18-23 mm/a is transformed into a deformation of 14 mm/a with a N-S direction across the Greater Caucasus, mainly the southern part (Vernant et al. 2004). Detailed studies in Azerbaijan (Kadirov et al. 2008) confirm a rotational convergence between Arabian and European plates. Shortening is distributed between the Northern Kura Basin and the outermost thrusts of the Dagestan FTB. Present-day slip rates decrease from 10 ±1 mm/a in eastern Azerbaijan to 4 ±1 mm/a in western Azerbaijan (Kadirov et al. 2008). A similar study in Georgia shows the opposite thrust directions between south-dipping thrusts in the Adjara-Trialet FTB and the Greater Caucasus front, which shows relative motion of 6.9 ±1.1 mm/a to the SW on north-dipping thrusts (Gamkrelidze & Kuloshvili 1998)These studies also show a marked change (decrease) in velocities across the MCT. Indeed north of the MCT velocities are almost 0, indicating no longitudinal displacement. All deformation appears to be taken up in uplift.

Across the more or less N-S oriented West Caspian Fault - at the transition Kura basin to Qobustan area near the eastern shores of the South Caspian Sea - a recent study indicates a dextral strike-slip motion and calculates a differential movement of 11 ±1 mm/a (Kadirov et al. 2008).

5.4. Uplift/Subsidence and Tectonics versus Topography

5.4.1. Subsidence studies

The Greater Caucasus basin was initiated by Mesozoic back-arc extension related to the subduction of the Tethys Ocean to the south (Barrier et al. 2008a; Brunet et al. 2003). A large part of the subsidence occurred during this rift-related crustal extension, prior to the subsequent Tertiary mountain building and the subsidence observed both north and south of the Greater Caucasus.

Rapid subsidence occurred there in a foreland basin setting, in different phases during the Tertiary. The north Caucasus foredeep (Kuban and Terek basins mainly) can be described in three major periods: Early Jurassic to Late Cretaceous related to initial rifting then cooling followed by a Late Cretaceous to Middle Eocene phase of alternating subsidence and uplift as a far field effect of the suturing of the Tethys Ocean to the south (Mikhailov et al. 1999). The period of Late Eocene to present relates to the development of a foreland basin coeval with shortening and uplift in the adjacent Greater Caucasus range. In the Black Sea and South Caspian basins (Brunet et al. 2003), the much more rapid Pliocene-Quaternary phase of sedimentary infill as well as subduction related subsidence in the north of South Caspian (Egan et al. 2009) occurred simultaneously with the asymmetrical subsidence of Caucasus-related molasse basins to the north and south (Ershov et al. 1999; Ershov et al. 2003). A crustal/lithospheric - scale model suggests that crustal thickening and removal of lithospheric roots are responsible for supporting the Caucasus Mountains. Subsidence is explained by loading of the lithospheric roots (Ershov et al. 1999). The Eocene - Early Oligocene phase of subsidence is associated with cessation of subduction in the southern areas of the Lesser Caucasus, while the rapid Middle Miocene to Present subsidence is linked to the final closure and inversion of the Greater Caucasus Basin.

5.4.2. Uplift-Exhumation

The Caucasus offers numerous geomorphic field lab conditions to apply classic methods such as terrace deposits studies or “young” marine sediment age/altitude studies, palaeogeography and palaeoclimate/environment, and more modern ones such as fission-track studies on apatite or zircon.

Geomorphologic research (Mitchell & Westaway 1999), and minor thermochronological investigations show a very young heterogeneous rock and surface uplift in the Greater Caucasus. A study on pre-alpine basement rocks shows ages based on apatite fission-track studies younger than 68 Myr in agreement with the general idea of an uplift that initiated in the Tertiary (Kral & Gurbanov 1996). Patterns of age distributions also indicate uplift of 7-4 Myr in some areas, suggesting a strong influence of recent tectonics in the process of exhumation/uplift. Studies on cooling history of recent granites in the western central Greater

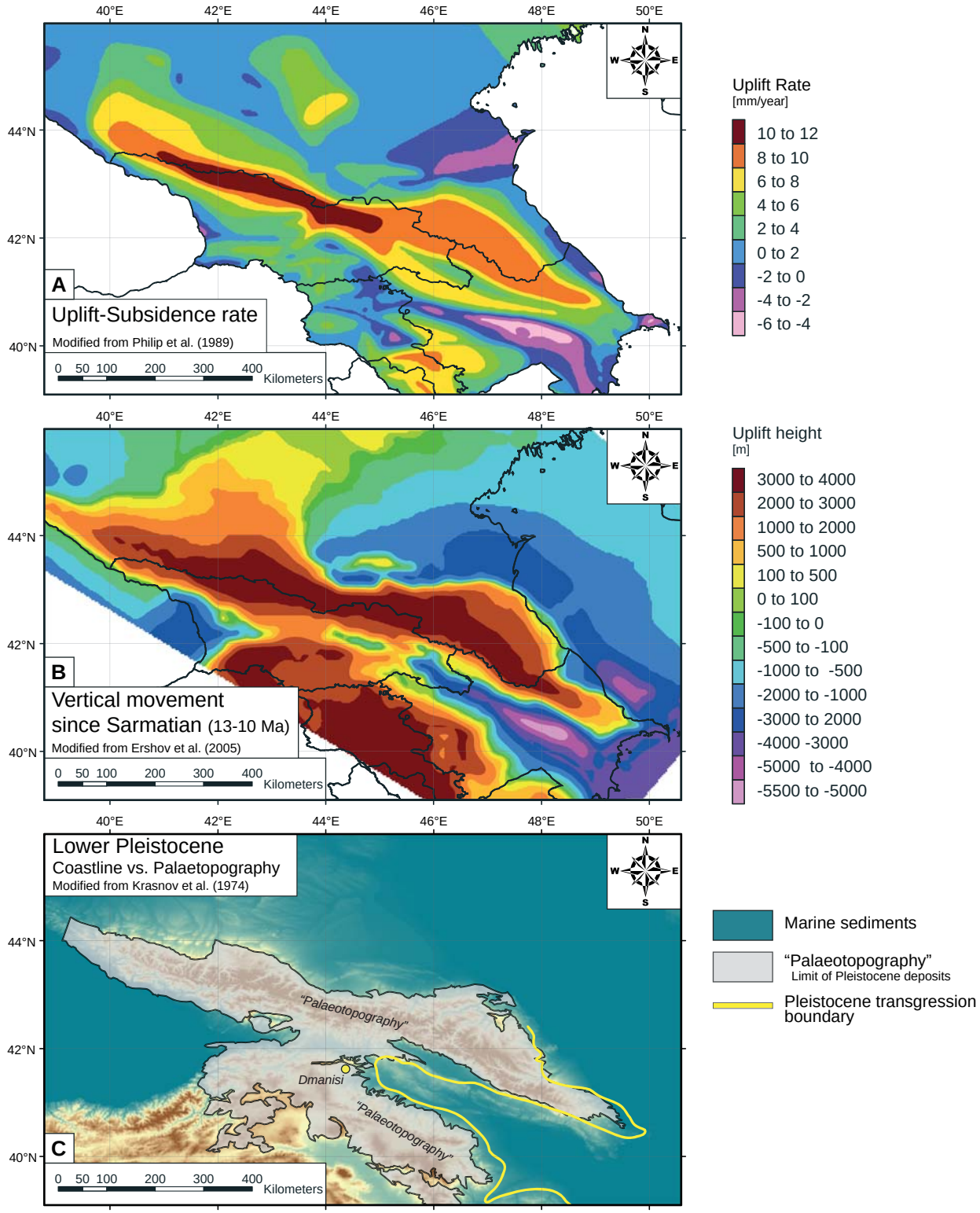

Figure 68: Maps of uplift rates, vertical movement, and Lower Pleistocene coastlines. (A) Uplift-subsidence rates: highest rates of 10-12 mm/year are found in the central part of the western Greater Caucasus (Philip et al. 1989). High subsidence is occurring in the Kura Basin; (B) Total vertical movement since Sarmatian (10-13 Myr). Strong subsidence is seen north and south of the eastern termination of the Greater Caucasus in Azerbaijan (Ershov et al. 2005); (C) Lower Pleistocene coastline – map of coastline (Krasnov et al. 1974) which separates the area of the former marine domain and zone above sea-level with Pleistocene deposits, and area with unknown amount of palaeotopography. Notice the position of Dmanisi (Georgia) where hominid remnants dated back to 1.8 Myr have been discovered.

Caucasus show ages between 2.5 and 1.2 Myr and suggest uplift rates of 4 mm/a (Hess et al. 1993), but thermal modelling difficulties linked to the close vicinity of hot intrusives may significantly modify modelling results leading to overestimates of the uplift rates.

Compilation of uplift amount and uplift rates (Ershov et al. 2005; Philip et al. 1989), confirm the very young uplift (figs. 68A and B) but show uplift rates in excess of 12 mm/a, which in light of field evidence (see Mitchell & Westaway, 2009, for discussion) seem very fast. However, they consistently show that the fastest and highest uplift is in the centre of the range. A more recent study on apatite fission tracks on the Early Miocene Maykop series of the western Greater Caucasus shows the detrital provenance of the clasts and suggests a minimum Early Oligocene age for subaerial uplift of the mountain range (Vincent et al. 2007). Work in progress by our group on apatite fission-track data in Azerbaijan, showed similar inherited ages of 12-56 Myr for samples taken in conglomerates of Pliocene age north of mount Sahdag (fig. 67). Ages of 21.8 Myr from samples taken in Aalenian sandstone in the central part of the range south of mount Sahdag (fig. 67) confirm the Tertiary uplift.

Detailed studies on geomorphology, including the young terraces along the Black Sea and Caspian Sea (Brod 1962; Krasnov et al. 1974), or the Kura Basin (Shirinov 1973; Shirinov 1975) exist but are all in Russian and difficult to access (Budagov 1969; Budagov 1973; Shcherbakova 1973; Shirinov 1975). One of the most prominent geomorphologic archives directly relating to uplift are the marine and river terraces. Up to 14 levels of terraces are recognized and reach into the valleys of the Greater Caucasus. A terrace at 475 m a.s.l. is given as latest Pliocene in age (fig. 68C), and is found along the western shore of the Caspian Sea (in Azerbaijan) and in the Kura basin along the foothill of the Greater and Lesser Caucasus. It reflects the location of the Pleistocene marine coastline corresponding to the Late Akchagyl transgression of the Caspian Sea (Krasnov et al. 1974; Popov et al. 2004). Its age is given between 2.5 and 1.8 Myr possibly as young as 1.2 Myr (see in Mitchell & Westaway (1999) for discussion and references). This is the same period that the oldest hominids in the Caucasus area were living in the Dmanisi (Georgia) area, near the ocean shores of the eastern Paratethys (Lordkipanidze et al. 2007). Many other terraces can be seen up to altitudes of 3000 m into the mountain valleys; their potential to help date uplift or show intermontane erosional/depositional processes remains to be investigated. Evidence from river incision of several hundred of meters since the last glaciations suggests uplift rates of 10 mm/a (Rastvorova & Shcherbakova 1967). Similar deep incisions are also observed in Plio-Pleistocene sediment of the Samur River in northern Azerbaijan; however detailed studies need to confirm the fast uplift rates.

The development of palaeo-rivers such as the Kura (Djavadova & Mamula 1999), Volga, Terek and Samur rivers, and provenance studies have been given great attention in recent years due to oil exploration studies (Guliyev et al. 2003; Morton et al. 2003; Reynolds et al. 1998). They transport the sediments from their source area to their final sinks. All this development, younger than 10 Myr, possibly even 5 Myr, led to the formation of very high quality reservoirs making the circum Caucasus basins unique oil provinces. The river systems and their deltas also underline the rapid lateral changes between areas with high and low topography or below and above sea-level. The long-lived river systems have also left a complex system of terraces, both in the valleys cutting into the mountain belt (mainly parallel and perpendicular to the main structural trend, (Lukina 1981). The existence of several levels and ages of river terraces document continued incision possibly due to uplift of the mountain range (Shirinov 1973). This is also shown by the important cliffs of Quaternary material cannibalized on the northern slopes of the eastern Greater Caucasus near Quba (figs. 65 and 67) (Kangarli 1982). Connecting these "events" to the different levels and ages of terraces along the Caspian Sea (Mamedov 1997; Shcherbakova 1973) opens the prospect of quantifying uplift vs. subsidence and basin infill.

One of the best data sets to directly quantify uplift are marine sediments such as those of Sarmatian age now found at an altitude of 3550 m a.s.l. such as in the Sahdag area of Azerbaijan (Budagov 1963) (fig. 67). Akchagylian marine clays are found in the Buduq syncline at altitudes of 2000 m a.s.l. in the Azerbaijan Greater Caucasus (Kangarli 1982). Combined information from different datasets suggest uplift rates between 0.33 and 1.00 mm/a for the last 10 Myr in eastern Greater Caucasus (Mitchell & Westaway 1999) but detailed rates for the different periods remain uncertain.

5.4.3. Palaeogeography

During the Tertiary the Greater Caucasus formed a vast island within the landlocked Paratethys Sea. Detailed palaeogeographic reconstructions indicate that the Greater Caucasus is emerging above sea level as lowland only after the mid Middle Miocene (13-14 Myr) to grow into a mountain range after Late Miocene (11-10 Myr) to Middle-Late Pliocene 3.4-1.8 Myr) (Popov et al. 2004). Palaeoclimate studies using spores and mostly pollen from Sarmatian (12-8Ma), mostly marine sediments, in Georgia north of Tbilisi

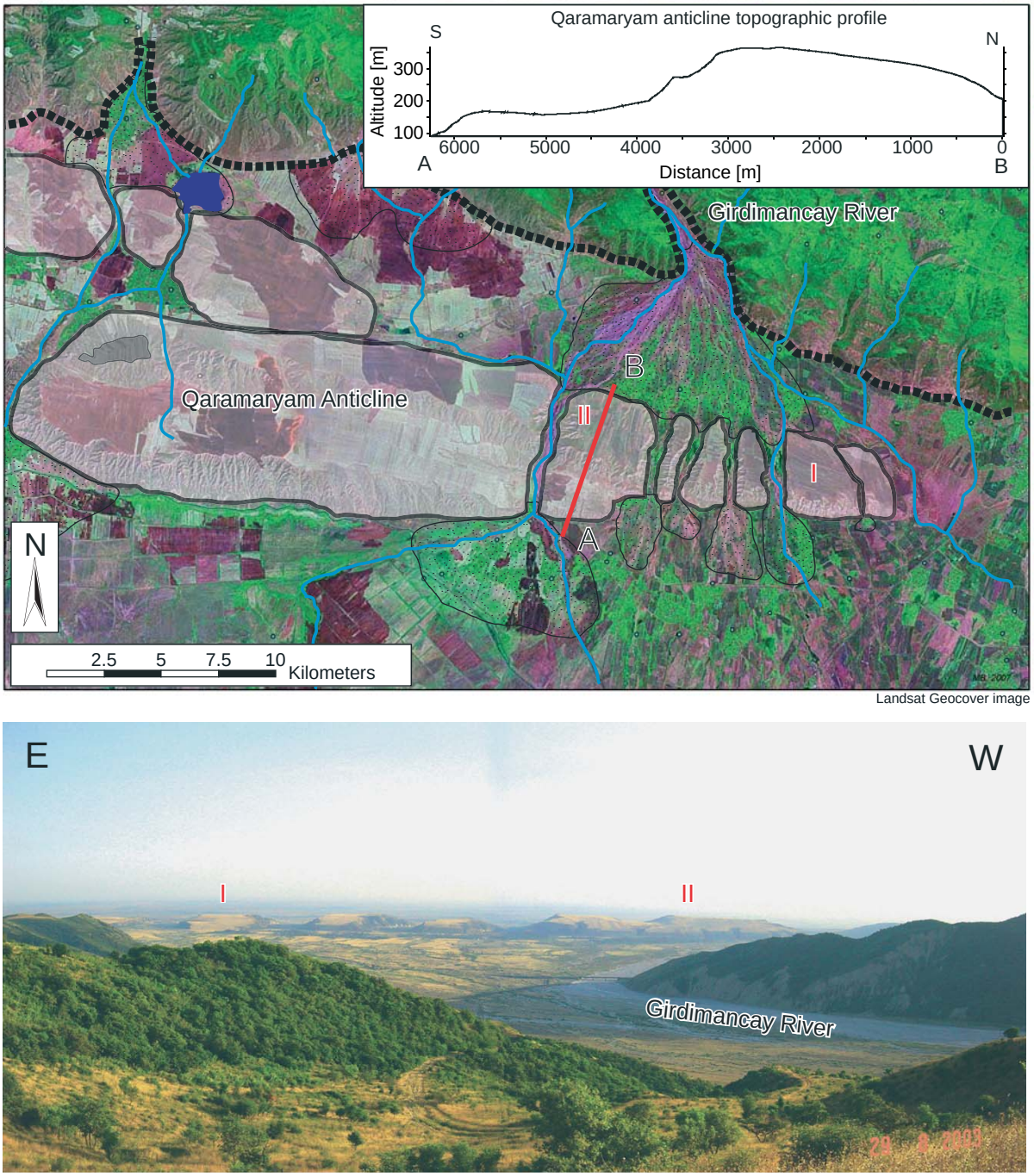

Figure 69: Pictures of the geomorphology of the Qaramaryam anticline (top image; Landsat 7 image) in the northern Kura basin of Azerbaijan, near the city of Agsu. The doubly plunging anticline is cut by the Girdimancay River to form water gaps due to river incision into the growing structure. Detailed topography along profile A-B (top right) shows the asymmetry of the Qaramaryam anticline, suggesting a buried thrust with top to the south movement. Dashed black line shows topographic limit of the southern steep slopes of the Basqal nappe unit (equivalent to the Alazani basin) to the north. Lower picture shows lateral view of the Qaramaryam anticline looking towards the south. See appendix A3.3 for other detailed topographical cross-sections.

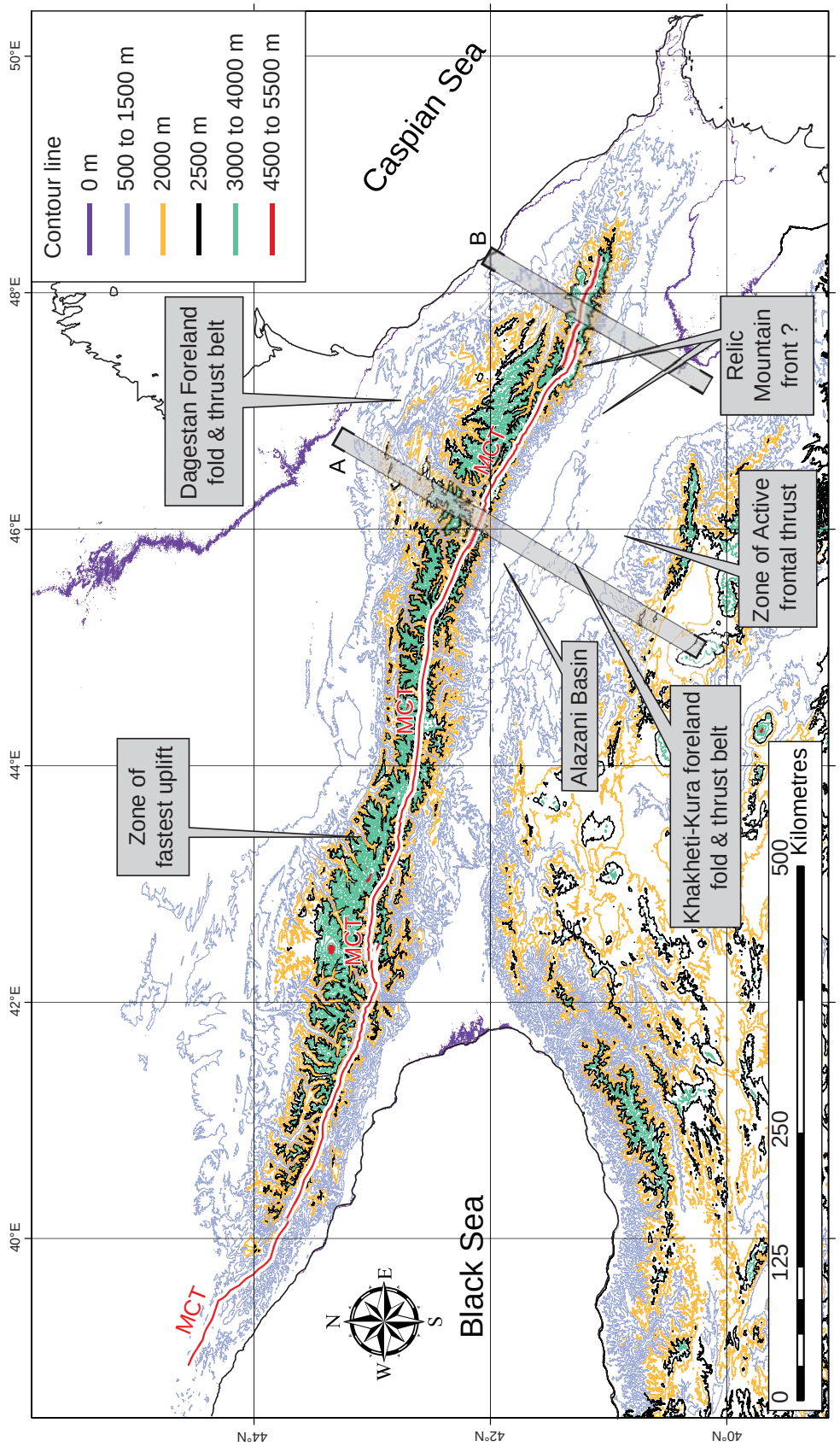

Figure 70: Faults versus topography: map showing majors faults (see also fig. 65) limiting zones of changing topography; MCT is highlighted. The zone of highest topography is mostly in the green color. Notice position of relic mountain/thrust front to the north of Alazani Basin. Qaramaryam anticline with water and wind gaps is at the northern edge of the Kura plain in Azerbaijan (see location in fig. 65).

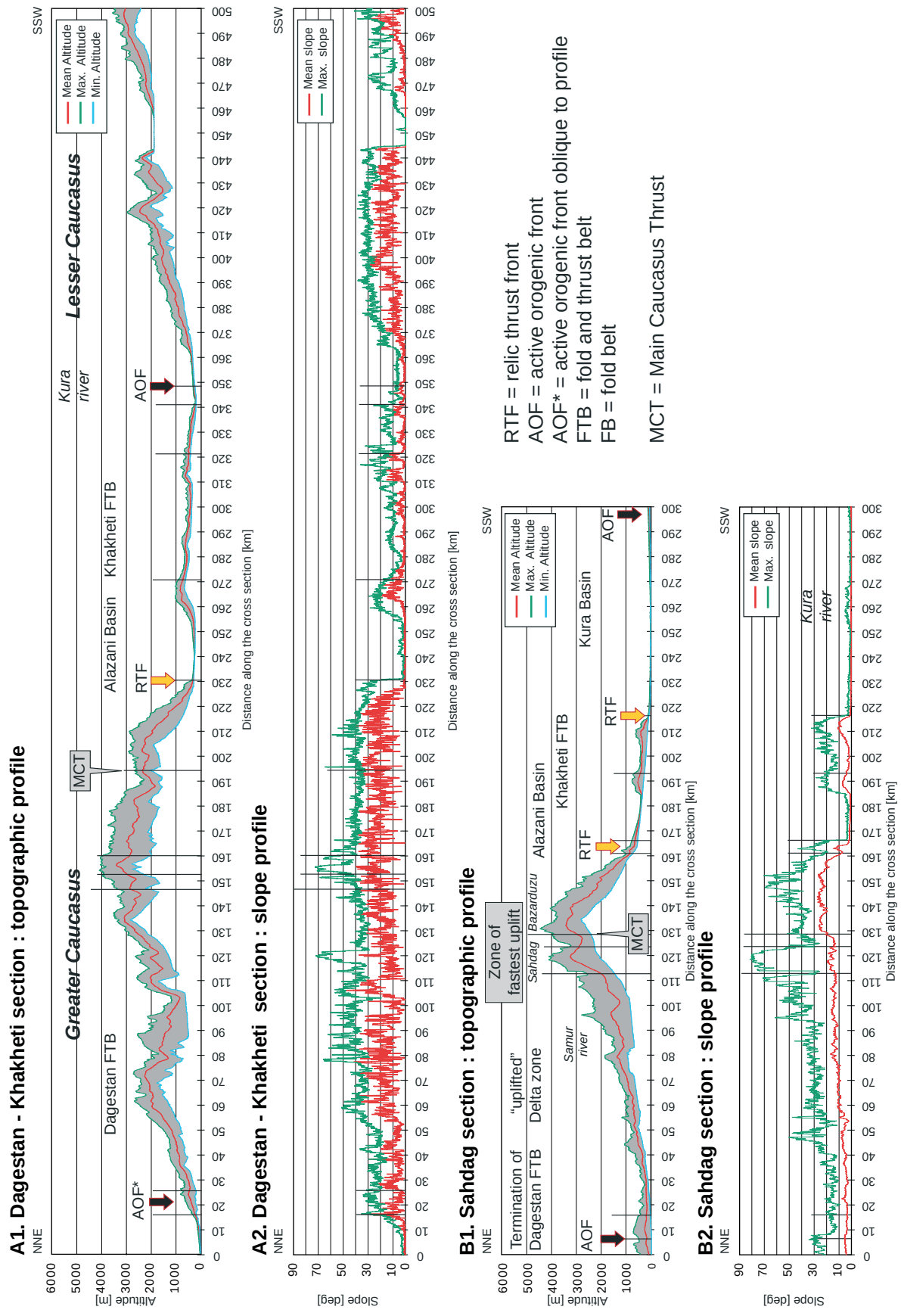

Figure 71: Sections across the Greater Caucasus showing the average evolution of topography along two transects as well as the changes in slope along the same transects. (Position of cross sections see fig. 70). More Eastern Greater Caucasus topographical profiles are available in appendix A3.2.

show the existence of pine forest at moderate to high altitudes and reflecting important climatic changes linked to mountainous topography and orogenic evolution (Kokolashvili & Shatilova 2009; Shatilova 1992; Shatilova et al. 2009). Prior to this Mid Miocene period, palaeogeographic reconstructions only indicate lowlands or islands or locally in the western Caucasus area mountainous areas. This is at odds with the fact that tectonic convergence and thrusting started already in Late Eocene times and most likely generated considerable topography. This is corroborated by the fact that important quantities of sediments are deposited in peripheral basins starting in Eocene-Oligocene, and that are most likely sourced in the nascent Greater Caucasus. An early Oligocene uplift is also confirmed by provenance studies and fission-track investigations in the Maykop series (Early Miocene) of the western Greater Caucasus (Vincent et al. 2007).

5.4.4. Tectonic Geomorphology

Only few combined studies on tectonics and geomorphology (Burbank & Anderson 2001; Delcaillau 2004; Keller & Pinter 2002) are available in the Greater Caucasus such as an investigation of the Alazani basin on the southern slope of the Greater Caucasus in Georgia (Philip et al. 1989; Triep et al. 1995).

This latter basin, runs parallel to the southern slope of the Greater Caucasus (figs. 65 and 70) and is filled with Pliocene - Quaternary sediments. This basin is bound to the north by one or several thrusts separating it from the steeper slopes rising into the high mountain range (Philip et al. 1989). To the east in Azerbaijan it can be shown that these faults are thrusting Cretaceous rocks over Oligocene series in the Basqal area (north of the town of Agsu; fig. 69 (Kangarli 1982). Its front to the south is bound by a thrust-related fold which leads to a sharp topographic drop down to the Kura plain. The Alazani basin is thus an intermontane, piggyback-type basin with a relic thrust front that was active in the Miocene along its northern edge and a frontal thrust which is active in Pliocene-Quaternary just south of the basin. In Georgia the Gagra-Dzhava zone located in the southern foothills of the main range is playing a similar role (Dotduyev 1986; Gamkrelidze 1991; Gamkrelidze & Gamkrelidze 1977). Its structure is similar to the Alazani Basin, but in addition shows somewhat farther travelled outliers of the main range, as is the case in the Basqal nappe structure in Azerbaijan (the eastern equivalent of the Alazani basin).

Further to the south the Quaternary sediments of the northern part of the Kura -Kartli basin are folded and thrusted. Very prominent in the morphology the Qaramaryam Quaternary Anticline in Azerbaijan (Girdimancay River - city of Agsu; figs. 65 and 69) is a large doubly plunging anticline showing well developed water gaps formed by tributaries of the Girdimancay River (fig. 69) (Shirinov 1975). A large asymmetric S-verging anticline is developed over a blind thrust with splays. The water gaps were cut during thrust-related folding and the fast changes in tectonics (leading to local uplift that was not matched by erosion) caused the change to wind gaps for some valleys. In western Azerbaijan the active thrust front extends all the way into the foothills of the Lesser Caucasus, folding alluvial fans and forming gentle topographic highs and tilted terraces.

Vertical faults with a strike-slip motion, are clearly reflected in the morphology as seen in examples from the Lesser Caucasus in Turkey and Georgia, as also discussed from earthquake focal mechanisms (Koçyigit et al. 2001; Rebaï et al. 1993). The importance of strike-slip tectonics in the Greater Caucasus has been suggested and discussed in many instances, however without conclusive or convincing evidence. Remote sensing studies of lineaments (rivers, and mountains crest, as well as faults (Cloetingh et al. 2007) and field investigations on faults with strike-slip movements show a general pattern of NNE-SSW oriented young anti-Caucasian faults crosscutting all the major fold and thrust structures. The general palaeostress orientation resulting from fault kinematic analyses shows a N-S to NNE-SSW oriented compression, with E-W extension and vertical intermediate stress axis confirming that they are recent faults that have suffered no rotation. However, no large-scale vertical faults or fault system crosscutting the whole mountain range could be observed.

5.4.5. Topography and Thrusts

Based on a digital elevation model at 90 m we have extracted a contour map (fig. 70) and superposed the main thrusts bounding the large changes in topography. Many thrusts coincide with changes in topography. In many other instances of topographic changes no thrusts are known, opening the possibility to denominate promising locations for thrusts, which remain to be ground-thrusted. The most striking feature is the MCT which forms the southern limit of the zone of highest topography throughout the Greater Caucasus. The relationship topography - thrust trace is even more clearly shown on two topographic profiles through the Eastern Greater Caucasus (fig. 71). Especially the relic thrust fronts of the Alazani basin and the folds and thrusts of the Qaramaryam-Khakheti zone stand out from the flat surface of the Kura basin. The morphological changes associated with the present active thrust front at the foothills of the Lesser Caucasus are too small to show on the profiles. A second set of pro-

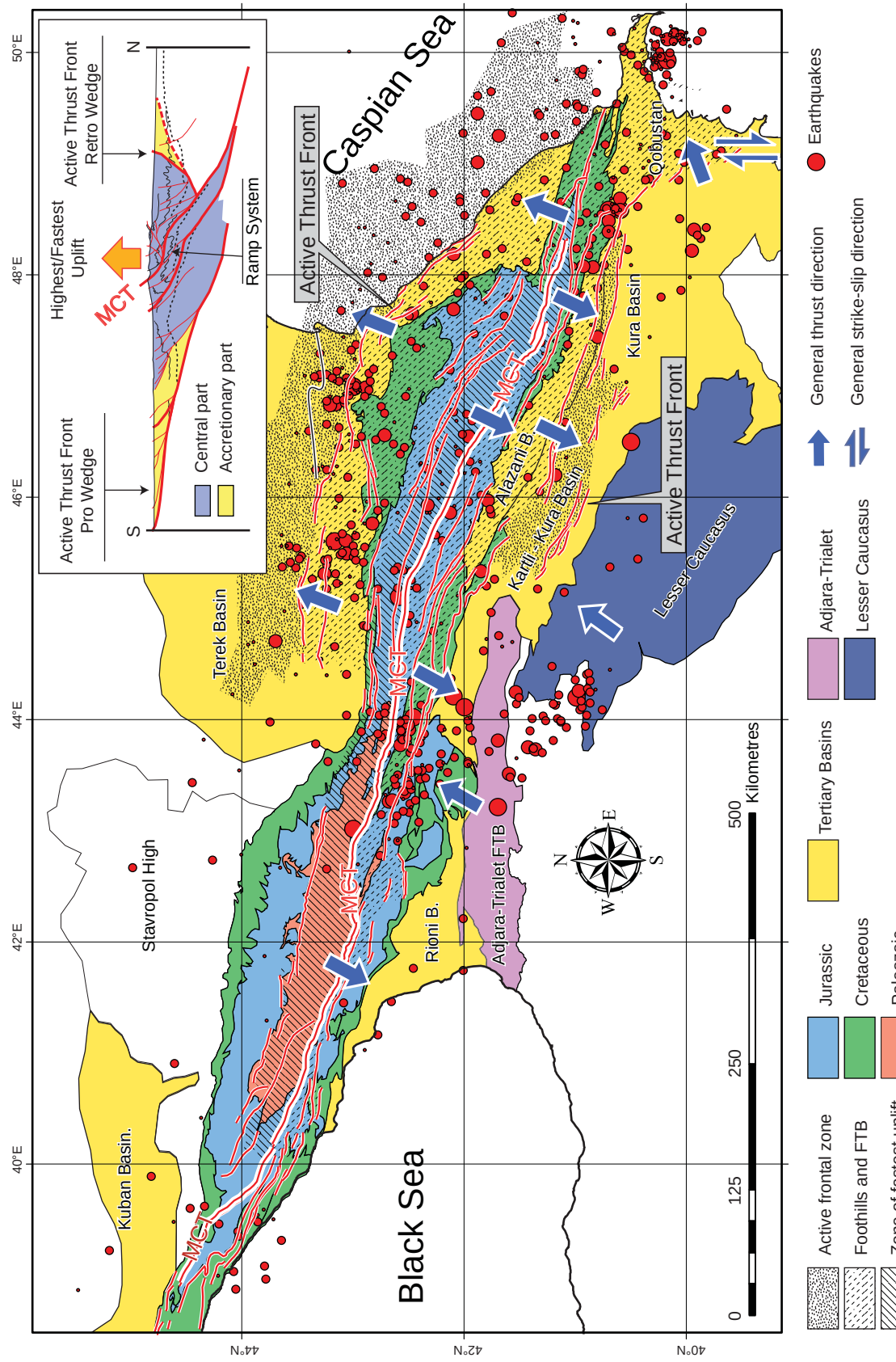

Figure 72: Simplified tectonic model of the GC linking topography and major geomorphic features with the major tectonic thrusts. The map shows the active fault strings of the MCT (in terms of seismicity) and the possible propagation outward to lower structural levels in the western GC in the Racha area.

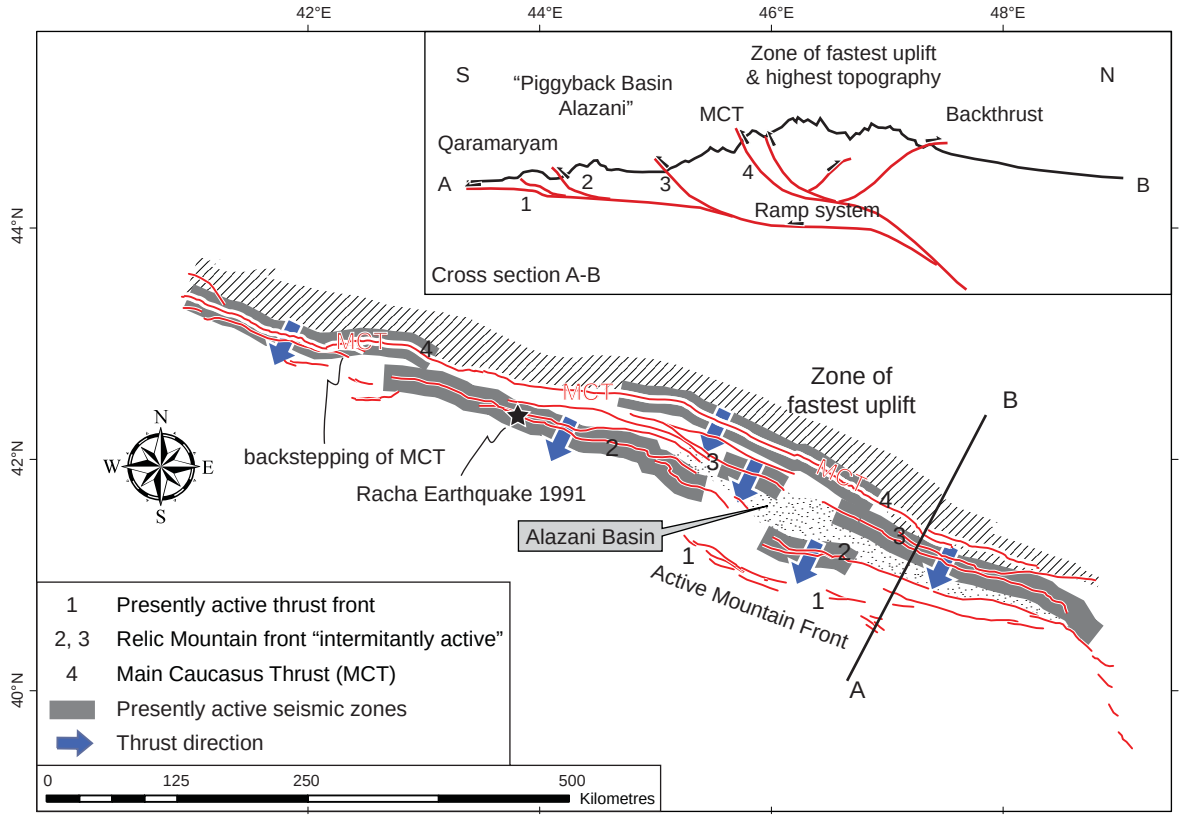

Figure 73: Topography versus tectonics: map showing the main areas of uplift and tectonic activity and an interpretative model which shows the link between thrusting and topography and seismic activity. The model proposes that due to motion over a ramp system at depth one can achieve fast uplift in narrow zone bound to forward thrust and back-thrust generated over the tectonic ramp.

files showing the changes in slope emphasize the position of the main thrusts!

The combined use of topography (figs. 71 A1 and B1) and slope (figs. 71 A2 and B2) helps to determine the position of the major thrusts which can be refined by the use of more detailed geological maps and satellite imagery (work in progress on a new tectonic map of the Greater Caucasus). This method can be used as a prospective tool to determine active (in combination with seismicity), but also fossil thrusts or orogenic fronts[1].

The major topographic changes and thrusts can be followed throughout the whole Greater Caucasus.

5.5. Discussion-Conclusions

New field evidence on thrust geometry, tectonic geomorphology, and tectonics combined with literature data on Tertiary tectonics in Azerbaijan led us to investigate the relationship between tectonics, topography and uplift in the eastern Greater Caucasus and correlate and expand our findings along strike to the whole Greater Caucasus.

The Greater Caucasus is an intracontinental doubly verging orogen resulting from the inversion of the Mesozoic, rift-related Greater Caucasus basin. The convergence between Arabia and Eurasia led to the closure of this basin and generated underthrusting and stacking of tectonic units. No subduction zone appears to exist under the Greater Caucasus, though incipient/young subductions are described for the western and eastern terminations of the Greater Caucasus into the Black Sea and Caspian Sea, respectively. During the orogenic development important foreland basins developed on both sides of the mountain range. Their development is contemporaneous with the infill of super deep sedimentary sinks in the Black Sea and the South Caspian Basin.

The Greater Caucasus is a fast growing orogen that started to build to its present topography since Late Eocene. Detailed timing of uplift above sea-level remains elusive, but there is clear evidence, including

1 13 detailed river topographic profiles in appendixes A3.4 and A3.6 were made to emphasize their relationship with the active faults. We also try to correlates them with the drainage patterns, river segment lengths and river segment numbers of 3 main rivers from the northern and southern slopes of the EGC (appendixes A3.7 to A3.10).

age and position of relic mountain fronts, that the orogen was growing in Oligocene and probably in Late Eocene already. The climax of growth was during the Late Tertiary, starting in middle Miocene and accelerating in Plio-Pleistocene. Information about uplift remains very unevenly distributed. Total uplift since Sarmatian is in excess of 3550 m as documented in the Eastern Greater Caucasus in Azerbaijan. Uplift rates in excess of 10-12 mm/a in the central part of the mountain range and based on river incision since the last glaciations, remain questionable and need to be confirmed especially when confronted with data showing more moderate uplift rates of 0.33 to 1.00 mm/a over the last 10 Myr.

The Main Caucasus Thrust is a discrete major thrust stretching across the whole Greater Caucasus from the shore of the Black Sea in the west to Azerbaijan in the east. In Azerbaijan and towards the shore of the Caspian Sea the MCT splits into several fault strings and affects a more diffuse zone, where both top to the north and top to the south thrusting is observed. The zone of highest topography, which correlates with the zone of fasted uplift, is bound to the south by the MCT which shows important top to the south movement. To the north this zone is bound by south dipping thrusts with top to the north movement. Detailed cross sections from northern Azerbaijan and insight from the Dagestan FTB suggest that this N-verging back-thrusting is linked to a thrust ramp system at depth. Thus the zone of highest uplift forms a triangular shaped domain limited to the south by the MCT and to the north by back-thrusts. This triangular zone of fast uplift and its associated major topographic/tectonic features can be correlated across the whole Greater Caucasus. Uplift over such a more or less steep ramp system may also explain why we observe such important uplift (a minimum of 3550 m since Sarmatian) in a rather restricted area.

Major displacement has been accommodated along the MCT as suggested from the location of the strongest earthquakes known is the area (>6 Mg). The 1991 earthquake of high magnitude in Georgia in the Racha area, but also by historical earthquakes in Azerbaijan such as in 1667 in the Samaxi area occur on thrusts located to the south of the MCT. These quakes area in similar structural position on a thrust system structurally beneath and to the south of the MCT and we interpret them as outward (to the south) propagating splays of the MCT.

Progressive southward migration of the thrust front during Tertiary formed successive active thrusts that were subsequently abandoned to form relic thrust fronts. The progression is registered in the geomorphology by clear changes in topography, deviation of rivers and water gaps. This is clearly documented in the thrust faults north, than south of the Alazani-Basqal (Basqal is a lateral structural equivalent of Alazani basin in Azerbaijan) structure, followed to the south by the Kartli FTP and the structures such as the Qaramaryam anticline. The active orogenic front zone, both to the north in Dagestan and to the south in the foothills of the Lesser Caucasus, can be deduced from morphological, structural and seismicity criteria.

Unlike the western Greater Caucasus, the eastern Greater Caucasus is seismically very active. This high seismicity correlates with higher present convergence rates in this area. We suggest that this reflects the continued growth of the foreland basins outboard of the main range into the Quaternary to recent sediment filled foredeeps. Simultaneously, as suggested by earthquakes in the central parts of the orogen, we observe continued growth and uplift in the central part. These zones correlate with the areas of high topographic gradients such as the MCT or other areas west of Tbilisi on the southern slope of the Georgian Greater Caucasus. The difference between east and west is due to different factors such as the E to W decreasing plate convergence rate. But, also the inherited structure possibly plays a major role. Indeed, the basement units present in the west are not observed to the east and this may be interpreted as a difference in the initial palaeotectonic setting that was subsequently differentially inverted during compression. In addition the observed recent magmatic activity in the west may suggest a difference in the crustal or whole lithosphere structure and strength contributing to a different evolution east and west.

Strain partitioning across and parallel to the Greater Caucasus is very heterogeneous, both vertically and horizontally. Present day plate convergence as observed from GPS data is oblique with a larger convergence in the east. Overall this convergence converted into a 6-14 mm/a horizontal deformation across the Lesser Caucasus and the Greater Caucasus. An important drop in velocities across the MCT in the Greater Caucasus, indicates, in agreement with what we suggest in this paper, that there is no horizontal displacement, but dominantly uplift! The MCT is a main boundary north of which we observe the development of triangular zone of uplift related to an important tectonic ramp system at depth. West of Tbilisi (Georgia) in Racha area seismicity indicates partitioning of strain between the MCT and the thrusts beneath the Gagra-Dzhava zone. As seen from GPS data and tectonic geomorphology the meridional FTB and the thrust front is clearly propagating, but the present activity is the Dagestan FTB and foreland basin.

An example of vertical strain partitioning between surface and deeper structures is suggested at the eastern transition of the GC into the South Caspian basin. Here in the Qobustan area GPS data suggest a dextral strike-slip motion along a major fault, the West Caspian Fault, whereas earthquake focal mechanisms suggest a thrust motion to the east which may be linked with westward subduction connected with subduction of the South Caspian Basin.

Clear links between geomorphology, seismicity and tectonics can be observed in the Greater Caucasus. With the exception of the Racha area in Georgia, mainly the eastern Greater Caucasus appears to be active at present. Strain partitioning across the mountain belt is very heterogeneous. In the absence of enough detailed data precise timing and assessment of rates of uplift and deformation and the partitioning of strain into uplift and horizontal deformation, as well as the partitioning between thrusting and strike-slip remain difficult to assess.

5.5.1. Acknowledgments

We would like to thank especially the MEBE Programme and its sponsors for supporting this research. We are further indebted to the Swiss national science foundation for their financial support (SCOPES project IB7320-110973) as well as INTAS (project 06-1000017-8930) and the University of Fribourg. We also would like to thank all the people in Azerbaijan and Georgia that were involved in this project and that helped in one way or another. We thank the reviewers for their constructive suggestions.

*****

6 - Geographical Information System (GIS) for the Eastern Greater Caucasus

The evolution of new GIS-supported technologies allowed modifying the habits of geologists, especially in the field, during data acquisition and mapping. Field-computers and GPS have nowadays the same importance as field-books, maps or compasses.

GIS improves the efficiency and extends the boundaries of the geological research, making it possible to share data with co-workers and facilitating the integration and the management of the collected data. GIS softwares now offer numerous tools for mapping, for calculations, and for data comparisons.

For the last 5 years, the tectonics group of the University of Fribourg works in a complete GIS environment including GPS, field-computers and GIS softwares in remote locations like the Eastern Greater Caucasus (EGC).

This chapter describes fieldworks with GIS, the tools (software and hardware), the geodatabase architecture, the main external data of the project and several GIS methods used to analyse the data acquired in the frame of this PhD project.

6.1. Fieldwork with GIS

GIS improves efficiency at all stages of fieldwork from preparation to publication. This section will detail all these stages.

6.1.1. GIS Preparation of fieldwork

GIS adds a new phase to fieldwork preparation. Most of the data can be digitalized and georeferenced. Therefore it is possible to use them directly on GPS or rugged computers in the field. A good data selection is necessary in order to not be submerged by useless data. A good GIS preparation permits losing less time in knowing geographical and geological characteristics of the studied area.

For several years 3D view and satellites images of the world are available in the World Wide Web trough applications such i.e. Google Earth®, NASA World Wind®, Microsoft Bing Maps 3D® and others. They contain data that are normally very difficult (or expensive) to obtain. These tools are very useful to visualize an area and must not be neglected for fieldwork preparation. In some cases, even geological structures like beddings, folds and faults can be seen.

In parallel it is important to obtain original files because it allows working independently of any connexions during the fieldwork. Topographical, geological and geomorphological data come mainly from publications, World Wide Web, universities and from other people working in this area. Like bibliographical work, this phase must not be underestimated in terms of time and importance. The collected data must be scanned and prepared to be introduced into the GIS. Before they can be uploaded in GPS or field computer, it is better to cut maps and data for the studied zones, thus limiting the size of files and uses less processor resources when working and consequently uses less battery energy.

Based on the EGC experience, it is necessary for fieldwork to have a good global geological and topographical map (~1:500'000), a detailed topographical map (1:25'000 or 1:50'000 if available, in our case 1:100'000) and a detailed geological map (scanned sketch, maps). Printed topographical maps are still necessary when talking to people that are not used to work with computer but also in terms of security.

The geodatabase structure must be designed to allow a high efficiency in entering data in GPS or field computer during the fieldwork. For a geodatabase feature, only the necessary data must be filled in the field (i.e. bedding azimuth and dip), data like date/hour and location can be filled automatically and for example if only one person will make the measures, its name

could be configured to be the default name for the corresponding database field. If the geodatabase and the interface are well designed, the time to fill it in the field will be acceptable compared to classical field book method. At the end the data will be directly georeferenced and time will be saved on the whole processus.

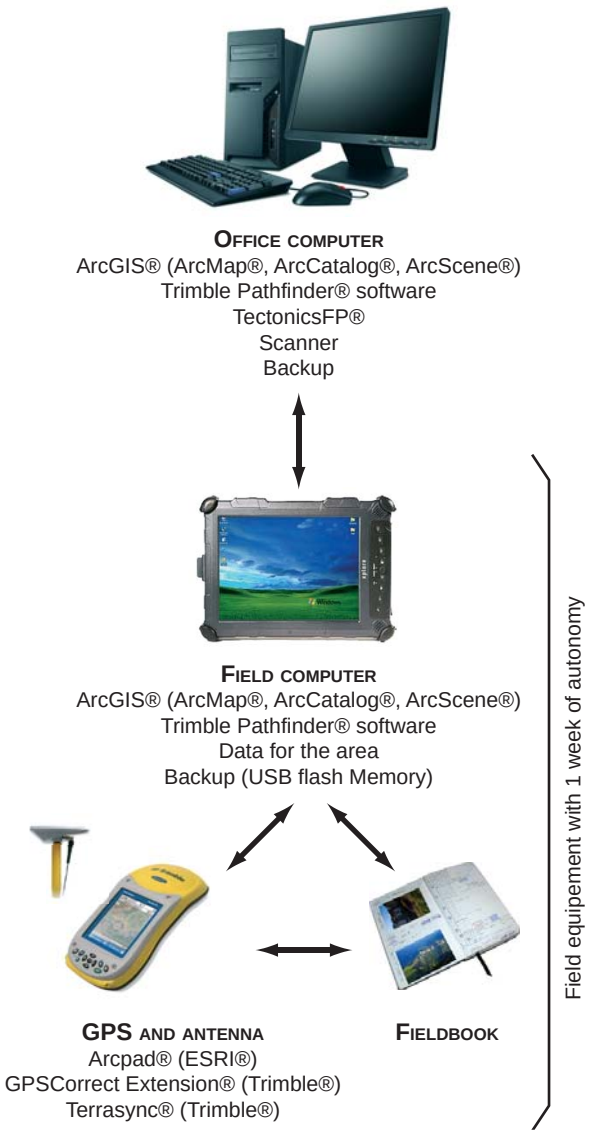

Figure 74: Hardware and software used for GIS work.

6.1.2. Fieldwork

In the field, a GPS was used to enter the measured data directly in the geodatabase and to have detailed map. A field-computer was used at the campsite to synchronize the data and to verify them. A second small GPS was taken in case of problem with the first one.

In terms of energy for the field-computer and the GPS, the spare batteries allowed one week of autonomy if taking care. In case of problem, a DC/AC converter (12VDC – 230VAV) allowed using the jeep battery to charge all systems.

The field-book was always necessary to draw outcrops, sketch maps and to make some annotations about a place. Measures were not systematically written in it. For each day, the most efficient content was: a first page with the date, the visited area, the participants and the weather; a sketched map of the area with the main infrastructure (road, houses and other significant details) where the main outcrops and structures can be drawn during the day; sketches of the outcrop with the associated observations and, when relevant, the associated measures; and finally a summary of the day.

In order not to lose data, they were first stand in the GPS (1st backup). Afterwards they were imported on the field-computer (2nd backup). Finally they were copied on a USB key (3rd backup). The three backups were never let at the same place in case of i.e. theft. When an Internet connection was available, a 4th backup was made towards a distant server.

6.1.3. Data validation and analysis

Back from fieldtrips, data are completed and corrected. Samples are numbered, sorted and sent to laboratories for analyses. A sample form (fig. 78) is filled out. Pictures are sorted, described and selected for the geodatabase. Some of them were printed at small scale (6 x 9 cm) to be paste in the field-book.

Afterwards, data were analysed in the GIS software itself but they were also exported in other softwares to apply other methods.

6.1.4. Publication

The advantage of a good geodatabase with numerous data is to have a global view on all data, to produce his own maps and finally the geodatabase can be easily shared with other people. Nowadays there are possibilities to publish PDF of a geodatabase giving the access to the data without buying expensive software.

6.2. SOFTWARE AND HARDWARE

The figure 74 shows the main hardware features and their respective softwares used by university for GIS work.

6.2.1. GIS softwares

The geodatabase and GIS environment was designed with ArcGIS® Desktop softwares (mostly Arc-

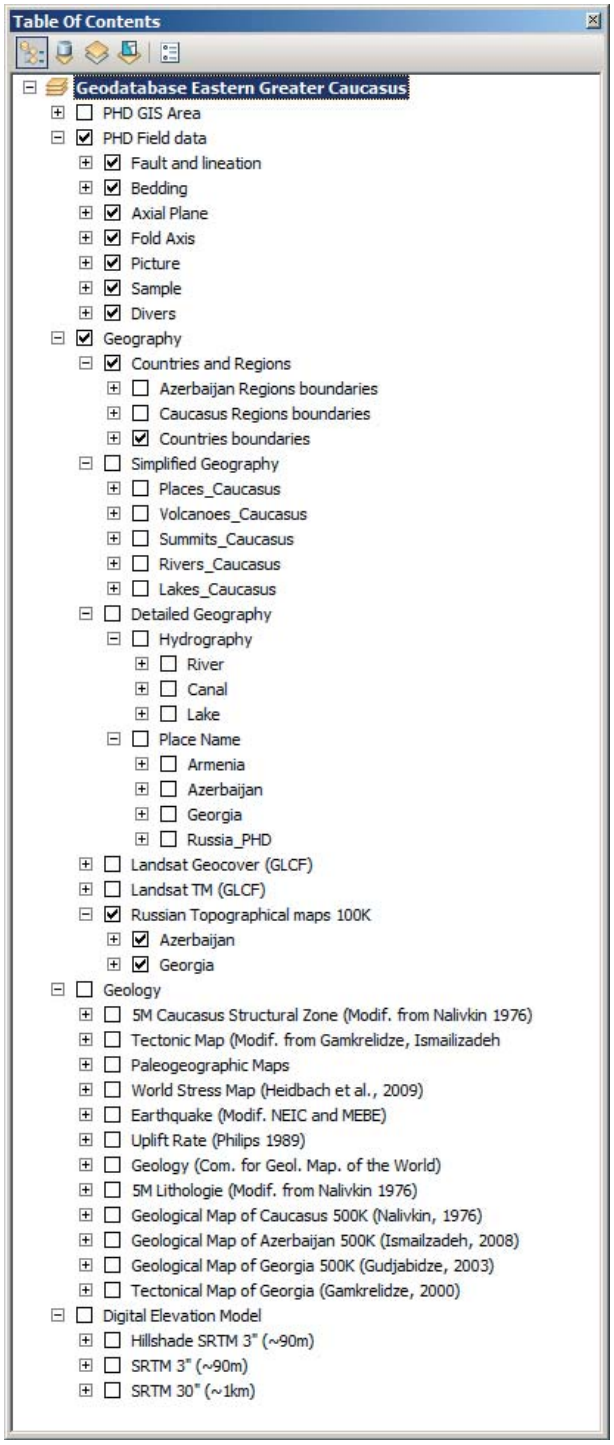

Figure 75: ArcMap's table of content.

Catalog® and ArcMap®) from ESRI®. Several extensions were used like 3D Analyst and Spatial Analyst. 3D models were generated with ArcScene® (ESRI®). Figure 76 show the working environment in Arcmap®.

In the field, ArcPad® (ESRI®) with the GPSCorrect® extension from Trimble were installed on the GPS. The field-computer was installed with ArcGIS Desktop®.

6.2.2. GPS and field computer

To enter and locate the measures, a Trimble GEOXH® GPS with ArcPad® software from ESRI and the GPScorrect® extension for ArcGIS® was used. This GPS was mostly used to enter data in the field but also to make accurate measures (< 50cm) of topographical features.

A rugged field computer Xplore iX104c3® was used to store and download the data, to complete and analyse them after one field day. It contained all the data available for the project. Rugged computers and GPS were completely necessary not only for rain and dust during the fieldwork but also for displacements with jeep or horses that were sometimes very rough during hours.

A backup was made on a USB external hard disk.

6.3. Architecture of geodatabase

The geodatabase was designed to integrate most of the field measures and field features: beddings and their associated schistosities, fault planes and their associated lineations, fold axes, axial planes, samples and photographies. As said before, features and their associated number, location and fields were designed to facilitate efficiency during the fieldwork. Data like the date, position or author name were automatically filled with defined default values.

All measures and data are represented by points with their respective position (longitude, latitude and altitude) and description fields. The World Geodetic System 1984 (WGS84) is chosen as coordinates systems for the geodatabase. It is a very common standard used in cartography, geodesy and navigation. It is also the default standard datum for GPS systems.

6.3.1. Measurements

Beddings, schistosity planes, fault planes, axial planes, fold axis and lineations are all characterized by their geographical position (latitude, longitude and altitude), azimuth, dip, date of measurement and their author.

Bedding and schistosity plane are recorded in the same features because when they are associated a fold axis can be calculated. Fault plane and its associated lineation (mostly slickensides) are also recorded in the same feature in order to be able to calculate stresses.

6.3.2. Pictures

More than 7300 pictures were taken during fieldtrips and approximatively 660 were selected to document outcrops.

For the picture integrated in the geodatabase, their GPS location and their direction of view were recorded to allow distinguishing afterwards, i.e., on which side of the valley the picture was taken. Each picture is also characterized by its date, author, an associated legend and remarks. To allow opening directly the file from ArcMap®, the relative path of the picture is also defined in the geodatabase (fig. 76).

Photoshop Lightroom® was used to sort the pictures and to fill the IPTC (International Press Telecomunication Council) metadata concerning place (Country, State/Province, City and Location field). This allows a fast search of the picture with classical search tools of Windows® and Mac®.

Almost all the 7300 pictures have the country and the region defined, the city/village is defined for 3/4 and finally the location within the village is defined for 1100 pictures. These data are stored directly inside the picture file.

6.3.3. Samples

Almost 220 rock samples were collected for different purposes. In the field a number was directly attributed to each sample and written on it, on a water resistant paper and on the plastic bag containing both.

The major problem was to send the sample to Switzerland. Authorizations from different ministries were necessary (generally depending on the custom officer). They were sent using an aerial freight company like Lutfhansa®.

In the lab, samples were sorted, renumbered based on the continuous numbering. Finally samples were prepared for their respective analyses. Remnants of sample were stored in a plastic bag with a label indicating the sample number, the provenance, the date of sampling and the type of analyses that were made. All the samples are stored in the same place.

The geodatabase contains the date, the sampling person, the sample number and the type of analysis that were made on the sample (i.e. apatite fission track, illite crystallinity, thin section and others) and a link that allows opening a PDF sample form (fig. 78).

The main page of the associated PDF sample form (fig. 78) contains informations about the sample number, the

Table 11: Description of geodatabase features and their corresponding fields.

Field	Type	Description
Bedding [Bedding table – Point feature]		
BedAuth	Text	Author of bedding measure
BedDate	Date	Date of bedding measure
BedAzm	Number	Azimuth of bedding plane [0 to 359°]
BedDip	Number	Dip of bedding plane [0 to 90°]
SchAzm	Number	Azimuth of schistosity [0 to 359°]
SchDip	Number	Dip of schistosity [0 to 90°]
BedRem	Text	Remarks about bedding measure
Fault [Fault table – Point feature]		
FltAuth	Text	Author of fault measure
FltDate	Date	Date of fault measure
FltAzm	Number	Azimuth of fault plane [0 to 359°]
FltDip	Number	Dip of fault plane [0 to 90°]
LinAzm	Number	Azimuth of associated lineation [0 to 359°]
LinDip	Number	Dip of associated lineation [0 to 90°]
LinSense	Number	Sense of lineation: S: sinistral / D : dextral / N : normal / R : reverse / U : unknown
FltRem	Number	Remarks about fault measure
Axial Plane [AxialPln table – Point feature]		
AplnAuth	Text	Author of axial plane measure
AplnDate	Date	Date of axial plane measure
AplnAzm	Number	Azimuth of axial plane [0 to 359°]
AplnDip	Number	Dip of axial plane [0 to 90°]
AplnRem	Text	Remarks about the axial plane measure
Fold Axis [FoldAxis table – Point feature]		
FldAuth	Text	Author of fold axis measure
FldDate	Date	Date of fold axis measure
FldAzm	Number	Azimuth of fold axis [0 to 359°]
FldDip	Number	Dip of fold axis [0 to 90°]

Field	Type	Description
Lineation [Lineation table – Point feature]		
LinAuth	Text	Author of lineation measure
LinDate	Date	Date of lineation measure
LinAzm	Number	Azimuth of lineation [0 to 359°]
LinDip	Number	Dip of lineation [0 to 90°]
LinRem	Text	Remarks about lineation measure
Sample [Sample table – Point feature]		
SmplAuth	Text	Person that collected the sample
SmplDate	Date	Date of sampling
SmplNo	Text	Sample Number (AZXXX)
SmplAge	Text	Age of sample
SmplAnly	Text	Analyses made on sample
SmplLink	Text	Link to the result of the analysis
SmplRem	Text	Remarks about sample
Picture [Picture table – Point feature]		
PictAuth	Text	Author of picture
PictDate	Date	Date when picture was acquired
PictNo	Text	Picture name
PictNo	Text	Direction of the picture [0 to 359°]
PictRem	Text	Remarks about picture
PictLeg	Text	Legend of picture
PictLink	Text	Link to picture file
Divers [Divers table – Point feature]		
DName	Text	Name of object
DRemarks	Text	Remarks about object

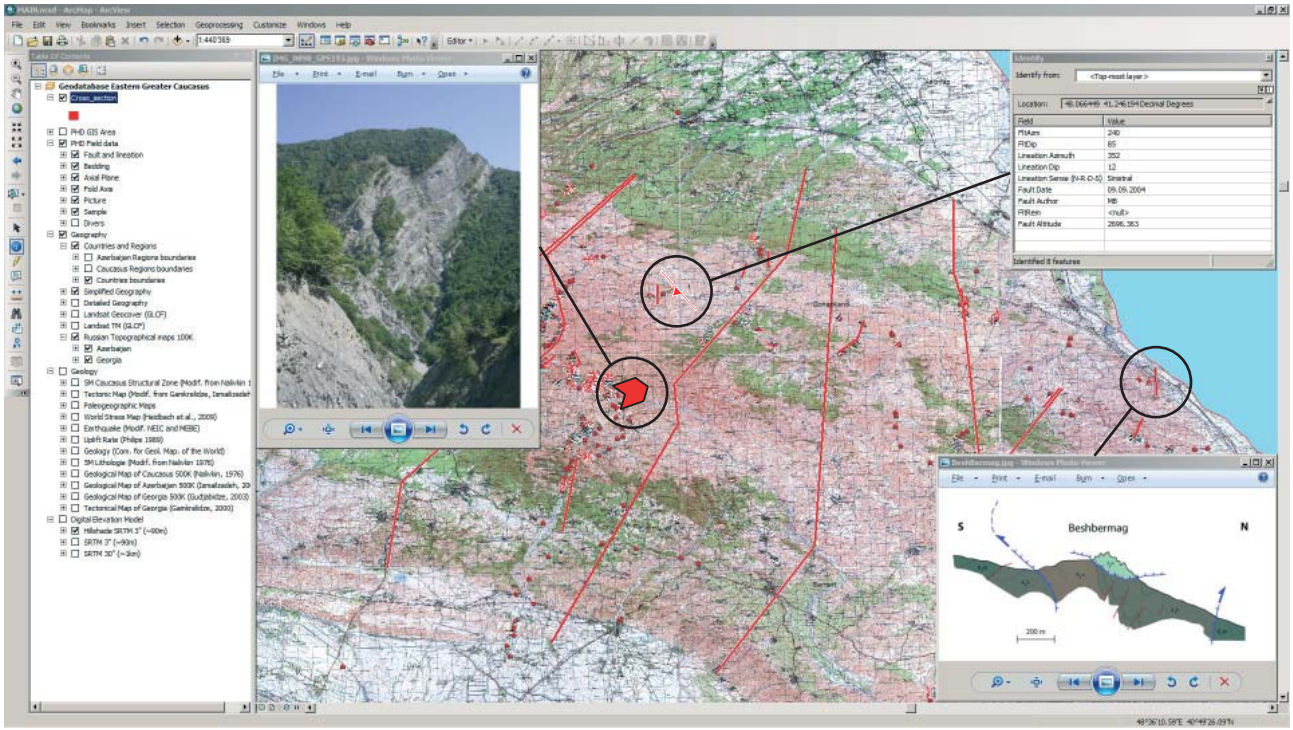

Figure 76: Arcmap® interface with some available data that can be consulted.

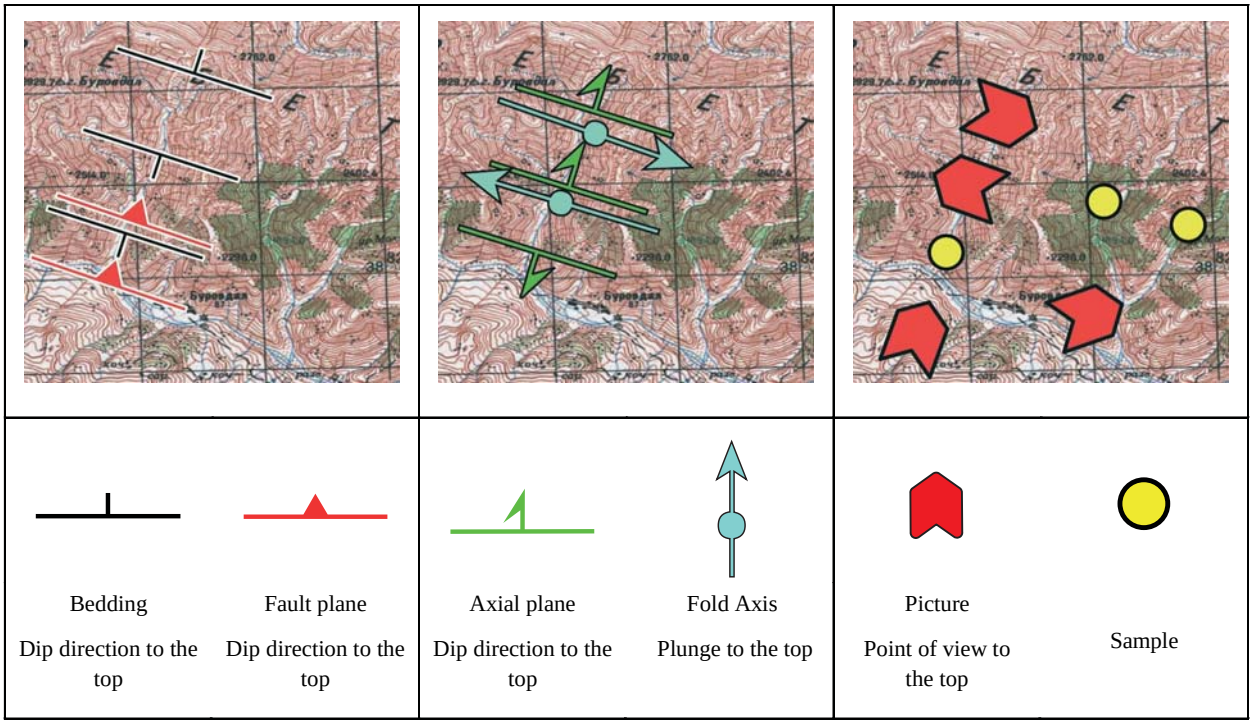

Figure 77: Main feature symbols for the field geodatabase.

geographic position (latitude, longitude and altitude), sampling author and date. A field allows defining the analysis that were made on the sample and for which results are available. It contains also fields to define precisely sedimentary rocks. Currently not all descriptions are filled and some future sedimentological projects could fill them.

6.4. Maps and vector data

Maps and vector data allow the geologist in remote areas such as the Eastern Greater Caucasus to always find his exact position and to quickly understand the environment of the study. The main sources for maps were the World Wide Web, publications, and data from our project colleagues and from the department.

In Azerbaijan essential data such as topographic maps turned out to be impossible to obtain. Especially topographic or geological maps at scales 1:25000 or 1:50000 fall under military restrictions. However, the large resources of the World Wide Web made it possible to find Russian maps at 1:100'000 (table 12-A), digital elevation model at 90 meters from the Shuttle Radar Topography Mission (SRTM) (table 12-B), free satellite images from Landsat (Geocover and ETM+ with seven spectral bands) (table 12-C) and a geodatabase with all locality and place names of Azerbaijan (NGA) (table 12-D). The place name list was not only helpful in the field; it also allowed to homogenize the place names and to avoid some misunderstanding in papers. The main geological maps were scanned and georeferenced. It include the geological map of Nilivkin (1976) covering the Caucasus, geological map of Azerbaijan (Ismailzadeh et al. 2008b), the geological map of Georgia (Gudjabidze 2003). Earthquake data were taken from USGS earthquake website (http://earthquake.usgs.gov/). Table 11 gives the most important sources and a sample of the data.

6.5. GIS applications in EGC

In this work, GIS was used to build several 3D models, maps or to do geomorphological analyses based on field data or on other data. This section will explain method used to build the models and the data that were used.

6.5.1. Geological maps

To illustrate this work several geological maps were drawn for this work and an original map as the base to draw them.

The maps at Caucasus scale (1:5'000'000) are mostly based on CCGM ("Commission de la Carte Géologique Mondiale") vector data.

The detailed geological maps of the EGC at scales smaller than 1:500'000 are based on:

- Fieldtrips all around the Eastern Greater Caucasus.
- Azerbaijan Geological Map at 1:500'000.
- Published local geological maps.
- Not published local geological maps from T. Kangarli.
- Articles.

6.5.2. Digital elevation models

A digital elevation model based on SRTM data at 3" (~90 m) was built for the PhD area and for Middle East Basin Evolution project Area (Table 12-B). The main work was to convert the data, to merge them together and to fill cells with no altitude data with an average value from the neighbouring cells.

A digital elevation model at 30" (~1km) including sea floor was built for the Middle East Area. The topography is based on SRTM data at 30" and the bathymetry is based on the General Bathymetric Chart of the Oceans (GEBCO) for the open waters and on the Caspian Environment program for the bathymetry of the Caspian Sea. The main work was first to convert the altitude lines of the GEBCO and Caspian Environment Program to a raster and secondly to merge it with the SRTM data. Cells with no altitude data were again filled with an average altitude based on the neighbouring cells. The result is used as a background for several maps of this work, for the topographical and slope analyses (see below), for the rivers analyses (see below).

6.5.3. 3D model of the Jurassic Basement

A 3D model was built for the Jurassic Basement based on a 2D Russian map of the basement (fig. 79) to allow a better visualisation of the situation.

It was necessary to digitalize the altitude line of the Jurassic basement on the original map and to interpolate them with the 3DAnalyst® toolbox in ArcGIS®.

6.5.4. Topographical and slope analyses

Topographical and slope analysis of 5 cross-sections of the Greater Caucasus and the Eastern Greater Caucasus were made. They could emphasize regional tectonic influence. To have relevant data, a GIS method was developed.

Based on the SRTM DEM at 3" (~90 m), this method calculates the maximum, mean and minimum alti-

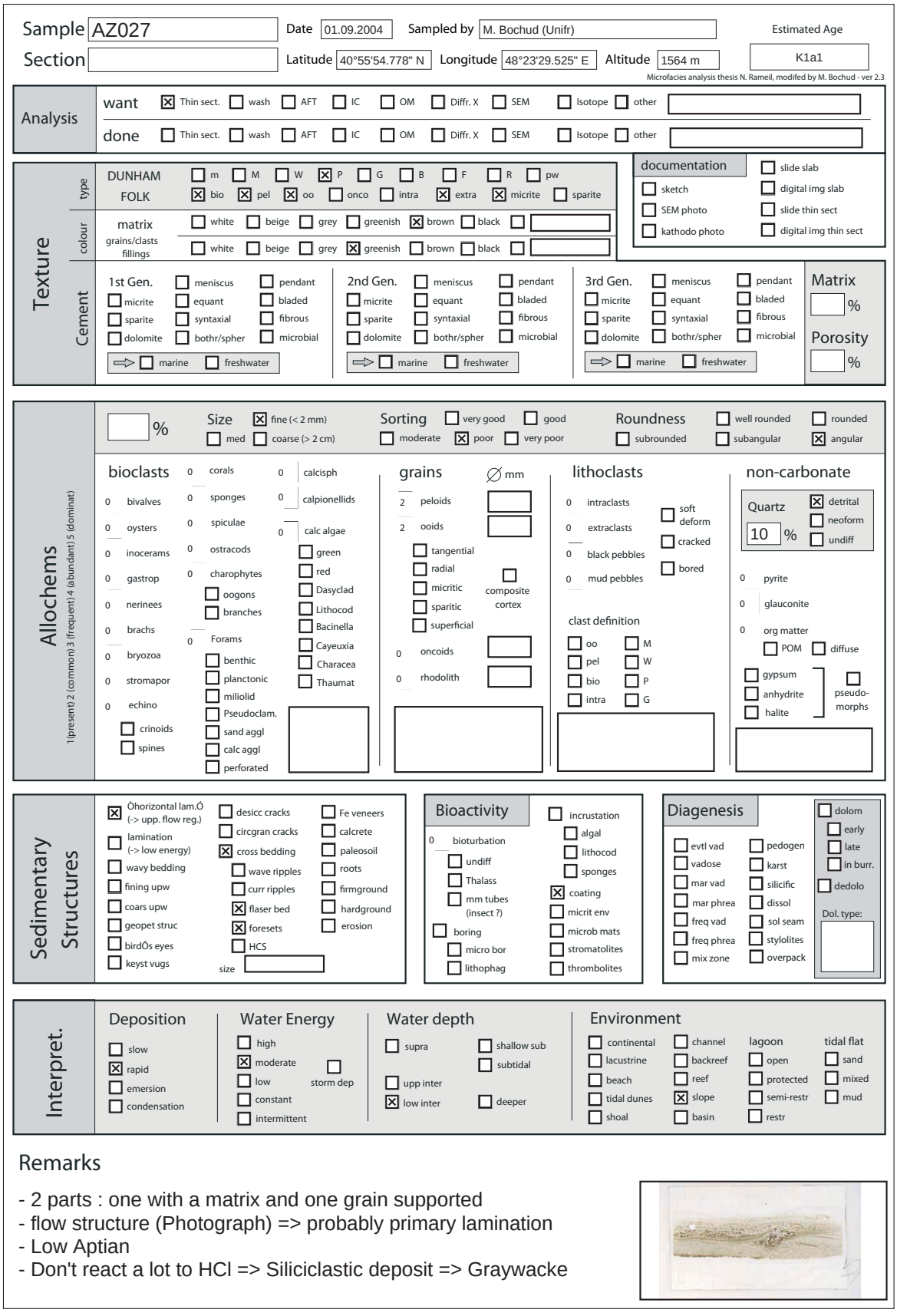

Figure 78: Example of a filling form that can be used to describe each rock sample collected in the EGC. As there is almost no magmatic or metamorphic rocks, form was made for sedimentary rocks. Fields for the sedimentological were defined by N. Rameil. The form can be filled directly in Adobe Acrobat®.

Table 12: Most used data downloaded from the World Wide Web with their respective download address.GIS applications in EGC.

Type of data	Data sample
A. Topographical maps of Azerbaijan at 1:100'000 **Source:** www.lib.berkeley.edu/EART/topo.html **Description:** Russian maps of Azerbaijan (1:100'000). They are available in UC Berkeley map Library. They were cutted and georeferenced to use them in ArcGIS®.	
B. Digital Elevation Models **Source:** http://www2.jpl.nasa.gov/srtm/ **Description:** Digital elevation model at 3" (~90 m) and 30" (~1 km) resolution from the Shuttle Radar Topography Mission of the NASA and NGA. The NASA obtained elevation data on a near-global scale to generate the most complete high resolution digital topographic database on the earth. Virtually the entire surface between +/- 60 degrees latitude was mapped by SRTM. The SRTM DEM data is not offered to the general public at full resolution (30 m) only the averaged 90 m is offered. The "Deutsches Zentrum für Luft und Raumfahrt" sell the full resolution SRTM (http://www.dlr.de). The price of a 15' x 15' DEM tile is 400 euros multiplied by the individual tile filling (0…100%: ocean areas, lakes and data gaps are not taken into account for pricing).	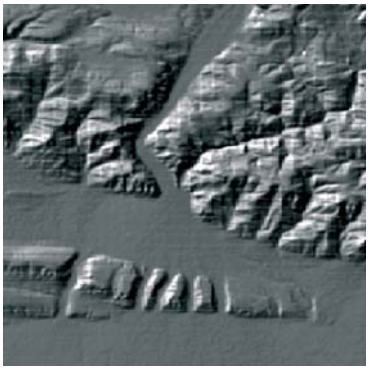
C. Landsat Satellite images (GLCF and Landsat TM) **Source:** http://glcf.umiacs.umd.edu/index.shtml **Description:** The University of Maryland's Global Land Cover Facility (GLCF) gives open source for Landsat TM and Landsat ETM satellite data. The site offers all Landsat TM bands and also a large number of the impressive enhanced (ETM) Landsat product which includes the 15m pan chromatic band, effectively doubling the maximum resolution of the images produced. The spectacular images are composed of Landsat TM bands 7, 4 and 2. These are not true colour images. Data are given in MRSID format that is readable in ArcMap (or in the free ArcExplorer). As said by Terrain map website, GLCF data archive represents the richest set of satellite imagery that exists anywhere.	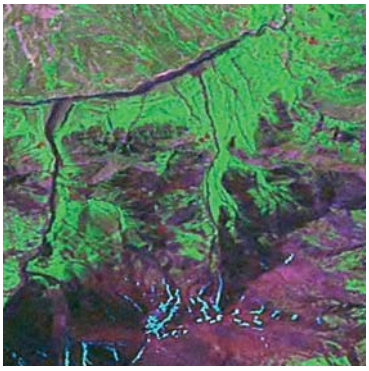
D. National Geospatial Intelligence Agency Places Names database **Source:** http://earth-info.nga.mil/gns/html/cntry_files.html **Description:** NGA (American National Geospatial-Intelligence Agency) GEOnet Names Server provides access to a database of foreign geographic feature names. The database is the official repository of foreign place name decisions approved by the U.S Board on Geographic Names. Approximately 20'000 of the database's features are updated monthly. **Vector Map Level 0 from the National Imagery and Mapping Agency (NIMA)** **Source:** http://geoengine.nga.mil/geospatial/SW_TOOLS/NIMAMUSE/webinter/ **Description:** The VMAP 0 (Vector Map Level 0) is an updated and improved version of the National Imagery and Mapping Agency's Digital Chart of the World. VMAP0 database provides worldwide coverage of vector-based geospatial data which can be viewed at 1:1'000'000 scale. It includes major road and rail networks, hydrologic drainage systems, utility networks, major airport, elevation contours, coastline, international boundary and populated places.	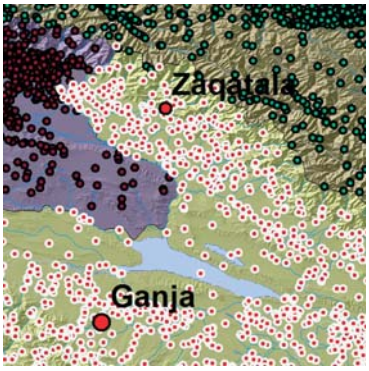

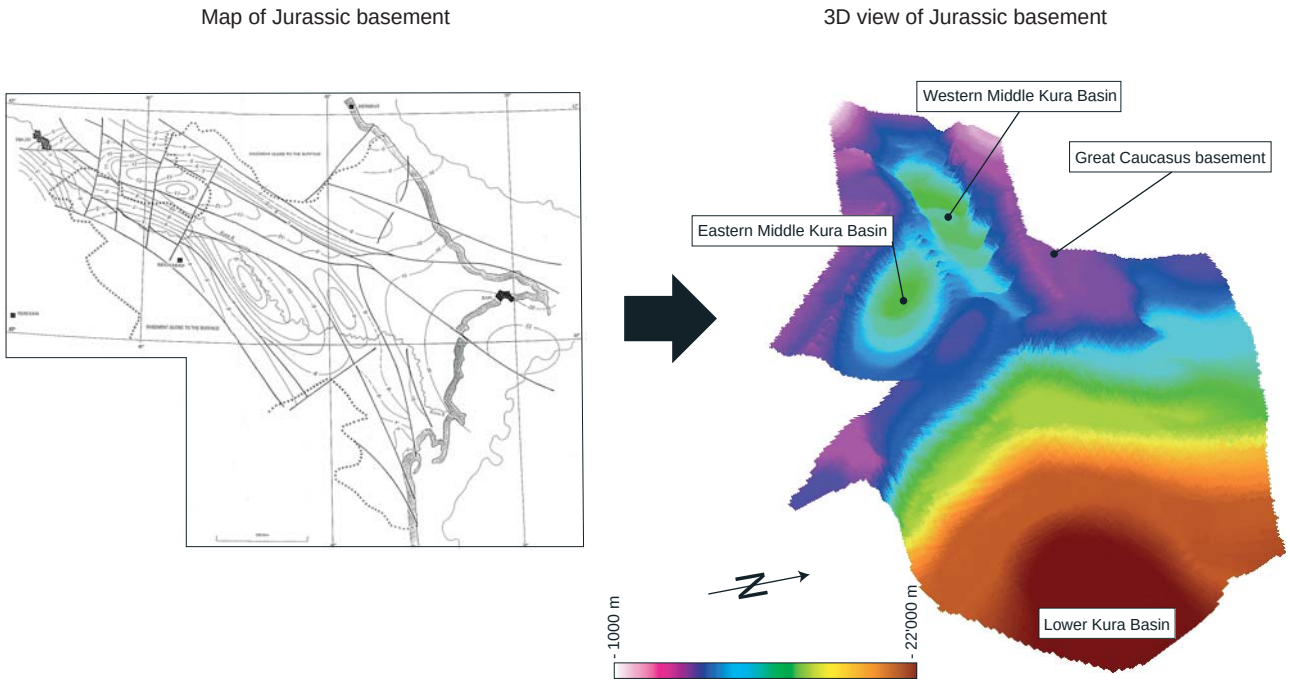

Figure 79: Building of a 3D model of the Jurassic Basement of the Kura Bassin based on a map

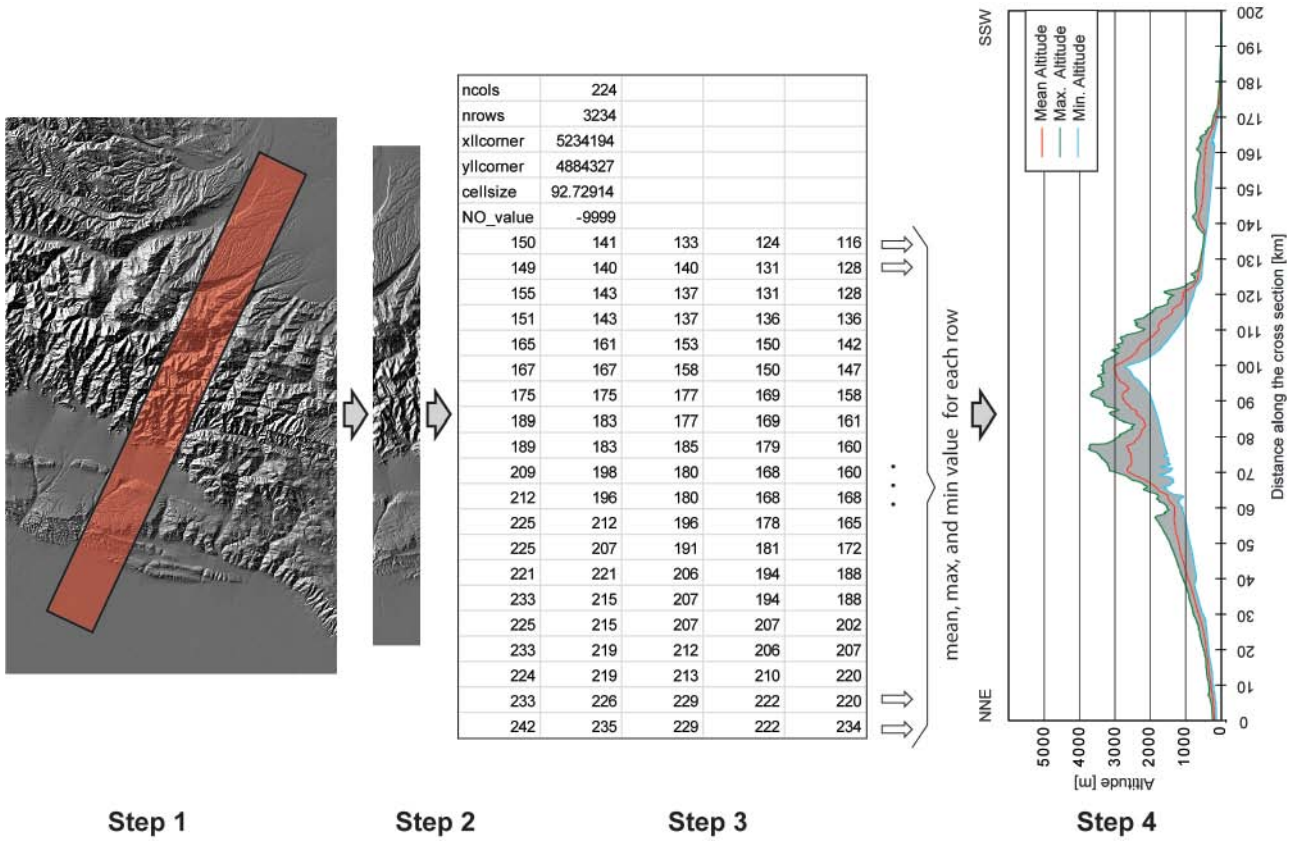

Figure 80: Method to obtains the maximum, minimum and mean topographic profile: (step 1) Defining a zone on the SRTM digital elevation model at 3'' (90 m) with, in this case, a width of 20 km and a length depending of the mountain width; (step 2) rotating the data to obtain a vertical or horizontal long side and extracting the data; (step 3) converting the data to a text file and importing them to a spreadsheet software allowing to calculate the maximum, minimum and mean value of each row; (step 4) creating a graph with the results.

tude profiles from a band with a width of 20 km and a length depending on the studied area (fig. 80).

To work in meter, the SRTM DEM is converted in a Mercator Projected coordinates system. As represented in figure 80, a rectangular area with a width of 20 km is selected on the DEM with the long side perpendicular to the main orogen direction. The area is then extracted and rotated to obtain a vertical long side for facilitating the analysis. The rotated rectangular area is exported as a text file and imported in spreadsheet software (i.e. Microsoft Excel®). Thus rows in the spreadsheet are parallel to the main orogen direction and minimum, maximum and mean altitude value for each row can be calculated and represented in an altitude – distance graph to compare visually the difference between the three calculated lines. The same work was done on a slope model calculated from the SRTM DEM and results were compared to the previous one. Results are in appendixes A3.1 and A3.2 and they are used in the chapter 5.

6.5.5. Accurate topographic measures

4 accurate topographical profiles of Qaramaryam hills were made with two high accuracy GPS to highlight an possible tectonic influence of a frontal thrust fault of the EGC on the topography.To reach an accuracy of less than 50 cm, the differential GPS measurements method was applied. Measurements were made with 2 Trimble GeoXH GPS receiver and their Zephir Antennas. The first GPS receiver was placed in one place and configured to measure continuously its positions. The second GPS receiver was mobile and it was moved through the hills. As there were no vegetation it was easy to walk straight along one direction. The GPS Correct Extension for ArcGIS (Trimble) allows correcting the data from the mobile GPS receiver with the data collected with the fixed one. As the absolute position of the fixed GPS is not known, the resulting accuracy is relative but as only the topographical shape is necessary for our study and not its absolute position, this small difference is not critical.

Results are in appendixes A3.2 and A3.3 and they are used in chapter 3 and 5.

6.5.6. River topographical profiles

13 rivers topographical profiles were built based on the DEM to emphasize tectonic influences on river profiles and combined with their estimated equilibrium profile. See appendix A3.4 for a description of the theory.

Results are in appendix A3.5 for 5 rivers of the northern slope and in appendix A3.6 for 6 rivers of the southern slope. They are used for helping to understand the general geodynamics of the area but a detailed study using them must be done.

6.5.7. River drainage patterns

We determined the drainage pattern data of 2 main river streams from the EGC northern slope (Qudiyalcay and Qusarcay rivers – fig. 81) and 1 main river from the EGC southern slope (Girdimancay River). For this study, approximatively 800 streams were drawn and their respective drainage data were determined. See appendix A3.4 for a theorical introduction.

Results for each river are combined with their respective topographical profiles: in appendix A3.7 for the rivers of the northern slope; in appendix A3.8 for the river of the southern slope. Statistics were also made on their length (app. A3.9) and on their level number (app. A3.10). As for the river profile, they are used for helping to understand the general geodynamics of the area but a detailed study using them must be done.

6.6. Conclusion

6-years' experience in field-work in remote areas of the Greater Caucasus have shown that the field computer and GPS handheld computer are rugged enough to tolerate difficult field conditions such as heat and shock as well as rain, or even short immersion in water.

Geographic Information System was the most used tool during this thesis from fieldwork to analyses. The data are stored in a way that they can be easily used by other. The data collected during this work are available on a DVD.

Based on field data and other data, numerous studies on geomorphology and geology have been made and allowed to make a link between topography and tectonics. The rapid uplift of the area and the fast eroding rocks make the EGC a very good laboratory for these methods. More precise data like 1" SRTM DEM could give better results.

GIS adds new perspectives for geological and geomorphological studies and become indispensable for geological study. The geographical parameters add a new dimension.

*****

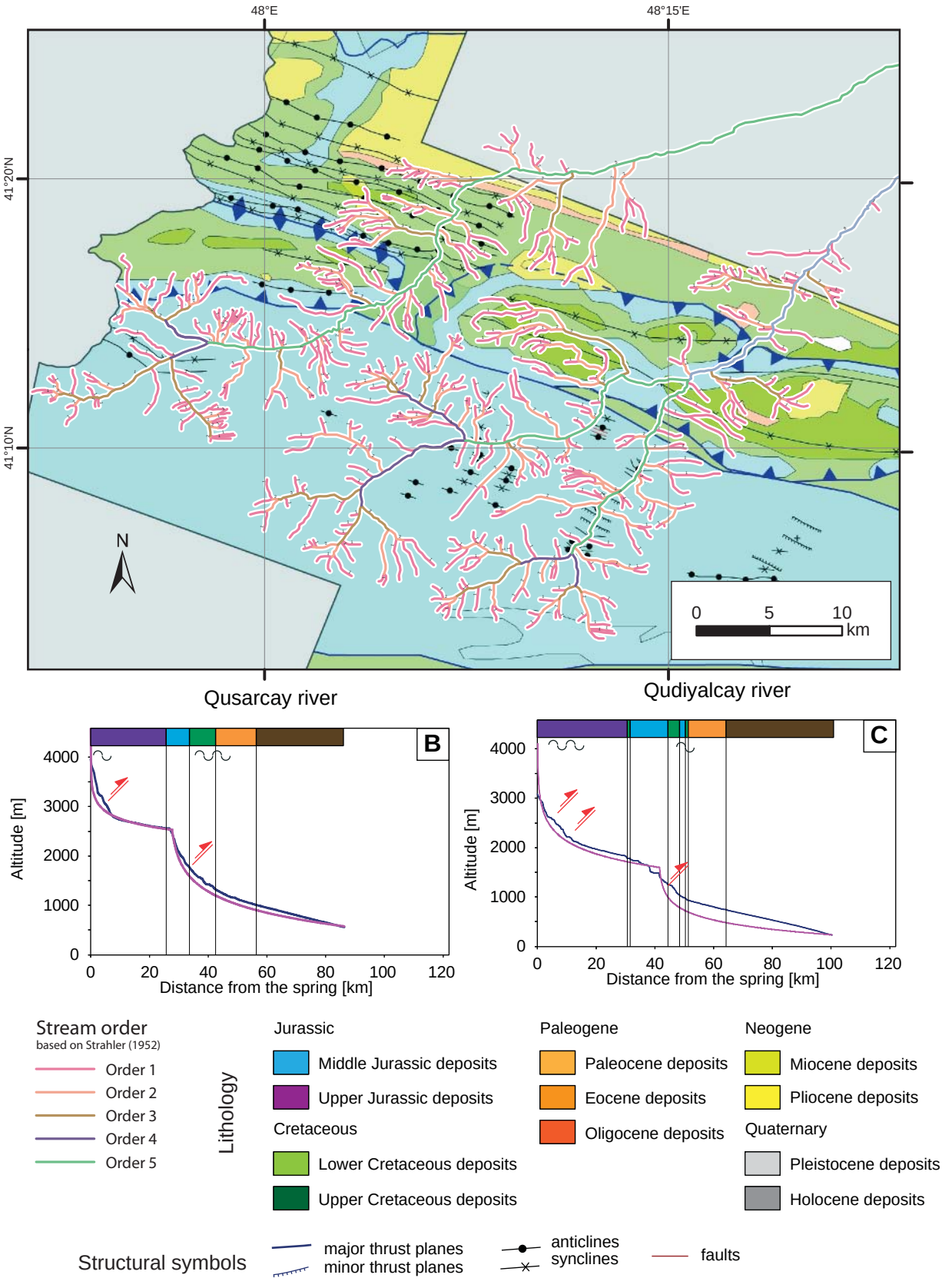

Figure 81: Drainage pattern and topographical analysis of two rivers from the northern slope.

7 - CONCLUSION

The Eastern Greater Caucasus (EGC) is located in the northern part of Azerbaijan. It is bordered by deep foreland basins, the Kura and Terek basins but also by the deep South Caspian Basin with a basement at a depth of 25 km. The area is also known since the antiquity for its hydrocarbon resources and its mud volcanoes. This particular context added to the high summits of its central area (Bazarduzu Mt. reaches 4466 m) made it interesting to study its geodynamic behaviour through the geological times. The eastern part of the Greater Caucasus started to build its present topography since Late Eocene. The climax of growth occurred during the Late Tertiary, starting in Middle Miocene and accelerating in Plio-Pleistocene.

The aims of this thesis were to first describe the geology and the evolution of the Eastern Greater Caucasus. Secondly, we detailed structural and geomorphological features of selected areas to determine a structural model for the EGC and to extend it to the Greater Caucasus. Finally we applied methods like Apatite Fission Track (AFT), Illite Crystallinity (IC) and subsidence curves to characterize the thermal evolution, the surface uplift and the exhumation of the area.

Lithologically, the EGC is mostly composed of sedimentary rocks. However, some intrusives can be observed on the southern slope. The core of the EGC is made of deep marine deposits of Middle Jurassic age. On the northern flank of the EGC, the deep marine Aalenian sediments lie under shallow marine and platform deposits from the Upper Jurassic and Lower Cretaceous. They are themselves eroded and covered by Paleocene to Quaternary sediments. The northern flank is also bordered by kilometric and massive limestone massifs (Sahdag Mt., Qizilqaya Massif, Cirax Mt and Besbarmaq Mt.) of Upper Jurassic and Lower Cretaceous. They lie on late Lower Cretaceous slope deposits. On the southern flank of the EGC marine slope deposits (turbidites) were deposited from the Lower Jurassic until at least the Middle Miocene. They are covered by alternating marine-continental deposits. Finally the foreland basins are filled with marine and continental deposits linked with the erosion of the growing Greater Caucasus.

7.1. BUILDING OF THE EGC

Field observation revealed several geological unconformities in different structural zones of the EGC. They helped to constrain several building phases.

The first observed unconformity occurred at the end of the Middle Jurassic (Callovian) in the Tahircal Zone (north of the EGC) where Callovian evaporites lie on folded deep marine Aalenian sediments. This folding and eroding phase can be associated to a compressive event that can be possibly correlated with the Mid-Cimmerian event described in northern Iran. The shallow-marine Callovian and Upper Jurassic sediments of the northern side of the EGC correspond to an uplift and a shallowing-up of the area.

Facies variations indicate that the basin was deeper in the south and in the east at the end of Upper Jurassic and beginning of Lower Cretaceous.

In the east, Berriasian conglomerates are deposited on folded Kimmeridgian deposits indicating a compressional event at the end of the Upper Jurassic.

The youngest rocks on which the northern Sahdag-Besbarmaq Nappe lies are of Barremian age. Consequently the setting-up of the nappe must be at the end of the Lower Cretaceous but, there is no other indication for a compression phase at this period. All deposits at the end of the Lower Cretaceous correspond to slope deposit (i.e flysch and presence of olistostromes). We propose that the Sahdag-Besbarmaq Nappe is a kilometric olistostrome sliding in a marine basin in a passive

margin context. Numerous smaller olistostromes can be found along the northern slope of the EGC.

In the east, near Xizi, a transgression of Turonian conglomerate deposits on folded Albian-Aptian sediments can be seen. This transgression is also present in the Sahdag area but with deeper sediment on top corresponding to slope deposits.

A regional uplift at the end of the Cretaceous and beginning of the Paleocene can be observed in the northern area. This period corresponds to the very first beginnings of the building of the Caucasus that definitively started during the Eocene-Oligocene when the Arabian plate collided with the Eurasian plate. The beginning was mostly caracterized by the formation of deep foreland basins filled with erosional products of the new orogen.

During the Miocene-Pliocene, the EGC area was characterized by low reliefs with local piggy back basins and numerous eustatic sea level variations. We sampled in the northern slope shallow marine deposits of the Middle Miocene on the Sahdag Mountain at an altitude of 3550m. There are also Pliocene sediments at an altitude of 2000 m near Buduq indicating a major orogenic event with a main uplift since the Pliocene.

7.2. EGC Structural Model

Based on our fieldwork and interpretation of our data we can discriminate 3 major structural features. They allow us to propose a general structural model for the EGC.

Overall in the EGC, structures trend WNW-ESE and are made of intermediate and large scale folds frequently fault related and locally associated with an axial plane parallel to rock cleavage.

A second group of structures are regional scale thrusts. They can be divided in two families: the first dips to the NNE with top to SSW movement and is mainly present in the south; the second dips to the SSW with top to the NNE movement and is mostly present in the north. The change of dip direction occurs in the central zone.

The third group of structures corresponds to strike-slip faults which can be subdivided in two sub-groups: dextral strike-slip faults with a NNW-SSE direction and sinistral strike-slip faults with a NNE-SSE direction. They are commonly named anticaucasian faults and are acting on the EGC at least since Plio-Quaternary time because of their great influence on the present geomorphology of the area.

A NNE-SSW compression stress can be associated with all these structures. It corresponds to the general movement of the Arabia-Eurasia convergence.

7.3. EGC surface uplift

In the Eastern Greater Caucasus we determined uplift rate of 0.31 mm/yr since the Sarmatian (~11.6 Myr) and of 0.77 mm/yr since the Pliocene (2.6 Myr). These rates are based on marine deposits in altitude.

Studies about the central part of the Greater Caucasus in Georgia and Russia determined surface uplift up to 10-12 mm/yr based in river incision since the last glaciations. Compared to our result in the EGC, this fast uplift remains questionable and needs to be confirmed.

Moreover, AFT and IC studies indicate that the exhumation was slower and longer in the central zone than in the northen area. The northern area (Tahircal-Sudur Zone and Sahdag Besbarmaq Nappe) underwent a fast exhumation since the Middle Miocene. The Tufan Zone underwent a longer and steady exhumation since at least the beginning of the Miocene that finally created the highest summits of Azerbaijan. The exhumation rate is certainly faster than 1mm/yr in the north (Tahircal Z.).

Based on AFT ages of pebbles composing Pliocene conglomerates, we concluded an eastward propagation of the main uplift.

7.4. Thermal evolution

During field work, we observed only a weak schistosity that develops in the central part. It corresponds to a low-grade metamorphism and develops in favorable lithologies.

Based on IC Index analyses, we observe a southwestward increase of metamorphism from the northern orogenic front (Samur River) to the central part of the EGC and a ESE decrease of metamorphism along the main EGC crest (along the line from the Bazarduzu Mt. to the Abseron Peninsula).

Both AFT t-T models and subsidence curves confirm a fast burial during the Middle Jurassic and Lower Cretaceous periods and a fast exhumation that started between Miocene and Quaternary. Data indicate that the northern area has a more complex behaviour than the central area: the initial burial is followed by an intermediate exhumation that lasts during the Upper Cretaceous and Paleogene. Afterwards, a burial acted

on the area since the beginning of Miocene and was finally followed by the main and recent exhumation.

7.5. Structure in the Greater Caucasus

Combining our structural and geomorphological study in the EGC with literature and GIS study on the other region of the Greater Caucasus, we expand our findings to the whole Greater Caucasus.

The Main Caucasus Thrust (MCT) is a discrete major thrust that crosses the whole Greater Caucasus from west to east. In Azerbaijan and towards the shore of the Caspian Sea the MCT splits into several fault strings and thrusting of both top to the north and top to the south is observed. The zone of highest topography is bound to the south by the MCT which shows important top to the south movement. To the north this zone is bound by south dipping thrusts with top to the north movement. Detailed structural studies of the EGC and the Dagestan Fold and Thrust Belt (FTB) suggest that this N-verging back-thrusting is linked to a thrust ramp system. Thus the zone of highest uplift forms a triangular shaped domain limited to the south by the MCT and to the north by back-thrusts. This triangular zone of fast uplift and its associated major topographic/tectonic features can be correlated across the whole Greater Caucasus. Uplift over such a more or less steep ramp system may also explain why we observe such important uplift in a rather restricted area.

The migration of the MCT to the south during Tertiary formed successive active thrusts that were subsequently abandoned to form relic thrust fronts. This resulted in the south of the Greater Caucasus in succesive foreland basins separated by clear changes in topography, deviation of rivers and water gaps.

A difference in the geodynamic behaviour between the east and west Greater Caucasus area is due to several factors such as the E to W decreasing plate convergence rate but the inherited structure certainly plays a major role. The basement units outcrop only in the west and are not observed to the east and this difference can induce a different behaviour during the orogen. Moreover the recent magmatic activity in the central and western part of the Greater Caucasus (Kasbek and Elbrus area) may suggest a difference in the crustal or whole lithosphere structure that contributed to a different evolution between the eastern and western regions.

Clear links between geomorphology, seismicity and tectonics can be observed in the Greater Caucasus. The Eastern Greater Caucasus appears to be active at present and numerous geomorphological features linked with the tectonics behaviour of the area can be observed.

*****

APPENDIXES

APPENDIX 1 - PT STRESS ANALYSES

The following stereonets are the result of the Pt axes calculation of the software Tectonic FP and are complementary to the data calculated with the dihedra method (figs. 44-1 and 44-2). The source data are represented on figures 40-1 and 40-2. Stereonets are located on the figure 43.

1. Middle Tahircal Valley (N=15)

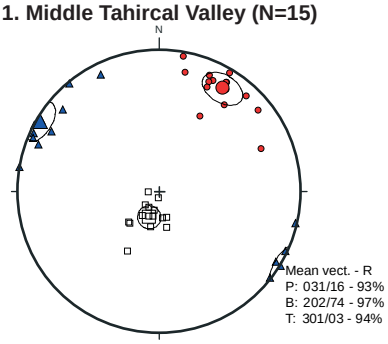

2. Laza Village (N=50)

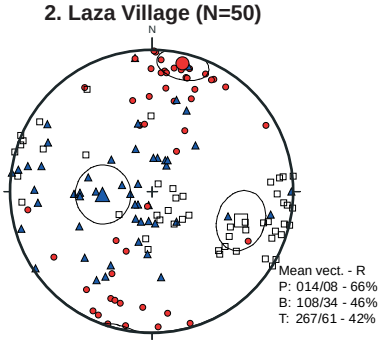

3. Tanga Alti Canyon (N=7)

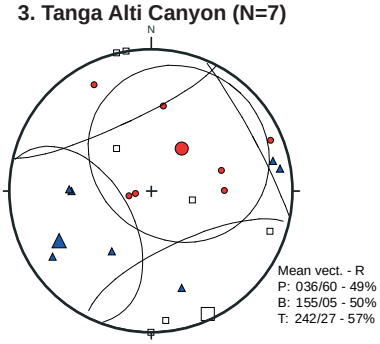

4. Base of Sahdag Nappe (N=30)

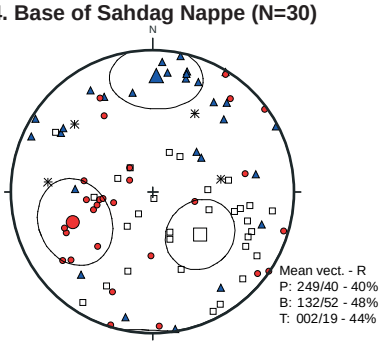

5. K1 on Sahdag Mt. (N=18)

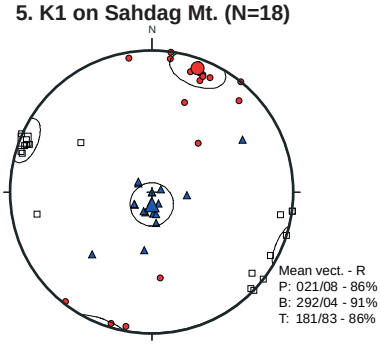

6. Sahdag Mt. Summit (N=11)

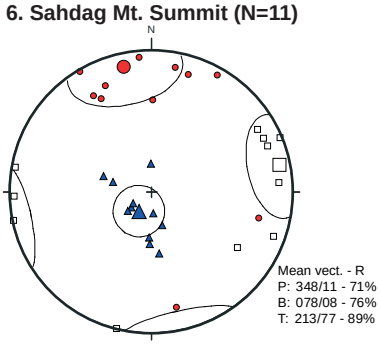

7. Qizilqaya Massif (N=18)

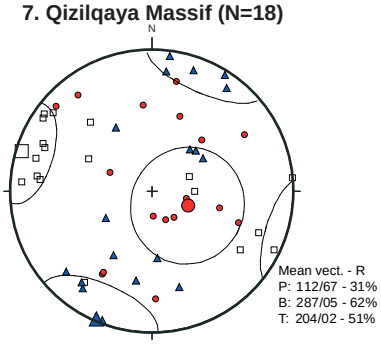

8. J3 Nappe of Cek Village (N=36)

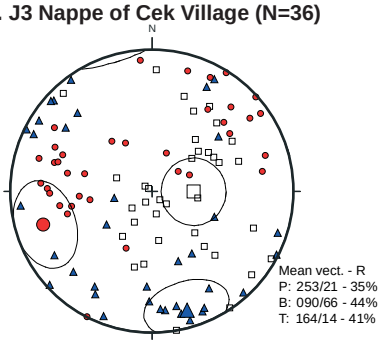

9. Cloudcatcher Canyon (N=10)

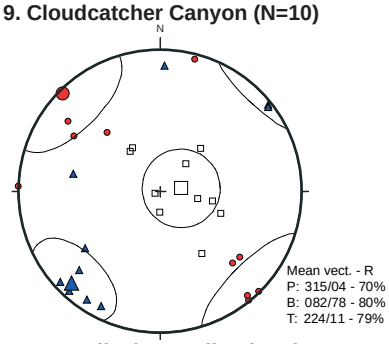

10. Nappe in Sahnabad Plain (N=64)

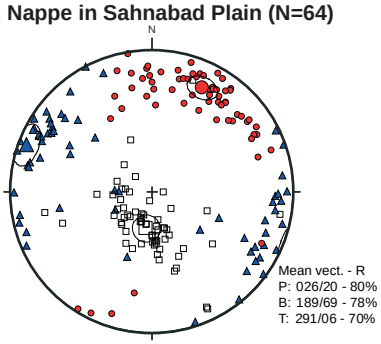

11. Small klippe in J2 deposit (N=29)

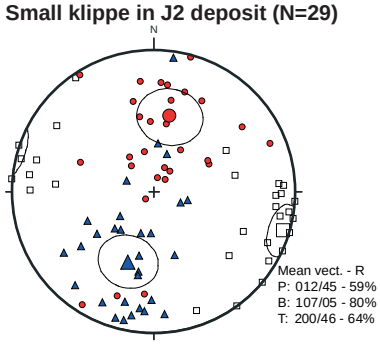

12. Qudiyalcay Valley (N=6)

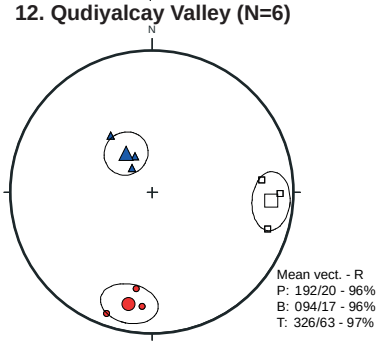

13. Hapit-Cek Valley (N=6)

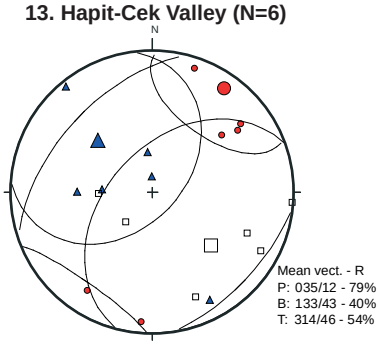

14. Yerfi Village (N=13)

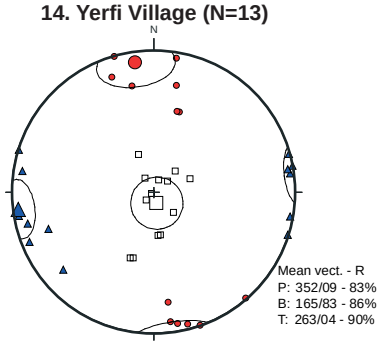

15. Cimicay River - Istisu (N=6)

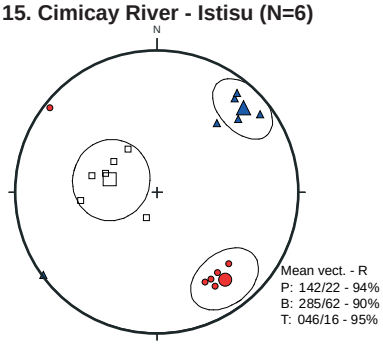

16. Gilgilcay River (N=9)

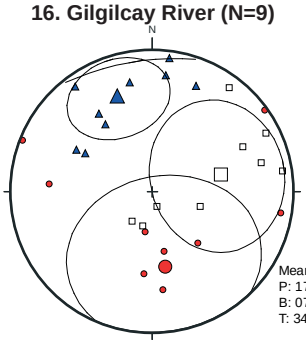

17. South of Qonaqkand Vill. (N=14)

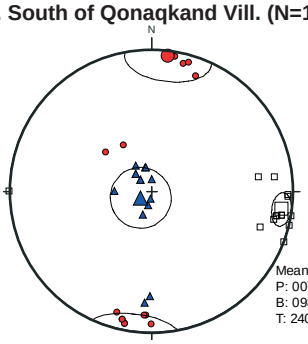

18. North of Babadag Valley (N=8)

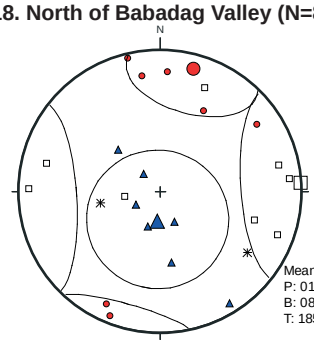

19. North of Tchötzarat Valley (N=14)

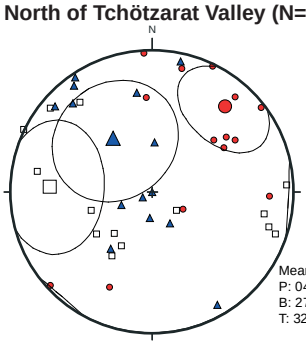

20. South of Tchötzarat Valley (N=12)

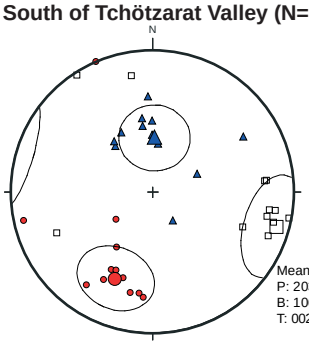

21. North of Març Valley (N=10)

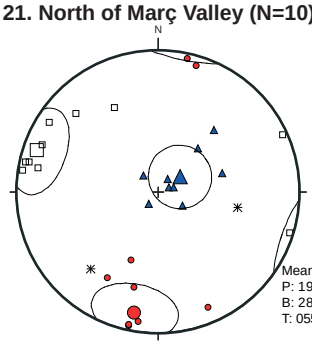

22. South of Març Valley (N=12)

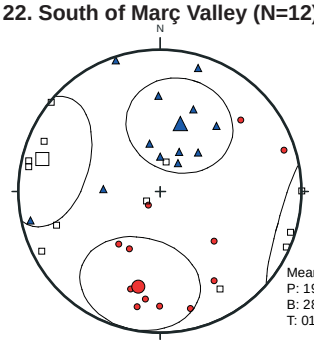

23. North of Molalar Valley (N=9)

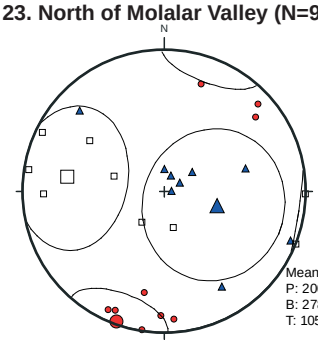

24. South of Molalar Valley (N=6)

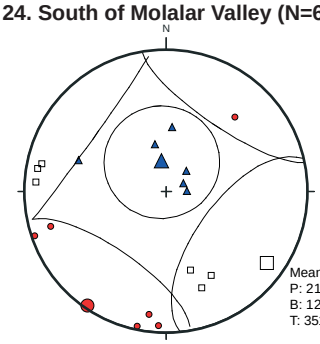

25. Lahic Canyon (N=17)

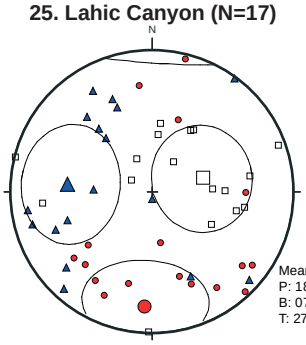

26. Candov Village (N=15)

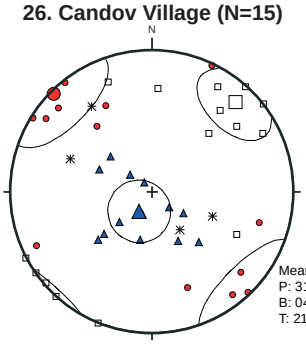

27. Qalaciq Village (N=2)

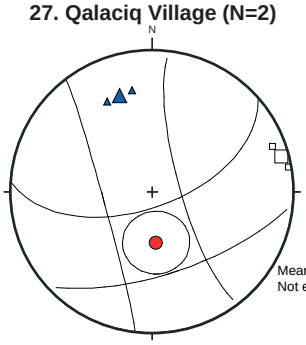

28. Vandam Zone near Qalaciq (N=11)

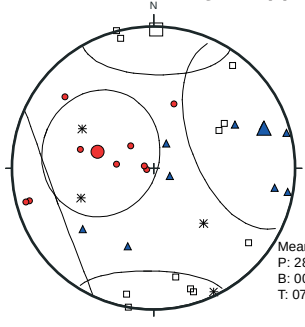

29. Vandam Zone near Vasa (N=7)

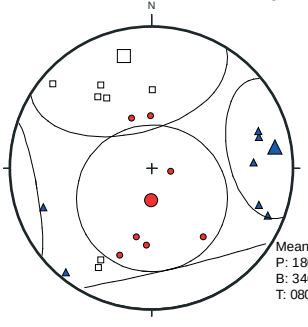

Schmidt equal area stereoplot
Lower hemisphere projection

P-Axes

T-Axes

B-Axes

APPENDIX 2 - ILLITE CRYSTALLINITY AND ORGANIC MATTER ANALYSES

A2.1. RESULTS OF IC ANALYSES MADE IN 2008 AT THE CENTRE SCIENTIFIQUE ET TECHNIQUE JEAN-FÉGER FROM THE TOTAL COMPANY IN PAU (FRANCE)

Sampling : T. Kissner – O. Kraft – U. A. Glasmacher - M. Bochud (2007)
Sample preparation : F. Champion (2008) – CSJF
Sample Analysis : M. Berut (2008) – CSJF

Sample	Altitude	POSITION [deg]			HEIGHT [cps]						FWHM [2th]		
		Chlorite	I/S R1	Illite	Chlorite		I/S R1		Illite		Chlorite	I/S R1	Illite
					k-a1	k-a2	k-a1	k-a2	k-a1	k-a2			
AZ159	**2224 m**	14.17	-	10.03	3.63	1.86	-	-	11.83	6.04	0.35	-	**0.42**
AZ161	**2074 m**	14.18	-	10.01	6.48	3.31	-	-	22.08	11.27	0.34	-	**0.47**
AZ163	**3313 m**	14.26	-	10.01	5.33	2.72	-	-	23.21	11.85	0.44	-	**0.71**
AZ165	**3063 m**	14.24	10.62	10.04	3.73	1.90	2.99	1.53	9.53	4.87	0.45	0.89	**0.52**
AZ167	**2877 m**	14.27	-	10.03	4.29	2.19	-	-	20.69	10.56	0.46	-	**0.78**
AZ169	**2641 m**	14.22	-	10.02	4.19	2.14	-	-	20.79	10.61	0.43	-	**0.74**
AZ171	**2200 m**	14.22	10.54	10.03	6.32	3.22	4.90	2.50	20.83	10.63	0.44	0.80	**0.54**
AZ173	**2141 m**	14.24	10.61	10.06	2.91	1.49	2.78	1.42	15.15	7.73	0.39	0.85	**0.57**
AZ175	**2761 m**	14.35	10.53	10.00	15.81	8.07	11.04	5.63	12.22	6.24	0.55	2.04	**0.37**
AZ176	**2547 m**	13.34	10.57	10.01	9.86	5.03	7.50	3.83	8.25	4.21	0.55	1.81	**0.38**
AZ177	**2398 m**	14.35	10.64	10.01	10.15	5.18	8.63	4.41	10.19	5.20	0.55	1.86	**0.41**
AZ180	**2212 m**	14.34	10.47	10.01	9.81	5.01	8.81	4.49	9.73	4.97	0.53	1.62	**0.38**
AT182	**2450 m**	14.34	10.24	9.98	6.76	3.45	8.15	4.16	4.51	2.30	0.51	1.61	**0.33**
AZ184	**2186 m**	14.27	10.42	10.01	5.52	2.82	9.43	4.82	7.51	3.83	0.46	1.55	**0.36**
AZ186	**2067 m**	14.22	10.41	10.03	6.34	3.23	13.84	7.06	11.48	5.86	0.39	1.49	**0.33**
AZ191	**1826 m**	14.22	10.25	10.01	5.00	2.55	17.74	9.06	9.53	4.87	0.38	1.39	**0.30**
AZ193	**2000 m**	14.23	10.66	10.06	4.17	2.13	4.71	2.40	19.85	10.13	0.42	0.94	**0.65**
AZ195	**1893 m**	14.23	-	10.05	2.11	1.08	-	-	12.79	6.53	0.38	-	**0.58**
AZ199	**1384 m**	14.22	10.65	10.03	1.98	1.01	5.68	2.90	9.81	5.01	0.34	1.10	**0.53**
AZ201	**1314 m**	14.43	10.43	10.26	18.44	9.41	13.68	6.98	12.56	6.41	0.49	1.50	**0.34**
AZ203	**1293 m**	14.18	11.02	10.02	7.94	4.05	16.60	8.47	20.07	10.24	0.52	1.44	**0.68**
AZ205	**1321 m**	14.15	10.66	9.99	4.16	2.12	7.03	3.59	7.47	3.81	0.41	1.57	**0.35**

A2.2. RESULTS OF IC ANALYSES MADE IN 2007 AT THE UNIVERSITY OF NEUCHÂTEL (SWITZERLAND)

Sampling : A. Rast and M. Bochud (2006) – University of Fribourg
Sample preparation : A. Rast (2006-2007) – University of Fribourg
Sample Analysis : Dr. Thierry Adatte (2007) - University of Lausanne

									5.2°	6.2°	8.8-8.9°	9.1-9.5°	12.3-12.4	17.7-17.8°	18.4°	20.85°	24.8-24.9°	25.1-25.2°	45° (2N)											
N° échantillon	N° GEA	Age litho	Lat	Long	Altitude	Sample Size	NE-SW [km]	Dév.	SM001	C001	M001	IS	K001 + C002	M002	C003	Qtz	Kaol	C004	M005	IC (2N) cm	IC (2N) deg	IC (2G) cm	IC (2G) deg	% IS	% SM001	% M001	%K001 *	% C002*	k001*	C002*
AZ079	0435	K2	41.22722	48.15077	3470 m	<2µm	25.4	0.16	115.55	0	249.25	20.23	0	97.77	0	0	0	0	45.93	0.28	0.61	0.11	0.24	5.25	30.01	64.74	0.00	0.00	0.00	0.00
AZ081	0436	K1br	41.19564	48.21297	1980 m	<2µm	26.2	-0.11	0	0	173.28	0	110.3	98.03	0	74.43	94.5	151.08	52.3	0.1	0.22	0.09	0.20	0.00	0.00	61.10	14.97	23.93	42.44	67.86
AZ084	0442	J2a	41.33986	48.15618	1200 m	<2µm	13.4	0.2	498.33	366.1	664.78	95	706.1	17.64	0	0	479.43	463.05	315.4	0.51	1.11	0.18	0.39	4.84	25.37	33.84	18.29	17.66	359.19	346.91
AZ089	0443	J2a	41.23285	48.06897	3080 m	<2µm	27.6	0.09	0	81.1	136.1	0	373.22	0	0	0	279.77	105	32.77	0.17	0.37	0.1	0.22	0.00	0.00	26.72	53.28	20.00	271.37	101.85
AZ091	0444	J2a	41.23344	47.90098	3947 m	<2µm	33.4	-0.01	0	118.92	166.15	0	632.28	45.05	70.55	0	0	265.93	22.95	0.16	0.35	0.1	0.22	0.00	0.00	20.81	0.00	79.19	0.00	632.28
AZ092	0445	J2a	41.23085	47.90223	3805 m	<2µm	33.8	0.13	0	96.1	104.53	0	420.03	0	51.67	0	0	214.32	0	0.1	0.22	0.12	0.26	0.00	0.00	19.93	0.00	80.07	0.00	420.03
AZ093	0446	J2a	41.22879	47.90676	3629 m	<2µm	34	0.1	0	71.08	103.13	18	403.43	56.67	72.22	52.22	0	216.48	0	0.19	0.41	0.09	0.20	3.43	0.00	19.66	0.00	76.91	0.00	403.43
AZ094	0447	J2a	41.22662	47.9111	3477 m	<2µm	34.2	-0.2	0	0	63.88	0	47.33	0	0	0	60.55	0	38.33	0.19	0.41	0.18	0.39	0.00	0.00	57.44	42.56	0.00	47.33	0.00
AZ095	0448	J2a	41.22428	47.92861	2834 m	<2µm	33.6	0.26	0	119.8	325.48	18	548.57	107.45	68.88	0	0	240.8	56.1	0.13	0.28	0.1	0.22	2.02	0.00	36.49	0.00	61.50	0.00	548.57
AZ098	0437	K1	41.27227	48.05244	3200 m	<2µm	24	0.27	0	0	181.1	0	86.67	99.42	0	0	0	0	60	0.17	0.37	0.5	1.09	0.00	0.00	100.00	0.00	0.00	0.00	0.00
AZ101	0438	K2	41.27506	48.03913	3324 m	<2µm	24.2	0.16	227.77	0	172.97	0	79.43	81.67	0	0	0	53.33	55.55	0.15	0.33	0.12	0.26	0.00	47.44	36.02	0.00	16.54	0.00	79.43
AZ102	0439	K2	41.27478	48.03881	3332 m	<2µm	24.4	0.05	72.77	69.43	280.55	89.43	0	78.33	0	0	0	0	59.43	0.45	0.98	0.26	0.57	20.20	16.44	63.37	0.00	0.00	0.00	0.00
AZ103	0440	K2	41.27437	48.03613	3411 m	<2µm	24.6	0.19	0	0	203.63	35.5	66.67	57.78	0	0	0	65	39.75	0.29	0.63	0.16	0.35	11.61	0.00	66.59	0.00	21.80	0.00	66.67
AZ105	0441	K2	41.27272	48.03405	3450 m	<2µm	24.8	0.06	98.88	60.25	116.67	10	0	0	0	0	0	0	0	0.19	0.41	0.07	0.15	4.43	43.84	51.73	0.00	0.00	0.00	0.00
AZ107	0449	J2a	41.42188	48.06016	1048 m	<2µm	8		28	37	117	0	497	47	15	0	511	135	58.33	0.08	0.17	0.09	0.20	0.00	4.36	18.22	61.24	16.18	393.14	103.86
AZ108	0450	J2a	41.43102	48.0664	963 m	<2µm	7	0.1	0	107.22	284.28	37	609.53	84.93	0	0	452.97	142.75	101.92	0.09	0.18	0.1	0.20	3.98	0.00	30.54	49.79	15.69	463.47	146.06
AZ109	0451	J2a	41.43801	48.07161	954 m	<2µm	6	0.1	0	55.83	151.03	0	623.52	55.55	0	0	477.63	18.28	37.22	0.19	0.39	0.11	0.22	0.00	0.00	19.50	77.53	2.97	600.54	22.98
AZ110	0452	J2a	41.44228	48.07692	862 m	<2µm	5.4	0.03	0	92.77	163.73	26	937.22	0	0	0	623.62	279.97	49.43	0.15	0.31	0.13	0.27	2.31	0.00	14.53	57.40	25.77	646.83	290.39
AZ111	0453	J2a	41.45288	48.08581	807 m	<2µm	3.8	0.07	0	66.1	160.72	28	148.77	0	0	0	62.78	95.47	31.67	0.24	0.52	0.24	0.52	8.30	0.00	47.62	17.49	26.59	59.02	89.75
AZ112	0454	J2a	41.46963	48.09452	735 m	<2µm	1.8	0.09	0	0	296.15	42	1332.77	129.82	0	0	907.83	447.2	65.98	0.58	0.97	0.63	1.05	2.51	0.00	17.72	53.44	26.32	892.92	439.85
AZ113	0455	J2a	41.47114	48.09556	725 m	<2µm	1.6	0.07	0	108.33	175.6	0	482.2	70.55	0	87.22	147.4	223.87	53.33	0.27	0.59	0.18	0.39	0.00	0.00	26.70	29.10	44.20	191.44	290.76
AZ114	0456	J2a	41.47814	48.09918	700 m	<2µm	0.8	-0.08	0	0	89.33	0	685.32	0	0	0	721.1	156.23	56.1	0.06	0.13	0.07	0.15	0.00	0.00	11.53	72.71	15.75	563.28	122.04
AZ115	0457	J2a	41.48418	48.10333	668 m	<2µm	0	0.05	0	47.77	65.48	0	324.63	0	0	48.88	239.8	71.12	0	0.16	0.35	0.13	0.28	0.00	0.00	16.79	64.18	19.03	250.37	74.26

: Données valides (M001>150) mais origine détritique (IC < 0.33 mais toujours présence de kaolinite ou smectite)

: Données valide (M001 >150)

: données non valides (M001<150)

A2.3. Organic Matter analysis

Organic matter analyses are used in this study to determine the maturity of the organic matter of each sample to evaluate the maximum temperature it reached and to correlate it with the diagenesis zones. Pyrolysis analyses were made based on the Rock Eval method described by Espitalié et al. (1977), Tissot & Welte (1978), and others.

As described by Pimmel & Claypool (2001), the Rock Eval pyrolysis method consists to heat in a pyrolysis oven ~100 mg of a sample with a programmed temperature in an inert atmosphere (helium). For each sample, the method allows determining quantitively and selectively the free hydrocarbons, the hydrocarbon and oxygen compounds (CO_2) that are volatilized during the cracking of the unextractable organic matter (kerogen) (Figure 82).

The parameters obtained for each sample by pyrolysis are (Tissot & Welte 1978):

- S_1 corresponds to the amount of free hydrocarbon (gas and oil) in mg per gram of rock. If S1>1 mg/g, it is indicative of oil presence. S1 normally increases with depth.

- S_2 corresponds to the amount of hydrocarbon generated by thermal cracking of kerogen (non-volatile hydrocarbon). It is an indication of the potential quantity of hydrocarbon that a rock can produce if burial and exhumation continue. S2 normally decreases with burial depths of more than 1 km.

- S_3 corresponds to the amount of CO_2 in mg of CO_2 per gram of rock that is produced during the pyrolysis of kerogen. It is an indication of the amount of oxygen in kerogen and is used to calculate the oxygen index. Contamination of the samples should be suspected if there is some abnormally high values are obtained. High S3 value can also be expected in rock with high concentrations of carbonate that break down at temperature <390°.

- Tmax corresponds to the temperature at which the cracking of kerogen during pyrolysis releases the maximum quantity of hydrocarbons. It corresponds to the top of S2 peak. Tmax is related to the stage of maturation of the organic matter. Tmax range of 400°-430°C represents immature organic matter; Tmax of 435°-450°C represents mature or oil zone; Tmax > 450°C represents the overmature zone.

- TOC corresponds to the total organic matter. It is determined by oxidizing the organic matter remaining after the pyrolysis (residual organic carbon and then adding it to the pyrolyzed organic carbon (measured from the hydrocarbon compound issued from pyrolysis).

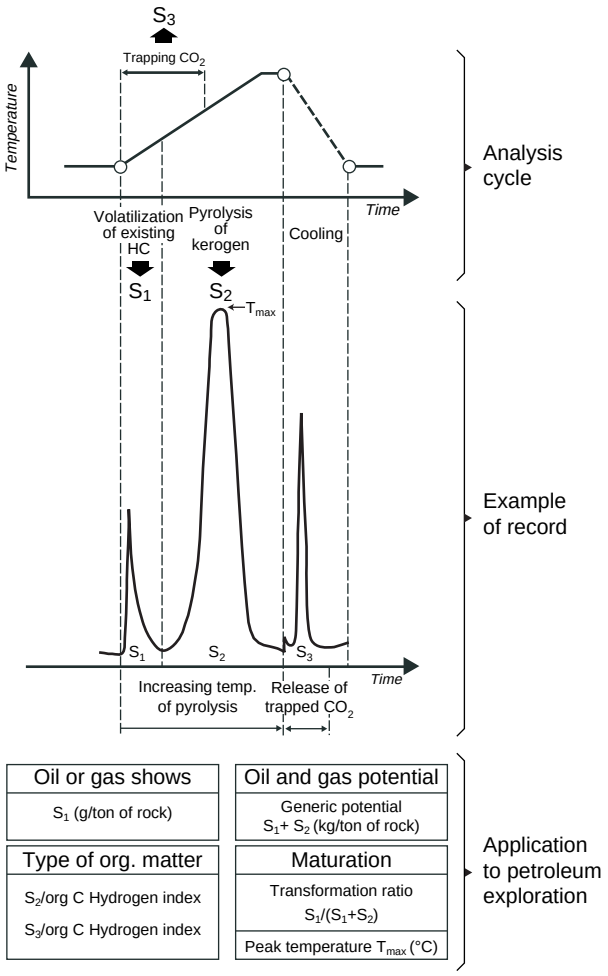

Figure 82: Example of Rock Eval trace. HC = hydrocarbon (modified from TISSOT & WELT, 1978).

Based on these parameters, several indexes can be calculated like the Hydrogen Index (HI = 100xS_2/TOC, the Oxygen Index (100xS_3/TOC), the Production Index (PI=S_1/[S_1+S_2]) and the pyrolyzable carbon Index (PC=0.083x[S_1+S_2]). Three of them are not interesting for this study: HI and OI allow characterizing the origin and the type of organic matter and PC corresponds to the carbon content of hydrocarbons volatilized and pyrolyzed during the analysis. Some graph combining HI and OI allow defining the maturity of the organic matter (Kerogen type). The Production Index is used to characterize the evolution level of the organic matter and could be linked with the depth and the temperature to which the sample was submitted during its evolution.

Sampling

It is the same samples that were analysed for the illite crystallinity.

Analysing

Organic Matter analyses were made in the same laboratory that made the illite crystallinity analyses: University of Neuchâtel and Centre Scientifique et Technique Jean-Féger (CSTJF) of the Total Company in Pau (France). They both use the Rock Eval 6 apparatus respectively with 100 mg and 80 mg of rock for each analysis.

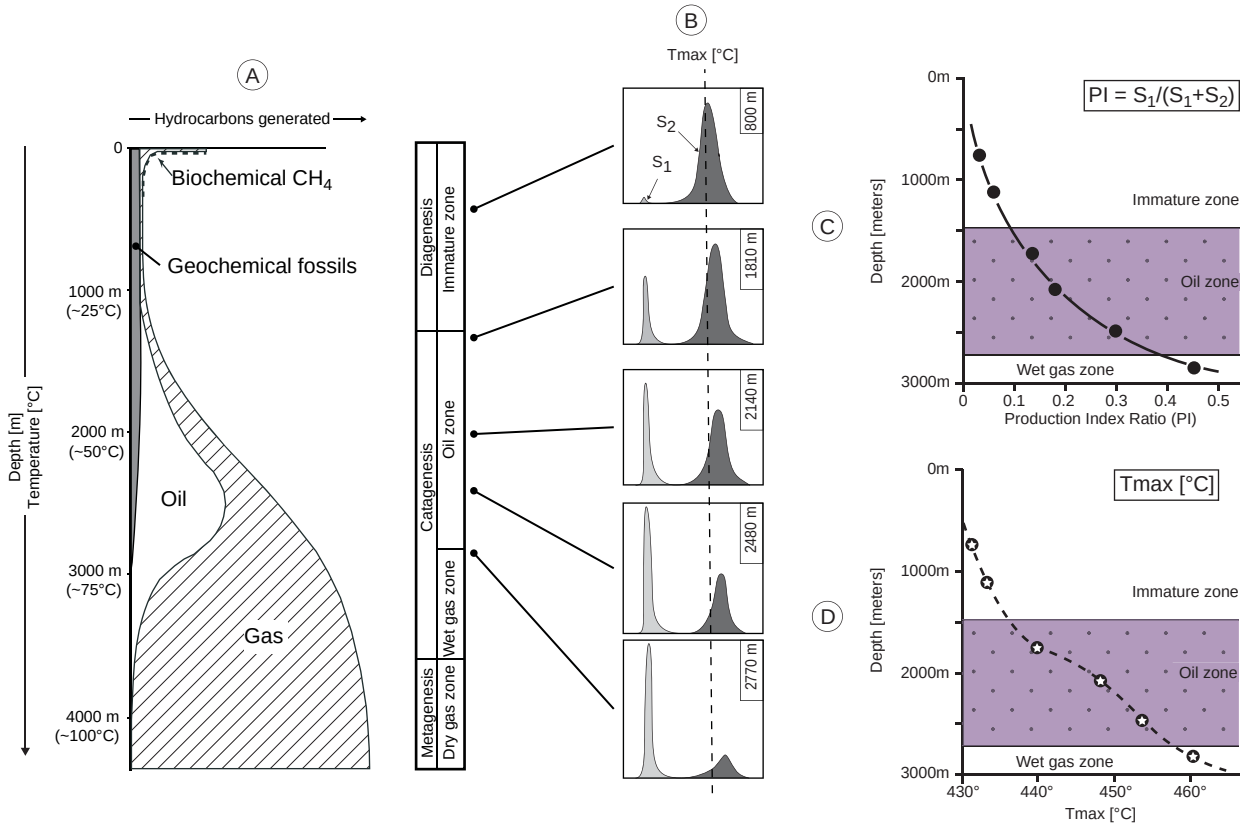

Figure 83: (A) General scheme of hydrocarbon formation as a function of burial of the source rock, depths are only indicative and correspond to an average on Mesozoic and Paleozoic source rocks, temperature are based on the average geothermal gradient of 25°C/km (modified from TISSOT & WELT, 1978); (B), (C), (D) correspond to an example of rapid characterization with pyrolysis of the evolution degree of sources rocks from a core in sedimentary deposits of Tertiary Age (modified from ESPITALIÉ et al., 1977).

A2.4. RESULTS OF ORGANIC MATTER ANALYSES MADE IN 2008 AT THE CSJF FROM THE TOTAL COMPANY IN PAU (FRANCE)

Sampling: T. Kissner – O. Kraft – U. A. Glasmacher - M. Bochud (2007)
Sample preparation: F. Champion (2008) - CSJF
Sample Analysis: M. Berut (2008) – CSJF
Method: Rockeval 6 Turbo (Pyrolysis method)

Sample	Lab.	Litho age	Lat	Long	Alti	Tmax	S1	S2	S3	TOC
			WGS 84 [Deg]		[m]	[°C]	[mg HC/g)	[mg HC/g)	[mg CO_2 /g]	[%]
AZ159	Total	J2a	41.14913	48.06697	2224 m	-	0.00	0.02		1.31
AZ161	Total	J2a	41.16219	48.08878	2074 m	-	0.00	0.02		1.12
AZ163	Total	J2a	41.14270	48.11435	3313 m	-	0.01	0.03		0.58
AZ165	Total	J2a	41.14504	48.12237	3063 m	-	0.00	0.02		0.49
AZ167	Total	J2a	41.14738	48.12361	2877 m	-	0.01	0.03		0.61
AZ169	Total	J2a	41.15259	48.12288	2641 m	-	0.01	0.06		0.86
AZ171	Total	J2a	41.16120	48.12101	2200 m	-	0.00	0.04		0.87
AZ173	Total	J2a	41.16308	48.12174	2141 m	-	0.00	0.06		0.85
AZ175	Total	J2a	41.20128	48.12609	2761 m	-	0.00	0.04		0.26
AZ176	Total	J2a	41.19646	48.12750	2547 m	448	0.01	0.18	0.2891	0.49
AZ177	Total	J2a	41.19200	48.12932	2398 m	449	0.01	0.14	0.376	0.4
AZ180	Total	J2a	41.18380	48.12786	2212 m	470	0.03	0.25	0.2624	0.64
AZ182	Total	J2a	41.20677	48.07617	2450 m	460	0.05	0.29	0.2573	0.83
AZ184	Total	J2a	41.19199	48.09864	2186 m	474	0.05	0.3	0.1848	0.77
AZ186	Total	J2a	41.18495	48.11352	2067 m	488	0.03	0.31	0.1183	0.91
AZ191	Total	J2a	41.14105	48.21865	1826 m	-	0.00	0.11	-	1.06
AZ193	Total	J2a	41.10332	48.19262	2000 m	-	0.00	0.03	-	0.87
AZ195	Total	J2a	41.11791	48.20382	1893 m	-	0.00	0.02	-	0.98
AZ199	Total	J2a	41.02836	48.53844	1384 m	477	0.05	0.3	0.305	0.5
AZ201	Total	J2a	41.05013	48.55832	1314 m	-	0.01	0.12	-	0.56
AZ203	Total	J2a	41.04628	48.55383	1293 m	-	0.01	0.13	-	0.74
AZ205	Total	J2a	41.04073	48.54726	1321 m		0.01	0.2	0.2871	0.99

A2.5. RESULTS OF ORGANIC MATTER ANALYSES MADE IN 2007 AT THE GEOLOGICAL INSTITUTE OF THE UNIVERSITY OF NEUCHÂTEL (SWITZERLAND)

Sampling: A. Rast – M. Bochud (2006)
Sample preparation: A. Rast (2006 – 2007)
Sample Analysis: Dr. Thierry Adatte (University of Lausanne) (2007)
Method: Rockeval 6 Turbo (Pyrolysis method)

Sample	Lab.	Litho age	Lat	Long	Alti	Tmax	S1	S2	S3	TOC
			WGS 84 [Deg]		[m]	[°C]	[mg HC/g)	[mg HC/g)	[mg CO_2 /g]	[%]
AZ081	UniNe	K1br	41.19564	48.21297	1980 m	-	0.00	0.00	1.19	0.59
AZ089	UniNe	J2a	41.23285	48.06897	3080 m	441	0.00	0.00	0.53	0.27
AZ094	UniNe	J2a	41.22662	47.91110	3477 m	447	0.00	0.00	0.25	0.38
AZ095	UniNe	J2a	41.22428	47.92861	2834 m	-	0.00	0.00	0.28	0.21
AZ108	UniNe	J2a	41.43102	48.06640	963 m	-	0.00	0.00	0.37	0.09
AZ109	UniNe	J2a	41.43801	48.07161	954 m	-	0.00	0.00	1.43	0.39
AZ111	UniNe	J2a	41.45288	48.08581	807 m	454	0.00	0.02	0.32	0.30
AZ112	UniNe	J2a	41.46963	48.09452	735 m	-	0.00	0.00	0.32	0.18
AZ113	UniNe	J2a	41.47114	48.09556	725 m	466	0.00	0.00	0.32	0.25
AZ114	UniNe	J2a	41.47814	48.09918	700 m	-	0.00	0.00	0.49	0.11

APPENDIX 3 - GEOMORPHOLOGICAL ANALYSES

A3.1. LOCATIONS OF THE 3 TOPOGRAPHIC SECTIONS OF THE APPENDIX A3.2.

3 topographic profiles across the EGC:

- (A) Sahdag – Bazarduzu – Kura
- (B) Qizilqaya – Cek – Qalaciq - Kura
- (C) Yerfi – Burovdal – Qaramaryam - Kura.

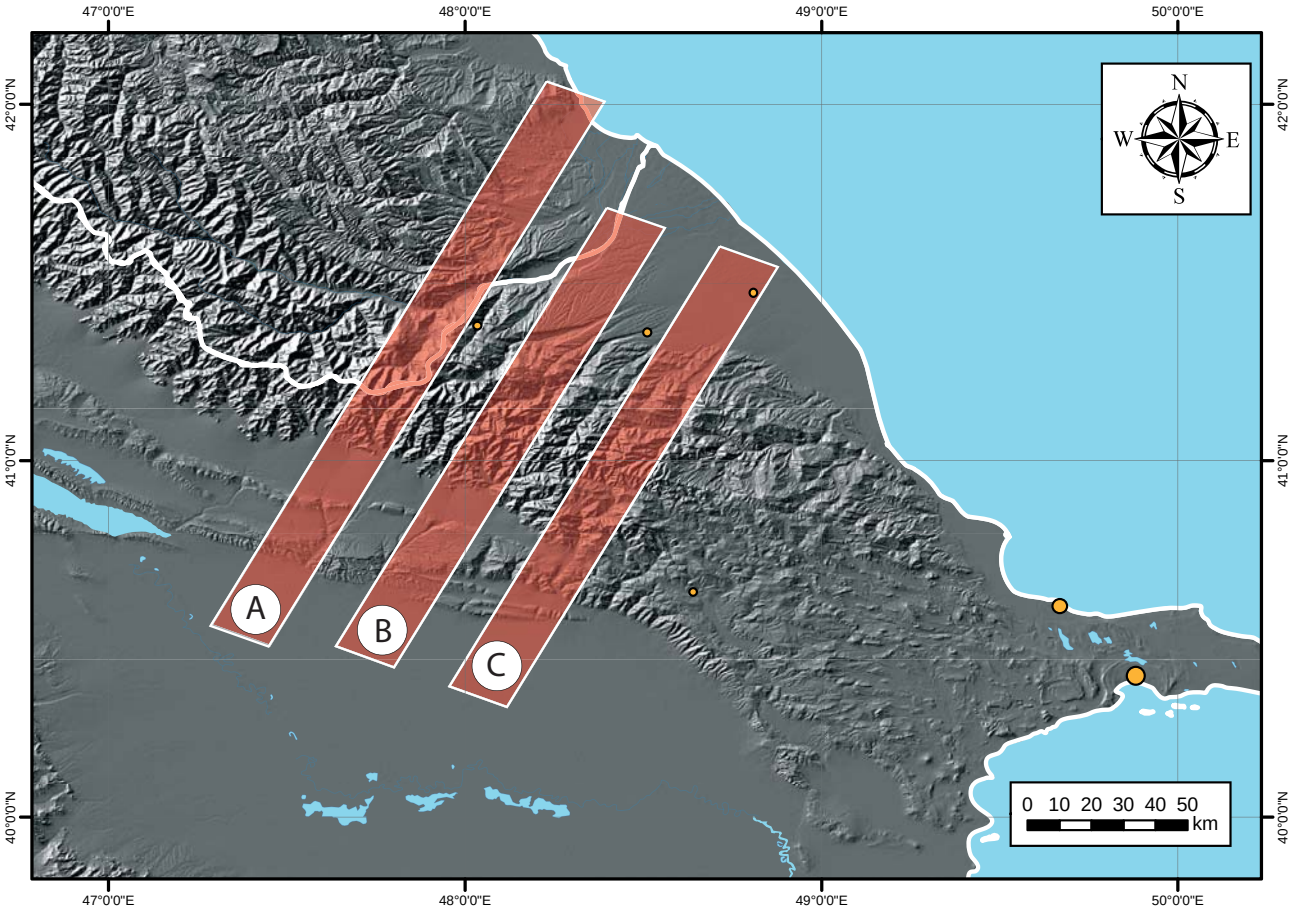

A3.2. Topographic profiles across the EGC

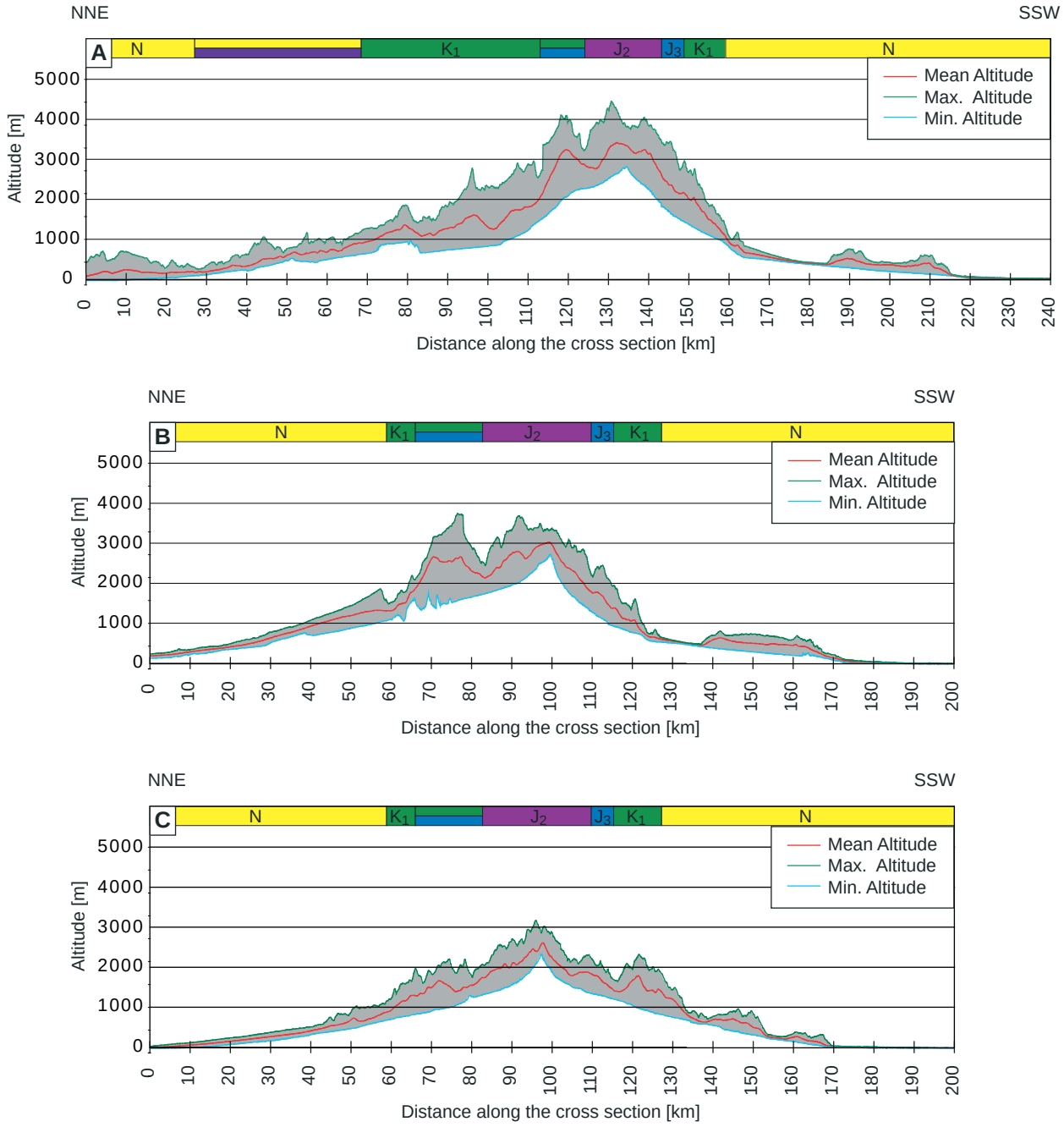

A3.3. 5 TOPOGRAPHIC PROFILES ACROSS QARAMARYAM HILLS (SOUTHERN SLOPE OF THE EGC)

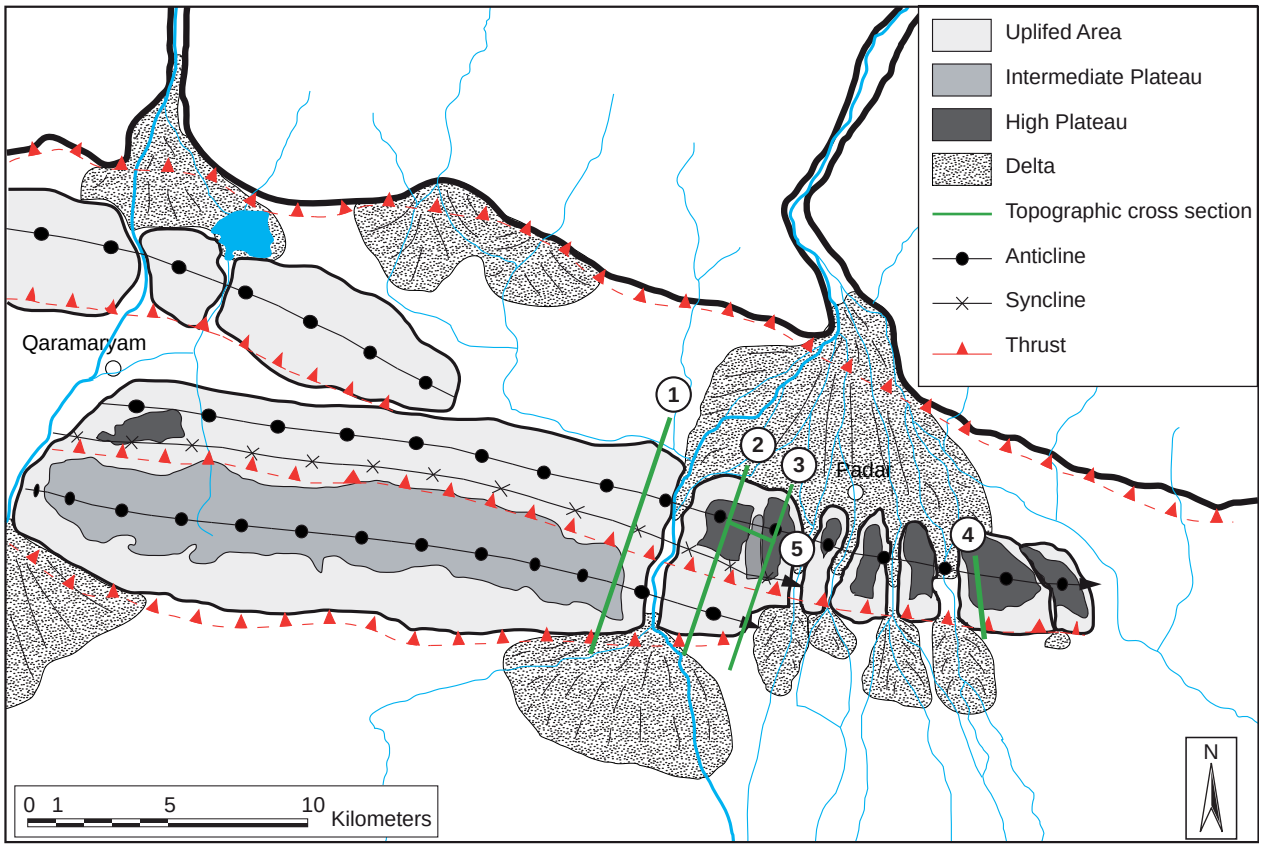

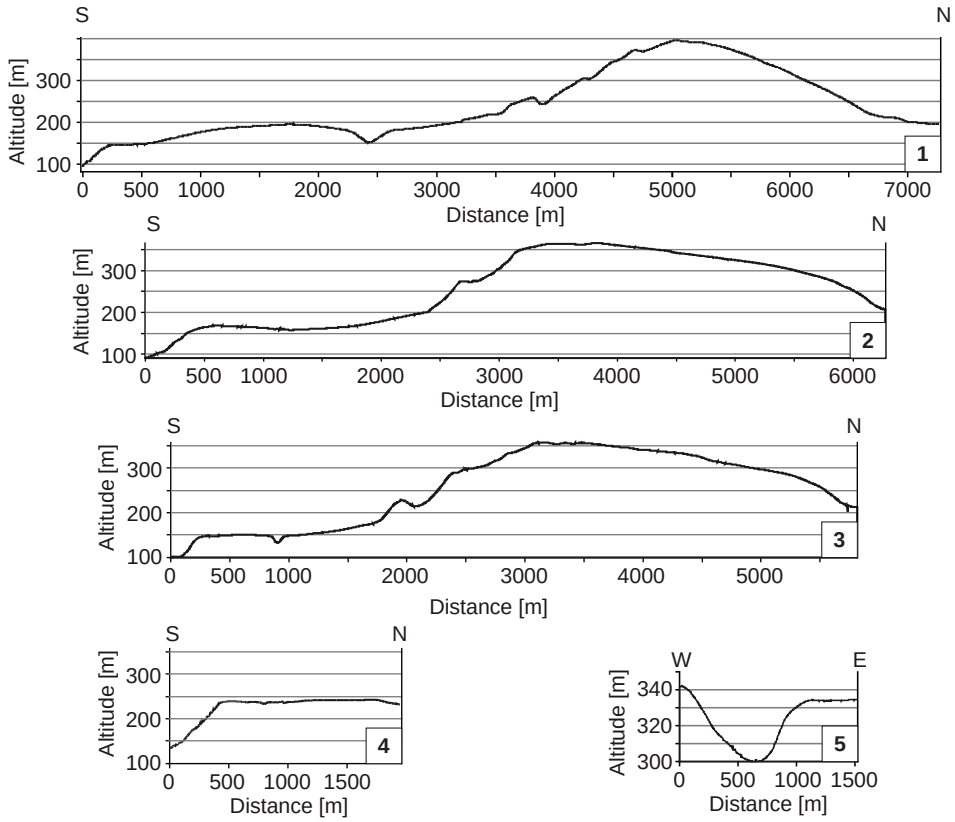

A3.4. Determining the topography and Drainage pattern of rivers

River topography

The longitudinal profile of a river is sensitive to the ongoing process of uplift and can be used to recognize active structures (Easterbrook 1999).

The method to build profiles was mainly based on the SRTM DEM at 3" (~90 m). However, as the accuracy of the 3D model is not good enough to use existing GIS tools for river analysis (they need a minimum accuracy of 25 m), river topographical profiles were built by "hand". The adjacent DEM pixel values were compared and, in case of same values or doubt, the river direction was based on topographical map at 1:100'000 scale. An estimated equilibrium profile was superposed to original profiles to accentuate differences. Finally, geological boundaries, main known faults and folded area were superposed on each profile to deduce a link between both of them.

Results in appendixes A3.5 and A3.6.

Drainage Pattern

The drainage pattern of rivers contains unique informations about the past and the present tectonic regime. Basically, its study allows determining the development degree of the drainage in one area. The comparison between surfaces, length and number of each drainage levels for several areas could emphasize a tectonic influence.

To build the drainage pattern in the EGC, the method is based on Strahler (1957) and consists of:

- Drawing of all studied rivers with their affluents. The 1:100'000 Russian maps were the basis to draw the streams.
- Drawing drainage areas from the smallest affluents to the main rivers. The limit between each drainage area was determined by the topography.
- Attributing the corresponding level to each stream segment starting from 1 to 6 (6 is the maximum level reached in this study). An upper level is reach when two same levels join.
- Calculating level, length and drainage surface for each surface.

Results in appendixes A3.7, A3.8, A3.9 and A3.10.

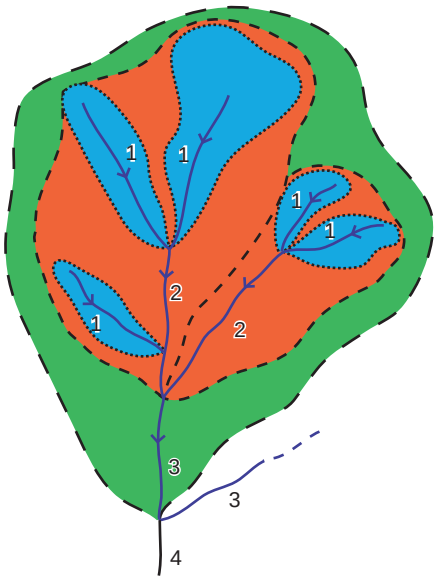

Figure 84: Sample of stream segments numbering based on STRAHLER (1957).

A3.5. River topographic profiles of the EGC northern slope

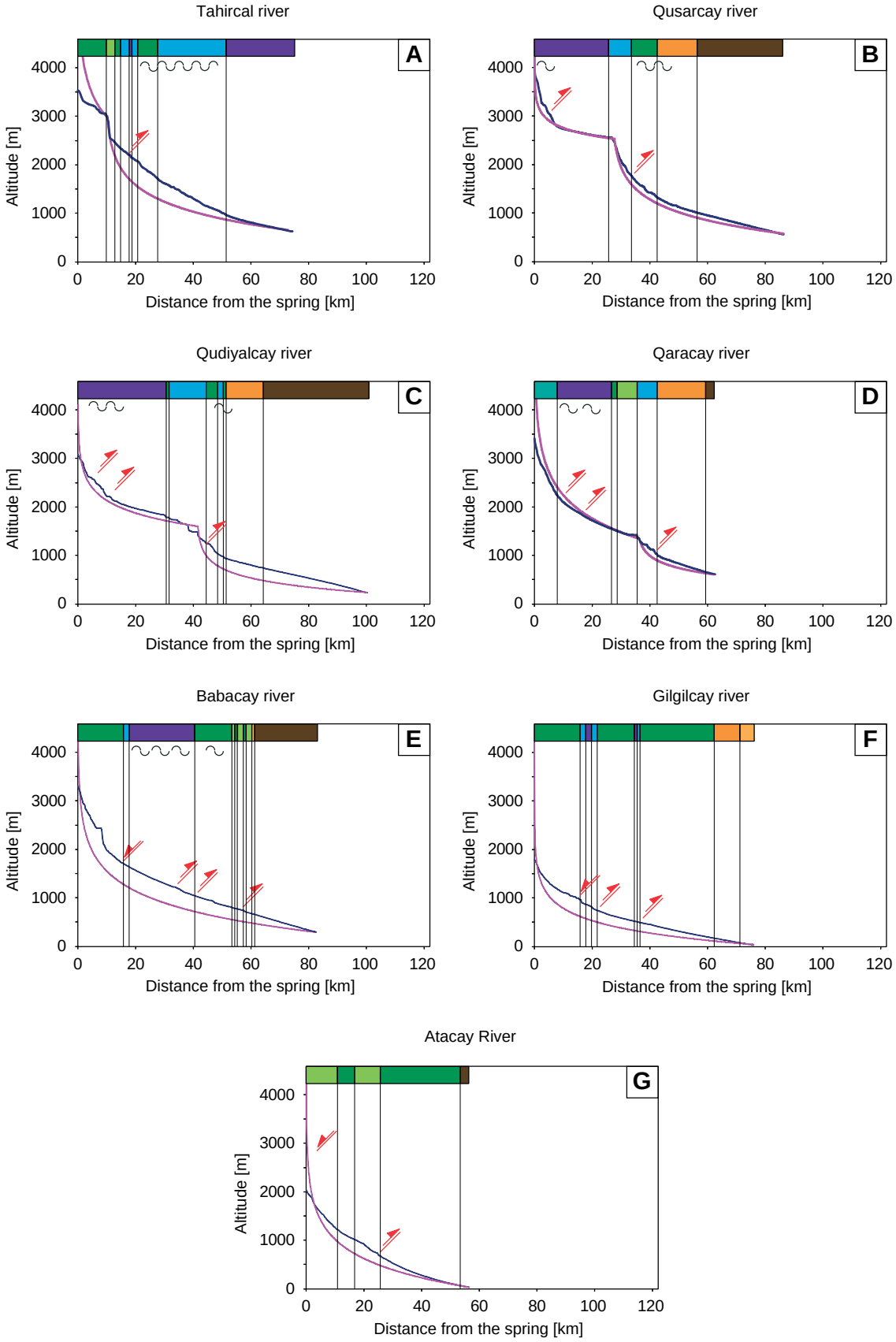

Blue line: topographical profile; Pink line : estimated equilibrium profile. Colors on top represent geological ages and see appendix A3.7 for their significance. See map of figure 11 in chapter 2 for localization.

A3.6. River topographic profiles of the EGC southern slope

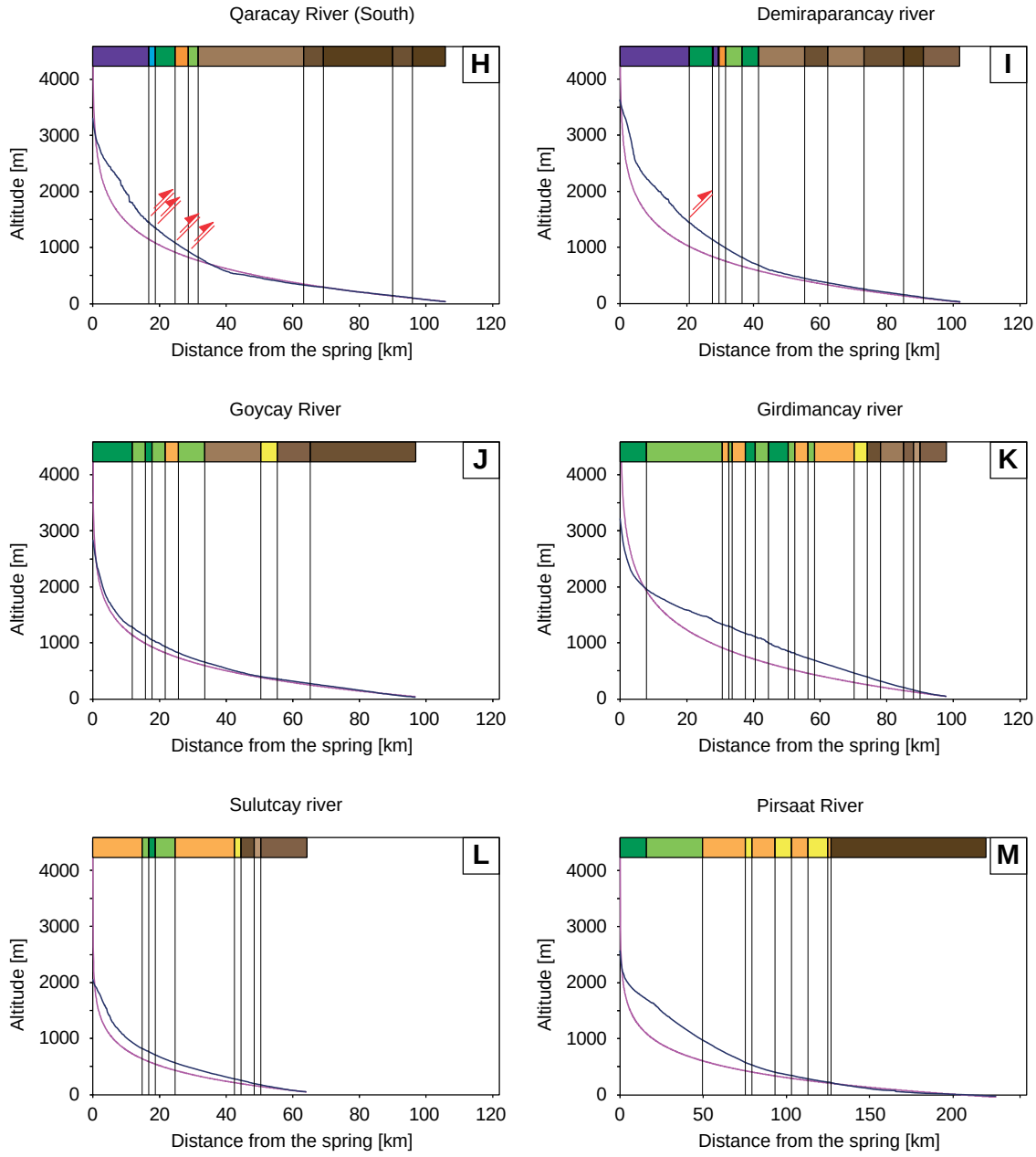

Blue line: topographical profile; Pink line : estimated equilibrium profile. Colors on top represent geological ages and see appendix A3.7 for their significance. See map of figure 11 in chapter 2 for localization.

A3.7. Drainage pattern of Qusarcay and Qudiyalcay rivers (EGC northern slope)

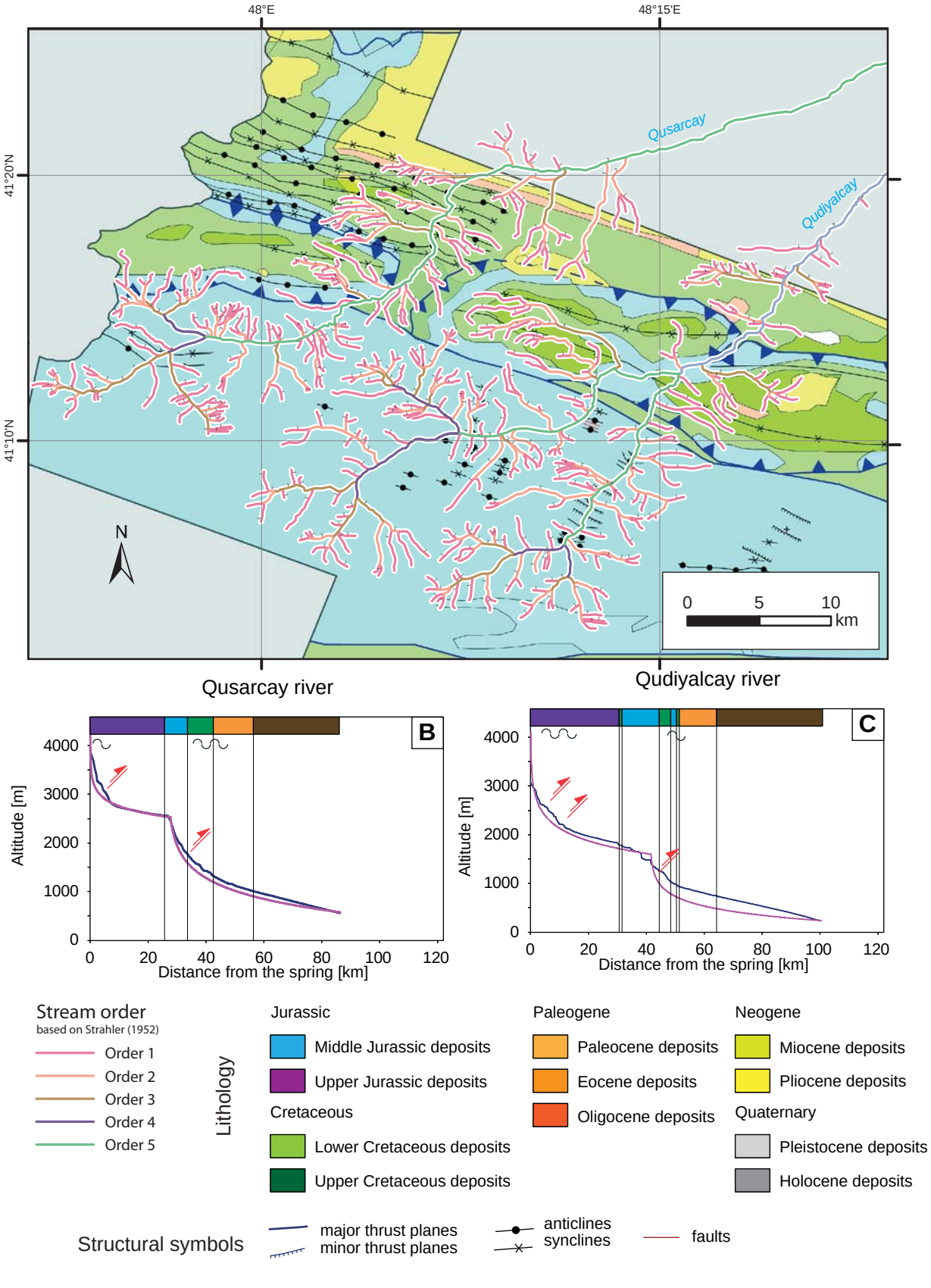

A3.8. Drainage pattern of Girdimancay River (EGC southern slope)

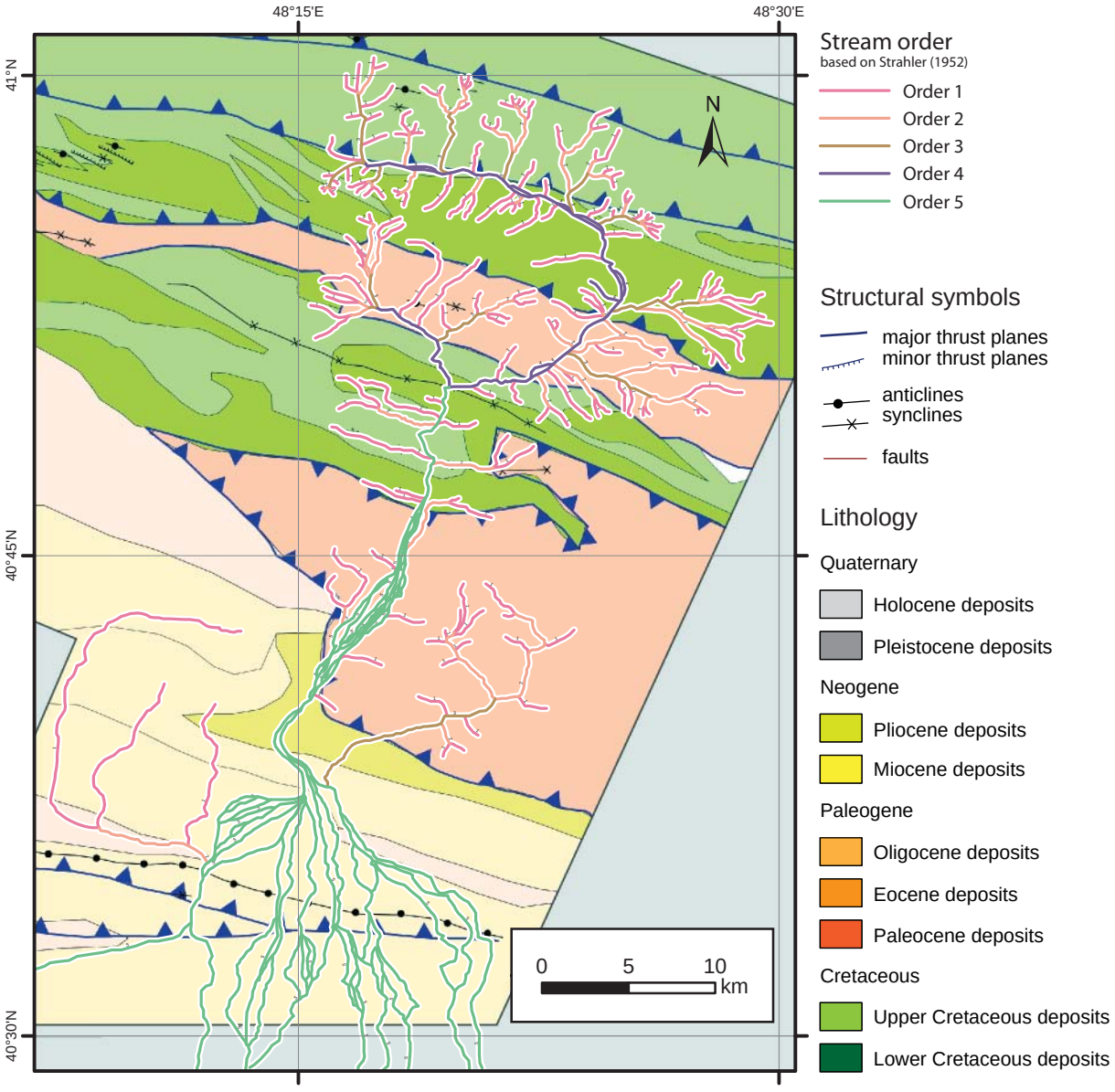

Girdimancay river

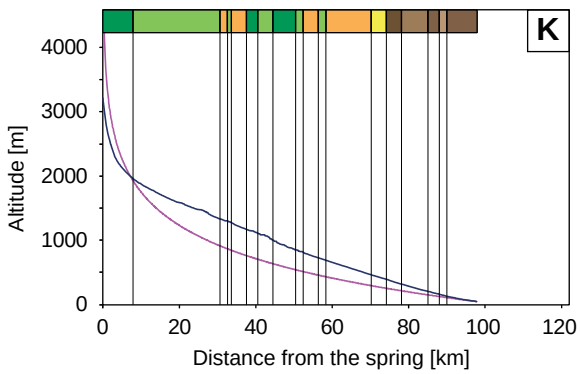

A3.9 Stream segments length statistics of Qusarcay, Qudiyalcay and Girdimancay rivers

	Girdimancay River	Qusarcay River	Qudiyalcay River
Order 1	514.6 km	385.3 km	538.3 km
Order 2	183.0 km	146.4 km	213.3 km
Order 3	85.2 km	55.2 km	86.9 km
Order 4	66.8 km	16.4 km	36.9 km
Order 5	94.8 km	192.5 km	59.3 km
Order 6	-	-	81.5 km
Total	944.4 km	795.8 km	1016.1 km

A3.10. Stream segments number statistics of Qusarcay, Qudiyalcay and Girdimancay rivers

	Girdimancay River	Qusarcay River	Qudiyalcay River
Order 1	167	161	236
Order 2	48	53	68
Order 3	13	11	21
Order 4	9	3	4
Order 5	1	1	2
Order 6	-	-	1
Total	238	229	332

REFERENCES

Abrams M.A. & Narimanov A.A. 1997. Geochemical evaluation of hydrocarbons and their potential ressources in the western South Caspian depression, Republic of Azerbaijan. Marine and Petroleum Geology 14, 4, 451-468.

Adamia Sh.A., Alania V., Chabukiani A., Chichua G., Enukidze O. & Sadradze N. 2010. Evolution of the Late Cenozoic basins of Georgia (SW Caucasus): A review. In: Sosson M., Stephenson R. A., Bergerat F. & Starostenko V. (Eds.), Sedimentary Basin Tectonics from the Black Sea and Caucasus to the Arabian platform. Geological Society of London, London, Special Publication 340, 239-259.

Adamia Sh.A., Chkhouta T., Kekelia M., Lordkipanidze M.B. & Zakariadze G.S. 1981. Tectonics of the Caucasus and adjoining areas: implications for the evolution of the Tethys ocean. Journal of Structural Geology 3, 4, 437-447.

Adatte T., Stinnesbeck W. & Keller G. 1996. Lithostratigraphic and mineralogic correlations of near K/T boundary clastic sediments in northeastern Mexico: Implications for origin and nature of deposition. Geological Society of America Special Papers 307, 211-226.

Ali-Zadeh K., Ali-Zadeh Ak., Abbasov A., Abdulkasumzadeh M., Agayev V., Azizbekova A., Aliyev R., Aliyeva L., Aliyulla Kh., Atayeva E., Babayev R., Babayev Sh., Vekilov B., Gasanov T., Gasanov T.Ab. & Idrisov V. 1997. Geology of Azerbaijan, volume 1, Stratigraphy, part 2 : Mesozoic-Cenozoic. Nafta Press, Baku, 580 pp.

Aliyev A., Guliyev I.S. & Belov I.S. 2002. Catalogue of recorded eruptions of mud volcanoes of Azerbaijan. Nafta Press, Baku, 94 pp.

Aliyev A., Guliyev I.S. & Rahmanov R.R. 2009. Catalogue of mud volcanoes eruptions of Azerbaijan (1810 - 2007). Nafta Press, Baku, 106 pp.

Allen M., Jackson J. & Walker R. 2004. Late Cenozoic reorganization of the Arabia-Eurasia collision and the comparison of short-term and long-term deformation rates. Tectonics 23, TC2008, 16 pp.

Allen M., Morton A.C., Fanning C.M., Ismail-Zade A.J. & Kroonenberg S.B. 2006. Zircon age constraints on sediment provenance in the Caspian region. Journal of the Geological Society 163, 647-655.

Allen M.B., Jones S., Ismail-Zadeh A., Simmons M. & Anderson L. 2002. Onset of subduction as the cause of rapid Pliocene-quaternary subsidence in the South Caspian basin. Geological society of America 30, 9, 775-778.

Allen M.B., Vincent S.J., Alsop G.I., Ismail-Zadeh A. & Flecker R. 2003. Late Cenozoic deformation in the South Caspian region: effects of a rigid basement block within a collision zone. Tectonophysics 6879, 1-17.

Allen Ph. & Allen J. 2005. Basin analysis, principles and applications. Blackwell Publishing, Oxford, 549 pp.

Angelier J. & Mechler P. 1977. Sur une méthode graphique de recherche des contraintes principales également utilisable en tectonique et en séismologie: la méthode des dièdres droits. Bulletin de la Société géologique de France 19, 6, 1309-1318.

Angevine C.L., Heller P.L. & Paola C. 1990. Quantitative sedimentary Basin modeling. American Association of Petroleum Geologists Shortcourse Note Series 32, 130-140.

Banks Ch., J., Robinson A.G. & Williams M.P. 1997. Structure and regional tectonics of the Achara-Trialet fold belt and the adjacent Rioni and Kartli foreland basins, Republic of Georgia. american Association of Petroleum Geologists, memoir 68, 331-346.

Barazangi M., Sandvol E. & Seber D. 2006. Structure and tectonic evolution of the Anatolian plateau in eastern Turkey. Geological Society of America Special Paper 409, 463-473.

Barrier E., Vrielynck B., Bergerat F., Brunet M-F., Mosar J., Poisson A. & Sosson M. 2008a. Paleotectonic maps of the Middle East - Tectono-sedimentary-palinplastic maps from Late Norian to Pliocene.

Barrier E., Vrielynck B., Brunet M.-F., Bergerat F. & Sosson M. 2008b. Toward a model of tectonic evolution of the Middle East since Mesozoic. International Geological Congress 2008, Oslo.

Bedford D.P. & Barry R.G. 1994. Glacier Trends in the Caucasus, 1960s to 1980s. Physical Geography 15, 5, 414-424.

Berberian M. 1983. The Southern Caspian: A compressional depression floored by a trapped modified oceanic crust. Canadian Journal of Earth Sciences. 287, 177-196.

Bravard Y. 1983. Le relief du Caucase oriental. Revue de Géographie Alpine 71, 3, 279-305.

Brod I.A. 1962. Structural-geomorphological investigations in the Caspian region. (Strukturno-geomorfologicheskie issledovaniya v Prikaspii). Leningrad, 512 pp.

Brunet M.-F., Granath J.W. & Wilmsen M. 2009a. South Caspian to Central Iran basins: introduction. In: Brunet M.-F., Wilmsen M. & Granath J.W. (Eds.), South Caspian to Central Iran Basins. The Geological Society of London, London, Special Publication 312, 1-10.

Brunet M.-F., Korotaev M.V., Ershov A.V. & Nikishin A.M. 2003. The South Caspian Basin: a review of its evolution from subsidence modelling. Sedimentary Geology 156, 1-4, 119-148.

Brunet M.-F., Wilmsen M. & Granath J.W. 2009b. South Caspian to Central Iran Basins. The Geological Society of London, London, 509 pp.

Budagov B.A. 1963. Neotectonic movements near the Shkhdag Massif (Southeatern Caucasus) reinterpreted after the discovery of Late Sarmatian fossils. Doklady Akademii Nauk Azerbajdzanskoj SSR 155, 30-32.

Budagov B.A. 1969. Geomorphology of the southern slope of the Bolshoi Caucasus (Azerbaidzhan). (Geomorfologiya yuzhnogo sklona bolshogo Kavkaza). Baku, 177 pp.

Budagov B.A. 1973. Geomorphology and latest tectonics of the South-Eastern Caucasus. (Geomorfologiya i noveishaya tektonika yugo-vostochnogo Kavkaza). Baku, 246 pp.

Burbank D.W. & Anderson R.S. 2001. Tectonic geomorphology. Blackwell Science, 274 pp.

Burtman V.S. 1989. Kinematics of the Arabian syntaxis. Geotectonics 23, 139-146.

Caspers H. 1957. Black Sea and Sea of Azov. Geological Society of America Memoirs 67, 1, 801-890.

Chalot-Prat F., Tikhomirov P. & Saintot A. 2007. Late Devonian and Triassic basalts from the southern continental margin of the East European Platform, tracers of a single heterogeneous lithospheric mantle source. Journal of Earth System Sciences 116, 6, 469-495.

Chernyshev I.V., Lebedev V.A. & Arakelyants M.M. 2006. K-Ar dating of Quaternary volcanics: mathodology and interpretation of results. Petrology 14, 1, 62-80.

Cloetingh S.A.P.L., Ziegler P.A., Bogaard P.J.F., Andriessen P.A.M., Artemieva I.M., Bada G., van Balen R.T., Beekmann F., Ben-Avraham Z., Brun J.-P., Bunge H.P., Burov E.B., Carbonell R., Facenna C., Friedrich A, Gallart J., Green A.G., Heidbach O., Jones A.G., Matenco L., Mosar J., Oncken O., Pascal C., Peters G., Sliaupa S., Soescoo A., Spakman W., Stephenson R.A., Thybo H., Torsvik T., de Vicente G., Wenzel F., Wortel M.J.R. & group TOPO-EUROPE Working 2007. 4-D topographic evolution of the intra-plate regions of Europe: a multidisciplinary approach linking geology, geophysics and geotechnology. Global and Planetary Change 58, 1-118.

Copley A. & Jackson J. 2006. Active tectonics of the Turkish-Iranian Plateau. Tectonics 25, TC6006, 19 pp.

Daukeev S.Zh., Uzhkenov B.S., Miletenko N.V., Morozov A.F., Leonov YuG., Futong W., Akhmedov N.A., Abdyllayev E.K., Murzagaziev S.M., Orifov A.O. & Alizade A.A. 2002. Atlas of lithology-paleogeographical, structural, palinspastic and geoenvironmental maps of Central Asia. Scientific Research Institute of Natural Resources YUGGEO, Almaty (Kazakhstan), 71 pp.

de Lumley M.-A. & Lordkipanidze D. 2006. L'Homme de Dmanissi (Homo georgicus), il y a 1810 000 ans. Comptes Rendus Palevol 5, 1-2, 273-281.

Delcaillau B. 2004. Reliefs et tectonique récente. Vuibert, Paris, 259 pp.

Dercourt J., Zonenshain L.P., Ricou L.E., Kazmin V.G., Le Pichon X., Knipper A.L., Grandjacquet C., Sbortshikov I.M., Geyssant J., Lepvrier C., Pechersky D.H., Boulin J., Sibuet J.C., Savostin L.A., Sorokhtin O., Westphal M., Bazhenov M.L., Lauer J.P. & Bijuduval B. 1986. Geological evolution of the Tethys belt from the Atlantic to the Pamirs since the Lias. Tectonophysics 123, 241-315.

Dilek Y., Imamverdiyev N. & Altunkaynak Å. 2010. Geochemistry and tectonics of Cenozoic volcanism in the Lesser Caucasus (Azerbaijan) and the peri-Arabian region: collision-induced mantle dynamics and its magmatic fingerprint. International Geology Review 52, 4-6, 536 - 578.

Djavadova A. & Mamula N. 1999. Petroleum geology of the "Akstafa Block" and surrounding Kura-Gabirry interfluve, Azerbaijan. Frontera Resources,

Donelick R.A., Ketcham R.A. & Carlson W.D. 1999. Variability of apatite fission-track annealing kinetics: II. Crystallographic orientation effects. American Mineralogist 84, 9, 1224-1234.

Donelick R.A., O'Sullivan P. & Ketcham R.A. 2005. Apatite Fission-Track Analysis. Rewiews in Mineralogy & Geochemistry 58, 49-94.

Dotduyev S.I. 1986. Nappe Structure of the Greater Caucasus Range. Geotectonics 20, 5, 420-430.

Doumitrachko N.V. & Milanovskii E.E. 1974. Formation of Present Relief of Caucasus - Geological Developments and Neotectonic Movements. Revue De Geographie Physique Et De Geologie Dynamique 16, 3, 271-283.

Dunkl I. 2002. Trackkey: a Windows program for calculation and graphical presentation of fission track data. Computers & Geosciences 28, 1, 3-12.

Easterbrook D.J. 1999. Surface Processes and Landforms. Prentice-Hall, New York, 546 pp.

Efendiyeva M.A. 2004. Anoxia in waters of the Maikop paleobasin (Tethys Ocean, Azeri sector), with implications for the modern Caspian Sea. Geo-Marine Letters 24, 3, 177-181.

Egan S.A., Mosar J., Brunet M.-F. & Kangarli T. 2009. Subsidence and Uplift Mechanisms Within The South Caspian Basin: Insights From The Onshore and Offshore Azerba-

ijan Region. In: Brunet M.-F., Wilmsen M. & Granath J.W. (Eds.), South Caspian to Central Iran Basins. The Geological Society of London, London, Special Publication 312, 219-240.

Ershov A.V., Brunet M.-F., Korotaev M.V., Nikishin A.M. & Bolotov S.N. 1999. Late Cenozoic burial history and dynamics of the Northern Caucasus molasse basin: implications for the foreland basin modelling. Tectonophysics 313, 219-241.

Ershov A.V., Brunet M.-F., Nikishin A.M., Bolotov S.N., Nazarevich B.P. & Korotaev M.V. 2003. Northern Caucasus basin: thermal history and synthesis of subsidence models. Sedimentary Geology 156, 95-118.

Ershov A.V., Nikishin A.M., Bolotov S.N. & Korotaev M.V. 2005. Mesozoic-Cenozoic subsidence evolution and geodynamics of the Caucasus. In: GEOKART-GEOS (Eds.), 400 million years of geological history of the meridional plateau of eastern Europe. Moscow, 1, 259-311.

Espitalié J., Laporte J.L., Madec M. & Marquis F. 1977. Méthode rapide de caractérisation des roches mères, de leur potentiel pétrolier et de leur degré d'évolution. Revue de l'Institut Français du Petrole XXXII, 1, 23-42.

Etiope G., Feyzullayev A., Baciu C.L. & Milkov A.V. 2004. Methane emission from mudvolcanoes in eastern Azerbaijan. Geology 32, 6, 465-468.

Eyubov A. 1993. Agroclimate Atlas of Azerbaijan. Academy of Sciences of Azerbaijan, Baku, pp.

Forte A.M., Cowgill E., Bernardin T., Kreylos O. & Hamann B. 2010. Late Cenozoic deformation of the Kura fold-thrust belt, southern Greater Caucasus. Geological Society of America Bulletin 122, 3-4, 465-486.

Fowler S.R., Mildenhall J., Zalova S., Riley G., Elsley G., Desplanques A. & Guliyev F. 2000. Mud volcanoes and structural development on Shah Deniz. Journal of Petroleum Science and Engineering 28, 4, 189-206.

Fürsich F.T., Wilmsen M., Seyed-Emami K. & Majidifard M.R. 2009. The Mid Cimmerian tectonic event (Bajocian) in the Alborz Mountains, Northern Iran: evidence of the break-up unconformity of the Southe Caspian Basin. In: Brunet M-F., Wilmsen M. & Granath J.W. (Eds.), South Caspian to Central Iran Basins. The Geological Society of London, London, Special Publication 312, 189-204.

Galbraith R.F. 1990. The radial plot - graphical assessment of spread in ages. Nuclear Tracks and Radiation Measurements 17, 3, 207-214.

Galbraith R.F. & Laslett G.M. 1993. Statistical models for mixed fission track ages. International Journal of Radiation Applications and Instrumentation. Part D. Nuclear Tracks and Radiation Measurements 21, 4, 459-470.

Gamkrelidze I.P. 1986. Geodynamic evolution of the Caucasus and adjacent areas in Alpine time. Tectonophysics 127, 261-277.

Gamkrelidze I.P. 1991. Tectonic Nappes and Horizontal Layering of the Earths Crust in the Mediterranean Belt (Carpathians, Balkanides and Caucasus). Tectonophysics 196, 3-4, 385-396.

Gamkrelidze I.P. 1997. Terranes of the Caucasus and adjacent areas. Bulletin of the Georgian Academy of Sciences 155, 3, 291-294.

Gamkrelidze I.P. & Kuloshvili S. 1998. Stress vector orientations and movement of the earth's crust of the territory of Georgia on the neotectonic stage. Bulletin of the Georgian Academy of Sciences 158, 2, 283-287.

Gamkrelidze I.P. & Shengelia D.M. 2005. Precambrian-Paleozoic regional metamorphism, granitoid magmatism and geodynamics of the Caucasus. Scientific World, Moscow, 460 pp.

Gamkrelidze P.D. & Gamkrelidze I.P. 1977. Tectonic covers of the southern slope of the Great Caucasus (in the limits of Georgia). Tbilisi, 80 pp.

Gamkrelidze P.D. & Rubinstein M.M. 1974. Problems of the geology of Adzharo-Trialetia (Problemy geologii Adzharo-Trialetii). Tbilisi, 184 pp.

Gazis C.A., Lanphere M., Taylor H.P. & Gurbanov A.G. 1995. 40Ar/39Ar and 18O/16O studies of the Chegem ash-flow caldera and the Eldjurta Granite: Cooling of two late Pliocene igneous bodies in the Greater Caucasus Mountains, Russia. Earth and Planetary Science Letters 134, 3-4, 377-391.

Giralt S., Julia R., Leroy S. & Gasse F. 2003. Cyclic water level oscillations of the KaraBogazGol-Caspian Sea system. Earth and Planetary Science Letters 212, 1-2, 225-239.

Gleadow A. J. W. & Duddy I. R. 1981. A natural longterm track annealing experiment for apatite. Nuclear Tracks 5, 169-174.

Godet A., Bodin S., Adatte T. & Follmi K.B. 2008. Platform-induced clay-mineral fractionation along a northern Tethyan basin-platform transect: implications for the interpretation of Early Cretaceous climate change (Late Hauterivian-Early Aptian). Cretaceous Research 29, 5-6, 830-847.

Green P.F. 1981. "Track-in-track" length measurements in annealed apatites. Nuclear Tracks 5, 1-2, 121-128.

Green P.F. 1988. The relationship between track shortening and fission track age reduction in apatite: combined influences of inherent instability, annealing anisotropy, length bias and system calibration. Earth and Planetary Science Letters 89, 3-4, 335-352.

Green P.F., Duddy I.R., Gleadow A.J.W., Tingate P.R. & Laslett G.M. 1986. Thermal annealing of fission tracks in apatite : 1. A qualitative description. Chemical Geology: Isotope Geoscience section 59, 237-253.

Green P.F. & Durrani S.A. 1977. Annealing studies of tracks in crystals. Nuclear Track Detection 1, 1, 33-39.

Green T., Abdullayev N., Hossack J., Riley G. & Roberts A.M. 2009. Sedimentation and subsidence in the South Caspian Basin, Azerbaijan. In: Brunet M.-F., Wilmsen M. & Granath J.W. (Eds.), South Caspian to Central Iran Basins. The Geological Society of London, London, Special Publication 312, 241-260.

Grist A.M. & Ravenhurst C.E. 1992a. Mineral separation techniques used at Dalhousie University. In: Zentilli M.

& Reynolds P.H. (Eds.), Short Course Handbook on Low Temperature Thermochronology. Mineralogical Association of Short Course Handbook, 20, 203-209.

Grist A.M. & Ravenhurst C.E. 1992b. A step-by-step laboratory guide to fission track thermochronology at Dalhousie University. In: Zentilli M. & Reynolds P.H. (Eds.), Short Course Handbook on Low Temperature Thermochronology. Mineralogical Association of Short Course Handbook, 20, 190-201.

Gudjabidze G.E. 2003. Geological Map of Georgia. Georgina State Department of Geology and National Oil Company "Saknavtobi".

Guliev I. & Panahi B. 2004. Geodynamics of the deep sedimentary basin of the Caspian Sea region: paragenetic correlation of seismicity and mud volcanism. Geo-Marine Letters 24, 3, 169-176.

Guliyev I.S., Levin L.E. & Fedorov D.L. 2003. Hydrocarbons potential of the Caspian Region (Sysem Analysis). 3-119.

Hafkenscheid E., Wortel M.J.R. & Spakman W. 2006. Subduction history of the Tethyan region derived from seismic tomography and tectonic reconstructions. Journal of Geophysical Research - Solid Earth 111, B08401, 26 pp.

Harzhauser M. & Piller W. 2004. Integrated stratigraphy of the Sarmatian (Upper Middle Miocene) in the western Central Paratethys. Stratigraphy 1, 1, 65-86.

Hess J.C., Lippolt H.J., Gurbanov A.G. & Michalski I. 1993. The cooling history of the late Pliocene Eldzhurtinskiy granite (Caucasus Russia) and the thermochronological potential of grain-size/age relationships. Earth and Planetary Science Letters 117, 393-406.

Hoesli E. 2006. A la conquête du Caucase. Epopée géopolitique et guerres d'influence. Editions des Syrtes, Paris, 682 pp.

Hoogendoorn R.M., Boels J.F., Kroonenberg S.B., Simmons M.D., Aliyeva E., Babazadeh A.D. & Huseynov D. 2005. Development of the Kura delta, Azerbaijan; a record of Holocene Caspian sea-level changes. Marine Geology 222, 359-380.

Hurford A.J. 1990. Standardization of fission-track dating calibration - recommendation by the fission-track working group of the IUGS subcommission on geochronology. Chemical Geology 80, 2, 171-178.

Hurford A.J. & Green P.F. 1982. A users' guide to fission track dating calibration. Earth and Planetary Science Letters 59, 343-354.

Hurford A.J. & Green P.F. 1983. The zeta age calibration of fission-track dating. Isotope Geoscience 1, 285-317.

Inan S. & Yalçin M.N. 1997. Deep petroleum occurences in the Lower Kura Depression, South Caspian Basin, Azerbaijan : an organic geochemical and basin modeling study. Marine and Petroleum Geology 14, 7/8, 731-762.

Ismail-Zade T.A., Gadjiev T.G., Guseinov A.N., Akhmedov A.M. & Yusufzade H.B. 1987. Atlas of oil and gas bearing and perspective structures of Azerbaijan. USSR Ministry of Geology, 132 pp.

Ismailzadeh A.D., Kangarli T., Korobanov V.V., Mustafayev G.V., Narimanov A.A. & Rustamov M.I. 2008a. Explanatory note of the Geological Map of Azerbaijan 1:500'000. Azerbaijan National Academy of Sciences (Geological Institute), Ministry of Ecology and Natural Ressources of Azerbaijan (National geological Survey), Ministry of fuel and Energetics of Azerbaijan, State Oil Company of the Azerbaijan Republic, Baku, 81 pp.

Ismailzadeh A.D., Kangarli T., Korobanov V.V., Mustafayev G.V., Narimanov A.A. & Rustamov M.I. 2008b. Geological Map of Azerbaijan 1:500'000. Azerbaijan National Academy of Sciences (Geological Institute), Ministry of Ecology and Natural Ressources of Azerbaijan (National geological Survey), Ministry of fuel and Energetics of Azerbaijan, State Oil Company of the Azerbaijan Republic.

Jaboyedoff M., Kubler B., Sartori M. & Thelin P. 2000. Basis for meaningful illite crystallinity measurements: an example from the Swiss Prealps. Schweizerische Mineralogische Und Petrographische Mitteilungen 80, 1, 75-83.

Jackson J. 1992. Partitioning of Strike-Slip and Convergent Motion between Eurasia and Arabia in Eastern Turkey and the Caucasus. Journal of Geophysical Research-Solid Earth 97, B9, 12471-12479.

Jackson J., Priestley K., Allen M. & Berberian M. 2002. Active tectonics of the South Caspian Basin. Geophysical Journal International 148, 214-245.

Kadirov F., Mammadov S., Reilinger R. & McClusky S. 2008. Some new data on modern tectonic deformation and active faulting in Azerbaijan (according to global positioning system measurements). Azerbaijan National Academy of Sciences Proceedings The Sciences of Earth 1, 82-88.

Kangarli T. 1982. Geological structures in the Azerbaijan lateral crest of the High Caucasus. Unpublished PhD Thesis, Azerbaijan State University, Baku.

Kangarli T. 2005. Greater Caucasus - chapter 3. In: Khain V.E. & Alizadeh A.Ak. (Eds.), Geology of Azerbaijan, Tectonics. Nafta-Press, Baku, Azerbaijan, IV, 43-213.

Kazmin V.G. & Tikhonova N.F. 2006. Late Cretaceous-Eocene marginal Seas in the Black-Sea-Caspian Region: Paleotectonic reconstructions. Geotectonics 40, 3, 162-182.

Keller E.A. & Pinter N. 2002. Active Tectonics. Earthquakes, uplift, and landscape. Prentice Hall, Upper Saddle River, 362 pp.

Ketcham R.A. 2005. Forward and inverse modeling of low-temperature thermochronometry data. In: Reiners P.W. & Ehlers T.A. (Eds.), Low-Temperature Thermochronology: Techniques, Interpretations, and Applications. The Mineralogical Society of America, Chantilly, 58, 275-314.

Ketcham R.A. 2009. HeFTy - Version 1.6.7. pp.

Ketcham R.A., Carter A., Donelick R.A., Barbarand J. & Hurford A.J. 2007a. Improved measurement of fission-track annealing in apatite using c-axis projection. American Mineralogist 92, 5-6, 789-798.

Ketcham R.A., Carter A., Donelick R.A., Barbarand J. & Hurford A.J. 2007b. Improved modeling of fission-track annealing in apatite. American Mineralogist 92, 5-6, 799-810.

Ketcham R.A., Donelick R.A., Balestrieri M.L. & Zattin M. 2009. Reproducibility of apatite fission-track length data and thermal history reconstruction. Earth and Planetary Science Letters 284, 3-4, 504-515.

Khain V.E. 1975. Structure and main stages in the tectono-magmatic development of the Caucasus: an attempt at geodynamic interpretation. American Journal of Science 275-A, 131-156.

Khain V.E. 1994. Geology of the Northern Eurasia (ex-USSR) : second part of the Geology of the USSR. Phanerozoic fold belts and young platforms. Borntraeger, Berlin; Stuttgart, pp.

Khain V.E. 1997. Azerbaijan - Greater Caucasus. In: Moores E.M. & Fairbridge R.W. (Eds.), Encyclopedia of European and Asian regional geology. Chapman and Hall, London, 60-63.

Klige R.K. & Myagkov M.S. 1992. Changes in the water regime of the Caspian Sea GeoJournal 27, 3, 299-307.

Knapp C.C., Knapp J.H. & Connor J.A. 2004. Crustal-scale structure of the South Caspian Basin revealed by deep seismic reflection profiling. Marine and Petroleum Geology 21, 1073-1081.

Koçyigit A., Yilmaz A., Adamia Sh.A. & Kuloshvili S. 2001. Neotectonics of the East Anatolian Plateau 8Turkey) and Lesser Caucasus: implication for transition from thrusting to strike-slip faulting. Geodinamica Acta 14, 177-195.

Kokolashvili I. & Shatilova I. 2009. The preliminary results of palynological investigations of Lower Sarmatian deposits of Kakheti. Proceedings Georgian Academy of Science, Biology Series. B 7, 1-2, 85-89.

Kopp M.L. & Shcherba I.G. 1985. Late Alpine development of the East great Caucasus. Geotectonics 19, 6, 497-507.

Koronovsky N.V., Kozhevnikov A.V., Panov D.I., Vishnevsky L.E., Guschin A.I., Nikitin M.Yu., Voronina A.A., Stafeev A.N., Panina L.V., Kopaevich L.F., Star M.A. & Belyakov G.A. 1987. The history of geologic development and structure formation of the central part of Terek–Caspian trough. In: Milanovsky E. E. & Koronovsky N. V. (Eds.), Geology and Mineral Resources of the Great Caucasus. Nauka, Moscow, 147–174.

Kotliakov V.M. & Krenke A.N. 1981. Glaciation actuelle et climat du Caucase. Revue de Géographie Alpine 64, 2, 241-264.

Kotliakov V.M. & Touchinski G.K. 1974. Present Regime of Glaciers and Avalanches in Caucasus. Revue De Geographie Physique Et De Geologie Dynamique 16, 3, 299-311.

Kovachev S.A., Kaz'min V.G., Kuzin I.P. & Lobkovsky L.I. 2006. New data on seismicity of the Middle Caspian Basin and their possible tectonic interpretation. Geotectonics 40, 5, 367-376.

Kral J. & Gurbanov A.G. 1996. Apatite fission track data from the Great Caucasus pre-alpine basement. Chemie der Erde 56, 177-192.

Krasnov I.I. 1974. Karta chetvertichnyh otlzhenii Evropeiskoi chasti SSSR. (Map of Quaternary deposits of the European part of the USSR scalle 1:1'500'000). Ministerstvo geologii SSR.

Krasnov I.I., Duphorn K. & Voges A. 1974. International Quaternary map of Europe - 12 Tbilisi.

Kübler B. 1964. Les argiles, indicateurs de métamorphisme. Revue de l'Institut Français du Petrole 19, 1093-1112.

Kübler B. 1987. Cristallinité de l'illite: méthodes normalisées de préparation, méthode normalisée de mesure, méthode automatique normalisée de mesure. Cahiers de l'Institut de Géologie, Université de Neuchâtel, Suisse Série ADX n°2, 10 pp.

Kübler B. & Goy-Eggenberger D. 2001. Illite cyrstallinity revisited: Review of studies over the past 30 years. Clay Minerals 36, 2, 143-157.

Kübler B. & Jaboyedoff M. 2000. Illite crystallinity concise review paper. Comptes Rendus de l'Académie des Sciences - Series IIA - Earth and Planetary Science 331, 2, 75-89.

Kurtubadze M. 2008. Climate zones of the Caucasus ecoregion. WWF-Caucasus.

Laslett G.M., Gleadow A.J.W. & Duddy I.R. 1984. The relationship between fission track length and track density in apatite. Nuclear Tracks and Radiation Measurements (1982) 9, 1, 29-38.

Lebedev V.A. 2005. Chronology of magmatic activity ofthe Elbrus volcano (Greater Caucasus): Evidence from K-Ar Isotope dating of lavas. Doklady Earth Sciences 405A, 9, 1321-1326.

Lebedev V.A. & Bubnov S.N. 2006. Pliocene granitoid massif in the Kazbek volcanic center: first geochronological and isotope-geochemical data. Doklady Earth Sciences 411A, 9, 1393-1397.

Lebedev V.A., Bubnov S.N., Chernyshev I.V. & Gol'tsman Y.V. 2006. Basic magmatism in the geological history of the Elbrus neovolcanic area, Greater Caucasus: Evidence from K-Ar and Sr-Nd isotope data. Doklady Earth Sciences 406, 1, 37-40.

Lisker F., Ventura B. & Glasmacher U.A. 2009. Apatite thermochronology in modern geology. Geological Society, London, Special Publications 324, 1, 1-23.

Ljubin V.P. & Bosinski G. 1995. The earliest occupation of the Caucasus region. In: Roedbroek W. & Van Kolfschoten T. (Eds.), The Earliest Occupation of Europe. University of Leiden Press, Leiden, 207-253.

Lordkipanidze D., Jashashvili T., Vekua A., Ponce de Leon M.S., Zollikofer C.P., Rightmire G.P. & al. et 2007. Postcranial evidence from early Homo from Dmanisi, Georgia. Nature 449, 305-310.

Lukina N.V. 1981. The age of the river terraces in the central Caucasian foreland. Geomorfologia 2, 68-75.

Mamedov A.V. 1997. The Late Pleistocene-Holocene history of the Caspian Sea. Quaternary International 41/42, 161-166.

Mangino S. & Priestley K. 1998. The crustal structure of the southern Caspian region. Geophysical Journal International 133, 630-648.

Mazzini A. 2009. Mud volcanism: Processes and implications. Marine and Petroleum Geology 26, 9, 1677-1680.

McClusky S., Balassanian S., Barka A. & Demir C. 2000. Global positioning system constraints on plate kinematics and dynamics in the eastern Mediterranean and Caucasus. Journal of Geophysical Research, Solid Earth 105, B3, 5695-5719.

Mellors R., Kilb D., Aliyev A., Gasanov A. & Yetirmishli G. 2007. Correlations between earthquakes and large mud volcano eruptions. Journal of Geophysical Research-Solid Earth 112, B04304, 11 pp.

Mengel K., Borsuk A.M., Gurbanov A.G., Wedepohl K.H., Baumann A. & Hoefs J. 1987. Origin of spillitic rocks from the southern slope of the Greater Caucasus. Lithos 20, 115-123.

Mikhailov V., Panina L.V., Polino R., Koronovsky N.V., Kiseleva E.A., Klavdieva N.V. & Smolyaninova E.I. 1999. Evolution of the North Caucasus foredeep: constraints based on the analysis of subsidence curves. Tectonophysics 307, 361-379.

Milanovski E.E. 1991. Geology of the USSR - Part 3. Univ. Press, Moscow, 272 pp.

Milanovsky E.E. 2008. Origin and development of ideas on Pliocene and Quaternary glaciations in northern and eastern Europe, Iceland, Caucasus and Siberia. In: Grapes R.H., Oldroyd D. & Grigelis A. (Eds.), History of Geomorphology and Quaternary Geology. The Geological Society of London, London, Special Publication 301, 87-115.

Mitchell J. & Westaway R. 1999. Chronology of Neogen and Quaternary uplift and magmatism in the Caucasus: constraints from K-Ar dating of volcanism in Armenia. Tectonophysics 304, 157-186.

Morton A. ,Allen M., Simmons M. , Spathopoulos F., Still J., Hinds D., Ismail-Zadeh A. & Kroonenberg S. 2003. Provenance patterns in a neotectonic basin: Pliocene and Quaternary sediment supply to the South Caspian. Basin Research 15, 321-337.

Mosar J., Kangarli T., Bochud M., Glasmacher U.A., Rast A., Brunet M.-F. & Sosson M. 2010. Cenozoic-Recent tectonics and uplift in the Greater Caucasus: a perspective from Azerbaijan. Geological Society, London, Special Publications 340, 1, 261-280.

Mustafayev M.A. 2001. Petrology and geodynamic conditions of formation of the early Alpine stage magmatic series of the East Caucasus, Azerbaijan. 4th International Symposium on Eastern Mediterranean Geology, Isparta.

Nadirov R.S., Bagirov E., Tagiyev M. & Lerche I. 1997. Flexural plate subsidence, sedimentation rates, and structural development of the super-deep South Caspian Basin. Marine and Petroleum Geology 14, 4, 383-400.

Narimanov N.P. 1992. Tectonic regionalization of offshore of South Caspian depression. Geologiya Nefti i Gaza 11, 22-24.

Nikishin A.M., Brunet M-F., Cloetingh S. & Ershov A. V. 1997. Northern Peri-Tethyan Cenozoic intraplate deformations: influence of the Tethyan collision belt on t he Eurasian continent from Paris to Tian-Shan. Comptes Rendus de l'Académie des Sciences de Paris, Série II 324, 49-57.

Nikishin A.M., Cloetingh S., Bolotov S. N., Baraboshkin E.Y., Kopaevich L.F., Nazarevich B.P., Panov D.I., Brunet M-F., Ershov A. V., Ilina V.V., Kosova S.S. & Stephenson R. A. 1998a. Scythian platform: Chronostratigraphy and polyphase stages of tectonic history. In: Crasquin S. & Barrier E. (Eds.), Peri-Tethys Memoir 3 - Stratigraphy and evolution of Peri-Tethyan platforms. Mémoires du Muséum national d'Histoire naturelle, Paris, 3, 153-161.

Nikishin A.M., Cloetingh S., Brunet M-F., Stephenson R.A., Bolotov S.N. & Ershov A.V. 1998b. Scythian Platform and Black Sea region: Mesozoic –Cenozoic tectonic and dynamics. In: Crasquin-Soleau S. & Barrier E. (Eds.), Peri-Tethys Memoir 3: Stratigraphy and Evolution of Peri-Tethyan Platforms. Mémoires du Muséum National d'Histoire Naturelle, Paris, 177, 165-176.

Nikishin A.M., Korotaev M.V., Ershov A.V. & Brunet M.-F. 2003. The Black Sea basin: tectonic history and neogene-quaternary rapid subsidence modelling. Sedimentary Geology 156, 149-168.

Nikishin A.M., Ziegler P., Panov D.I., Nazarevich B.P., Brunet M.-F., Stephenson R.A., Bolotov S.N., Korataev M.V. & Tikhomirov P.L. 2001. Mesozoic and Cainozoic evolution of the Scythian Platform - Black Sea - Caucasus domain. In: Ziegler P., Cavazza W., Robertson A.H.F. & Crasquin-Soleau S. (Eds.), Peri-Tethys Memoir 6 - Peri-Tethyan rift/wrench basins and passive margins. Mémoires du Muséum national d'Histoire naturelle, Paris, 186, 295-346.

Nilforoushan F., Masson F., Vernant Ph., Vigny C., Martinod J., Abbassi M.R., Nankali H., Hatzfeld D., Bayer R., Tavakoli F., Ashtiani A., Doerflinger E., Daignières M., Collard P. & Chéry J. 2003. GPS network monitors the arabia-Eurasia collision deformation in Iran. Journal of Geodesy 77, 411-422.

Nilivkin V. 1976. Geological map of the Caucasus at 1:500'000 scale.

Nosova A.A., Sazonova L.V., Dokuchaev A.Ya., Grekov I.I. & Gurbanov A.G. 2005. Neogen Late-collisional subalkaline granitoids in the area of Mineral'nye Vody, Caucasus: T-P-fo crystallization conditions, fractional and fluid-magmatic differentiation. Petrology 13, 2, 122-160.

Ortner H., Reiter F. & Acs P. 2002. Easy handling of tectonic data: the programs TectonicVB for Mac and TectonicFP for Windows. Computers and Geosciences 28, 1193 - 1200.

Parsons B. & Sclater J.G. 1977. An analysis of the variation of ocean floor bathymetry and heat flow with age. Journal of Geophysical Research 32, 803-827.

Peresson H. 1992. Computer aided kinematic analysis of fault sets. Mitteilungen der Gesellschaft für Geologie und Bergbaustudien 38, 107-119.

Philip H., Cisternas A., Gvishiani A. & Gorshkov A. 1989. The Caucasus: an actual example of the initial stages of continental collision. Tectonophysics 161, 1-21.

Pimmel A. & Claypool G. 2001. Introduction to shipboard organic geochemistry on the JOIDES Resolution. ODP Technical Note 30, 29 pp.

Planke S., Svensen H., Hovland M., Banks D.A. & Jamtveit B. 2003. Mud and fluid migration in active mud volcanoes in Azerbaijan. Geo-Marine Letters 23, 3-4, 258-268.

Popov S.V., Rögl F., Rozanov A.Y., Steininger F.F., Shcherba I.G. & Kovac M. 2004. Lithological-Paleogeographic maps of Paratethys. 10 maps Late Eocene to Pliocene. Courier Forschungsinstitut Senckenberg, Stuttgart, 46 pp.

Priestley K., Baker C. & Jackson J. 1994. Implications of earthquake focal mechanism data for the active tectonics of the south Caspian Basin and surrounding regions. Geophysical Journal International 118, 111-141.

Pryde P. R. 1979. Geothermal Energy Development in the Soviet Union. Geo-Heat Center Quarterly Bulletin 4, 2, 8-14.

Ramsay J.G. & Lisle R.J. 2000. The Techniques of Modern Structural Geology : Applications of continuum mechanics in structural geology. Academic Press, 1061 pp.

Rast A. 2007. Topographie, soulèvement et tectonique dans la partie nord du Grand Caucase d'Azerbaijan. Master Thesis, University of Fribourg, Fribourg.

Rastvorova V.A. & Shcherbakova E.M. 1967. The uplift of the Central Caucasus during late-glacial times. In: Gerasimov I. P. (Eds.), Recent crustal movements. Israel Program Scientific Translation, 318-326.

Rebaï S., Philip H., Dorbath L., Borissoff B., Haessler H. & Cisternas A. 1993. Active tectonics in the Lesser Caucasus: coexistance of compressive and extensional structures. Tectonics 12, 5, 1089-1114.

Reilinger R., McClusky S., Vernant Ph., Lawrence S., Ergintav S., Cakmak R., Ozener H., Kadirov F., Guliev I., Stepanyan R., Nadariya M., Hahubia G., Mahmoud S., Sakr K., ArRajehi A., Paradissis D., Al-Aydrus A., Filikov S.V., Gomez F., Al-Ghazzi R. & Karam G. 2006. GPS constraints on continental deformation in the Africa-Arabia-Eurasia continental collision zone and implications for the dynamics of plate interactions. Journal of Geophysical Research B, solid earth and planets 111, B05411, 26 pp.

Reiners P.W. & Brandon M.T. 2006. Using Thermochronology to Understand Orogenic Erosion. Annual Review of Earth and Planetary Sciences 34, 419-466.

Reynolds A.D., Simmons M.D., Bowman M.B.J., Henton J., Brayshaw A.C., Ali-Zade A.A., Guliyev I.S., Suleymanova S.F., Ateava E.Z., Mamedova D.N. & Koshkarly R.O. 1998. Implications of Outcrop Geology for Reservoirs in the Neogene Productive Series: Apsheron Peninsula, Azerbaijan. American Association of Petroleum Geologists Bulletin 82, 1, 25-49.

Riedel W. 1929. Zur Mechanik geologischer Brucherscheinungen. Centralblatt für Mineralogie, Geologie und Paläontologie 1929B, 354-368.

Robinson A.G., Banks C.J., Rutherford M.M. & Hirst J.P.P. 1995. Stratigraphic and structural development of the Eastern Pontides, Turkey. Journal of the Geological Society 152, 5, 861-872.

Rogozin E.A. & Ovsyuchenko A.N. 2005. Seismic and geological activity of tectonically faulted structures in the Northern Caucasus. Physics of solid Earth 41, 6, 449-461.

Rogozin E.A., Yunga S.L., Marakhanov A.V., Ushanova E.A., Ovsyuchenko A.N. & Dvoretskaya N.A. 2002. Seismic and tectonic activity of faults on the south slope of the NW Caucasus. Russian journal of earth sciences 4, 3, 233-241.

Rychagov G.I. 1993a. The level of the Caspian Sea in historic times. Bulletin of Moscow State University 5, 4(1), 42-49.

Rychagov G.I. 1993b. The sea-level regime of the Caspian Sea during the last 10,000 years. Bulletin of Moscow State University 5, 4 (2), 38-49.

Rychagov G.I. 1997. Holocene oscillations of the Caspian Sea, and forecasts based on palaeogeographical reconstructions. Quaternary International 41-42, 167-172.

Saintot A. & Angelier J. 2000. Plio-Quaternary paleostress regimes and relation to structural development in the Kertch-Taman peninsulas (Ukraine and Russia). Journal of Structural Geology 22, 1049-1064.

Saintot A., Angelier J., Ilyn A. & Goushtchenko O. 1998. Reconstruction of paleostress fields in Crimea and the North West Caucasus, relationship with major structures. Mémoires du Muséum national d'histoire naturelle 177, 89-112.

Saintot A., Brunet M.-F., Yakovlev F., Sebrier M., Stephenson R.A., Ershov A.V., Chalot-Prat F. & McCann T. 2006a. The Mesozoic-Cenozoic tectonic eveolution of the Greater Caucasus. Geological Society London, Memoirs 32, 277-289.

Saintot A., Stephenson R.A., Stovba S., Brunet M.-F., Yegorova T.P. & Starostenko V. 2006b. The evolution of the southern margin of Eastern Europe (Eastern European and Scythian platforms) from the latest Precambrian-Early Paleozoic to Early Cretaceous. Geological Society, London, Memoirs 32, 481-505.

Schmoker J.W. & Halley R.B. 1982. Carbonate porosity versis depth; a predictable relation for South Florida. American Association of Petroleum Geologists Bulletin 66, 12, 2561-2570.

Sclater J.G. & Christie P.A.F. 1980. Continental stretching on explanation of the post-mid Cretaceous subsidence of the central north sea Basin. Journal of Geophysical Research 85, 3711-3739.

Shatilova I. 1992. The late Cenozoic climate and vegetation of western Georgia. Paleontologia I Evolucio 24-25, 465-481.

Shatilova I., Maissuradze L., Koiava K., Mchedlishvili N., Rukhadze L., Spezzaferri S. & Strasser A. 2009. Foraminifers and Palynomorphs in the Sarmatian deposits of Kartli (Eastern Georgia): Stratigraphical and paleoclimato-

logical implications. Proceedings Georgian Academy of Science, Biology Series. B No 3-4, 65-76.

Shcherbakova E.M. 1973. The ancient glaciation of the Great Caucasus. (Drevnee oledenenie Bolshogo Kavkaza). Moscow, 271 pp.

Shikalibeily E.S. & Grigoriants B.V. 1980. Principal features of the crustal structure of the South-Caspian Basin and the conditions of its formation. Tectonophysics 69, 113-121.

Shirinov N.Sh. 1973. Geomorphological structure of the Kura-Araksa depression (Geomorfologicheskoe stroenie Kura-Araksinskoi depressii). Baku, 215 pp.

Shirinov N.Sh. 1975. Latest tectonics and development of the relief of the Kura-Araska depression (Noveishaya tektonika i razvitie relyefa Kura-Araksin-skoi depressii). Baku, 190 pp.

Sholpo V.N. 1993. Strucure of inversion anticlinoria in the core of the Greater Caucasus: an advection hypothesis. Geotectonics 23, 3, 245-251.

Sobel E.R. & Seward D. 2010. Influence of etching conditions on apatite fission-track etch pit diameter. Chemical Geology 271, 59-69.

Sobornov K.O. 1994. Structure and petroleum potential of the Dagestan thrust belt, northeastern Caucasus, Russia. Bulletin of Canadian Petroleum Geology 42, 3, 352-364.

Sobornov K.O. 1996. Lateral variations in structural styles of tectonic wedging in the northeastern Caucasus, Russia. Bulletin of Canadian Petroleum Geology 44, 2, 385-399.

Somin M.L., Kotov A.B., Sal'nikova E.B., Levchenko O.A., Pis'mennyi A.N. & Yakovlev S.Z. 2006. Paleozoic rocks in infrastructure of the metamorphic core, the Greater Caucasus Main Range Zone. Stratigraphy and Geological Correlation 14, 5, 475-485.

Sosson M., Kaymakci N., Stephenson R. A., Bergerat F. & Starostenko V. 2010a. Sedimentary Basin Tectonics from the Black Sea and Caucasus to the Arabian Platform. The Geological Society of London, London, 509 pp.

Sosson M., Kaymakci N., Stephenson R.A., Bergerat F. & Starostenko V. 2010b. Sedimentary basin tectonics from the Black Sea and Caucasus to the Arabian Platform: introduction. In: Sosson M., Stephenson R.A., Bergerat F. & Starostenko V. (Eds.), Sedimentary Basin Tectonics from the Black Sea and Caucasus to the Arabian platform. The Geological Society of London, London, Special Publication 340, 1-10.

Sosson M., Rolland Y., Muller C., Danelian T., Melkonyan R., Adamia Sh.A., Kangarli T., Avagyan A., Galoyan G. & Mosar J. 2010c. Subductions, obduction and collision in the Lesser Caucasus (Armenia,Azerbaijan, Georgia), new insights. In: Sosson M., Stephenson R.A., Bergerat F. & Starostenko V. (Eds.), Sedimentary Basin Tectonics from the Black Sea and Caucasus to the Arabian platform. The Geological Society of London, London, Special Publication 340, 329-352.

Stampfli G.M., Borel G., Cavazza W., Mosar J. & Ziegler P. 2001. Palaeotectonic and palaeogeographic evolution of the western Tethys and PeriTethyan domain. Episodes 24, 4, 222-228.

Stephenson R.A. & Schellart W.P. 2010. The Black Sea back-arc basin: insights to its origin from geodynamic models of modern analogues. In: Sosson M., Stephenson R.A., Bergerat F. & Starostenko V. (Eds.), Sedimentary Basin Tectonics from the Black Sea and Caucasus to the Arabian platform. The Geological Society of London, London, Special Publication 340, 11-21.

Stokes C.R., Gurney S.D., Shahgedanova M. & Popovnin V. 2006. Late-20th-century changes in glacier extent in the Caucasus Mountains, Russia/Georgia. Journal of Glaciology 52, 176, 99-109.

Strahler A.N. 1957. Quantitative analysis of watershed geomorphology. Transactions of the American Geophysical Union 38, 913-920.

Tan O. & Taymaz T. 2006. Active tectonics of the Caucasus: Earthquake source mechanisms and rupture histories obtained from inversion of teleseismic body waves. Geological Society of America, Special paper 409, 531-578.

Tchalenko J.S. 1970. Similarities between Shear Zones of Different Magnitudes. Geological Society of America Bulletin 81, 1625-1640.

Tissot B.P. & Welte D.H. 1978. Petroleum Formation and Occurence, a new approach to oil and gas exploration. Springer-Verlag, Berlin, 538 pp.

Triep E.G., Abers G.A., Lerner-Lam A.L., Mishatkin V., Zakharchenko N. & Starovoit O. 1995. Active thrust front of the Greater Caucasus : The April 29, 1991 Racha earthquake sequence and its tectonic implications. Journal of Geophysical Research 100, B3, 4011-4034.

Tzereteli D.V. 1974. Quaternary Glaciation in Caucasus. Revue De Geographie Physique Et De Geologie Dynamique 16, 3, 293-298.

Ulminshek G.F. 2001. Petroleum geology and resources of the Middle Caspian Basin, former Soviet Union. U.S. Geological Survey Bulletin 2201-A, 38.

Van Hinte J.E. 1978. Geohistory analysis - Application of micropaleontology in exploration geology. American Association of Petroleum Geologists Bulletin 62, 201-222.

Vernant Ph., Nilforoushan F., Hatzfeld D., Abbassi M.R., Vigny C., Masson F., Nankali H., Martinod J., Ashtiani A., Bayer R., Tavakoli F. & Chéry J. 2004. Present-day crustal deformation and plate kinematics in the Middle East constrained by GPS measurements in Iran and northern Oman. Geophysical Journal International 157, 381-398.

Vialon P., Ruhland M. & Grolier J. 1976. Eléments de tectonique analytique. Masson, Paris, 118 pp.

Vincent S.J., Morton A.C., Carter A., Gibbs S. & Barabadze T.G. 2007. Oligocene uplift of the western Greater Caucasus: an effect of initial Arabia-Eurasia collision. Terra Nova 19, 160-166.

Wagner G.A. 1972. Spaltspurenalter von Mineralen und natürlichen Gläsern: eine Übersicht. Fortschritte der Mineralogie 49, 114–145.

Wagner G.A. & Van den haute P. 1992. Fission-Track Dating. Kluwer Academic Publishers, Dordrecht, 285 pp.

Westaway R. 1990. Seismicity and tectonic deformation rate in Soviet Armenia : Implications for local earthquake hazard and evolution of adjacent regions. Tectonics 9, 3, 477-503.

Wilcox R.E, Harding T.P. & Seely D.R. 1973. Basic Wrench Tectonics. American Association of Petroleum Geologists Bulletin 57, 1, 74-96.

Yakubov A.A., Ali-Zade A.A. & Zeinalov M.M. 1971. Mud Volcanoes of the Azerbaijan SSR Atlas. Baku, 258 pp.

Zanchi A., Zanchetta S., Garzanti E., Balini M., Berra F., Mattei M. & Muttoni G. 2009. The Cimmerian evolution of the Nakhlak-Anarak area, Central Iran, and its bearing for the reconstruction of the history of the Eurasian margin. In: Brunet M-F., Wilmsen M. & Granath J.W. (Eds.), South Caspian to Central Iran Basins. The Geological Society of London, London, Special Publication 312, 261-285.

Zenkevich L.A. 1957. Caspian and Aral Seas. Geological Society of America Memoirs 67, 1, 891-916.

Zonenshain L.P., Kuzmin M.I. & Natapov L.M. 1990. Geology of the USSR: A plate tectonic synthesis. American Geophysical Society, Washington, 242 pp.

Zonenshain L.P. & Le Pichon X. 1986. Deep Basins of the Black-Sea and Caspian Sea as Remnants of Mesozoic Back-Arc Basins. Tectonophysics 123, 1-4, 181-211.

*****

CURRICULUM VITAE

Martin BOCHUD

Dr. in Geology / ETS Engineer in electronics

Born in Posieux (Switzerland)
Birthdate : 20.10.1977

Legal status : married
Nationality : Swiss
E-mail : martin.bochud@bluewin.ch

Educational background

PhD in tectonics and general geology at the University of Fribourg. PhD thesis : *« Tectonics of the Eastern Greater Caucasus in Azerbaijan ».*	July 2006 - October 2011
Diploma in tectonics and general geology at the University of Fribourg. Diploma thesis : *« Tectonic evolution of the Eastern Greater Caucasus ».* **Erasmus Exchange** in the Earth Sciences and Geography department at Keele University (UK).	October 2002 - June 2006 February - May 2005
ETS Engineer in Electronics at the College of Engineering and Architecture of Fribourg. Diploma thesis : *«Système de mesure et de traitement des ultrasons pour l'observation des chauves-souris »*, Vibrometer award.	October 1996 - December 1999
Federal VET Certificate in electronics and Professional Baccalaureate at the Ecole des Métiers of Fribourg.	August 1993 - July 1996

Professional activities

Swiss Institute for Speleology and Karst Studies (SISKA), non-military national service, inventory and study of the karst areas and karst springs of the Fribourg region.	January - April 2011
University of Fribourg, part-time assistant in the Geosciences Department : geographic information system, cartography and field trips.	July 2006 - December 2010
Softcom Technologies SA, part-time electronics engineer : project manager for energy management, expertises for PLC in tunnels, electronic board development.	January 2006 - April 2011
University of Fribourg, part-time assistant : cartography.	October 2004 - June 2006
College of Engineering and Architecture of Fribourg, part-time assistant in the Energy department. Electronic board development and processor programming.	May 2002 - March 2006
Montena MCO, installation of an active electrical network filter in Colombia.	February 2002
ITN Sàrl in Fribourg, Labview project for the Swiss National Metrology Institute (METAS).	May 2001 - January 2002
College of Engineering and Architecture of Fribourg, full time assistant in the Energy department : development of an electrical network filter in collaboration with the EPFL and Montena MCO and EMC.	December 1999 - September 2000
Ilford AG in Marly, electrician during summer academic holidays.	1997 - 1999

Languages

French : mother tongue.

English : Read / Write / Speak (B2-C1 level).

Spanish : Read / Write / Speak (B2 level).

German : Read / Write / Speak (B2 level).

Softwares

Geology and GIS: ArcGIS (ArcCatalog, ArcMap, ArcGlobe, ArcScene), Tectonics FP, Binomfit, Hefty, Popshare, Trackkey.

Graphic and photography : Adobe Illustrator, Adobe Photoshop, Adobe Acrobat, Adobe Lightroom.

Electronics and programming : Mentor Graphics, Code Composer Studio (Texas), HC11 processor, CPLD, RFID card, C programming, assembly language and Labview.

Office software : Microsoft Office (Excel, Word, Access, Outlook, Visio), LaTeX, Adobe Acrobat.

Miscellaneous : Joomla (CMS), network configuration (Ethernet, CANbus, RS-485).

Associations and hobbies

Geology - Engineering : Swiss Geological Society, CH-GEOL and Swiss Engineering.

Speleology : president of the Spéléo Club des Préalpes fribourgeoises, Société Suisse de Spéléologie, Spéléo Secours Suisse.

Outdoor Sport : hiking, ski-touring, mountaineering, canyoning and climbing.

Travels: Algeria, Tunisia, Mali, Azerbaijan, Georgia, Colombia, Mexico, Venezuela, Europe and 6 months in South America (Argentina, Chile, Bolivia, Peru and Ecuador).

Photography : Photo Club Fribourg, 2 exhibitions.

Publications

Morard, S., Bochud, M., & Delaloye, R. (2010). Rapid changes of the ice mass configuration in the dynamic Diablotins ice cave – Fribourg Prealps, Switzerland. *The Cryosphere*.

Morard, S., Bochud, M., & Delaloye, R. (2010). *Rapid changes of the ice mass configuration in the dynamic Diablotins ice cave– Fribourg Prealps, Switzerland*. Paper presented at the Swiss Geoscience Meeting 2010, Fribourg.

Mosar, J., Kangarli, T., Bochud, M., Glasmacher, U., Rast, A., Brunet, M. F., & Sosson, M. (2010). Cenozoic-Recent tectonics and uplift in the Greater Caucasus: a perspective from Azerbaijan. In M. Sosson, N. Kaymakci, R. A. Stephenson, F. Bergerat & V. Starostenko (Eds.), *Sedimentary Basin Tectonics from the Black Sea and Caucasus to the Arabian Platform* (Vol. 340, pp. 261-280). London: Geological Society.

Bochud, M., & Mosar, J. (2008). *GIS-supported Geology and Fieldwork in the Eastern Greater Caucasus.* Paper presented at the Swiss Geoscience Meeting, Lugano.

Bochud, M., Mosar, J., & Kangarli, T. (2008). *Structural geology, stress and strain across the Eastern Greater Caucasus.* Paper presented at the Swiss Geoscience Meeting, Lugano.

Bochud, M., Blant, M., Braillard, L., Magnin, B., & Jutzet, J. M. (2007). Les ours des cavernes et la faune du Pleistocène supérieur de la grotte du Baerenloch (Charmey,FR). [Acte du 12e Congrès national de Spéléologie.]. 148-154.

Bochud, M., Mosar, J., Rast, A., & Kangarli, T. (2007a). *GIS and Geodatabase for fieldwork in Azerbaijan.* Paper presented at the 2nd International Scientific Conference of young scientists and students, Baku.

Bochud, M., Mosar, J., Rast, A., & Kangarli, T. (2007b). *Tectonics of the Eastern Greater Caucasus.* Paper presented at the 2nd International Scientific Conference of young scientists and students, Baku.

Bochud, M. (2006). *Tectonic evolution of the Eastern Greater Caucasus.* Diploma, University of Fribourg, Fribourg.

Vrielynck, B., Bochud, M., Barrier, E., Brunet, M. F., Bergerat, F., Brouillet, J.-F., Pasquier, D. (2006). *The Mebe Gis Database: A Tool for Middle East Geology.* Paper presented at the GEO2006, 7th Middle East Geosciences Conference and Exhibition, Bahrain.

Vrielynck, B., Bochud, M., Brouillet, J.-F., Morgant, I., & Pasquier, D. (2006). *From field to GIS*. Paper presented at the MEBE conference.

Egan, S., Mosar, J., Brunet, M.-F., Bochud, M., Kangarli, T., & Mountney, N. (2004). Subsidence Mechanisms within the South Caspian Basin - Year 2 Report (pp. 80): Middle East Basin Evolution Programme.

Blant, M., Bochud, M., Braillard, L., & Magnin, B. (2004). Bärenloch, Le dernier repaire d'ours des Cavernes dans les Alpes suisses ? . *Stalactite, 54*(1).

Bochud, M. (2001). *Région du Vanil Blanc dans les Préalpes Fribourgeoises.* Paper presented at the Actes du 11e Congrès National de Spéléologie, Genève.

Bochud, M. (2000). La Grotte de l'Alfredo, Albeuve (FR). *Cavernes, 2000*(1), 13-17.

Already published:

Vol. 1 **HILLGÄRTNER, Heiko** (1999) The evolution of the French Jura platform during the Late Berriasian to Early Valanginian: controlling factors and timing (203 pp.).

Vol. 2 **DUPRAZ, Christophe** (1999) Paléontologie, paléoécologie et évolution des faciès récifaux de l'Oxfordien Moyen-Supérieur (Jura suisse et français) (247 pp.).

Vol. 3 **BASSANT, Philip** (1999) The high-resolution stratigraphic architecture and evolution of the Burdigalian carbonate-siliciclastic sedimentary systems of the Mut Basin, Turkey (278 pp.).

Vol. 4 **COLOMBIÉ, Claude** (2002) Sédimentologie, stratigraphie séquentielle et cyclostratigraphie du Kimméridgien du Jura suisse et du Bassin vocontien (France): relations plate-forme - bassin et facteurs déterminants (198 pp.).

Vol. 5 **PICOT, Laurent** (2002) Le Paléogène des synclinaux du Jura et de la bordure sud-rhénane: paléontologie (Ostracodes), paléoécologie, biostratigraphie et paléogéographie (240 pp.).

Vol. 6 **DAPPLES, Florence** (2002) Instabilités de terrain dans les Préalpes fribourgeoises (Suisse) au cours du Tardiglaciaire et de l'Holocène: influence des changements climatiques, des fluctuations de la végétation et de l'activité humaine (158 pp.).

Vol. 7 **HUG, Wolfgang Alexander** (2003) Sequenzielle Faziesentwicklung der Karbonatplattform des Schweizer Jura im Späten Oxford und frühesten Kimmeridge (156 pp.).

Vol. 8 **OSWALD, Daniel** (2003) Analyse de l'activité de glissements de terrain et relation avec les conditions climatiques: Exemples dans les Préalpes fribourgeoises (Suisse) (147 pp.).

Vol. 9 **BECKER, Damien** (2003) Paléoécologie et paléoclimats de la Molasse du Jura (Oligo-Miocène): apport des Rhinocerotoidea (Mammalia) et des minéraux argileux (327 pp.).

Vol. 10 **DELALOYE, Reynald** (2005) Contribution à l'étude du pergélisol de montagne en zone marginale (240 pp.).

Vol. 11 **FREUDIGER-BONZON, Jeanne** (2005) Archaeometrical study (petrography, mineralogy and chemistry) of Neolithic Ceramics from Arbon Bleiche 3 (Canton of Thurgau, Switzerland) (187 pp.).

Vol. 12 **STOFFEL, Markus** (2005) Spatio-temporal variations of rockfall activity into forests - results from tree-ring and tree analysis (188 pp.).

Vol. 13 **RAMEIL, Niels** (2005) Carbonate sedimentology, sequence stratigraphy, and cyclostratigraphy of the Tithonian in the Swiss and French Jura Mountains - a high-resolution record of changes in sea level and climate (246 pp.).

Vol. 14 **BRAILLARD, Luc** (2006) Morphogenèse des vallées sèches du Jura tabulaire d'Ajoie (Suisse): rôle de la fracturation et étude des remplissages quaternaires (224 pp.).

Vol. 15 **GOYETTE-PERNOT, Joëlle** (2006) L'Ambroisie: analyse statistique et modélisation numérique de sa trajectoire aérobiologique (274 pp.).

Vol. 16 **TRESCH, Jonas** (2007) History of a Middle Berriasian transgression (Switzerland, France, and southern England) (271 pp.).

Vol. 17 **BONNET, Cécile** (2007) Interactions between tectonics and surface processes in the Alpine foreland: Insights from analogue model and analysis of recent faulting (189 pp.).

Vol. 18 **VONLANTHEN, Pierre** (2007) EBSD-based investigations of upper mantle xenoliths, snowball garnets and advanced ceramics (114 pp.).

Vol. 19 **VÉDRINE, Stéphanie** (2007) High-frequency palaeoenvironmental changes in mixed carbonate-siliciclastic sedimentary systems (Late Oxfordian, Switzerland, France, and southern Germany) (216 pp.).

Vol. 20 **BOLLSCHWEILER, Michelle** (2008) Spatial and temporal occurrence of past debris flows in the Valais Alps - results from tree-ring analysis (182 pp).

Vol. 21 **MARTY, Daniel** (2008) Sedimentology, taphonomy, and ichnology of Late Jurassic dinosaur tracks from the Jura carbonate platform (Chevenez-Combe Ronde tracksite, NW Switzerland): insights into the tidal-flat palaeoenvironment and dinosaur diversity, locomotion, and palaeoecology (278 pp.).

Vol. 22 **STIENNE, Noémie** (2010) Paléoécologie et taphonomie comparative en milieux carbonatés peu profonds (Oxfordien du Jura Suisse et Holocène du Belize) (248 pp.).

Vol. 23 **WAITE, Richard** (2010) The palaeoecology of high-spired gastropods and the lost palaeosols: depositional reconstructions on a shallow carbonate platform (Late Kimmeridgian, Swiss Jura Mountains) (149 pp.).

Vol. 24 **MARGRET, Stephan** (2010) Benthic foraminifera associated to cold-water coral ecosystems (248 pp.).

Vol. 25 **VON ALLMEN, Katja** (2010) Variations of calcium and barium isotopes and elemental contents in biogenic and abiogenic geological archives (97 pp.).

Vol. 26 **VOUILLAMOZ, Naomi / SAUDAN, Corinne / MOSAR, Jon** (2010) Microzonage sismique du canton de Fribourg - Cartographie au 1:25'000 des sols de fondation selon la norme SIA 261 (57 pp.).

Vol. 27 **IBELE, Tobias,** (2011) Tectonics of the Western Swiss Molasse Basin during Cenozoic Time (166 pp.).

Vol. 28 **GENNARI, Giordana, (2011)** The Mediterranean - Black Sea connections: The fundamental role of foraminifera as a multifaceted tool for the geological reconstruction of the last 10 ky (171 pp.).

Vol. 29 **MORARD, Sébastien, (2011)** Effets de la circulation d'air par effet de cheminée dans l'évolution du régime thermique des éboulis froids de basse et moyenne altitude (220 pp.).

ISSN 1424 - 1463

GeoFocus is the publication series of the Department of Geosciences, University of Fribourg, Switzerland, and can be ordered at:
Department of Geosciences - Earth Sciences - University of Fribourg - 1700 Fribourg, Switzerland - http://www.unifr.ch/geoscience/geology